

STRUCTURE AND STABILITY OF EUROPIUM DOPED β -ALUMINA"
TYPE PHOSPHOR"

BY"

ZHEHUA WU"

A THESIS"
SUBMITTED TO THE FACULTY OF"

ALFRED UNIVERSITY"

IN PARTIAL FULFILLMENT OF THE REQUIREMENTS"
FOR THE DEGREE OF"

DOCTOR OF PHILOSOPHY"

IN"

CERAMICS"

ALFRED, NEW YORK
JULY, 2002

Alfred University theses are copyright protected and may be used for education or personal research only. Reproduction or distribution in any format is prohibited without written permission from the author.

STRUCTURE AND STABILITY OF EUROPIUM DOPED b-ALUMINA
TYPE PHOSPHOR

BY

ZHEHUA WU

B.S. TSINGHUA UNIVERSITY (1998)

SIGNATURE OF AUTHOR _____ (Signature on file)

APPROVED BY _____ (Signature on file)

ALASTAIR N. CORMACK, ADVISOR

(Signature on file)

PAUL F. JOHNSON, ADVISORY COMMITTEE

(Signature on file)

DOREEN D. EDWARDS, ADVISORY COMMITTEE

(Signature on file)

ROBERT CONDRADE, ADVISORY COMMITTEE

(Signature on file)

ARUN VARSHNEYA, CHAIR, ORAL THESIS DEFENSE

ACCEPTED BY _____ (Signature on file)

RONALD S. GORDON, DEAN, SCHOOL OF
CERAMIC ENGINEERING AND MATERIALS SCIENCE

ACCEPTED BY _____ (Signature on file)

DAVID SZCZERBACKI,
DIRECTOR OF GRADUATE SCHOOL, ALFRED UNIVERSITY

Acknowledgments

Sincerely, I would like to thank my advisor, Dr. Alastair N. Cormack, who leads me into the world of computer simulation, for his guidance, support and advice during my four-year study at Alfred University. Also I want to express thanks to my thesis advisory committee members, Dr. Robert A. Condrate, Dr. Paul F. Johnson, Dr. Doreen Edwards, for their great help especially in refining my thesis work. I would like to show my gratitude to all my group members, especially Byeongwon Park, JinCheng Du and Darren Stohr, who had helped me with the research difficulties. I am deeply appreciated for Ann Baldwin to help me improve my English skills. I acknowledge the U.S. Department of Energy for financing my Ph.D. thesis and U. C. Berkeley for computational resources.

I would like to show my thank for Dr. YaoZhong Jiang in the Tsinghua University, Beijing, China, who recommended Alfred University for graduate study. My acknowledgements are also given to the past the current Chinese students, especially XiangLong Yuan, ChangQing Shen, who made my life in Alfred much more fun and enjoyable. Special thanks are given to my family and friends in China for their supports and encouragement.

Table of Contents

	Page
Acknowledgments	iii
List of Tables	vi
List of Figures.....	viii
Abstract	x
1. General Introduction	1
References	4
2. The Crystal Structure	6
2.1 Structure of β -Alumina	6
2.2 Beta Triple-Prime Phase	9
2.3 Beta Double-Prime Phase	11
2.4 Barium Magnetoplumbite	13
References	15
3. Atomistic Computer Simulation Techniques	21
3.1 Introduction	21
3.2 Inter Atomic Potentials	22
3.3 Minimization Techniques.....	25
3.4 Defect Energy Calculations.....	27
References	31
4. Defects in $\text{BaMgAl}_{10}\text{O}_{17}:\text{Eu}^{2+}$ Blue Phosphor	34
4.1 Introduction	35
4.2 Results.....	39
4.3 Defect Complexes.....	48
4.4 Europium Ion Size Consideration.....	51
4.5 Calculations with the Bush Potential	53
4.6 Conclusions	55
References	57
5. Ion Migration In BAM.....	64

5.1 Introduction	65
5.2 Experiments.....	68
5.3 Results.....	69
5.4 Related Phases Containing Eu.....	74
5.5 Conclusions	76
References.....	77
6. Eu in Barium Hexa-aluminates Containing No Mg	81
6.1 Introduction	82
6.2 The Barium-Poor Phase $Ba_{0.75}Al_{11}O_{17.25}$	84
6.3 Emission Band Calculations.....	94
6.4 $Ba_3Al_3O_5$	98
6.5 Conclusions	102
References.....	103
7. Defects in β'' - and β''' - Barium Hexa-aluminates	114
7.1 Introduction:	115
7.2 Equilibrated Structures	119
7.3 Intrinsic Defects.....	122
7.4 Extrinsic Defects: Europium	126
7.5 Potential at Tetrahedral and Octahedral Sites	128
7.6 Conclusions	128
References.....	130
8. Summary and Future Work.....	135
8.1 Summary	135
8.2 Suggestions for Future Work	137

List of Tables

	Page
Table II.1. Positional and Occupation Parameters for β -Alumina (I)	8
Table II.2. Positional and Occupation Parameters for β -Alumina (II)	9
Table II.3. Positions of Ions in β''' -Alumina	10
Table II.4. Positions of Ions in β'' -Alumina	11
Table IV.1. Crystallographic Information for the β -Alumina Structure	36
Table IV.2. Potential Parameters Derived by Lewis and Catlow	38
Table IV.3. Potential Models Derived by Bush et al.	38
Table IV.4. Lattice Energies of Mg Distributions in Al(2) and Al(3) Sites	40
Table IV.5. Comparison of Measured and Calculated Structures	41
Table IV.6. Calculated Point Defect Energies (eV)	42
Table IV.7. Calculated Intrinsic Defect Energies (eV)	45
Table IV.8. Europium Point Defect Energies (eV)	46
Table IV.9. Eu^{2+} Ion Incorporation into BAM	47
Table IV.10. Eu^{3+} Ion Incorporation into BAM	48
Table IV.11. Defect Complexes Containing Eu^{3+} and O^{2-}	49
Table IV.12. Defect Complexes with Three Point Defects	50
Table IV.13. Defect Reaction of Defect Complex	50
Table IV.14. Bond Valence of Cations in BAM	52
Table IV.15. Bond Length vs. Coordination Number	52
Table IV.16. Point Defect in Config. I with Bush Potential	53
Table IV.17. Intrinsic Defect Energy of BAM with Bush Potential	54
Table IV.18. Incorporation of Eu into BAM (Bush Potential)	55
Table V.1. Defect Complex with Two Oxygen and One Eu^{3+}	75

Table VI.1. Lattice Energies of Five Structures	86
Table VI.2. Lattice Energies of Five Structures (with Reidinger-Defect)	86
Table VI.3. Vacancy Defect Energies of Super-Cells	88
Table VI.4. Point Defects of 1-2 Super-Cell	89
Table VI.5. Point Defects of 1-3 Super-Cell	90
Table VI.6. Point Defects of b1 Super-Cell	90
Table VI.7. Intrinsic Defect Energies of Super-Cells (eV)	91
Table VI.8. Europium Point Defects in the Three Super-Cells	92
Table VI.9. Incorporation of Eu into Super-Cells	93
Table VI.10. Estimated Emission Wavelength of Eu	95
Table VI.11. Site Energy Comparison of Eu ²⁺ Positions	96
Table VI.12. Lattice Energies of Four Possible Structures	99
Table VI.13. Point Defect in Ba ₃ Al ₃₂ O ₅₁	100
Table VI.14. Europium Point Defects	101
Table VI.15. Defect Reaction of Eu in Ba ₃ Al ₃₂ O ₅₁	101
Table VII.1. Potential Parameters Derived by Lewis and Catlow	118
Table VII.2. Lattice Energy of Barium β"-Alumina	120
Table VII.3. Lattice Energy of Barium β'''-Alumina	121
Table VII.4. Defect Energy of Barium β"-Alumina	124
Table VII.5. Defect Energies of Barium β'''-Alumina	125
Table VII.6. Point Defect of Europium in Barium β"-Alumina	127
Table VII.7. Defect Formation Energies of Eu ²⁺ in Barium β"-Alumina	127
Table VII.8. Defect Formation Energies of Eu ³⁺ in Barium β"-Alumina	127

List of Figures

	Page
Figure 2.1. Structure of ideal β -alumina $\text{NaAl}_{11}\text{O}_{17}$.	17
Figure 2.2. Structure of ideal β''' -alumina $\text{Na}_2\text{O} \cdot \text{MgO} \cdot 15\text{Al}_2\text{O}_3$. All Mg are shown as Al.	18
Figure 2.3. Structure of ideal β'' -alumina.	19
Figure 2.4. Structure of ideal manetoplumbite $\text{MAl}_{12}\text{O}_{19}$.	20
Figure 3.1. Two regions for defect energy calculation. Defect is in the center of region I.	33
Figure 4.1. Primitive cell of β -alumina.	59
Figure 4.2. Two configurations of BAM. a) Configuration I possesses Mg at ab sites; b) Configuration II possesses Mg at ac sites.	60
Figure 4.3. Projection of mirror plane of BAM with ion positions on X-Y plane.	61
Figure 4.4. Three types of oxygen interstitial of BAM.	62
Figure 4.5. Configuration of Reidinger defect.	63
Figure 5.1. Primitive cell of BAM, configuration I.	78
Figure 5.2. Projection of mirror plane of BAM on X-Y plane.	79
Figure 5.3. Magnesium positions related to $\text{Eu}_i^{\bullet\bullet\bullet} + V_{\text{Al}(2)}^{\bullet\bullet}$.	79
Figure 5.4. Barium interstitialcy migration.	80
Figure 5.5. Trajectory of Eu^{2+} in the conduction plane.	80
Figure 6.1. $\text{Ba}_6\text{Al}_{88}\text{O}_{138}$ super-cell.	105
Figure 6.2. Structure of 1-2 super-cell of barium-poor phase.	106
Figure 6.3. Structure of 1-3 super-cell of barium-poor phase.	107
Figure 6.4. Lattice energy of solid solution between BAM and barium-poor phase.	108
Figure 6.5. Crystal structure of b1 super-cell.	109

Figure 6.6. Mirror plane structures. a) BAM; b) magnetoplumbite.	110
Figure 6.7. a) Mirror plane of 1-2 super-cell; b) Mirror plane of 1-3 super-cell; c) Mirror plane of b1 super-cell.	110
Figure 6.8. Eu^{2+} environment in mirror plane. a) Associated without O_{BR} ; b) Associated with O_{BR} .	111
Figure 6.9. Selection of $\sqrt{3} \times \sqrt{3}$ super-cell.	112
Figure 6.10. $\sqrt{3} \times \sqrt{3}$ unit cell of $\text{Ba}_3\text{Al}_{32}\text{O}_{51}$.	113
Figure 7.1. Comparison of BR and anti-BR positions.	132
Figure 7.2. Unit cell of barium β'' -alumina.	133
Figure 7.3. Primitive cell of barium β''' -alumina.	134

Abstract

BaMgAl₁₀O₁₇ (BAM) has been widely used as the host material for Eu-active phosphors for lamps and display panels. It has a luminescent wavelength ranging from 430nm to 450nm, blue in color. However, there is a degradation problem for this phosphor material: the luminescent intensity decreases and the emission band shifts from blue toward green in color with an increase in application period and annealing procedure of manufacture. The suggestion that the luminescent degradation is related to the oxidation of europium from a 2+ to 3+ oxidation state forms the basis for the first part of this thesis. A computer simulation study of the behavior of europium in BAM (based on the classical Born model description the ionic materials) was carried out. Europium ions were found to prefer different lattice positions depending on their valence state: Eu²⁺ prefers the BR site in the mirror plane; Eu³⁺ prefers the Al(2) site in the spinel block.

Because there are many other barium hexa-aluminate phases besides BAM and because they can also be used as the phosphor host materials, the phase relationship between these phases and the properties of the Eu dopant in these phases were also investigated, in particular, for the barium-poor phase, Ba_{0.75}Al₁₁O_{17.25}. The barium-poor phase, after doping with Eu²⁺, shows a broader and shifted emission band compared to BAM. The formation of barium-poor phase has also been proposed as the reason for the observed luminescent degradation in BAM. Calculations on the barium-poor phase were performed to investigate the origin of the emission band differences between it and BAM, and the complete solid solution between them. The coexistence of multiple O_{BR}-distributions in the barium-poor phase was found to be the origin of the observed broader and shifted emission band of Eu²⁺.

Since the hypotheses about luminescent degradation involve phase changes or structural adjustments, molecular dynamics simulations of ion migration were also performed to study the defect and structural changes after the europium oxidation. It was found that Eu³⁺ ions can migrate from the mirror plane to the spinel block at relatively low temperature, and that Eu²⁺ ions have a tendency to congregate in BAM.

1. General Introduction

Barium hexa-aluminates, widely used as host materials for rare-earth elements for optical applications, have many forms with different chemistries but their structures are mainly based on that of β -alumina and are closely related to each other.¹⁻⁴ They are also candidates for gas turbine applications because of their high thermal stability. The structures of barium aluminates are actually nonstoichiometric.⁵⁻⁷ For some phases, additional elements, other than Ba, Al and O, are required in the structure or the structure will not be stable, which adds to the complexity of the material.

β -alumina has the chemical formula of $\text{NaAl}_{11}\text{O}_{17}$, and there are two formula units in a primitive cell. Its structure can be described in terms of oxygen cubic-like closely packed spinel blocks separated by sodium-oxygen planes. In barium aluminates, sodium has been substituted by barium and other structural changes have to be made to compensate for the effective charge of the substitution. The details of the possible forms of barium hexa-aluminates are discussed in Chapter 2.

Experiments to determine these structures have the shortcomings of not being able to determine the detailed local structure and local defect properties. In addition, experimental measurement is always the combination of several factors, and it is hard to differentiate between. For example, the measured unit cell size varies with the temperature, strain, external force field and experimental error. As the material structure gets more complex, there will be too many parameters of structure determination (such as partial occupation and dopant locations) for experiments to handle.

Computer simulation provides a way to overcome these problems and has been used successfully in the study of many aspects of materials science. The structure model in the simulation can be changed systematically so that the effect of any individual parameter can be studied. As computer simulation works on the mathematical description of materials, the detailed arrangement of ions around point defects and the ion distribution are readily obtained. Properties determined by long-range periodicity that are hard to measure can easily be found from super-lattice simulations. Furthermore, computer

simulation can be used to predict material properties and thus, can provide microscopic explanation of macroscopic measurements.

Optically related defect properties are the main concern of this work. When doped with Eu^{2+} ions, barium aluminates become the blue phosphors used for lamps and display panels. There are many phases of barium aluminates that are possible candidates for phosphor host-materials and they show different luminescent properties.⁴ The most widely used phase is $\text{BaMgAl}_{10}\text{O}_{17}$ (BAM). However, there is a problem with this blue phosphor: its luminescent intensity decreases in the annealing step of the manufacturing process, and there is also an emission band shift, which is believed to be the result of Eu oxidation and is thought to be defect or phase-related.⁹⁻¹¹ This problem will shorten the application period of the phosphor material and lower the energy efficiency. Because of the complexity of this structure and of many closely related phases, there is no full understanding of the degradation mechanism from the experiments at this time.

Oshio et al. have suggested that after degradation, an Eu^{3+} magnetoplumbite structure, $\text{EuMgAl}_{11}\text{O}_{19}$, will form inside the barium aluminate.¹¹ But there is another hypothesis for forming a barium-poor phase, $\text{Ba}_{0.75}\text{Al}_{11}\text{O}_{17.25}$, suggested by Yokota et al., because the emission band of the barium-poor phase doped with Eu^{2+} ions is broader than BAM:Eu^{2+} , and the band also shifts.^{10,12} $\text{EuMgAl}_{11}\text{O}_{19}$ has not been proved to exist yet, and the barium-poor phase is actually a mixture of phases as shown in the work of Park and Cormack.¹³ These two hypotheses are tested in our study.

The goal of this study was to determine the phase relationship between barium hexa-aluminates, and their possible structures. As additional types of cation are required in certain phases, their distribution in the lattice and their effect on defect properties were investigated. Understanding the behavior of europium in different phases is the main objective. The europium related defects and positions were examined and included both divalent and trivalent europium ions to address the degradation issue. From this work, we want to understand the degradation mechanism so that possible adjustments in chemistry or fabrication can be made to solve the problem of luminescent degradation.

Chapter 2 discusses the structural details of barium hexa-aluminates and their basis, β -alumina. Chapter 3 concentrates on the theory of our simulation methodology: its benefits and shortcomings.

Investigation of the structure and defect properties of BAM is discussed in Chapter 4. The potential dependence of the calculations is also discussed to show the results are independent of the potential used, so that it can be applied for further simulation. Positions of europium ions were determined and are discussed.

Chapter 5 focuses on the migration properties of ions in BAM because it shows some kind of two-dimensional ionic conduction. The effect of the structure of the fast-ionic conduction plane on the behavior of europium ion is presented. The temperature dependence of the migration of Eu ions is also described in order to get an idea of what happens at the thermal degradation temperature. The hypothetical of formation of $\text{EuMgAl}_{11}\text{O}_{19}$ is addressed.

In Chapter 6, a phase, known as the barium-poor phase which is possibly formed during degradation of the luminescence, is considered in detail. Several possible structures are calculated and compared. The intrinsic and extrinsic defects in those structures are also compared. The objective is to understand the difference in the observed emission band between BAM and the barium-poor phase.

Chapter 7 discusses the stability and defect properties of other phases closely related to BAM structure. The involvement of these phases in the degradation process is also discussed. Behavior of europium ions is compared between different phases.

These four chapters are written in a way that they can be published easily. Thus, some information is repeated. A summary and suggestions for future work are provided in the last chapter.

References

1. D. Ravichandran, S.T. Johnson, S. Erdei, R. Roy, and W.B. White, "Crystal Chemistry and Luminescence of the Eu^{2+} -Activated Alkaline Earth Aluminate Phosphors," *Displays*, **19**[4] 197-203 (1999).
2. C.R. Ronda and B.M.J. Smets, "Chemical Composition of and Eu^{2+} Luminescence in the Barium Hexa-aluminates," *J. Electrochem. Soc.*, **136**[2] 570-3 (1989).
3. A.L.N. Stevels and J.M.P.J. Verstegen, " Eu^{2+} Luminescence in Hexagonal Aluminates Containing Large Divalent or Trivalent Cations," *J. Electrochem. Soc.*, **123** 691-7 (1976).
4. B. Smets, J. Rutten, G. Hoeks, and J. Verlijsdonk, " $2\text{SrO}\cdot 3\text{Al}_2\text{O}_3\text{:Eu}^{2+}$ and $1.29(\text{Ba,Ca})\text{O}\cdot 6\text{Al}_2\text{O}_3\text{:Eu}^{2+}$," *J. Electrochem. Soc.* **136**[7] 2119-23 (1989).
5. V. Delacarte, A.K. Harari, and J. They, "Barium Hexaaluminoferrites with New Structural Features," *Mater. Res. Bull.*, **28**[5] 435-43 (1993).
6. M. Bettman and L.L. Turner, "On the Structure of $\text{Na}_2\text{O}\cdot 4\text{MgO}\cdot 15\text{Al}_2\text{O}_3$, a Variant of Beta-Alumina," *Inorg. Chem.*, **10**[7] 1442-6 (1971).
7. N. Iyi, Z. Inoue, and S. Kimura, "The Crystal Structure and Cation Distribution of Highly Nonstoichiometric Magnesium-Doped Potassium Beta-Alumina," *J. Solid State Chem.*, **61**[2] 236-44 (1986).
8. D. Ravichandran, R. Roy, W.B. White, and S. Erdei, "Synthesis and Characterization of Sol-Gel Derived Hexa-aluminate Phosphors," *J. Mater. Res.*, **12**[3] 819-24 (1997).
9. S. Tanaka, I. Ozaki, T. Kunimoto, K. Ohmi, and H. Kobayashi, "Blue Emitting $\text{CaAl}_2\text{O}_4\text{:Eu}^{2+}$ Phosphors for PDP Application," *J. Lumin.*, **87-89**[1] 1250-3 (2000).
10. K. Yokota, S.X. Zhang, K. Kimura, and A. Sakamoto, " Eu^{2+} -Activated Barium Magnesium Aluminate Phosphor for Plasma Displays - Phase Relation and Mechanism of Thermal Degradation," *J. Lumin.*, **92**[3] 223-7 (2001).
11. S. Oshio, K. Kitamura, T. Nishiura, T. Shigeta, S. Horii, and T. Matsuoka, "Analytical Research of Decrease in Luminance Following Annealing of $\text{BaMgAl}_{10}\text{O}_{17}\text{:Eu}^{2+}$ Blue Phosphor for Fluorescent Lamps and Plasma Display Panels," *Natl. Tech. Rep. (Matsushita Electr. Ind. Co.)*, **43**[2] 181-7 (1997).
12. B.M.J. Smets and J.G. Verlijsdonk, "The Luminescence Properties of Eu^{2+} and Mn^{2+} -Doped Barium Hexa-aluminates," *Mater. Res. Bull.*, **21**[11] 1305-10 (1986).

13. J.G. Park and A.N. Cormack, "Crystal/Defect Structures and Phase Stability in Ba Hexa-aluminates," *J. Solid State Chem.*, **121**[1] 278-90 (1996).

2. The Crystal Structure

2.1 Structure of β -Alumina

Beta alumina, unlike other phases of alumina (α, γ, δ), is not a pure two-elements crystal with formula of Al_2O_3 . Although, when it was first reported in 1916, β -alumina was thought to contain no other cations except aluminum. It was suggested by Bragg et al. later that the presence of sodium ion was essential for the stability of the structure.¹ They assigned the formula of $\frac{1}{2}\text{Na}_2\text{O} \cdot 11\frac{1}{2}\text{Al}_2\text{O}_3$ to the crystal but they could not devise a satisfactory structure for it. Later Beevers and Ross confirmed the existence of this phase and refined the structure to the chemical formula of $\text{Na}_2\text{O} \cdot 11\text{Al}_2\text{O}_3$.² After that refinement in 1956, Saalfeld suggested that β -alumina is not stoichiometric. Instead there tends to be excess sodium in the phase: it would be more appropriate to write the formula as $(\text{Na}_2\text{O})_{1+x} \cdot 11\text{Al}_2\text{O}_3$.

There is actually a series of sub-structures in the family of β -alumina labeled β' , β'' , β''' and so on. They can be classified into two groups -- one with a two-fold screw axis and the other with a three-fold screw axis. β - and β''' -alumina have the two-fold screw axis while β'' and β'''' have a three-fold axis. Whether or not β' -alumina is a new phase other than non-stoichiometric β -alumina remains unclear.³

As described in the work of Bragg and the work of Beevers and Ross, β -alumina is a column-like structure. It consists of blocks of cubic close-packed oxygen layers with aluminum in the tetrahedral and octahedral positions. A mirror plane that contains same number of sodium and oxygen ions separates adjacent blocks with the bridge-like Al-O-Al structure parallel to the c-axis.¹ In 1967, β -alumina was discovered to be a fast Na^+ ion conductor.⁴ Since then it has been found that the conduction occurs two-dimensionally in the reflection plane via an interstitialcy mechanism. Because of this the mirror plane is also known as the conduction plane.

Because the blocks, with the formula of $[\text{Al}_{11}\text{O}_{16}]^{1+}$, are quite similar to the structure of spinel, MgAl_2O_4 , with Mg substituted by Al, the blocks are also called spinel blocks.

There are four oxygen layers in a block with the oxygen having a cubic-like stacking order of ABCA. Because of the mirror plane between adjacent blocks, two blocks are required to generate periodicity. In a primitive cell there are two stacking orders, ABCA and ACBA along the c direction. The requirement of two spinel blocks in a primitive cell gives the structure space group of $P6_3/mmc$.

There are four crystallographically distinct aluminum ions in the spinel block: Al(1) ion is in the center of an octahedron formed with six oxygen ions not in the middle of the spinel block; Al(2) ion is in a tetrahedral site across the middle of the spinel block; Al(3) ion, also coordinated with four oxygen ions, is found at the edge of the spinel blocks; Al(4), another six coordinated site, is at the central symmetry site in the middle of the spinel blocks (Fig 1).

Sodium ions were thought to occupy two possible sets of positions in Beevers and Ross' study.² One is at $(\frac{2}{3} \frac{1}{3} \frac{1}{4})$ and the other is at $(0 \ 0 \ \frac{1}{4})$. These two positions seem similar to each other if considering their environment only in the mirror plane. Actually the environments are quite different outside the mirror plane. The first coordinating ions of the $(\frac{2}{3} \frac{1}{3} \frac{1}{4})$ site are six oxygen ions, three above and three below the mirror plane. For the $(0 \ 0 \ \frac{1}{4})$ position, there are two oxygens immediately above and below. Beevers and Ross found that having a sodium ion in the $(\frac{2}{3} \frac{1}{3} \frac{1}{4})$ position would provide a more accurate fit to the x-ray intensity, and concluded that Na^+ would stay there. So this position was named after them to be the Beevers-Ross (BR) site, and the other position was called the anti-BR site. In the notation of the $P6_3/mmc$ space group, BR sites are the 2(d) sites and anti-BR sites are the 2(b) sites. After the discovery that β -alumina is rich in sodium relative to the idealized sodium/aluminum ratio of 1:11, many efforts have been put to accommodate excess sodium into the structure.^{4,5} Peters and Bettman found another position for sodium, $(\frac{5}{6} \frac{1}{6} \frac{1}{4})$, that is referred to as the mO position because it is between two oxygen ions in the mirror plane. Actually, the sodium was not exactly located in the mO site but deviates a little away from it toward an anti-BR site namely "A

site”. Three positions have been defined but only two of them are thought to be occupied by sodium. The anti-BR sites are thought to be impossible for sodium ions. Even for the two possible sites, BR and A sites, the occupancy is not the same. Unlike the ideal structure, only about 75% of the BR sites are occupied by sodium in the material. Table II.1 and 2.2 give the crystallographic data of β -alumina based on the work of Peters et al. and the work of Edstrom et al., respectively.^{4,5}

Table II.1. Positional and Occupation Parameters for β -Alumina (I)
From the work of Peters and Bettman⁴

$$a = 5.594 \text{ \AA} \quad c = 22.53 \text{ \AA}$$

Position	Wyck off	Occupancy	X	Z
O(1)	12(k)	0.996	0.15711	0.05011
O(2)	12(k)	0.998	0.50318	0.14678
O(3)	4(f)	0.993	2/3	0.05552
O(4)	4(e)	1.014	0	0.14253
O(5)	2(c)	1.018	1/3	1/4
Al(1)	12(k)	0.989	-0.16775	0.10630
Al(2)	4(f)	1.028	1/3	0.02477
Al(3)	4(f)	1.006	1/3	0.17555
Al(4)	2(a)	1.025	0	0
Na(1)	2(d)	0.750	-0.2938	1/4
Na(2)	6(h)	0.174	-0.1269	1/4

Excess sodium in the conduction plane needs a charge compensation mechanism. This could be achieved by the occurrence of oxygen interstitials or aluminum vacancies. Actually both defects exist in the material. Roth et al., using neutron diffraction analysis, discovered that aluminum vacancy and aluminum interstitial pairs, aluminum Frenkel defects, exist in the spinel blocks.⁶ But as the aluminum vacancy and interstitial exist as pairs, they would not contribute to the charge compensation. It is the oxygen interstitial that compensates the positive charge introduced by excess sodium. The oxygen interstitials are on the mO sites and are stabilized by adjacent aluminum ions in the spinel

blocks displacing toward it from above and below. Then, a $V_{Al}-Al_i-O_i-Al_i-V_{Al}$ defect complex is formed across the mirror plane. After Reidinger published this work in 1979, the idea became widely accepted, and this kind of defect is called a Reidinger Defect.

Table II.2. Positional and Occupation Parameters for β -Alumina (II)
From the work of Edstrom, Thomas and Farrington⁵

$$a = 5.5929 \text{ \AA} \quad c = 22.526 \text{ \AA}$$

Position	Wyck off	Occupancy	x	Z
O(1)	12(k)		0.15712	0.04998
O(2)	12(k)		0.50305	0.14632
O(3)	4(f)		2/3	0.05525
O(4)	4(e)		0	0.14219
O(5)	2(c)		1/3	1/4
Al(1)	12(k)	0.963	-0.16798	0.10610
Al(2)	4(f)		1/3	0.02482
Al(3)	4(f)		1/3	0.17576
Al(4)	2(a)		0	0
Na(1)	2(d)	0.734	2/3	1/4
Na(2)	6(h)	0.162	0.89702	1/4
Al(5)	12(k)	0.037	-0.16045	0.17523
O(6)	6(h)	0.037	5/6	1/4

2.2 Beta Triple-Prime Phase

The first discovery of β''' -alumina was made by Bettman and Turner in 1970 in an attempt to grow β'' -alumina crystals.³ Its ideal chemical formula is $Na_2O \cdot 4MgO \cdot 15Al_2O_3$. Its structure is similar to that of β -alumina with the same space group of $P6_3/mmc$, except that there are six oxygen layers in a spinel block instead of four. The stacking order of oxygen layers in spinel blocks is also cubic close-packed with aluminum and magnesium in the tetrahedral and octahedral positions just like in $MgAl_2O_4$. The stacking order for

two spinel blocks in a unit cell is CAB CAB and BAC BAC, respectively, separated by the Na-O mirror plane. Table II.3 lists the positions of ions in β''' -alumina.

Table II.3. Positions of Ions in β''' -Alumina
 $a = 5.63 \text{ \AA}$ $c = 31.85 \text{ \AA}$

Position	Wyck off	X	Z
O(1)	12(k)	-1/6	0.0334
O(2)	12(k)	1/2	0.1109
O(3)	12(k)	1/6	0.1765
O(4)	4(f)	1/3	0.0334
O(5)	4(e)	0	0.1109
O(6)	4(f)	2/3	0.1765
O(7)	2(c)	1/3	1/4
Al(1)	12(k)	-1/6	0.1474
Al(2)	4(f)	2/3	0.0701
Al(3)	4(f)	1/3	0.0932
Al(4)	4(f)	1/3	0.1972
Al(5)	4(e)	0	0.0577
Al(6)	6(g)	1/2	0
Na(1)	2(b)	0	1/4
Na(2)	2(d)	2/3	1/4
Na(3)	6(h)	-1/6	1/4

Another mismatch between the β and β''' phases lies in the positions of sodium ions. It was suggested that in β''' phase all three positions, 2(b), 2(d) and 6(h) could be occupied by sodium ions, with different occupancy. Sodium most commonly occurs on the 2(b) sites. Since the two oxygen layers immediately above and below the conduction plane have changed from the A-A stacking in the β phase to B-B and C-C stacking in the β''' phase, the BR site has changed from 2(d) to 2(b) in the symmetric notation, if considering the surroundings.

2.3 Beta Double-Prime Phase

In 1968 Yamaguchi and Suzuki reported a compound namely β' -alumina which was unusually rich in sodium oxide.⁸ Because there is normally excess sodium oxide in β -alumina, whether it was a new phase or just a nonstoichiometric β alumina is doubtful. In the same paper, they also described a new crystal structure, $\text{Na}_2\text{O} \cdot 5\text{Al}_2\text{O}_3$, β'' -alumina. Later Bettman and Peters found a compound, β'' -alumina, containing MgO and analyzed the single crystal using X-ray diffraction.⁹ The ideal chemical formula of the compound was found to be $\text{Na}_2\text{O} \cdot \text{MgO} \cdot 5\text{Al}_2\text{O}_3$. It was suggested that small quantities of Mg or Li stabilize the structure because the β'' -alumina containing no MgO or Li_2O is not stable. Table II.4 shows the crystallographic information of β'' -alumina.

Table II.4. Positions of Ions in β'' -Alumina
 $a = 5.614 \text{ \AA}$ $c = 33.85 \text{ \AA}$

Position	Wyck off	X	Z
O(1)	18(h)	0.156	0.0339
O(2)	18(h)	0.1657	0.2357
O(3)	6(c)	0	0.0961
O(4)	6(c)	0	0.2955
O(5)	3(b)	0	$\frac{1}{4}$
Al(1)	18(h)	0.336	0.0708
Al(2)	6(c)*	0	0.3501
Al(3)	6(c)	0	0.4498
Al(4)	3(a)	0	0
Na(1)	6(c) ¹	$\frac{2}{3}$	$\frac{1}{4}$
Na(2)	18(h) ²	$\frac{1}{2}$	$\frac{1}{4}$

* share with Mg

1 nearly full occupancy

2 two thirds occupancy

Like the β phase, β'' -alumina consists of oxygen close-packed spinel blocks separated by sodium-oxygen planes. Instead of two spinel blocks as in the primitive cell of the β

phase, there are three spinel blocks in a primitive cell of β'' -alumina. β'' -alumina can be seen as a rhombohedral variant of β -alumina. Three spinel blocks are stacked along the three-fold screw axis. Adjacent spinel blocks are no longer mirror symmetric to each other across the sodium-oxygen plane; instead they rotate 120° to each other so the sodium-oxygen plane is no longer a mirror plane. As the screw axis is three-fold, the stacking orders of oxygen close-packed layers in the three spinel blocks are ABCA, CABC and BCAB. The space group of β'' -alumina becomes $R\bar{3}m$.

The actual spinel blocks are distorted (i.e. the oxygen layers are not strictly two-dimensional). They are affected by the distribution of magnesium ions and partial occupancy of sodium ions in the conduction plane, as in the β phase. But in a spinel block, the upper half is centrosymmetric with the lower half at the aluminum ion in the middle of the spinel block.

The conduction plane of β'' -alumina is similar to the β phase but is not exactly the same and the terms “BR, anti-BR and mO” also apply to it. However, now the coordination of BR and anti-BR sites are the same in the β'' phase because of the change in oxygen stacking order. The BR and anti-BR sites are shifted to the centers of elongated tetrahedra rather than octahedra. Sodium ions occupy two thirds of the A sites and nearly fully occupy the BR positions. Bettman and Peters have suggested that the number of sodium ions per conduction plane is less than 2 so that sodium vacancies in the conduction plane make it a fast ion conductor. There is no need for oxygen interstitials in the conduction plane because the charge compensation can be achieved by ions with valence charge less than the $3+$ of aluminum. Therefore, Reidinger defects do not exist in β'' -alumina.

Both β'' and β''' phases have 12 oxygen close-packed layers in one primitive cell but the β''' phase has only two conduction planes instead of three, so the β''' phase is more dense in the c direction than β'' -alumina. The corresponding rhombohedral structure of the β''' phase, known as the β'''' phase, was discovered by Weber and Venro in 1970. It has six oxygen close-packed layers in a spinel block as in the β''' phase and a three-fold screw axis as in β'' phase.

2.4 Barium Magnetoplumbite

Many analogous and similar structures related to β -alumina have been found and studied after the discovery of β -alumina. They are based on Ga_2O_3 or Fe_2O_3 in place of Al_2O_3 such as $\text{K}_2\text{O}\cdot 11\text{Fe}_2\text{O}_3$ and $\text{K}_2\text{O}\cdot 5\text{Fe}_2\text{O}_3$.¹¹ Later a similar compound, $\text{PbO}\cdot 6\text{Fe}_2\text{O}_3$ was determined by Adelsköld and named magnetoplumbite (MP).¹⁰ It has nearly the same structure as β -alumina, except for the mirror plane. Its mirror plane is fully packed with three oxygen ions, one aluminum and one lead ion. Oxygen positions in the mirror plane have changed from 2(c) in the β phase to 6(h) in MP. 6(h) is the mO site in β -alumina in which an oxygen ion in the mirror plane connects with three other oxygen ions in the same plane. So there are three 6(h) sites (mO sites) per mirror plane in a primitive cell, all of them are occupied in MP structure. The aluminum in the mirror plane is at the center of a trigonal bipyramid consisting of five oxygen ions. Three out of the five oxygen ions are at 6(h) sites in the mirror plane; the other two are immediately above and below the mirror plane at the edge of spinel blocks.

MP structures have also been found in the $\text{BaO}\text{-FeO}\text{-Fe}_2\text{O}_3$ ternary system. $\text{BaFe}_{12}\text{O}_{19}$ has been widely investigated to improve the magnetic properties of barium ferrite. During a study of aluminum-substituted barium ferrite, Batti et al. discovered a miscibility gap between barium ferrite and barium aluminate, which led to the reclassification of the structure of barium aluminate from MP to β -alumina. Since then a lot of effort has been put into the investigation of barium aluminates.¹²⁻¹⁶ Two structures are believed to exist in the phase diagram of barium aluminates. One is a barium-poor phase with the 'ideal' formula of $\text{Ba}_{0.75}\text{Al}_{11}\text{O}_{17.25}$ and the other is a barium rich phase that is not fully determined yet.

The barium-poor phase has the same structure as β -alumina but with 75% barium vacancies in the two BR sites in the primitive cell. There is a Reidingen defect, $\text{V}_{\text{Al}}\text{-Al}_i\text{-O}_i\text{-Al}_i\text{-V}_{\text{Al}}$, close to the vacant BR site to compensate the charge. Normally it is described in a 2×2 super-cell, a four primitive-cell superstructure. Three of the four primitive cells are the ideal β -alumina structures with barium in BR sites. One of them is a defect cell without barium ion but with two Reidingen defects. Actually, there are many possible configurations for the barium-poor phase, with different distributions of two

Reidinger defects in the super-cell. Park and Cormack have shown that although the lattice energies of these configurations vary, the differences are small.¹⁷

The barium-poor phase can be considered in this way: taking β -alumina, $\text{Na}_2\text{O}\cdot 11\text{Al}_2\text{O}_3$, as the prototype, 75% of sodium are changed to barium and the effective positive charge generated is compensated by substituting the other 25% sodium with oxygen. It is the uncertainty of the locations of barium or substituted oxygen that makes the barium-poor phase uncertain. $\text{BaMgAl}_{10}\text{O}_{17}$ (BAM) can be described in a similar way but this time all the sodium become barium and the same number of aluminum change to magnesium. When applying the same kind of change to β'' -alumina, one will get barium β'' -alumina. Structures obtained in this way are used as the starting structures for our simulations, but they are surely not in equilibrium and may be heavily strained. In this work, these derived structures will be equilibrated by METAPOCS, using lattice energy minimization technique; the unit cell strain is also minimized¹⁸. Defect calculations are performed after the lattice relaxation.

References

1. W.L. Bragg, C. Gottfried, and J. West, "The Structure of Beta Alumina," *Z. Kristallogr.*, **77**[2] 255-74 (1931).
2. C.A. Beevers and M.A.S. Ross, "The Crystal Structure of "Beta Alumina" $\text{Na}_2\text{O}\cdot 11\text{Al}_2\text{O}_3$," *Z. Kristallogr.*, **97**[1] 59-66 (1937).
3. M. Bettman and L.L. Turner, "On the Structure of $\text{Na}_2\text{O}\cdot 4\text{MgO}\cdot 15\text{Al}_2\text{O}_3$, a Variant of Beta-Alumina," *Inorg. Chem.*, **10**[7] 1442-6 (1971).
4. C.R. Peters and M. Bettman, "Refinement of the Structure of Sodium β -Alumina," *Acta Crystallogr., Sect. B: Struct. Crystallogr. Cryst. Chem.*, **B27**[9] 1826-34 (1971).
5. K. Edstrom and J.O. Thomas, "Sodium-Ion Distribution in Na^+ Beta-Alumina: Crystallographic Challenge," *Acta Crystallogr., Sect. B: Struct. Sci.*, **B47**[2] 210-6 (1991).
6. W.L. Roth, F. Reidinger, and S.L. Placa, "Studies of Stabilization of Transport Mechanisms in Beta and Beta" Alumina by Neutron Diffraction," pp. 223-41 in *Superionic Conductors*. Edited by G. D. Mahan and W. L. Roth. Plenum, New York, 1976.
7. M. Bettman and L.L. Turner, "On the Structure of $\text{Na}_2\text{O}\cdot 4\text{MgO}\cdot 15\text{Al}_2\text{O}_3$, a Variant of Beta-Alumina," *Inorg. Chem.*, **10**[7] 1442-6 (1971).
8. G. Yamaguchi and K. Suzuki, *Bull. Chem. Soc. Jap.*, **41** 93 (1968). As cited in M. Bettman and L.L. Turner, "On the Structure of $\text{Na}_2\text{O}\cdot 4\text{MgO}\cdot 15\text{Al}_2\text{O}_3$, a Variant of Beta-Alumina," *Inorg. Chem.*, **10**[7] 1442-6 (1971).
9. M. Bettman and C.R. Peters, "The Crystal Structure of $\text{Na}_2\text{O}\cdot \text{MgO}\cdot 5\text{Al}_2\text{O}_3$ with Reference to $\text{Na}_2\text{O}\cdot 5\text{Al}_2\text{O}_3$ and Other Isotypal Compounds," *J. Phys. Chem.*, **73**[6] 1774-80 (1969).
10. V. Adelskold, "X-Ray Studies on Magnetoplumbite, $\text{PbO}\cdot 6\text{Fe}_2\text{O}_3$ and Other Substances Resembling β -Alumina, $\text{Na}_2\text{O}\cdot 11\text{Al}_2\text{O}_3$," *Ark. Kemi, Mineral. Geol.*, **12A** 1-9 (1938).
11. C.J.M. Rooymans, C. Langereis, and J.A. Schulkes, " KFe_5O_8 , a New Phase in the $\text{K}_2\text{O}\text{-Fe}_2\text{O}_3$ System," *Solid State Commun.*, **4**[3] 85-7 (1965).
12. H.W. Zandbergen, F.C. Mijlhoff, D.J.W. Ijdo, and G.V. Tendeloo, "A Model for the Structure of $1.31\text{BaO}\cdot 6\text{M}_2\text{O}_3$; M = Al, Ga; An Electron Microscopy Study," *Mater. Res. Bull.*, **19**[11] 1443-50 (1984).

13. S. Kimura, E. Bannai, and I. Shindo, "Phase Relations Relevant to Hexagonal Barium Aluminates," *Mater. Res. Bull.*, **17**[2] 209-15 (1982).
14. N. Iyi, S. Takekawa, Y. Bando, and S. Kimura, "Electron Microscopic Study of Barium Hexa-aluminates," *J. Solid State Chem.*, **47**[1] 34-40 (1983).
15. F.P.F. van Berkel, H.W. Zandbergen, G.C. Verschoor, and D.J.W. Ijdo, "The Structure of Barium Aluminate, $Ba_{0.75}Al_{11}O_{17.25}$ " *Acta Crystallogr., Sect. C: Cryst. Struct. Commun.*, **C40**[7] 1124-7 (1984).
16. N. Yamamoto and M. O'Keefe, "Electron Microscopy and Diffraction of Phases in the Al_2O_3 - $BaAl_2O_4$ System," *Acta Crystallogr., Sect. B: Struct. Sci.*, **B40**[1] 21-6 (1984).
17. J.G. Park and A.N. Cormack, "Crystal/Defect Structures and Phase Stability in Ba Hexa-aluminates," *J. Solid State Chem.*, **121**[1] 278-90 (1996).
18. C.R.A. Catlow, A.N. Cormack, and F. Theobald, "Structure Prediction of Transition-Metal Oxides Using Energy-Minimization Techniques," *Acta Crystallogr., Sect. B: Struct. Sci.*, **B40**[3] 195-200 (1984).

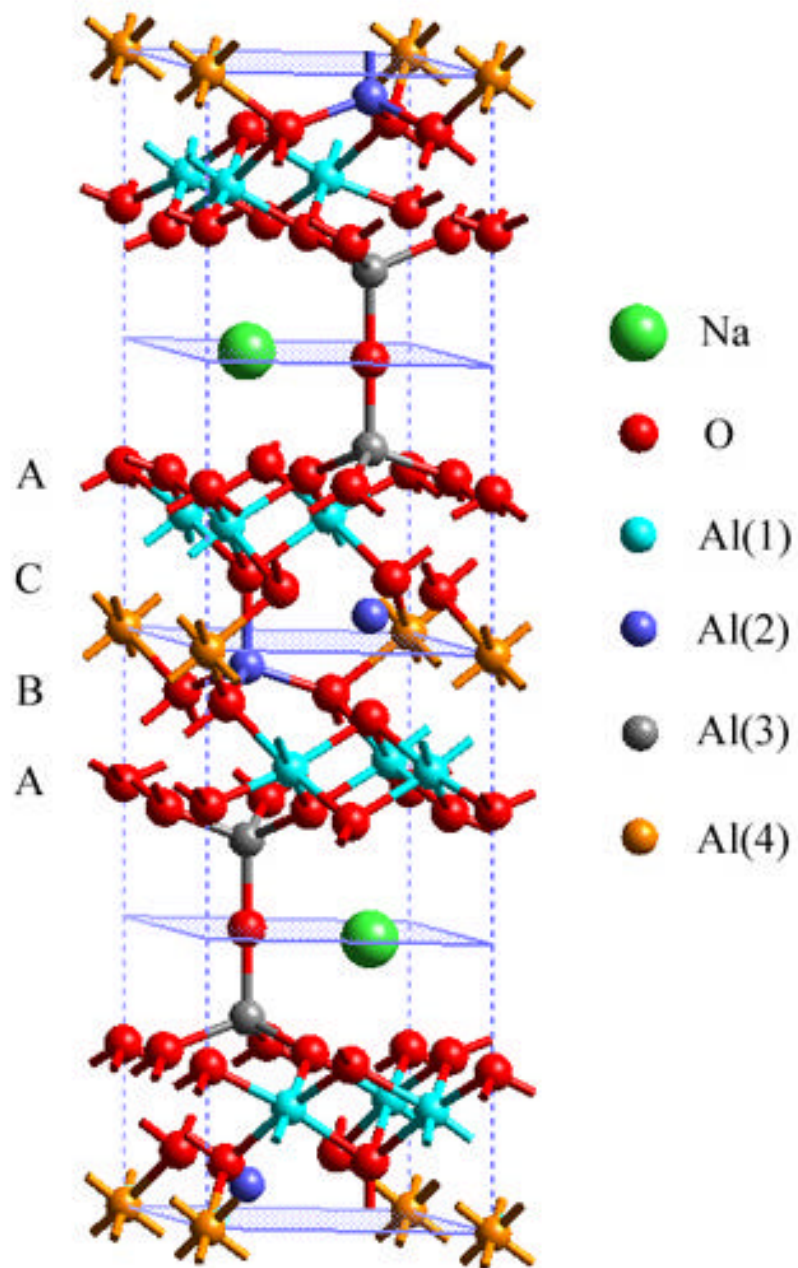


Figure 2.1. Structure of ideal β -alumina $\text{NaAl}_{11}\text{O}_{17}$.

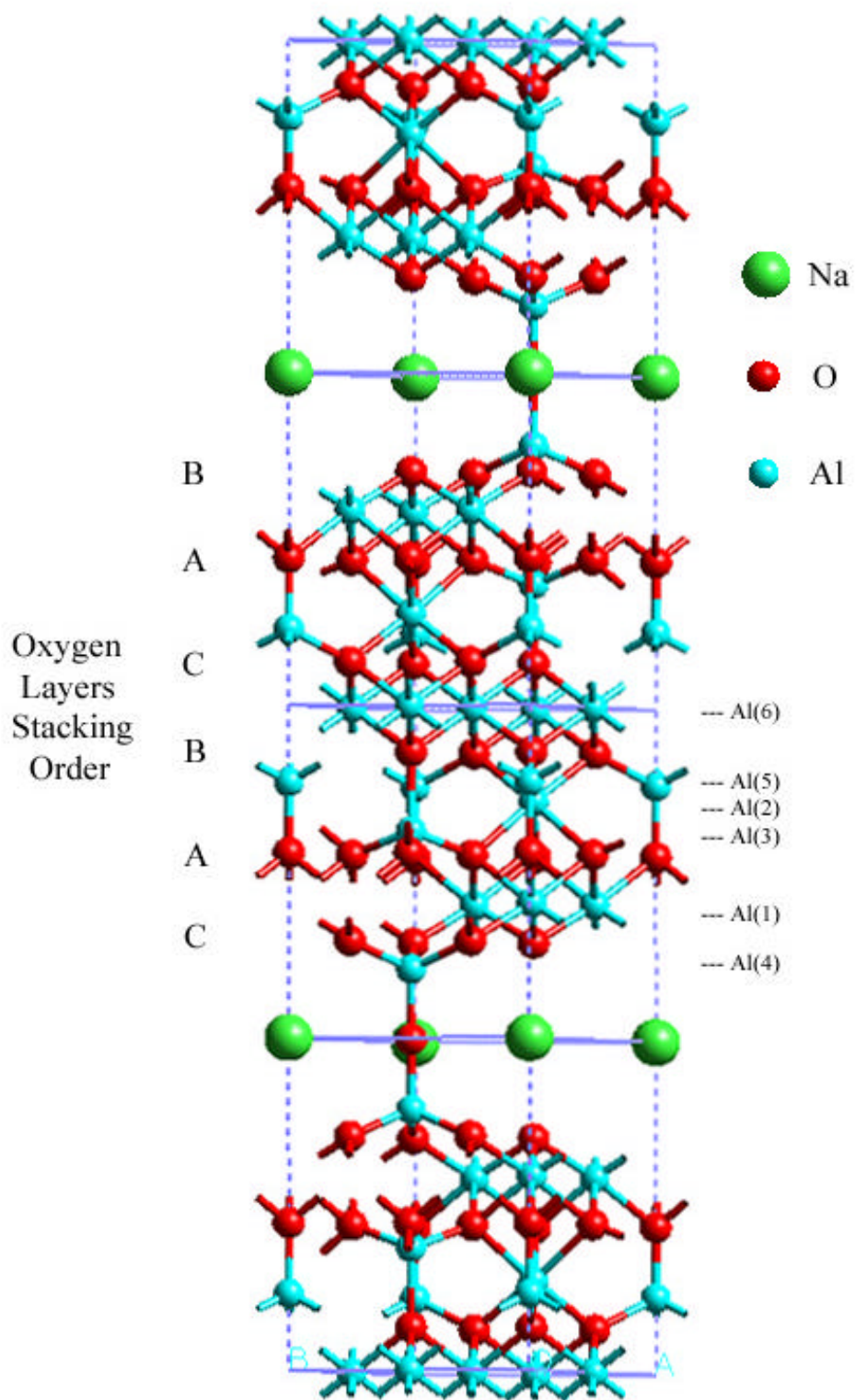


Figure 2.2. Structure of ideal β''' -alumina $\text{Na}_2\text{O}\cdot\text{MgO}\cdot 15\text{Al}_2\text{O}_3$. All Mg are shown as Al.

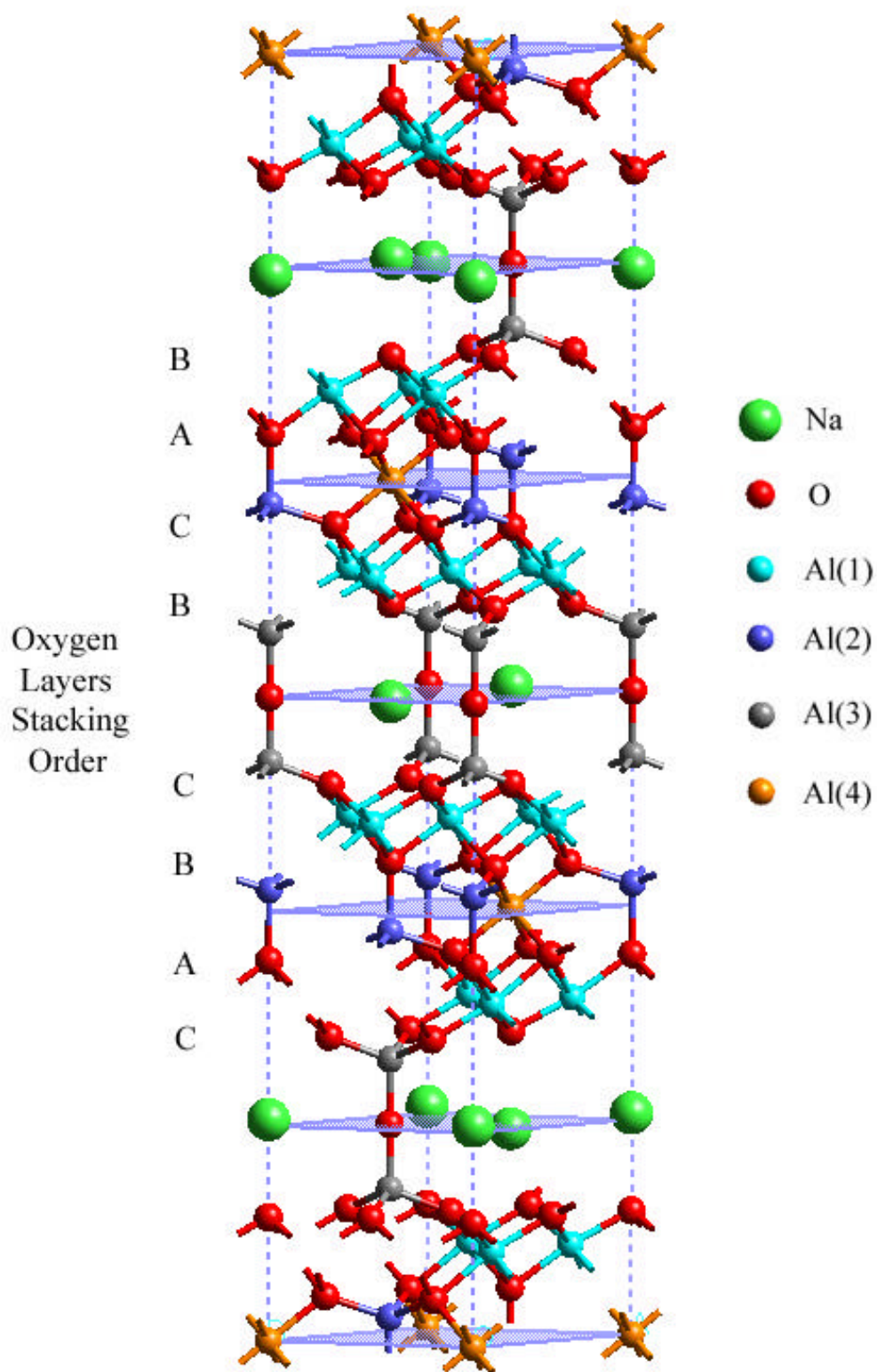


Figure 2.3. Structure of ideal β'' -alumina.

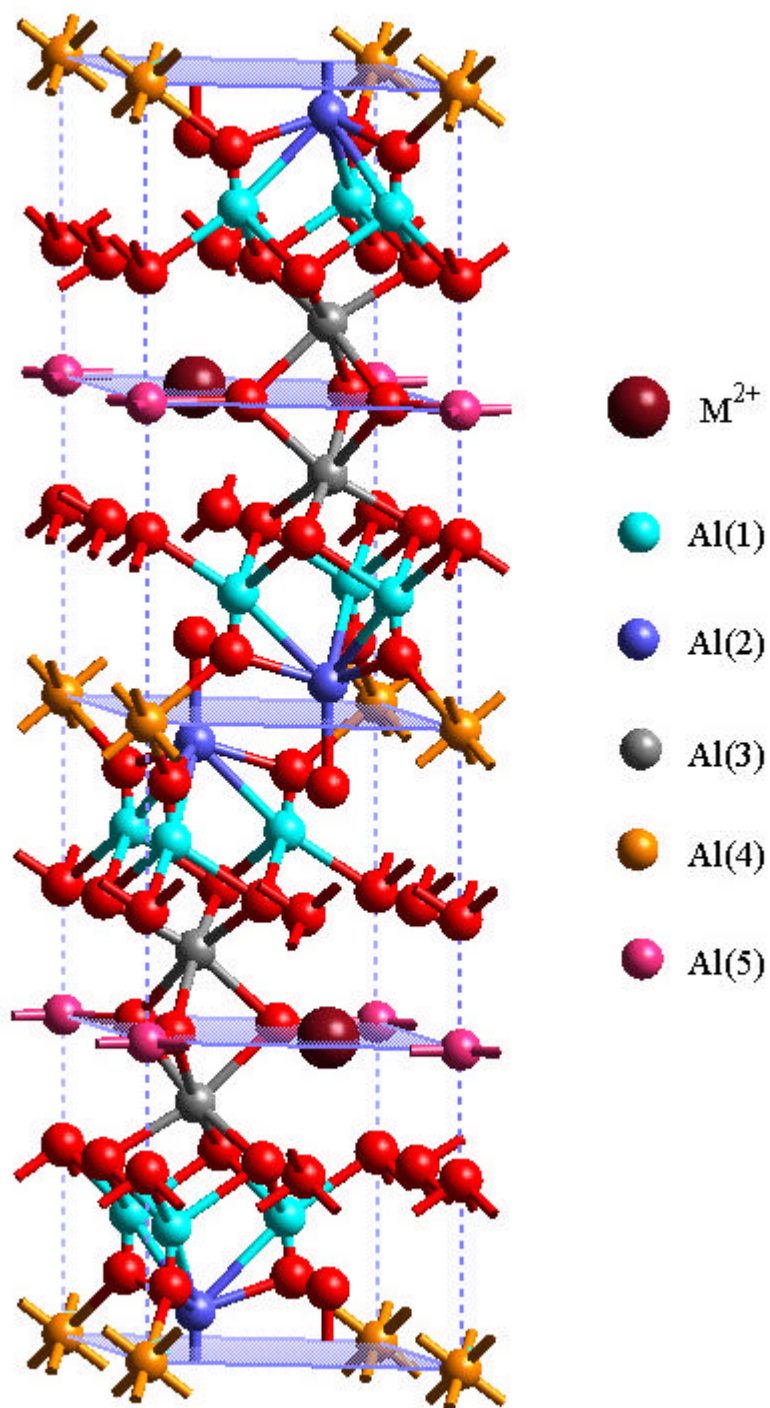


Figure 2.4. Structure of ideal manetoplumbite $MA_{12}O_{19}$.

3. Atomistic Computer Simulation Techniques

3.1 Introduction

With expansion of the region of human life, materials become more and more important to society. Ceramic materials, an important class of materials, have found applications in nearly all advanced technologies. Ceramic science was studied empirically initially. Later, as the characterization techniques, such as X-Ray diffraction and transmission electron microscopy, were developed, more and more principles and theories were suggested by experience. Now, computer simulation has assumed importance in the study of materials science.

Compared to computer simulation, traditional experimental studies have some shortcomings in studying the disorder and complex materials. First of all, a lot of parameters need to be determined for complex systems: not only the unit cell dimensions but also the coordinates of asymmetric ions. One would not be surprised to see that long periods of experiment time and intense arguments occur before general acceptance of some hypotheses. Secondly, detailed local information such as defect structure and ion distribution in non-stoichiometric phases is difficult to determine experimentally. Thirdly, the measurement of a specific property may be the combination of effects of several factors, and it may not be easy to differentiate between them. According to Moore's law, the power of computer doubles every eighteen months, which is unimaginable for experimental techniques. So, computer simulation has become more and more widely adopted in scientific research. The validity of many simulation studies has been demonstrated by later experiments.¹⁻³ Right now, computer simulation has covered many scales, electronic scale for superconductivity, atomistic scale for crystal structure and larger scale for finite element study of mechanical properties. In the present work, atomistic scale of simulation has been practiced and compared to the experiment results. This chapter briefly describes the atomistic simulation methodology.

Simulation speed is an important issue that needs to be addressed. Practically, simulation time should not last too long or the benefits of computer simulation will be lost. A compromise between the time consumed and the calculation algorithm must be made. Even today, the speed of computer does not quite match the need for many simulations such as first-principle simulations and large-size molecular dynamics simulations (more than ten thousand atoms). Many algorithms with approximations have been applied to calculations in order to shorten the simulation time, and therefore, some precision will be lost in this process. So, the properties calculated are sometimes more qualitative than quantitative.

Simulations in this study are based on inter atomic potentials (i.e. the description of interactions between particles in a numerical way). The extent to which the potential model represents the reality affects the accuracy of calculated results, and thus the potential model is the key factor in the simulation.

3.2 Inter Atomic Potentials

The materials being studied in this work are mainly ionic materials. For ionic materials, the interatomic potentials can be divided into two parts, Coulombic and non-Coulombic terms.⁴

$$V_{ij} = Z_i Z_j / r_{ij} + U_{ij}(r). \quad (1)$$

The first term in the above equation is the long-range Coulombic interaction. Normally, integer charges are assigned to each species of ion. But it is possible to assign to them an effective partial charge. It all depends on the actual determination process of the potential model. It has been found for most systems, including oxides, that integral ionic charges are adequate.^{3,5}

The second term on the right side in Eqn.1, $U_{ij}(r)$, represents both short-range (overlap of electronic clouds) and long-range (dispersion) interactions. An assumption has been made about the potential model of ionic materials that the covalent distortion of the electron cloud is so small that it can be treated as polarization perturbation. This assumption limits the potential model to ionic, or mainly ionic, materials.⁴ Then $U_{ij}(r)$ is separated into two terms, one with and one without polarization contributions.

$$V_{ij} = Z_i Z_j / r_{ij} + U_{ij}^N(r) + U_{ij}^P(r, F_i, F_j). \quad (2)$$

The polarizative contribution not only depends on the separation of ions but also on the electronic static field (F_i and F_j).

Many methods have been proposed to address the simulation of polarization in ionic materials. Among them, the core-shell model introduced by Dick and Overhauser is widely used, and it is also the mechanism used in the present work.⁶ In the core-shell model, ions are treated as atomic cores associated with a massless shell by a harmonic spring. Normally, the massless shell possesses a charge Y calculated by the ion polarizability, but the sum of charges on the core and shell must be equal to the total ionic charge. The polarization of ions is modeled by the contraction and expansion of the spring between the core and shell, with spring constant K . The polarizability of the free ion is described as

$$a = Y^2 / K. \quad (3)$$

The values; Y and K can be fitted by ab-initio (quantum mechanical) methods. Since ab-initio calculations take a very long time to run and the results are not very satisfactory, Y and K parameters are often fitted to elastic, dielectric, phonon frequencies and crystal data. It is not easy to get a single set of parameters to make calculation of all these properties agree with the observed value. Normally, the crystal data are considered the most important factor compared to other properties; the principal criterion of an adequate potential model is the extent of similarity between calculated and measured crystal structures.

A lot of forms have been suggested for the non-polarization potential term such as the 12-6 potential, Lennard-Jones potential and Buckingham potential.⁷ The model established by Fumi and Tosi, a Buckingham potential model, is used in this work; it has the following functional form:⁸

$$U_{ij}^N(r) = A_{ij} \exp(-r_{ij} / r) - C_{ij} / r^6. \quad (4)$$

Sometimes an additional term D_{ij}/r^8 is also included in the model.⁴ Like the parameters in the shell model, the parameters A , r and C are determined by least squares fitting to lattice properties. The calculated structure must be strain-free as in the real material in its thermally equilibrated state; this must be able to be achieved by a proper potential model.

Another problem may arise in fitting the potential: so many constants need to be determined at the same time that the existing lattice properties are not sufficient. For example, in the simple binary compound, three interactions exist: cation-cation, anion-anion and cation-anion. If all five constants (A , r , C , Y and K) are to be determined for each interaction, thirteen constants are necessary to be determined (there is no Y and K for cation-anion interaction). Things will become worse for more complex compounds. So additional approximations have been made to limit the number of parameters. First, as the polarisabilities of cations, especially those with charges greater than 2, are low, it is quite reasonable to assume that cations are non-polarisable. Second, because the cation-cation separations are large enough and because of the anion screening effect, the short-range interactions between cations are so small that they may be neglected. Third, it has been found that a common anion-anion interaction can be used for a series of materials such as alkaline-earth oxides.⁹ For example, the O-O potential derived from MgO can be applied to much more complex structures like MgAl₂O₄.

Because of the above assumptions, the generated potential will not be perfect, and it has limitations in application. If two ions are far away from each other, the short-range interaction becomes so small that it can be treated as zero without problem. A distance cutoff is used to define the range beyond which short-range interaction is zero. The use of a short-range potential cutoff also improves the calculation speed.

Another thing to which attention should be paid is that the potential may be coordination dependent. There is no doubt that cation-anion distances are different for different numbers of anions around the cation, so the cation radius differs in tetrahedral and octahedral sites. To take into account of the effect of coordination number, a modification of the potential model may be necessary. Cormack et al. used an approach of adjusting the pre-exponential term, A , to represent the change in radius.¹⁰

For the Huggins-Mayer relationship

$$A = b \exp(r / r) \quad (5)$$

the difference between tetrahedral and octahedral positions in radius is

$$\Delta r = r_{oct} - r_{tet} \quad (6)$$

so the pre-exponential term A of ion in tetrahedral site is given by

$$A_{tet} = A_{oct} \exp(-\Delta r / r). \quad (7)$$

This kind of potential adjustment has been applied to the aluminum-oxygen potential for the different aluminum sites in our study.

3.3 Minimization Techniques

A lattice simulation consists of two parts, calculation of the lattice energy and the minimization of the lattice energy. The perfect lattice energy calculation sums all of the interaction potentials, both Coulombic and non-Coulombic. As the long-range Coulombic potential does not converge quickly, a technique developed by Ewald is normally used, in which the point charge is replaced by an electron cloud with a Gaussian distribution and then, the whole system is translated into reciprocal space.⁷ Summation of the Fourier series in reciprocal space converges quickly, and the overlap between electron clouds is subtracted in real space, a procedure that also converges quickly.

The concept of energy minimization is simple; lattice parameters and the ion coordinates are adjusted toward the direction that will lower the lattice energy. The equilibrated structure is considered as an equilibrium state between structure and lattice energy (i.e. the equilibrated lattice structure has the lowest lattice energy compared to any other lattice structures with small perturbation to it). If the potential model precisely described the crystal, one would reach the observed structure from a closely related structure by energy minimization with the assumption that there is no other energy minimum between the starting structure and equilibrated structure. That is, the basis used to estimate structure from a similar crystal but with different chemical composition. The lattice energy minimization technique can also be used to test the credibility of a potential model by comparing the calculated structure with the observed one.

Similar to experiments, the simulation conditions also affect the minimization process. A minimum lattice energy can be achieved by adjusting the coordinates only, or by adjusting both lattice parameters and coordinates at the same time. The former condition is called Constant Volume, and the latter is called Constant Pressure. As indicated earlier, the thermally equilibrated observed structure is strain free so that the minimization process must also maintain structure in this situation. The internal strain on an ion can be calculated by the differentiation of the sum of the potential on this ion with respect to its coordinates.

Here, the lattice energy minimization discussed by Catlow and Norgett is described under the constant pressure condition. For a unit cell with N ions, the increase in the lattice energy with the displacement of one ion can be written as

$$U(r') = U(r) + g^T \cdot d + (1/2)d^T \cdot w \cdot d \quad (8)$$

where the new ion position r' is displaced from r by the strain vector d . d has $N+6$ dimensions for the whole structure: three dimensions x , y and z for each ion and 6 independent bulk strain terms for the unit cell. For ions, $d = r' - r = dr$ and $g = \nabla U / \nabla dr$, the first derivative of U with respect to displacement. For the other six bulk strains, $d = de$. e is a component of the reduced strain matrix Δe .

$$\Delta e = d \begin{vmatrix} e_1 & (1/2)e_6 & (1/2)e_5 \\ (1/2)e_6 & e_2 & (1/2)e_4 \\ (1/2)e_5 & (1/2)e_4 & e_3 \end{vmatrix} \quad (9)$$

and the related $g = \nabla U / \nabla de$. W is the second derivative of lattice energy given by the relations,

$$W = \begin{vmatrix} \frac{\partial^2 U}{\partial dr \partial dr} & \frac{\partial^2 U}{\partial dr \partial de} \\ \frac{\partial^2 U}{\partial de \partial dr} & \frac{\partial^2 U}{\partial de \partial de} \end{vmatrix} = \begin{vmatrix} W_{rr} & W_{re} \\ W_{er} & W_{ee} \end{vmatrix} \quad (10)$$

Applying the equilibrium condition

$$\nabla U / \nabla dr = 0 \quad (11)$$

to differentiate equation (8) will generate

$$0 = g + W_{rr} \cdot dr \rightarrow g = -W_{rr} \cdot dr \quad (12)$$

which determines the condition for the minimum $U(r)$. Rewriting equation (12) in order to get the function of displacement of ions,

$$dr = -W_{rr}^{-1} \cdot g. \quad (13)$$

If only one ion is allowed to move, equation (13) gives the optimum displacement of the ion. Since every ion is allowed to relax (i.e. the strain field varies after the minimization), energy minimization must be done by iteration, updating the coordinates with equation (13). In this process, the most time-consuming step is to calculate the inverse matrix of W_{rr} for each ion because it must be recalculated at each iteration.

The simulation time can be dramatically reduced if the fast matrix method used by Norgett and Fletcher is adopted.¹¹ W_{rr}^{-1} is not calculated at each iteration, instead it will be estimated from the value of last iteration. The inverse matrix at iteration $n+1$ can be estimated from the matrix at iteration n as:

$$W_{rr}^{-1}(n+1) = W_{rr}^{-1}(n) + \frac{dr \cdot dr^T}{dr^T \cdot dg} - \frac{W_{rr}^{-1}(n) \cdot dg \cdot dg^T \cdot W_{rr}^{-1}(n)}{dg^T \cdot W_{rr}^{-1}(n) \cdot dg} \quad (14)$$

where $dr = r_{n+1} - r_n$ and $dg = g_{n+1} - g_n$. In this way, not only has the time to invert the matrix been shortened but also the time spent on the calculation of the W_{rr} matrix. Its limitation is that the error in the estimation process is cumulative so that the matrix must be recalculated after every 10 to 30 iterations.

Constant Volume minimization is simpler than Constant Pressure for it does not need to consider the change of lattice parameters (i.e. d has only 3N dimension and W has only one term W_{rr}).

3.4 Defect Energy Calculations

After introducing a defect into structure, the defective lattice is relaxed to minimize the energy, to make the system stable. Thus, the defect energy calculation is also known as a lattice relaxation process. In defect energy calculations, the internal energy of the perfect lattice is set to zero. Since energy is required to move an ion from the lattice to infinity, the vacancy defect energy is always positive. The introduction of an additional ion into the crystal is not the same; normally, the interstitial defect energy is negative, but if it causes too large a stress in the lattice, it can be positive.

Since the relaxation of the structure closest to the defect is greatest and decreases with distance from the defect, Lidiard and Norgett have developed a two-region strategy.¹² As shown in Fig. 3.1, an inner region immediately surrounding the defect is simulated on the atomic scale by solving the equation (13) as in the perfect lattice simulation; and an outer region which is slightly disturbed is approximately treated as a dielectric continuum inside which ions are displaced according to the electric field of the defect. The boundary between these two regions must be addressed explicitly.

The total energy of a defect system is written as

$$E = E_I(X) + E_{II}(Y) + E_{I,II}(X, Y). \quad (15)$$

$E_I(X)$ is the energy of inner region I and X are the vectors describing ions' positions in region I. $E_{II}(Y)$ is the energy of outer region II and Y is the corresponding vector for the displacement of ions in region II which is determined by the detailed X configuration in region I. $E_{I,II}(X, Y)$ is the interaction energy between region I and region II.

The energy of region is assumed to be a quadratic function of Y ,

$$E_{II}(Y) = \frac{1}{2} Y^T \cdot A \cdot Y, \quad (16)$$

and the equilibrium condition for displacements in region II is

$$\frac{\partial E}{\partial Y} = 0 = A \cdot Y + \frac{1}{2} \frac{\partial E_{I,II}(X, Y)}{\partial Y} \Big|_{Y=Y'}. \quad (17)$$

Y' is the equilibrium value of Y corresponding to arbitrary X . The energy of region II can be rewritten as

$$E_{II}(Y) = -\frac{1}{2} \frac{\partial E_{I,II}(X, Y)}{\partial Y} \Big|_{Y=Y'} \cdot Y \quad (18)$$

and the total energy changes to

$$E = E_I(X) + E_{I,II}(X, Y) - \frac{1}{2} \frac{\partial E_{I,II}(X, Y)}{\partial Y} \Big|_{Y=Y'} \cdot Y. \quad (19)$$

X can be determined now by applying the equilibrium condition for X

$$\frac{dE}{dX} = \frac{\partial E}{\partial X} \Big|_{Y=Y'} + \frac{\partial E}{\partial Y} \Big|_{X'} \cdot \frac{\partial Y}{\partial X} = 0 \quad (20)$$

since Y is in equilibrium with respect to arbitrary X' , $\frac{\partial E}{\partial Y} = 0$, we can rewrite Eqn. (20) as

$$\frac{\partial E}{\partial X} \Big|_{Y=Y'} = \frac{\partial E_I(X)}{\partial X} + \frac{\partial E_{I,II}(X, Y)}{\partial X} \Big|_{Y=Y} - \frac{1}{2} \frac{\partial^2 E_{I,II}(X, Y)}{\partial X \partial Y} \Big|_{Y=Y'} \cdot Y = 0. \quad (21)$$

The position of the ions can be calculated from equation (21) and the lattice relaxation is solved. In order to get a self-consistent solution, equations (18) and (21) must be calculated iteratively until no further changes in X and Y are seen.

The above process is theoretically deduced from the pure energy and equilibrium condition. In order to include the potential model, the energy terms must be expanded in terms of the potential model. For a perfect lattice, the energy is summed as

$$E = \sum_{ij} U_{ij} (|R_i - R_j|) \quad (22)$$

where R is the vector position of the ion. In the same way, the defect lattice energy is written as

$$E = \sum_{ij} U_{ij} (|r_i - r_j|) \quad (23)$$

where r is the vector describing the relaxed ion's position. The defect energy is the difference between these two energies:

$$E = \sum_{ij} U_{ij} (|r_i - r_j|) - \sum_{ij} U_{ij} (|R_i - R_j|) \quad (24)$$

Considering the separation of the summation into sums within regions and sums between two regions, there are an infinite number of ions in region II so that it will take a long time for the sum to converge. Further simplification has been made. The defect energy can be rewritten in the following way:

$$\begin{aligned} E = & \sum_{ij(I)} [U_{ij} (|r_i - r_j|) - U_{ij} (|R_i - R_j|)] \\ & + \sum_{\substack{i(I) \\ j(II)}} [U_{ij} (|r_i - r_j|) - U_{ij} (|R_i - R_j|)] \\ & + \sum_{\substack{i(I) \\ j(II)}} [\partial U_{ij} (|r_i - r_j|) / \partial r_{ij} - \partial U_{ij} (|R_i - R_j|)] \cdot (r_j - R_j). \end{aligned} \quad (25)$$

here the summation in region II has been transformed into a summation between region I and region II, but there are still an infinite number of interactions. Mott and Littleton have defined two parts in the outer region to get over this problem.¹³ Part IIa has the size of at least the short-range potential cutoff outside region I. Ions in IIa interact with ions in region I with the full potential model, while region IIb only interacts with the effective defect charge in region I by Coulombic force. Hence, the energy of region IIb is

$$E_{I,II}^b(X, Y) = -Q^2 \sum_{j(IIb)} \frac{q_j M_j}{|R_j|^4} \quad (26)$$

where Q is the effective charge of region I, $q_j M_j$ and R_j are the charge, Mott-Littleton parameter and position vector, respectively, of the ion j in region IIb.

As long as the region I size is large enough so that the assumption of the two-region technique is valid, the defect energy will converge quickly to some value and not depend

on the region size any more. Normally, region I will contains more than one hundred ions. The software used in this work is METAPOCS and CASCADE:¹⁴ the former is for lattice relaxation, and the later is for defect calculation.

References

1. A.S. Nowick and B.S. Lim, "Electrical Relaxations: Simple Versus Complex Ionic Systems," *Phys. Rev.*, **B63**[18] 184115-22 (2001).
2. A.N. Cormack, C.R.A. Catlow, and A.S. Nowick, "Theoretical Studies of Off-Center Sc^{3+} Impurities in CeO_2 ," *J. Phys. Chem. Solids*, **50**[2] 177-81 (1989).
3. G.V. Lewis and C.R.A. Catlow, "Defect Studies of Doped and Undoped Barium Titanate Using Computer Simulation Techniques," *J. Phys. Chem. Solids*, **47**[1] 89-97 (1986).
4. W.C. Mackrodt, "Theory of Defect Calculations for Ionic And Semi-Ionic Materials," pp. 107-30 in NATO ASI Series: *Mass Transport in Solids*. Edited by F. Beniere and C. R. A. Catlow. Plenum Press, New York and London, 1983.
5. T.S. Bush, J.D. Gale, C.R.A. Catlow, and P.D. Battle, "Self-Consistent Interatomic Potentials for the Simulation of Binary and Ternary Oxides," *J. Mater. Chem.*, **4**[6] 831-7 (1994).
6. B.G. Dick and A.W. Overhauser, "Theory of the Dielectric Constants of Alkali Halide Crystals," *Phys. Rev.*, **112**[1] 90-103 (1958).
7. T.B. Forester and W. Smith, *DL_POLY Reference Manual*, 2.0 ed.; pp. 45-7. CCLRC, Daresbury Laboratory, Warrington, UK., 1995.
8. F.G. Fumi and M.P. Tosi, "Ionic Sizes and Born Repulsive Parameters in the NaCl-Type Alkali Halides-I," *J. Phys. Chem. Solids*, **25**[1] 31-43 (1964).
9. G.V. Lewis and C.R.A. Catlow, "Potential Models for Ionic Oxides," *J. Phys. C: Solid State Phys.*, **18**[6] 1149-61 (1985).
10. A.N. Cormack, G.V. Lewis, S.C. Parker, and C.R.A. Catlow, "On the Cation Distribution of Spinels," *J. Phys. Chem. Solids*, **49**[1] 53-7 (1988).
11. M.J. Norgett and R. Fletcher, "Fast Matrix Methods for Calculating the Relaxation about Defects in Crystals," *J. Phys. C: Solid State Phys.*, **3**[11] L190-2 (1970).
12. A.B. Lidiard and M.J. Norgett, "Point Defects in Ionic Crystals," pp. 385-412 in *Computational Solid State Physics*. Edited by F. Herman, N. W. Dalton, and T. R. Koehler. Plenum, New York, 1972.
13. N.F. Mott and M.J. Littleton, "Conduction in Polar Crystals. I. Electrolytic Conduction in Solid Salts," *Trans. Faraday Soc.*, **34**[1] 485-99 (1938).

14. C.R.A. Catlow, A.N. Cormack, and F. Theobald, "Structure Prediction of Transition-Metal Oxides using Energy-Minimization Techniques," *Acta Crystallogr., Sect. B: Struct. Sci.*, **B40**[3] 195-200 (1984).

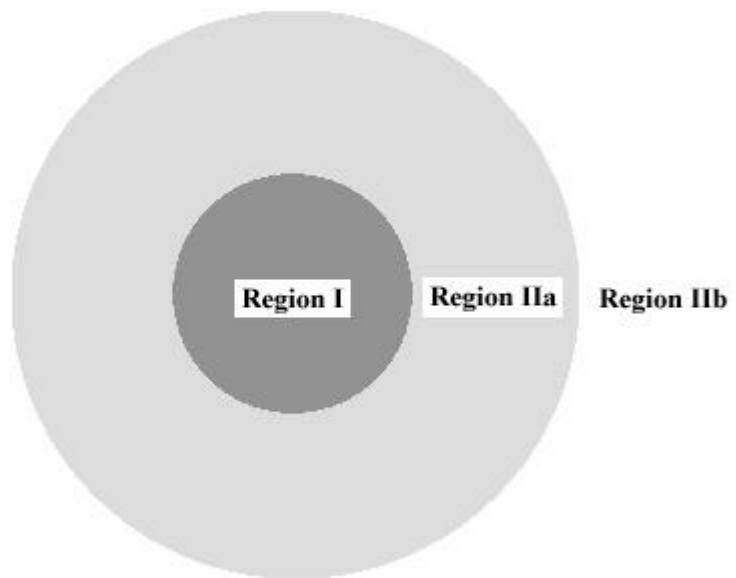


Figure 3.1. Two regions for defect energy calculation. Defect is in the center of region I.

4. Defects in BaMgAl₁₀O₁₇: Eu²⁺ Blue Phosphor

Abstract:

The luminescent properties of BaMgAl₁₀O₁₇: Eu²⁺ blue phosphor are closely related to the valence state of europium inside the crystal and its defect structure. Because of the complexity of the BAM structure, research was carried out to study the europium-related defects by computer simulation. Two lattices with different Mg distributions were found to have the same lattice energy, but the arrangement of Mg affects the defect energy and position. Eu³⁺ behavior was also discussed to address the oxidation-induced luminescent degradation. Two energetically most-favorable positions were found for europium, one is the Beavers-Ross site on the conduction plane for Eu²⁺, and the other is the Al(2) site in the middle of the spinel block for Eu³⁺. Results of defect complex and bond-valence calculations have suggested that the large europium ion can reside in the oxygen close-packed spinel blocks. A comparison of europium defect properties calculated with two different potential models suggests that results of the simulations are potential independent.

4.1 Introduction

The optical properties of phosphor materials depend not only on the active elements but also on the host materials. The active ions, typically rare-earth ions, are introduced into the host material as dopants. The local environment of the active element will change the emission spectrum of the final phosphor material. In an increasing number of cases, host compounds have somewhat complex crystal structures, which provide several possible sites for the active ion.

$\text{BaMgAl}_{10}\text{O}_{17}$ (BAM): Eu^{2+} is widely used as a blue phosphor for lamp and display panels. It is not clear where the exact positions of europium ions are in the structure, from experiment because of the complex crystal chemistry of BAM structure. Computer simulation based on the classical Born model has been found to be a successful method in the defect studies.

In this paper, various aspects of barium β -aluminates (BAM) have been investigated with the aid of computer simulation; these include the BAM structure itself, magnesium distributions and defect properties. The intrinsic defects, besides the europium extrinsic defects, have also been studied because they affect charge compensating mechanisms when europium ions are introduced into the structure. The potential dependence of the results has also been investigated.

4.1.1 Detail of Structure

The BAM structure was derived from that of β -alumina ($\text{NaAl}_{11}\text{O}_{17}$) and the β -alumina was first discovered by Rankin and Merwin.¹⁻³ Bragg, and Beevers and Ross have refined the β -alumina structure with x-ray diffraction; the atom positions are summarized in Table IV.1.^{4,5} The structure has a space group of $P6_3/mmc$ and can be described as consisting of oxygen close-packed spinel blocks of composition $[\text{Al}_{11}\text{O}_{16}]^{+1}$ separated by mirror planes of composition $[\text{NaO}]^{-1}$ (Fig. 4.1). The stacking order of oxygen close-packed layers in one spinel block is ABCA. Sodium occupies the Beevers-Ross (BR) site in the mirror plane. Aluminum ions partially occupy octahedral

and tetrahedral sites. Based on the symmetry, there are four aluminums, five oxygens and one sodium in symmetrically independent positions. In forming BAM, sodium is replaced by barium and the same number of aluminum ions is replaced by magnesium in order to keep the unit cell charge neutral. Thus the chemical formula of the spinel blocks becomes $[\text{MgAl}_{10}\text{O}_{16}]$ and the mirror plane changes to $[\text{BaO}]$; both are charge neutral. Magnesium may substitute in any of the four aluminum sites in the crystal but the structure will be more stable if the original symmetry is kept as far as possible after the substitution as shown in our simulations. Because the spinel blocks are similar to the structure of MgAl_2O_4 and Mg occupies the tetrahedral positions in spinel, the possible positions of Mg in the spinel blocks are most likely also the tetrahedral sites: Al(2) and Al(3).

Table IV.1. Crystallographic Information for the β -Alumina Structure
 $a=5.594 \text{ \AA}$ $c=22.53 \text{ \AA}$

Atom	Wyckoff position	Type of Site	x	y	z
Na(1)	2c	BR	2/3	1/3	1/4
Al(1)	12k	Octahedral	0.832	-x	0.106
Al(2)	4f	Tetrahedral	1/3	2/3	0.025
Al(3)	4f	Tetrahedral	1/3	2/3	0.176
Al(4)	2a	Octahedral	0	0	0
O(1)	12k	Tetrahedral	0.157	-x	0.05
O(2)	12k	Tetrahedral	0.503	-x	0
O(3)	4f	Tetrahedral	1/3	2/3	0.056
O(4)	4e	Tetrahedral	0	0	0.143
O(5)	2c	Tetrahedral	1/3	2/3	1/4

The simulations in this study are based on the Born model description of a solid, which treats the solid as a collection of point ions with long-range and short-range forces acting between them. This approach has enjoyed a wide range of success, but it has been found that the reliability of the simulations depends on the validity of the potential model

used in the calculations. The non-Coulombic potentials are usually described by a simple analytical Buckingham function,

$$V_{ij}(r_{ij}) = A_{ij} \exp(-r_{ij} / r_{ij}) - C_{ij} r_{ij}^{-6} \quad (1)$$

where r_{ij} is the distance between the ions i and j .

The polarizability of individual ion is included through the core-shell model originally developed by Dick and Overhauser, in which the outer valence electron cloud of the ion is simulated by a massless shell of charge Y and the nucleus and inner electrons by a core of charge X .⁶ The total charge of the ion ($X+Y$) is equal to the oxidation state of the ion. The interaction between core and shell of any ion is harmonic with a spring constant k , and is given by

$$V_i(r_i) = \frac{1}{2} k_i d_i^2 \quad (2)$$

where d_i is the relative displacement of core and shell of ion i .

For the core-shell model, the value of the free-ion electronic polarizability is given by

$$a_i = Y_i^2 / k_i. \quad (3)$$

The potential parameters (A , r , and C in Eq. (1)), the shell charges Y , and the spring constant k associated with the shell-model description of polarizability need to be determined for the interactions between each ion pair in the crystal. In the present study, they were taken from our earlier studies of hexa-aluminates following the original compilation of Lewis and Catlow⁷⁻⁹. Another set of potentials derived independently by Bush et al. was also tested.¹⁰

4.1.2 Lattice Energy Calculations

The lattice energy is the binding or cohesive energy of the perfect crystal and is usually defined as the energy that must be released to the crystal to separate its component ions into free ions at rest at infinite separation. It is calculated by the relation:

$$U = 1/2 \sum \sum V_{ij}. \quad (4)$$

The interatomic potential, V_{ij} , includes the long-range Coulombic interactions and the non-Coulombic potential described above. The lattice energy is minimized through a

second derivative Newton-like procedure, coded into METAPOCS.¹¹ Details of the procedure have been outlined by Cormack and outlined in the previous chapter.¹²

In the present work, this perfect lattice approach has been used to establish an equilibrated crystal structure for BAM using the previously published potential summarized in Table IV.2.⁷ In addition, Bush potentials, shown in Table IV.3 were used to justify whether the results are potential independent.

Table IV.2. Potential Parameters Derived by Lewis and Catlow

Interaction	A (eV)	ρ (Å)	C (eV·Å ⁶)
Al(o) – O	1474.40	0.30059	0
Al(t) – O	1334.31	0.30059	0
Ba – O	931.70	0.39490	0
Mg – O	710.50	0.32420	0
O – O	22764.2	0.14910	17.89
Eu(2+) – O	665.20	0.39490	0
Eu(3+) – O	1358.0	0.35560	0
Interaction	Shell charge	K	
Ba (core) – Ba (shell)	1.46	14.78	
O(core) – O(shell)	-2.207	27.29	

Table IV.3. Potential Models Derived by Bush et al.

Interaction	A (eV)	ρ (Å)	C (eV·Å ⁶)
Al – O	2409.505	0.2649	0
Ba – O	4818.416	0.3067	0
Mg – O	2457.243	0.2610	0
O – O	25.41	0.6937	32.32
Eu(2+) – O	6212.907	0.27948	0
Eu(3+) – O	847.868	0.3791	0
Interaction	Shell charge	Spring constant	
Al(core) – Al(shell)	2.957	403.98	
Ba(core) – Ba(shell)	1.831	34.05	
O(core) – O(shell)	-2.513	20.53	
Eu(3+ core) – Eu(3+ shell)	3.991	304.92	

4.1.3 Defect Energy Calculations

Calculations of defect structure and energy introduce one vital feature in addition to those for the perfect lattice methods. That is, the occurrence of relaxation of lattice atoms around the defect species. The effect is large because the defect generally provides an extensive perturbation of the surrounding lattice, and, in the case of ionic crystals, the relaxation field is long-range as the perturbation provided by the defect is mainly Coulombic in origin.

The defect calculation is based on the Mott-Littleton theory, which allows one to calculate the defect-induced static polarization of a dielectric continuum.¹³ The basic approach is to contain, within the dielectric continuum, a region, immediately surrounding the defect, which is treated atomistically within the framework of the Born model described above. In this region, the forces and resulting atom displacements are too large to be treated properly using continuum theory, which can, nevertheless, be used to model the more distant parts of the crystal. This two-region approach is coded in CASCADE that was the program used in this work.

4.2 Results

4.2.1 Structures of BAM

Using β -alumina as a prototype, the BAM structure was obtained by substituting all Na with Ba and two Al with Mg in a primitive cell; the structure was then put into METAPOCS to relax it to a minimum energy configuration. Mg ions were put in Al(2) or Al(3) positions (four Al(2) positions are labeled as a-d and four Al(3) positions are labeled as a'-d' along c axis in Fig. 4.2). It was determined that the lattice energy of the unit cell with all Mg in Al(2) site was lower than for the other Mg distributions (Table IV.4). Furthermore, there are three possible ways to put two magnesium ions in four Al(2) sites.

After checking all the possibilities, in which magnesium ions are in ab, ac and bc sites respectively, we have found two types of Mg distribution having nearly the same lattice energy (a 0.06eV difference). This suggests that there will be a variety of Mg distributions in BAM crystals, since apart from the preference for the Al(2) site there is no driving force for Mg ordering in the equivalent sites. We have defined these two

possible structures of BAM as configuration I and II. Configuration I has Mg in a and c sites, and configuration II has Mg in a and b sites (Fig. 4.2). In configuration II, the two mirror planes in the unit cell are now different from each other because of the Mg distribution and then the defect properties may vary in different regions. In configuration II, all Mg are located in the lower half of the unit cell (IIM) and no Mg is in the upper half (IIA). Actually, configuration I has lost the mirror symmetry but kept the 2-fold screw axis, whereas configuration II has kept the mirror symmetry but lost the 2-fold screw axis. For convenience, the phrase “mirror plane” is generally used to refer to the barium-oxygen plane in both configurations.

Table IV.4. Lattice Energies of Mg Distributions in Al(2) and Al(3) Sites

Configuration with Al(2) and Al(3) mix	aa'	ab'	ac'	ad'
Lattice Energy (eV)	-1733.27	-1734.91	-1735.09	-1733.60
Configuration with only Al(2)	ab	ac	bc	
Lattice Energy (eV)	-1736	-1736.06	-1733.83	
Configuration with only Al(3)	a'b'	a'c'	b'c'	
Lattice Energy (eV)	-1733.32	-1734.42	-1733.71	

The calculated crystal structure parameters for BAM (configuration I) are given in Table IV.5, in which they are compared with the experimental data of Iyi et al.² Because the structure has been changed after the substitution of Mg, the coordinates are averaged for each symmetrically independent position. In addition, the Mg in the spinel block was introduced as a defect, and the lattice must relax in some way to allocate the defect. This relaxation changes the size and shape of the spinel block slightly; that is the reason for the fact that Ba and O(5) ions did not remain exactly on the mirror plane ($z=0.25, 0.75$). Having magnesium and barium in the structure has expanded the unit cell and the cell parameters become $a=5.72 \text{ \AA}$ and $c=22.65 \text{ \AA}$. Although the calculated structure is slightly different from the β -alumina structure, the agreement between our modeled structure and

the experiment data of BAM is very good, as can be seen from the Δx and Δz columns in Table IV.5, which represents the difference between calculation and experiment.

Table IV.5. Comparison of Measured and Calculated Structures

Atom type	$X_{\text{obs.}}$	$X_{\text{calc.}}$	ΔX	$Z_{\text{obs.}}$	$Z_{\text{calc.}}$	ΔZ
Ba	0.6678	0.6667	0.0011	0.2500	0.24662	0.00338
Al(1)	0.8343	0.8338	0.0005	0.10544	0.10268	0.00276
Al(2)	0.3333	0.3333	0	0.02400	0.01848	0.00552
Al(3)	0.3333	0.3333	0	0.17416	0.17052	0.00364
Al(4)	0.0000	0.0000	0	0.00000	0.00000	0
O(1)	0.1534	0.1488	0.0046	0.05152	0.05130	0.00022
O(2)	0.5042	0.5040	0.0002	0.14799	0.14333	0.00466
O(3)	0.6667	0.6667	0	0.05901	0.05409	0.00492
O(4)	0.0000	0.0000	0	0.14437	0.139590	0.00478
O(5)	0.3333	0.3333	0	0.25000	0.24789	0.00211

Because of the good agreement between calculated and measured structural data, the potential was ready for further defect simulations. Although the Mg distribution does not affect the lattice energies significantly for configurations I and II, they may be expected to have a significant effect on the energies of point defects.

4.2.2 Intrinsic Disorder

Point defect energies of all ion species in the two configurations and the two regions of configuration II have been calculated with CASCADE and are compared in Table IV.6. These are energies associated with bringing the defects into the crystal from infinity. No ionization processes have been included. As the introduction of Mg into the structure has changed the symmetry, defect energies in BAM are not necessarily the same for the originally symmetry-similar positions of β -alumina. It is appropriate to calculate defects on all possible lattice sites as well as sites that are normally symmetrically equivalent. For example, all aluminum vacancies of Al(2) in β -alumina should have the same defect energy. But in BAM, the aluminum ions in the Al(2) position have different

environments compared to each other; i.e. one Al(2) would have a magnesium close to it but the other has magnesium further away. Although their environments, or site symmetries, are different, they are still described as being in the Al(2) position, as classified in β -alumina, to keep the problem simple. Thus all aluminums in the Al(2) sites must be calculated individually. When looking at the Table IV.6, it must be kept in mind that the defect energy listed was the lowest one for that class of positions.

Table IV.6. Calculated Point Defect Energies (eV)

Defect	Config. I	Config IIM	Config. IIA
V_{Ba}^{\bullet}	17.01	17.70	16.16
V_{Mg}^{\bullet}	29.30	29.39	29.39
$V_{Al(1)}^{\bullet\bullet}$	58.34	58.66	56.78
$V_{Al(2)}^{\bullet\bullet}$	58.52	-	58.31
$V_{Al(3)}^{\bullet\bullet}$	59.39	59.78	58.92
$V_{Al(4)}^{\bullet\bullet}$	57.08	57.07	57.07
$V_{O(1)}^{\bullet\bullet}$	23.31	23.18	24.90
$V_{O(2)}^{\bullet\bullet}$	24.92	24.62	26.00
$V_{O(3)}^{\bullet\bullet}$	25.44	25.47	25.62
$V_{O(4)}^{\bullet\bullet}$	23.33	23.13	25.79
$V_{O(5)}^{\bullet\bullet}$	25.16	24.02	26.23
$Ba_i^{\bullet\bullet}$	-11.21	-12.19	-10.25
$Mg_i^{\bullet\bullet}$	-18.22	-18.91	-16.94
$Al_i^{\bullet\bullet}$	-42.51	-42.86	-42.57
O_i^{\bullet}	-14.76	-15.52	-15.24

When considering the interstitial defect, one will wonder where are the possible interstitial positions for ions. Since the mirror plane region is quite open in β -alumina and symmetry has been impaired, it is not so straightforward to select all the possible positions beside the special sites such as unoccupied octahedral sites and the anti-BR site. In order to consider all of the possibilities, a computer program was designed to find the possible positions automatically. The basic idea of the program is that as long as the site is large enough (i.e. the distance from this site to its nearest ion is larger than a prescribed threshold), it can be a candidate to hold an interstitial ion. The smaller is the size of the

interstitial position is, the bigger the relaxation is needed to accommodate the interstitial ion, and the higher the defect energy may be, and the more sites are selected. No distance between two interstitial positions is shorter than the threshold to limit the number of selected sites. Another criterion is that no two sites have the same environment surrounding them. Even though many limitations have been applied to the structure, the program still generated around 200 candidates. The lower the symmetry is, the more candidates are generated. All of the generated interstitial sites have been tested for each ion species and the position with the lowest point defect energy has been considered as the interstitial position for that ion species. However, that does not mean interstitials only occur at that position; it merely means that the probability of finding an interstitial of that ion at that position is the greatest.

In configuration I, the aluminum vacancy seems most likely to occur at Al(4) in the middle of spinel block, but it was the Al(1) site that became vacant in configuration II. Other vacancy positions were the same for the two Mg distributions.

The barium interstitial prefers to occupy the anti-BR site in the mirror plane and was the same for both configurations. Since the divalent barium ion is quite large relative to other ions (its radius is 1.5 Å, which is nearly double the size of an aluminum ion), it is not surprising that barium can not reside inside the spinel block since it is oxygen close-packed. Magnesium was also found to occupy the anti-BR site, but with a little deviation toward a nearby O(5) ion. Aluminum behaves differently from other cations because its size is so small that it can enter into the spinel block. Aluminum ion prefers to take the octahedral sites across the middle of the spinel block. Since there are three cation layers in the middle of a spinel block, Mg-Al(4)-Al(2), two oxygen layers at the edge of this region have been separated further away from each other, and they are no longer strictly close-packed. The octahedron formed by these two oxygen layers has become distorted and longer in the *c* direction. The aluminum interstitial was not found in the center of the octahedron but closer to the Al(2) layer, because of the relaxation around magnesium ion. The fact that aluminum interstitial ions are inside the spinel blocks is consistent with the observation of neutron diffraction by Roth et al.¹⁴ Oxygen interstitials in configuration I sit in the Al(1) layer and close to the unoccupied octahedral site; this is different from the observation in β -alumina.¹⁵

For oxygen in β -alumina, the favorite interstitial position is the mO site in the conduction plane, between two adjacent O(5) ions. After relaxation, two Al(1) ions above and below the mO site move automatically toward the conduction plane to stabilize the interstitial ion. This creates a $V_{Al}-Al_i-O_i-Al_i-V_{Al}$ defect cluster, called a Reidinger defect, across the mirror plane (see Fig. 4.4a). The interstitial oxygen stayed strictly on the mirror plane. After its migration, the coordination number of the aluminum in the Reidinger defect changes from six to four. However, for configuration I of BAM, only one aluminum ion moved toward the O_i , forming a $V_{Al}-Al_i-O_i$ defect cluster (Fig. 4.4c) if the oxygen interstitial ion was put into the mO position. In this case the interstitial oxygen no longer stayed on the mO site but relaxed away from the nearby barium and the mirror plane. The reason is because the size of barium is larger than sodium so that the oxygen interstitial is pushed away and the two corner-shared tetrahedra of the Reidinger defect become bent and stretched. Then, the Reidinger defect was no longer stable, and it broke. However oxygen can still be stabilized by a single aluminum ion moving toward it. Therefore, the defect energy for the oxygen interstitial in the mirror plane is no longer the lowest one, even if we forced the structure to form a Reidinger defect before the defect relaxation.

Another kind of defect cluster of oxygen interstitials has been found in configuration II. The oxygen interstitial ion tends to stay between the barium and a nearby O(5) ion that normally associates with two Al(3) ions to form a bridge perpendicular to the mirror plane; we define this position as the mOB site. The O(5) ion shared the aluminum ions with the interstitial oxygen and formed a two-bridge configuration. The Al(3)-O(5)-Al(3)- O_i defect cluster forms a parallelogram (see Fig. 4.4b). It should be mentioned that this parallelogram is mirror symmetric across the conduction plane. That is the reason why this defect has the lowest defect energy for it keeps the symmetry of the configuration II structure. While testing this two-bridge configuration in configuration I, the defect energy was -14.23eV , a little higher than the lowest one found earlier. It is not surprising to see this because the structure of configuration I has no mirror symmetry so the two-bridge defect-cluster with mirror symmetry has no benefit over other defects.

The chemical formula of region IIM is $[\text{BaMg}_2\text{Al}_9\text{O}_{17}]^{-1}$ while the formula of region IIA is $[\text{BaAl}_{11}\text{O}_{17}]^{+1}$. It is reasonable to say that a net-positive-charged point defect should prefer the IIM region and vice versa; this proves to be true in the calculation.

Energies of Schottky and Frenkel defects have been calculated from the point defect energies.¹⁶ These intrinsic defect energies have been normalized (per defect) for comparison. A Frenkel defect consists of one vacancy and one interstitial point defect while the Schottky defect consists of a formula unit of vacancies. The intrinsic defect energies are actually defect formation enthalpies.

Frenkel defect energy calculation involve

$$A_A \rightarrow A_i + V_A$$

$$\Delta E_{FA} = E_{Ai} + E_{VA} .$$

Schottky defect energy calculation involve

$$\text{null} \rightarrow \text{BaMgAl}_{10}\text{O}_{17} + V_{Ba}'' + V_{Mg}'' + 10V_{Al}''' + 17V_O^{\bullet\bullet}$$

$$\Delta E_S = E_{VBa} + E_{VMg} + 10E_{VAl} + 17E_{VO} + E_{latt} .$$

In order to compare different defects, the intrinsic defect energy was calculated per single point defect. Table IV.7 lists the final comparable defect energies. The barium Frenkel defect has the lowest defect energy, and therefore, it will be predominant in thermally generated defects. The energetically favorable barium interstitial position is the anti-BR site on the mirror plane. In addition, point defects will be created for charge compensation after the introduction of europium or other optically active ions.

Table IV.7. Calculated Intrinsic Defect Energies (eV)

Disorder	Config. I	Config. IIM	Config. IIA	Lowest
Schottky	5.01	4.93	5.82	4.93
Frenkel: O	4.28	3.81	4.83	3.81
Frenkel: Ba	2.90	2.76	2.96	2.76
Frenkel: Mg	5.54	5.24	6.23	5.24
Frenkel: Al	7.29	7.11	7.11	7.11

4.2.3 Europium Incorporation

It is important to determine the sites of europium ion to understand the luminescent behavior of BAM phosphor. There are many processes available for Eu to enter into the structure, and the way to distinguish between them lies in the heat of solution; the incorporation process with the lowest heat of solution will be the one that dominates. The Eu ion may substitute for cations or enter into interstitial sites. First, the sites with lowest defect energy were found (see Table IV.8) while allocating Eu to where it could possibly reside. The second step was to write down the solution reaction.

Table IV.8. Europium Point Defect Energies (eV)

Defect	Config. I	Config. II
Eu_{Ba}	-1.34	-1.47
Eu_{Mg}	10.59	10.59
Eu'_{Al}	38.47	38.34
$Eu_i^{\bullet\bullet}$	-12.88	-14.00
Eu_{Ba}^{\bullet}	-21.67	-22.22
Eu_{Mg}^{\bullet}	-13.23	-13.29
Eu_{Al}	14.44	14.37
$Eu_i^{\bullet\bullet\bullet}$	-31.56	-33.32

The defect energies in Table IV.8 are the lowest one for each kind of defect. For example, Eu^{2+} ions can substitute for four different Al ions in different symmetry locations. There is no doubt that we will get four different defect energies. Here the defect energy of Eu_{Al}' corresponds to the one of Eu^{2+} ions substituting for the Al(2) ion since it has the lowest point defect energy. There was no difference in the positions of the europium defect for the two structural configurations. Interstitial ions were located on the anti-BR site. The Al(2) ion was easy to be substituted by the europium ions. Since there is only one kind of position each for Ba and Mg, there is no ambiguity in the europium substitution of them.

The absolute value of the point defect energy is itself meaningless except for the comparison between the same kind of defects (such as interstitials). There is no way to tell which kind of defect will occur more easily than the others from the point defect energy alone unless they are put into a defect reaction and reaction enthalpies are calculated. The quasi-defect reactions, along with the corresponding reaction energies, or heats of solution, are shown in Table IV.9 and 4.10.

Table IV.9. Eu^{2+} Ion Incorporation into BAM

Defect Reaction	Enthalpy (eV)	
	Conf. I	Conf. II
$\text{EuO} \rightarrow \text{Eu}_i^{\bullet\bullet} + \text{O}_i''$	5.56	3.68
$\text{EuO} \rightarrow \text{Eu}'_{\text{Al}} + \text{Al}_i^{\bullet\bullet\bullet} + \text{O}_i''$	14.4	13.16
$\text{EuO} \rightarrow 1/2\text{Al}_2\text{O}_3 + \text{Eu}'_{\text{Al}} + 1/2\text{V}_\text{O}^{\bullet\bullet}$	3.94	3.72
$\text{EuO} \rightarrow \text{Eu}_{\text{Mg}} + \text{Mg}_i^{\bullet\bullet} + \text{O}_i''$	10.81	9.36
$\text{EuO} \rightarrow \text{MgO} + \text{Eu}_{\text{Mg}}$	3.35	2.35
$\text{EuO} \rightarrow \text{BaO} + \text{Eu}_{\text{Ba}}$	0.55	0.42
$\text{EuO} \rightarrow \text{Eu}_i^{\bullet\bullet} + \text{V}_{\text{Ba}}'' + \text{BaO}$	6.02	4.05

It has been shown that the barium Beavers-Ross site is the most energetically favorable site for Eu^{2+} ion. This is most likely because mirror plane is more open than inside the spinel block and the doping process requires only a straight swap of barium for europium. The other possible mechanisms require a compensating defect, which will raise the overall energy of the defect reaction. Note that for interstitial Eu^{2+} , a barium vacancy could be an alternative compensating defect. If Eu_i and V_{Ba} are close to each other, the Eu_i will relax into the adjacent vacancy, which gives a simple swap process. Otherwise, the overall energy is somewhat higher.

Table IV.10. Eu^{3+} Ion Incorporation into BAM

Defect Reaction	Enthalpy (eV)	
	Conf. I	Conf. II
$1/2\text{Eu}_2\text{O}_3 \rightarrow \text{Eu}_i^{\bullet\bullet\bullet} + 3/2\text{O}_i''$	11.74	8.84
$1/2\text{Eu}_2\text{O}_3 \rightarrow \text{Eu}_{\text{Al}} + \text{Al}_i^{\bullet\bullet\bullet} + 3/2\text{O}_i''$	15.23	13.66
$1/2\text{Eu}_2\text{O}_3 \rightarrow \text{Eu}_{\text{Al}} + 1/2\text{Al}_2\text{O}_3$	0.49	0.42
$1/2\text{Eu}_2\text{O}_3 \rightarrow \text{Eu}_{\text{Mg}}^\bullet + \text{MgO} + 1/2\text{O}_i''$	4.39	3.95
$1/2\text{Eu}_2\text{O}_3 \rightarrow \text{Eu}_{\text{Ba}}^\bullet + \text{BaO} + 1/2\text{O}_i''$	5.08	4.15

Lattice Energy (eV): $E_{\text{BaO}} = -31.31$ $E_{\text{MgO}} = -40.99$ $E_{\text{EuO}} = -33.2$

$E_{\text{Al}_2\text{O}_3} = -158.78$ $E_{\text{Eu}_2\text{O}_3} = -130.88$

Oxidation, a detrimental process for BAM phosphors, changes the valence of europium from 2 to 3. It is important to understand whether (or to what extent) the behavior of trivalent europium differs from divalent Eu. In a similar way, we can write incorporation reactions for Eu^{3+} as shown in Table IV.10.

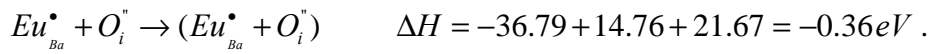
The important thing that should be mentioned is that the trivalent europium ion no longer prefers to substitute for the barium ion, as the divalent europium ion did. Instead we found that it would prefer to substitute for an aluminum ion in the Al(2) position, that is, a tetrahedral site. This raises a problem: Is it possible for the large Eu^{3+} ion to sit between close-packed oxygen layers? As can be seen in Table IV.10, the substitution of barium by Eu^{3+} ions needs half the amount of oxygen interstitials to compensate the charge generated. What would happen if the europium and oxygen ions associated with each other? Would the association of O ions stabilize the Eu^{3+} ions at BR site? Further simulations have been done to investigate this kind of interaction between point defects.

4.3 Defect Complexes

When two defects are close to each other, they interact and may decrease or increase the total defect energy. There is a limit of defect separation in a defect complex, beyond which there is no discernable interaction. Actually, the closer the defects are, the bigger is the interaction. We were interested in defect complexes in the mirror plane containing

europium ions. It has been shown above that the divalent europium ion stayed in the mirror plane and trivalent ion stayed close to the middle of spinel block. In the mirror plane, two positions were available for europium ions: Beevers-Ross and anti-Beevers-Ross sites. Also, two positions have been found for oxygen interstitial ions: mO and mOB sites. Defect complexes with two point defects were calculated first (Table IV.11). The two point defects were placed as close as possible to get the maximum interaction.

The formation of defect complex did lower the defect energy. For example in configuration I,



The Eu^{3+} and O interstitials came close to each other and that lowered the defect energy by 0.36eV. If the decrease in the defect energy is large enough, it may be possible for Eu^{3+} ions to stay in the mirror plane.

Table IV.11. Defect Complexes Containing Eu^{3+} and O^{2-}

Oxygen position	Europium position	Config. I (eV)	Config. II (eV)
mO	BR	-36.79	-
mO	Anti-BR	-50.38	-50.25
mOB	BR	-39.06	-39.47
mOB	Anti-BR	-51.96	-52.92

Defect complexes with three point defects have also been considered. BR and anti-BR sites were occupied by europium at the same time while oxygen interstitials were put into mO or mOB sites. The association of divalent and trivalent europium ions was also calculated in Table IV.12.

The more complicated defect complexes were energetically unfavorable because they generated big dipole moments in a small region that resulted in a large stress of their surroundings. For example, a $O_i^{\bullet}(\text{mOB}) - Eu_{Ba}^{\bullet} - Eu_i^{\bullet\bullet\bullet} - O_i^{\bullet}(\text{mOB})$ had a defect energy of -90.82eV that was bigger than -91.02eV, the sum of energies of two separated defect complexes, $O_i^{\bullet}(\text{mOB}) - Eu_{Ba}^{\bullet}$ and $Eu_i^{\bullet\bullet\bullet} - O_i^{\bullet}(\text{mOB})$. And, the association between

defects in a big defect complex would become weaker because of the larger separation of point defects from one end to the other.

Table IV.12. Defect Complexes with Three Point Defects

Defect complex	Config. I (eV)	Config. II (eV)
$Eu_{Ba}^{\bullet} - O_i'' (\text{mO}) - Eu_i^{\bullet\bullet\bullet}$	-73.83	-75.03
$O_i'' (\text{mOB}) - Eu_{Ba}^{\bullet} - Eu_i^{\bullet\bullet\bullet}$	-70.54	-71.92
$Eu_{Ba}^{\bullet} - Eu_i^{\bullet\bullet\bullet} - O_i'' (\text{mOB})$	-73.12	-74.47
$Eu_{Ba} - O_i'' (\text{mO}) - Eu_i^{\bullet\bullet\bullet}$	-52.23	-52.28
$O_i (\text{mOB}) - Eu_{Ba} - Eu_i^{\bullet\bullet\bullet}$	-49.00	-50.00
$Eu_{Ba} - Eu_i^{\bullet\bullet\bullet} - O_i'' (\text{mOB})$	-53.44	-54.39
$Eu_{Ba}^{\bullet} - O_i'' (\text{mO}) - Eu_i^{\bullet\bullet}$	-53.12	-52.93
$O_i'' (\text{mOB}) - Eu_{Ba}^{\bullet} - Eu_i^{\bullet\bullet}$	-51.76	-52.52
$Eu_{Ba}^{\bullet} - Eu_i^{\bullet\bullet} - O_i'' (\text{mOB})$	-52.07	-52.82

Based on the defect reaction enthalpies in Table IV.13, defect complexes can not limit the trivalent europium ion to the mirror plane for either structural configuration. Although forming defect complexes sometimes lowers the reaction enthalpy, the decrease is not big enough: the enthalpy of forming the defect complex is still much larger than for europium substituting for Al(2). Thus, the defect complex can not prevent the trivalent europium ion from entering into the tetrahedral Al(2) sites in the spinel block.

Table IV.13. Defect Reaction of Defect Complex

Defect reaction	Enthalpy (eV)	
	Config. I	Config. II
$1/2Eu_2O_3 \rightarrow (Eu_i^{\bullet\bullet\bullet} + O_i'')_{com} + 1/2O_i''$	6.10	4.76
$1/2Eu_2O_3 \rightarrow (Eu_{Ba}^{\bullet} + O_i'')_{com} + BaO + 1/2V_O^{\bullet\bullet}$	6.72	6.22
$1/2Eu_2O_3 \rightarrow 1/2(Eu_i^{\bullet\bullet\bullet} + O_i'' + Eu_{Ba}^{\bullet})_{com} + 1/2BaO + 1/2O_i''$	5.49	4.51
$1/2Eu_2O_3 + EuO \rightarrow (Eu_i^{\bullet\bullet\bullet} + O_i'' + Eu_{Ba}^{\bullet})_{com} + BaO + 1/2O_i''$	6.51	5.18
$1/2Eu_2O_3 + EuO \rightarrow (Eu_i^{\bullet\bullet} + O_i'' + Eu_{Ba}^{\bullet})_{com} + BaO + 1/2O_i''$	6.83	6.64

com: Defect complex

4.4 Europium Ion Size Consideration

Although it seems that the large Eu^{3+} ion should not reside in the spinel block because the spinel block is oxygen close-packed, the distance between two oxygen layers across the middle of spinel block (2.431 Å) is larger than distance between other neighboring oxygen layers (2.016 Å) in the spinel block. Therefore, the mid-region of spinel block is not strictly close-packed. There are three cation-layers, Mg-Al(4)-Al(2), in the middle of the spinel block. Normally, the coordination number of rare-earth elements is equal to or larger than six because they are large in size and they prefer to reside in the larger octahedral sites. Thus, there is not much information about the Eu^{3+} radius in tetrahedral sites in the literature. However, it can be calculated from bond-valence theory and then can be compared with the distances in the calculated structure. Based on the bond valence theory, the valence of an ion is related to its bond lengths with the form¹⁷

$$V_i = \sum_j v_j = \sum_j \exp\left(\frac{R_{ij} - d_{ij}}{b}\right) \quad (5)$$

where V_i , the valence of ion i , is the summation of bond valences v_i between the central ion and its neighbors. d_{ij} is the bond length, R_{ij} is the bond valence parameter for the ion pair (i,j) and b is a constant equal to 0.37.¹⁸ The Eu^{3+} -O distances were 2.144 Å x 3 and 2.111 Å when Eu^{3+} ion was in the preferred position, the Al(2) tetrahedral site of BAM. The bond valence sum for that position is calculated to be 3.389 (see Table IV.14) and is close to the europium oxidation state of 3 and the 13% difference is in reasonable range compared to other ions. It seems that the Eu^{3+} ion just has a bond valence higher than the theoretical value, which means that Eu^{3+} ions will be tightly pinned by the environment and will hardly move. In contrast, those ions in the mirror plane, which can move easily, have bond valences far below their ideal values.

Table IV.14. Bond Valence of Cations in BAM

Ion	V_i	n	V_i/V_0 (%)
Al(1)	2.966	6	98.9
Al(2)	2.564	4	85.5
Al(3)	2.827	4	94.2
Al(4)	2.624	6	87.5
Ba	1.413	9	70.7
Mg	1.955	4	97.8
Eu ²⁺ (BR)	1.071	9	53.6
Eu ³⁺ (Al2)	3.389	4	113

V_0 : theoretical valence

If we assume that all Eu³⁺ - O lengths are the same in a tetrahedron, we can rewrite equation [5] as:

$$d_{ij} = R_{ij} + b \ln \left(\frac{n}{V_i} \right) \quad (6)$$

where n is the coordination number. This gives the predicted bond length for different coordination conditions.

Table IV.15. Bond Length vs. Coordination Number

n (Eu-O)	4	5	6
d (Eu-O) Å	2.1804	2.263	2.3305

The bond length of Eu³⁺ - O in BAM is smaller than the predicted value from bond valence theory. This may be related to the cation rich environment in the mid-spinel region. The oxygen ions around Eu³⁺ can not relax too much. Before the substitution, the Al-O bond lengths for Al(2) are 1.797 Å and 1.822 Å x 3. The substitution did relax the surrounding oxygen ions to a suitable distance to accommodate the large Eu³⁺ ion. The shortened Eu³⁺-O bond length is the compromise between normal bond length and the actual surroundings.

4.5 Calculations with the Bush Potential

The potentials used to generate the above results were taken from the work of Lewis and Catlow and adjusted from our earlier studies.³ It is important for the results to be the same using different potential models to confirm the results. It has been shown above that the calculated structure fits the experimental data well. Further verification of the potential model has been done. Another set of totally different potentials (derived by Bush et al.¹⁰) deduced independently was used to calculate the structure. Bush et al. used core-shell models for all cations, and the potential model might be considered to be more accurate. However, they did not define the $\text{Eu}^{2+}\text{-O}$ potential in their work, so the potential was fitted to the properties of EuO later using the new oxygen-oxygen potential. Because of the lack of physical data for fitting, i.e. it did not reproduce well all of the physical data, the fitted potential was not very satisfactory. As with the earlier potential, we found two Mg distributions with the new potential. Since we only want to test the potential dependence of calculations, only the data for configuration I calculated by the Bush potential are listed (see Table IV.16).

Table IV.16. Point Defect in Config. I with Bush Potential

Intrinsic Point Defect	Defect Energy (eV)	Extrinsic Point Defect	Defect Energy (eV)
V_{Ba}''	19.06	Eu_{Ba}	-1.58
V_{Mg}''	27.90	Eu_{Mg}	8.53
$V_{Al(1)}'''$	58.88	Eu_{Al}'	35.88
$V_{Al(2)}'''$	56.34	Eu_i''	-14.64
$V_{Al(3)}'''$	59.60	Eu_{Ba}^\bullet	-19.65
$V_{Al(4)}'''$	60.24	Eu_{Mg}^\bullet	-12.99
$V_{O(1)}''$	18.54	Eu_{Al}	14.53
$V_{O(2)}''$	20.83	Eu_i'''	-31.28
$V_{O(3)}''$	19.96		
$V_{O(4)}''$	19.14		
$V_{O(5)}''$	25.16		
Ba_i''	-12.84		
Mg_i''	-19.34		
Al_i''	-47.31		
O_i''	-11.61		

On substituting for aluminum, europium ions preferred the Al(2) sites which is the same as the results with Lewis potential. The preferred positions of the defect are the same except for the aluminum vacancy. Using the Bush potentials, it is the Al(2) position that has the lowest vacancy energy. The europium point defects occur at exactly the same places with both two sets of potentials.

Table IV.17. Intrinsic Defect Energy of BAM with Bush Potential

Disorder	Energy (eV)
Schottky	1.87
Frenkel: O	4.28
Frenkel: Ba	3.11
Frenkel: Mg	4.28
Frenkel: Al	4.52

The predominant intrinsic defect was the barium Frenkel defect for the Lewis and Catlow potential, which was expected, but the Schottky defect has the lowest reaction enthalpy for the Bush potential.

Although the absolute values of reaction energies show small differences, Eu^{3+} ions entering into the Al(2) site and Eu^{2+} ions substituting for barium still consumes the lowest energy (Table IV.18). Another interesting thing is that Eu^{2+} ions substituting Al(2), the favorite site for Eu^{3+} , has a dramatically decreased heat of solution and comes close to that of Eu^{2+} ions sitting in the BR site. It seems that Eu^{2+} may occur inside the spinel block; this is contrary to the previous results with the Lewis and Catlow potential. Since the fitting of Eu^{2+} -O potential was not satisfactory, the results obtained from the Lewis & Catlow potentials may be considered to be more reliable: only one Eu^{2+} position exists.

The environment of the Eu^{3+} ion on the Al(2) site consists of three Eu^{3+} - O bonds with a bond-length equal to 2.102 Å and one Eu^{3+} - O bond-length equal to 2.098 Å. This is close to the configuration obtained with Lewis and Catlow potential, but the size is a little smaller. From this comparison, it is clear that the europium ion positions are insensitive to the potentials.

Table IV.18. Incorporation of Eu into BAM (Bush Potential)

Defect Reaction	Enthalpy (eV)
$EuO \rightarrow Eu_i^{\bullet\bullet} + O_i^{\prime\prime}$	8.28
$EuO \rightarrow 1/2Al_2O_3 + Eu_{Al}^{\prime} + 1/2V_O^{\bullet\bullet}$	0.93
$EuO \rightarrow MgO + Eu_{Mg}$	2.18
$EuO \rightarrow BaO + Eu_{Ba}$	0.54
$1/2Eu_2O_3 \rightarrow Eu_i^{\bullet\bullet\bullet} + 3/2O_i^{\prime\prime}$	15.87
$1/2Eu_2O_3 \rightarrow Eu_{Al} + 1/2Al_2O_3$	0.37
$1/2Eu_2O_3 \rightarrow Eu_{Mg}^{\bullet} + MgO + 1/2O_i^{\prime\prime}$	4.83
$1/2Eu_2O_3 \rightarrow Eu_{Ba}^{\bullet} + BaO + 1/2O_i^{\prime\prime}$	6.7

Lattice Energy (eV): $E_{BaO} = -32.46$ $E_{MgO} = -40.99$ $E_{EuO} = -34.58$
 $E_{Al_2O_3} = -157.6$ $E_{Eu_2O_3} = -129.28$

4.6 Conclusions

Based on our calculations, the BAM structure may accommodate two Mg distributions that can not be distinguished by their lattice energies. We think both configurations will exist in the real material, which makes the defect structures much more complicated. Although two Mg distributions exist, the predominant defect is the same for both configurations, namely the Barium Frenkel defect. The distribution of Mg changes the defect properties and the most significant change in the defect properties is the oxygen interstitial position. The Mg distribution that retains the mirror symmetry at the barium-oxygen plane constrains the oxygen interstitial ion in the mirror plane to form a two-bridge configuration instead of a Reidinger defect as in β -alumina. However, if the Mg distribution destroys the mirror symmetry, the oxygen will stay inside the spinel block in the half unit cell without Mg. It seems that the relative charge of Mg_{Al}^{\prime} plays an important role in determining the positions of defects.

Two sets of potential models have been tested. The results show a difference in the predominant thermal defect, but the europium defects had the same properties. Two europium sites were found: divalent ions prefer to occupy the Beevers-Ross site in the

mirror plane while trivalent europium ions prefer the Al(2) tetrahedral position in the spinel block. Although the calculated Eu^{3+} -O bond length is smaller than the expected value, the difference is small and the bond length is in the reasonable range.

Defect complexes with two and three defects, at least one of which is Eu^{3+} , have been calculated and compared. The defect complexes did show smaller defect energies than the sum of individual defects, but the amount of energy decrease was not big enough to stabilize the Eu^{3+} ion in the mirror plane.

Although Eu^{3+} was predicted to prefer the Al site, this was a thermodynamic conclusion, and kinetic factor was not considered. For example, if Eu^{3+} was formed during application by oxidation from Eu^{2+} , it would not be necessary for it to be at the Al(2) site. As the Eu^{2+} ion resides at the BR position in the conduction plane, Eu^{3+} could be formed at that position. There is about 5 Å distance between the BR and Al(2) sites. Whether Eu^{3+} ions can migrate such a distance is a kinetic problem that will be investigated later.

References

1. M. Bettman and L.L. Terner, "On the Structure of $\text{Na}_2\text{O}\cdot 4\text{MgO}\cdot 15\text{Al}_2\text{O}_3$, a Variant of Beta-Alumina," *Inorg. Chem.*, **10**[7] 1442-6 (1971).
2. N. Iyi, Z. Inoue, and S. Kimura, "The Crystal Structure and Cation Distribution of Highly Nonstoichiometric Magnesium-Doped Potassium Beta-Alumina," *J. Solid State Chem.*, **61**[2] 236-44 (1986).
3. G.A. Rankin and H.E. Merwin, "The Ternary System $\text{CaO}\text{-Al}_2\text{O}_3\text{-MgO}$," *J. Am. Chem. Soc.*, **38**[3] 568 (1916).
4. W.L. Bragg, C. Gottfried, and J. West, "The Structure of Beta Alumina," *Z. Kristallogr.*, **77**[2] 255-74 (1931).
5. C.A. Beevers and M.A.S. Ross, "The Crystal Structure of "Beta Alumina" $\text{Na}_2\text{O}\cdot 11\text{Al}_2\text{O}_3$," *Z. Kristallogr.*, **97**[1] 59-66 (1937).
6. B.G. Dick and A.W. Overhauser, "Theory of the Dielectric Constants of Alkali Halide Crystals," *Phys. Rev.*, **112**[1] 90-103 (1958).
7. J.G. Park and A.N. Cormack, "Potential Models for Multicomponent Oxides: Hexa-Aluminates," *Philos. Mag.*, **73**[1] 21-31 (1996).
8. J.G. Park and A.N. Cormack, "Crystal/Defect Structures and Phase Stability in Ba Hexa-aluminates," *J. Solid State Chem.*, **121**[1] 278-90 (1996).
9. G.V. Lewis and C.R.A. Catlow, "Potential Models for Ionic Oxides," *J. Phys. C: Solid State Phys.*, **18**[6] 1149-61 (1985).
10. T.S. Bush, J.D. Gale, C.R.A. Catlow, and P.D. Battle, "Self-Consistent Interatomic Potentials for the Simulation of Binary and Ternary Oxides," *J. Mater. Chem.*, **4**[6] 831-7 (1994).
11. C.R.A. Catlow, A.N. Cormack, and F. Theobald, "Structure Prediction of Transition-Metal Oxides Using Energy-Minimization Techniques," *Acta Crystallogr., Sect. B: Struct. Sci.*, **B40**[3] 195-200 (1984).
12. A.N. Cormack, "A Perfect Lattice Approach to Nonstoichiometry," *Solid State Ionics*, **8**[1] 187-92 (1983).
13. N.F. Mott and M.J. Littleton, "Conduction in Polar Crystals. I. Electrolytic Conduction in Solid Salts," *Trans. Faraday Soc.*, **34**[1] (1938).

14. W.L. Roth, F. Reidinger, and S.L. Placa, "Studies of Stabilization of Transport Mechanisms in Beta and Beta" Alumina by Neutron Diffraction," pp. 223-41 in *Superionic Conductors*. Edited by G. D. Mahan and W. L. Roth. Plenum, New York, 1976.
15. K. Edstrom and J.O. Thomas, "Sodium-Ion Distribution in Na⁺ Beta-Alumina: Crystallographic Challenge," *Acta Crystallogr., Sect. B: Struct. Sci.*, **B47**[2] 210-6 (1991).
16. A.N. Cormack, "Defect Processes in Ceramics," pp. 63-98 in *Advances in Solid-State Chemistry*. Edited by C. R. A. Catlow. Jai Press, Greenwich, Connecticut, 1993.
17. I.D. Brown, "The Bond-Valence Method: An Empirical Approach to Chemical Structure and Bonding," pp. 1-30 in *Structure and Bonding in Crystals*. Edited by M. O'Keeffe and A. Navrotsky. Academic Press, New York, 1981.
18. N.E. Brese and M. O'Keeffe, "Bond-Valence Parameters for Solids," *Acta Crystallogr., Sect. B: Struct. Sci.*, **B47**[1] 192-7 (1991).

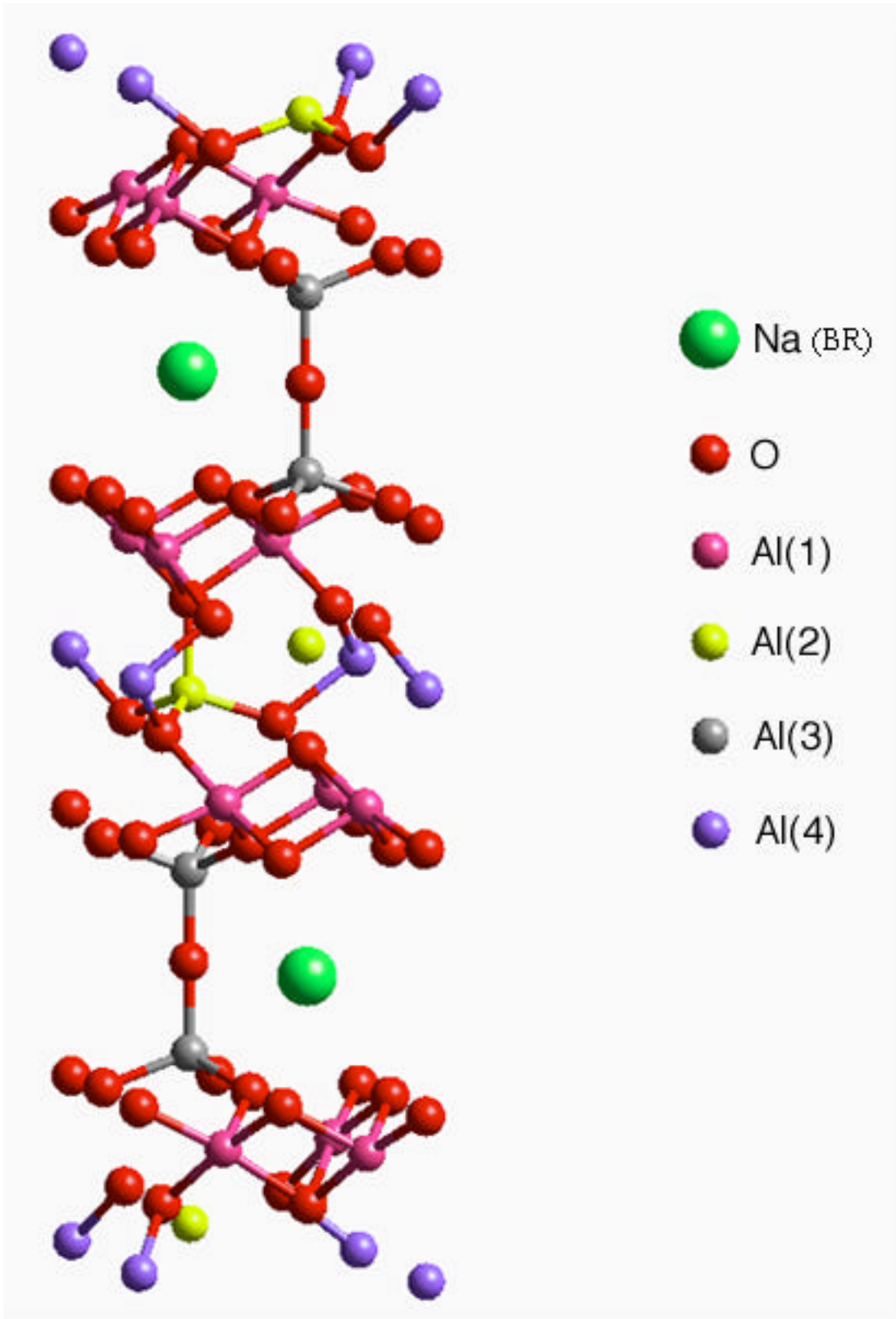


Figure 4.1. Primitive cell of β -alumina.

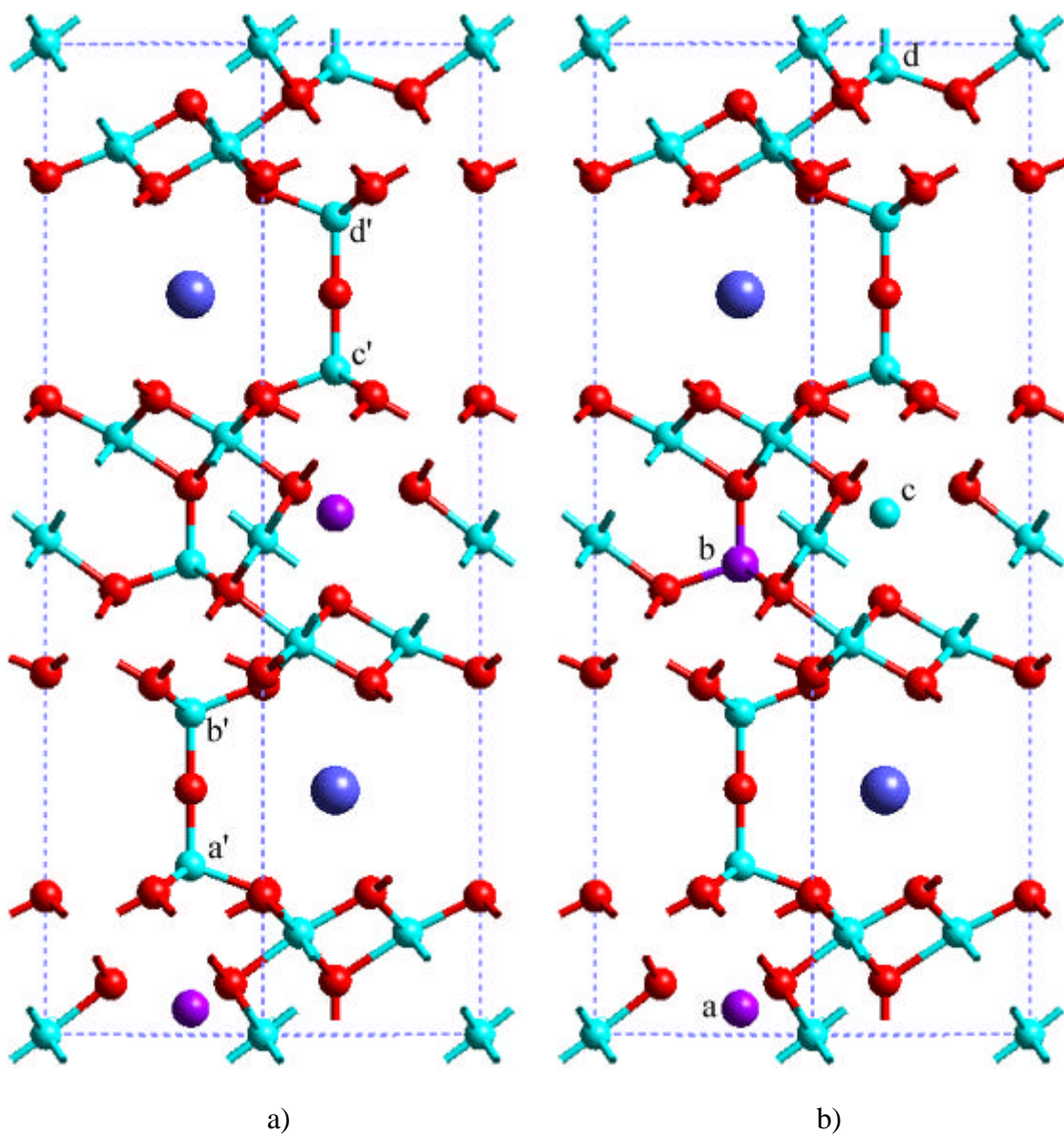


Figure 4.2. Two configurations of BAM. a) Configuration I possesses Mg at ab sites; b) Configuration II possesses Mg at ac sites.



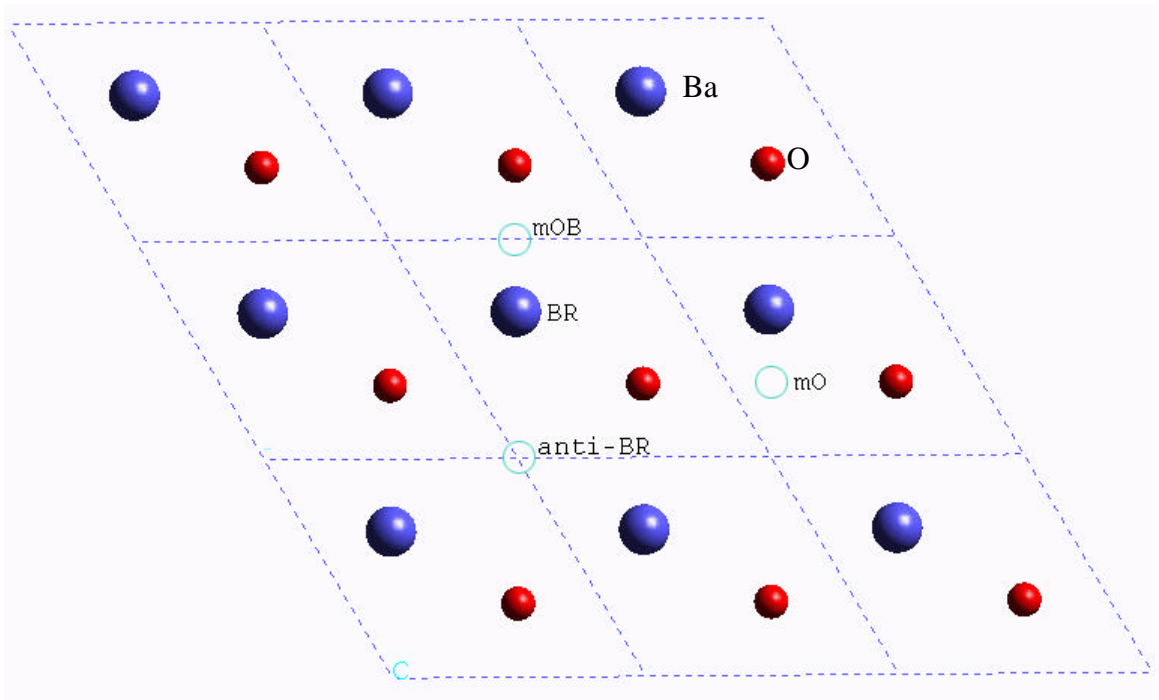


Figure 4.3. Projection of mirror plane of BAM with ion positions on X-Y plane.

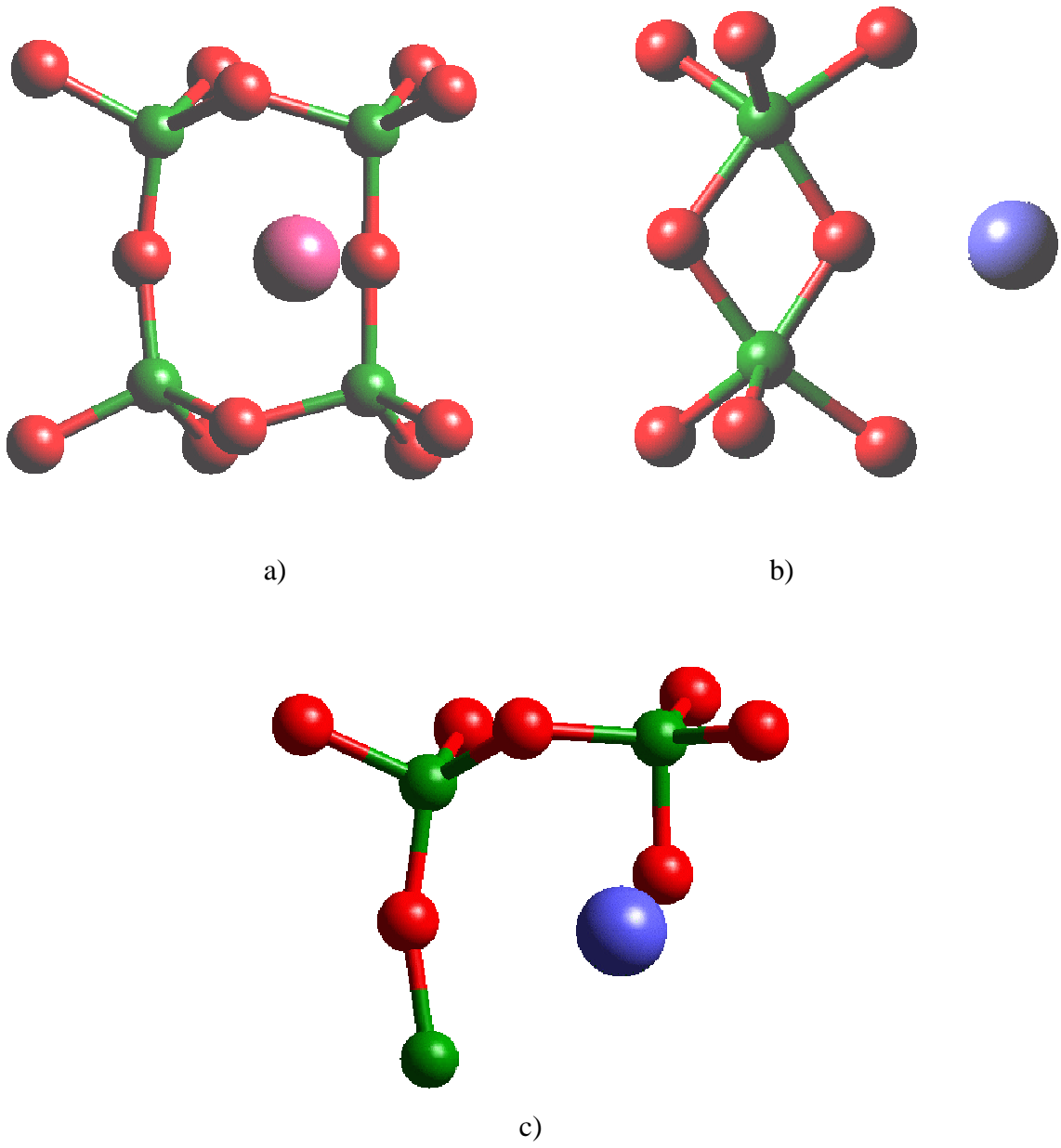


Figure 4.4. Three types of oxygen interstitial of BAM.



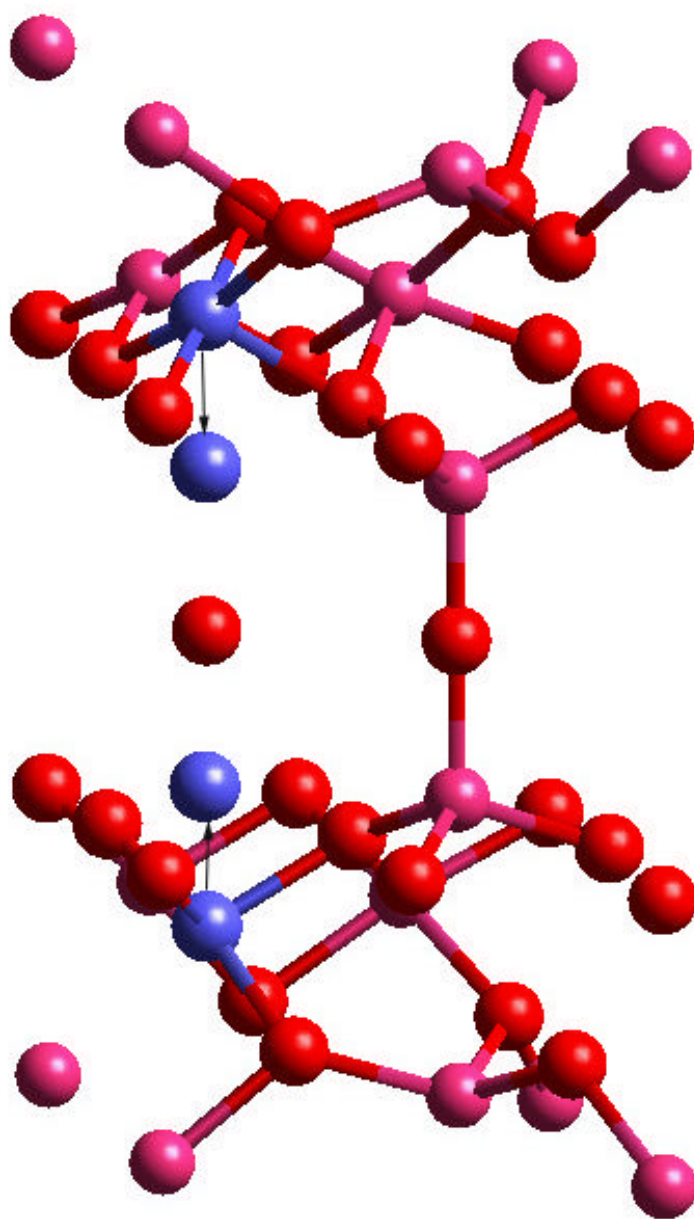


Figure 4.5. Configuration of Reidinger defect.

● Ba ● O ● Al

5. Ion Migration In BAM

Abstract:

$\text{BaMgAl}_{10}\text{O}_{17}:\text{Eu}^{2+}$, a blue phosphor material, has a luminescent property degradation problem, in which the emission intensity decreases with time and heating process. It is believed that the degradation process is related to the oxidation of europium from the divalent state to the trivalent state. Earlier simulation work has shown that the europium ion prefers to occupy two different positions in the BAM lattice, in different oxidation states. The two positions are about 5 \AA away from each other. In this work, molecular dynamics simulation was adopted to investigate the migration of ions in BAM, particularly the Eu ions.

Our results suggest that regardless of the position of Eu^{3+} in the conduction plane (BR or anti-BR), it can migrate into the spinel block at relatively low temperature, under certain conditions, such as the presence of a nearby Mg ion. The probability of migration increases with the temperature. Eu^{2+} ion migrates very differently from the trivalent ion; instead of entering into the spinel block, it migrates inside the conduction plane with a mobility close to or larger than the mobility of Ba ion. The hypothesis of forming $\text{EuMgAl}_{11}\text{O}_{19}$ after degradation is discussed from the aspect of ionic migration.

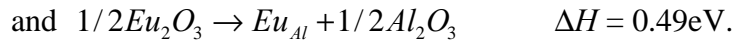
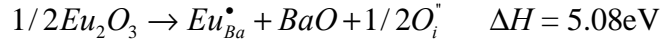
5.1 Introduction

The structure prototype of BAM ($\text{BaMgAl}_{10}\text{O}_{17}$) is β -alumina ($\text{NaAl}_{11}\text{O}_{17}$).¹ The structure of β -alumina can be described as oxygen close-packed spinel blocks separated by sodium-oxygen planes.² It has the space group symmetry of $P6_3/mmc$ that requires two spinel blocks and two Na-O planes in one primitive cell. On changing the material from β -alumina to BAM, magnesium ions are substituted for two aluminum ions on tetrahedral sites in order to compensate the charge generated by the $\text{Ba}_{\text{Na}}^{\bullet}$ substitution. Although it has been found that there are two structures, with different Mg distributions, having nearly the same lattice energy, only the structure with the lower lattice energy (configuration I) was investigated in this chapter to check the migration property of europium ions (see Fig. 5.1).

The aluminum sites in BAM can be classified into four asymmetric positions labeled as Al(1)-Al(4), in which Al(1) and Al(4) are octahedral positions and the other two are tetrahedral positions. Magnesium has been found to occupy the Al(2) position. The Mg distribution of the structure investigated here has the two Mg ions in different spinel blocks and retains the 2-fold screw axis symmetry. This kind of distribution destroys the mirror symmetry at the barium-oxygen plane in between the two adjacent spinel blocks along the *c*-axis. The barium-oxygen plane is referred to as a conduction plane instead of a mirror plane because of the above reason, and because of the high mobility of barium in this plane.

In the conduction plane (Fig. 5.2) there are three different positions, labeled as BR, anti-BR and mO sites, named after the work of Beevers and Ross.³ Although BR and anti-BR sites are both surrounded by three oxygen ions in the conduction plane, their neighboring ions above and below them in the *c* direction are different. The BR site is in the center of an octahedron with three oxygen ions above and another three below. For the anti-BR site, there are oxygen ions immediately above and below it, and the three ions form a straight line parallel to the *c*-axis.

It has been found that Eu^{2+} ion is incorporated into the structure at the BR site, while Eu^{3+} ion prefers to substitute on the Al(2) site in the middle of spinel block from our earlier work (Chapter 4). As one would imagine, Eu^{3+} ion is quite likely to form at the BR site, through oxidation of the Eu^{2+} at that site. It has been found that there is about 4.5eV difference in the defect reaction enthalpy for Eu^{3+} entering into these two positions.



Although the enthalpy difference is quite large, it is not clear whether it is large enough for the Eu^{3+} ion to move through the oxygen close-packed layers. Therefore, it is necessary to investigate the possibility of europium migration. Molecular dynamics (MD) simulation provides a useful tool to study the migration of ions at different temperature, and was used to investigate the migration of Eu in our study.

5.1.1 Molecular Dynamics Simulation

As its name implies, molecular dynamics simulation models the movement of particles: ions, atoms and molecules. In ionic crystals, ions are under the influence of all the other ions, long-range and short-range. They will move according to the summation of all the influences. Normally, ions just oscillate at their equilibrium position in an equilibrated material, and jump randomly with small jump frequency unless a gradient is established somehow (thermal, electrical, chemical etc.). If the temperature of the material is high enough, the frequency of an ion obtaining a kinetic energy large enough to overcome the migration obstacle formed by all other ions becomes larger. Actually, any kind of migration can occur at any temperature above 0K, but with different probability. The higher the temperature is, the larger the probability.

The first thing in setting up a MD simulation is to describe the system. For the ionic material of BAM, the system consists of many individual ions with charges determined by their valence state. Boundary conditions can be periodical or restrictive (nonperiodic in any of the x, y and z directions), depending on the simulation requirement. Periodic boundary conditions are used frequently to simulate bulk materials. The system size can be altered to adjust some species' concentration, such as dopants and defects. Normally,

the core-shell model used in energy minimization simulations would not be adopted in a MD simulation, because the frequency of the core-shell vibration is very high which requires the simulation to work at that infinitesimal time-step and the time of the simulation becomes unacceptably long.⁴

Secondly, the interaction between ions in the system is defined. The interaction includes long-range Coulombic and short-range non-Coulombic interactions. The potential energy of one pair of ions is described as

$$V_{ij}(r_{ij}) = z_i z_j / r_{ij} + A_{ij} \exp(-r_{ij} / r_{ij}) - C_{ij} r_{ij}^{-6}. \quad (1)$$

In the above equation, the non-Coulombic potential is in Buckingham form for the consistency with earlier work.

For summation of the long-range potentials, the Ewald approach is used for periodic systems; the direct Coulombic sum can be used for periodic or non-periodic systems, but with long calculation time. The Ewald sum calculates the long-range potential in two steps. First, a spherical Gaussian cloud of opposite charge centered on each ion is superimposed on the system; this changes the long-range interaction to short-range and then the summation converges quickly. Second, another set of Gaussian clouds of the same charge as each ion is superimposed, so that the total effect of the two superimpositions is zero. The second set of Gaussian clouds can be summed quickly in reciprocal space. Therefore, the Ewald sum replaces an infinite sum in real space into two infinite sums: one in real space and the other in reciprocal space, but both converge quickly.⁵

The force acting on each ion can be calculated by differentiating the potential at that ion with respect to its coordinates. Ions will move under those forces for an infinitesimal period of time and then the forces have to be recalculated because the potential at each ion has changed after the ions' positions have changed. Normally, the scale of the time-step is about 10^{-3} picosecond. It can not be too large or the calculation will become unrealistic; because the frequency of phonon motion is about 10^{13} Hz, and thus, the simulation time-step must be far smaller than 10^{-13} s. The small scale of the time-step limits the capability of MD simulation because it can not simulate in real time scale; one-second simulation requires about 10^{14} time-steps for which the calculation will last "forever". For example, the calculation of one time-step for a one-thousand-atom

system lasts 0.1 second (based on our calculation), a simulation of 10^{14} time-steps will last 10^{13} seconds which is definitely unacceptable.

Normally MD simulations use the Verlet leapfrog scheme as standard to calculate the positions and velocities of ions in a system at each time-step, in the microcanonical (NVE) ensemble in which the total energy of the system is conserved.⁵ The temperature of the system may vary in a small range. This kind of algorithm is also used in our studies. Constant temperature MD simulation uses other algorithms to calculate the trajectories; the system energy may be conservative or not depending on the actual algorithm used.⁵

5.2 Experiments

As the possibility to observe migration is dependent on the temperature, it is necessary to find the effective temperature at which Eu^{3+} migration occurs frequently, if Eu^{3+} does migrate into the spinel block. To control the concentration of europium ions, the size of the super-cell used in the simulation contains about 1000 ions. Only one europium ion is incorporated into the structure and the europium defect concentration is about 3% of total number of Ba ions, which is inside the range of the commercial phosphor product⁶.

In the beginning, the simplest defect configuration was tested: an Eu^{3+} interstitial and an Al(4) vacancy. The Al vacancy acted as the charge compensation mechanism and the possible destination of the Eu migration. The reason to choose the Al(4) vacancy instead of the Al(2) vacancy where Eu^{3+} prefers to reside, is that the Al(4) vacancy has a lower defect energy than the Al(2) vacancy in the tested BAM structure based on our earlier study. The defect energy difference is about 1.26eV. Neutron diffraction analysis of Roth et al. has shown a large number of aluminum Frenkel defects of aluminum ions in the spinel block so this kind of set-up is reasonable.⁷ The europium interstitial and aluminum vacancy were put in the same primitive cell to increase the possibility of migration occurrence. They were separated in distance by 6.6 Å. The simulation was run, beginning from 550K and the temperature increased in 100K intervals until migration was observed.

After the determination of the temperature at which the probability of observing migration was high, other aluminum vacancies, including the Al(2) (the favored position

of Eu^{3+} ions), as the Eu^{3+} migration destinations, were tested at that temperature or at temperatures a little higher. Migration properties of Eu^{2+} , Ba and O ions were also investigated.

5.3 Results

5.3.1 Europium Migration for Configurations of Eu Interstitial + Al Vacancy

5.3.1.1 $\text{Eu}_i^{\bullet\bullet\bullet} + V_{\text{Al}(4)}^{\bullet\bullet\bullet}$

The first observation of migration occurred at 850K, in which one Al(1) ion moved up to the middle region of the spinel block to occupy the vacant Al(4) position and then the Eu^{3+} interstitial migrated from the conduction plane to the nearby vacant Al(1) position. These two migrations seem to occur continuously, Al(1) migrating first and then the Eu^{3+} . The simulation was rerun several times to test the probability of the migration occurring. None of the later runs showed the migration. This implies that Eu^{3+} migration can occur at 850K but with very small probability. After increasing the temperature to 950K, all of the tested runs showed the same kind of migration that occurred at 850K. Thus a temperature of 950K was used as the starting temperature in later simulations. Actually, the temperature in the simulation does not correspond to the real temperature. The simulation temperature is normally higher than the real temperature because the integer charges have been assigned to each ion (because of the assumption of fully ionic material) and then the Coulombic binding energy is bigger than in the real case.

Although Eu migration had been observed, it needed to be investigated further. As seen in the BAM structure (see Fig. 5.1), an ion in the conduction plane will experience different environments when moving up or down. Moving up, it will encounter an Al(2) ion earlier than an Mg ion (substituting at Al(2) site) but it will see Mg ion earlier when moving down; this is because only one Al at the two Al(2) sites in a spinel block is substituted by Mg. As the Al(4) vacancy can occur above or below the europium interstitial, these two situations must be investigated individually. Another thing that needs to be considered is that the two defects can reside in different primitive cells and that the migration path and mechanism may change for different kinds of defect

arrangement. More simulations were carried out at three different temperatures, 950K, 1050K and 1150K for each defect arrangement.

When the two defects were in the same primitive cell, migration of an Al(1) to the vacant Al(4) occurred. Whether or not the migration of Eu^{3+} to the vacant Al(1) would occur was dependent on the presence of magnesium in the migration path. Migration would happen when there was an Mg in between the Eu^{3+} interstitial and the vacant Al(4) position initially, but not in the case when an Al(2) ion was in between them. In the case of an Al ion in between, the Eu^{3+} ion did move above the conduction plane and appeared to try to enter the spinel block but it just stayed there, even with extended simulation time.

When the two defects were not in the same primitive cell, no Eu^{3+} migration into the spinel block was observed. Instead, the Eu^{3+} ion moved to a nearby BR position and stayed there by displacing the Ba ion in the BR position to an interstitial position. That is because BR site is larger than the anti-BR site; i.e. the distance from a BR site to its nearest neighboring ion is larger than for an anti-BR site. The barium ion pushed into the interstitial position by the Eu^{3+} ion migrated inside the conduction plane toward the vacant aluminum site. The migration of an Al(1) ion to the vacant Al(4) position did not occur in all simulations; it showed up at high temperature, but not at lower temperature, which is reasonable because the Al(4) vacancy is more energetically favorable and the change from Al(4) vacancy to Al(1) vacancy increases the system energy.

5.3.1.2 $\text{Eu}_i^{\bullet\bullet\bullet} + V_{\text{Al}(2)}^{\text{m}}$

Al(2) is a tetrahedral position close to the middle of spinel block. It is a little closer to the conduction plane than Al(4). Many defect arrangements were tested to find the possibility and mechanism of migration. No direct migration of Eu^{3+} ion into the Al(2) position was observed. Instead when the two defects were in the same primitive cell with no Mg in between them, the Eu^{3+} moved into a vacant Al(3) position generated by the Al(3) ion migrating to the vacant Al(2) position. The europium ion just stayed at the edge of the spinel block and did not migrate any further because there is no longer an available position in the spinel block. This migration is not contrary to the magnesium effect shown in the previous results because this time the vacancy is further away from

the interstitial and their correlation is weakened by the cation-rich region in the middle of spinel block, as well as the large separation, if the Mg ion is in between (see Fig. 5.3).

For all of the other arrangements of these two defects, Eu^{3+} ion occupied a nearby BR position and the generated barium interstitial moved inside the conduction plane to a position close to the vacancy. But no migration of barium into the spinel block was observed. Al(3) was found sometimes to migrate to the vacant Al(2) in the spinel block at higher temperature.

5.3.1.3 $\text{Eu}_i^{\bullet\bullet\bullet} + V_{\text{Al}(1)}^{\prime\prime}$ and $\text{Eu}_i^{\bullet\bullet\bullet} + V_{\text{Al}(3)}^{\prime\prime}$

As Eu^{3+} occupation of the Al(1) and Al(3) positions was observed in the previous migration study, it is not surprising to see the direct migration of Eu^{3+} ion into these two aluminum positions if they are vacant at the beginning of simulations. But the limitation was that the aluminum vacancy must be in the same primitive cell as the europium or the migration did not occur. And, if in the migration direction, Al(2) was closer to Eu than the Mg, Eu^{3+} did not pass through the oxygen close-packed layer. However it did jump to the vacant Al(3) at the edge of spinel block easily, no matter the position of the magnesium ion. For simulations of both defect configurations without Eu^{3+} long-range migration, it was the barium ion that moved close to the vacancy and stabilized the system. Eu^{3+} ion just underwent a short-range displacement to a nearby BR position.

The above results imply that Mg plays a key role in the migration of europium into the spinel block. The reason could be the relaxation caused by local strain field around Mg ion whose radius is larger than Al and so the substitution of Al with Mg opens up the spinel block. Or it could be the effective local charge of -1 associated with the substitution; the local charge would attract the Eu^{3+} and help its migration. The Mg influence could also be the combination of these two issues.

No Eu^{3+} long-range migration inside the conduction plane was observed in all defect configurations and at all three temperatures. It was the barium long-range migration that occurred when the europium interstitial and aluminum vacancy were not in the same primitive cell. The Ba interstitial migrated in the conduction plane to a position close to the vacancy, which also stabilized the system, but to a smaller extent than when Eu^{3+} was inside the spinel block.

Since Eu^{3+} ion is supposed to form at the BR position, migration from the BR position also needs to be considered. Besides the aluminum vacancy acting as the destination of migration, a barium interstitial ion is also required to keep the whole system charge neutral (which is the requirement of the MD program, DLPOLY). So the defect configuration becomes $\text{Eu}_{\text{Ba}}^{\bullet} + V_{\text{Al}}^{\text{m}} + \text{Ba}_i^{\bullet\bullet}$. When the barium interstitial was in the same conduction plane as the europium ion, the europium behaved as the same as when it was in the interstitial position. It should be noted that when $\text{Eu}_{\text{Ba}}^{\bullet}$ and $\text{Ba}_i^{\bullet\bullet}$ were the same distance away from the V_{Al}^{m} , it was the europium ion that migrated to the vacancy, otherwise the vacancy remained unoccupied. In the conduction plane, Ba ion migrated much more easily than Eu^{3+} but it never went into the spinel block. If $\text{Eu}_{\text{Ba}}^{\bullet}$ and $\text{Ba}_i^{\bullet\bullet}$ were in different conduction planes, the europium remained where it was but deviated a small distance toward the vacancy. In this case, if the europium began to migrate towards the aluminum vacancy, another vacancy would be generated in the conduction plane at the BR site, and this seemed to hinder the Eu^{3+} migration toward the aluminum vacancy.

5.3.2 Migration of Other Ions

Barium migration in the conduction plane occurred by an interstitialcy mechanism, in which a barium interstitial pushed another barium in a normal BR position into an adjacent interstitial position (see Fig. 5.4) and then occupied the normal lattice position. The final configuration after an interstitialcy migration looks like the interstitial ion migration to a nearby interstitial position. This result is consistent with the experimental observations.⁸

The migration properties of divalent europium ion were also investigated. Eu^{2+} ion was put at a BR position with a barium interstitial in the same conduction plane and a barium vacancy in the other to test the mobility of Eu^{2+} inside the conduction plane. The trajectory plot of Eu^{2+} in the conduction plane shows that the europium almost moved through all the BR positions (see Fig. 5.5). Thus the mobility of Eu^{2+} ion must be the same as barium, or larger. The hexagonal shape in the trajectory map implies an interstitialcy migration mechanism; otherwise the shape should be triangular.

The defect set up to test the possibility of Eu^{2+} migration into the spinel block was the following: an Eu^{2+} was placed in its favorite BR position, an aluminum vacancy was placed inside the spinel block in the same primitive cell as the Eu^{2+} ion, and an Eu^{3+} interstitial was placed in the other conduction plane (without Eu^{2+}) and in a different primitive cell away from the Eu^{2+} . As shown above, when the Eu^{3+} ion was not in the same primitive cell as the Al vacancy, it did not migrate and thus would not disturb the migration of Eu^{2+} ion. Although a barium interstitial would form close to the aluminum vacancy, it is in the conduction plane where it would not seriously affect the Eu^{2+} migration. In all simulations with different aluminum vacancies, no long-range migration of Eu^{2+} ions was observed, although there was a little relaxation off the conduction plane. It seems that the divalent and trivalent europium ions behave quite differently in the migration process, although they are only different in the electronic charge they possess and in their size.

The migration of the only anion, O^{2-} , in the material has also been tested. There are three oxygen positions of interest: the position inside the spinel block, where it is the favorite oxygen interstitial position for configuration I of BAM; the mO site where is the oxygen interstitial position in β -alumina, and the mOB site which oxygen will occupy in configuration II of BAM. An Eu^{2+} interstitial in the conduction plane will be the compensating defect.

When inside the spinel block according to the interstitial position of configuration I of BAM, the oxygen migrated to the conduction plane, only if there was an Eu^{2+} interstitial in the same unit cell. Otherwise, the oxygen remained in place. When the oxygen migrated to the conduction plane, it formed a defect complex with the Eu^{2+} .

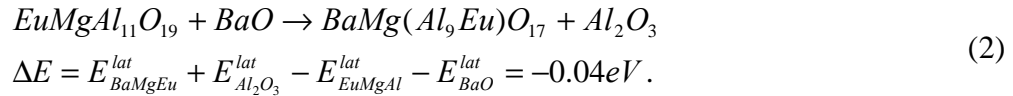
If the oxygen interstitial at the mOB site formed a two-bridge configuration with an O(5) in the conduction plane, it did not migrate at all. Instead the two oxygen ions rotated around the Al(3)-Al(3) axis, with a trajectory of a circle. When put in the third position, the mO site at the conduction plane, the oxygen did not stay there; instead it moved close to a nearby O(5) ion and formed a two-bridge configuration, as it did in the mOB site. There was no observation of Al(1) moving toward conduction plane to form a Reidinger defect, which is consistent with the previous defect energy calculations. In a

word, there was no long-range oxygen migration in the conduction plane at the tested temperatures.

5.4 Related Phases Containing Eu

Shozo et al. have proposed that oxidation converts the BAM:Eu²⁺ phosphor into a mixture of two compounds, BaMgAl₁₀O₁₇ and EuMgAl₁₁O₁₉ which was proposed to have a magnetoplumbite (MP) structure with three oxygen ions in the mirror plane.⁹ But in this migration study, oxygen and Eu³⁺ did not migrate inside the conduction plane, at the temperature at which Eu³⁺ can migrate into the spinel block easily. Thus the Eu³⁺ MP structure can not form, at least at that temperature where luminescent degradation begins to occur. Instead, based on our earlier result that Eu³⁺ prefers to substitute for Al in the spinel blocks of BAM, the phase after oxidation should be BaMg(Al₉Eu)O₁₇ keeping the β-alumina type structure.

These two structures were modeled and their lattice energies are compared below:



The negative reaction enthalpy means that the reaction will process toward right side of the reaction automatically, in other words, BaMg(Al₉Eu)O₁₇ is thermodynamically more stable, although the difference is small. Another thing that should be noted is that the unit cell parameter along 2-fold screw axis for BaMg(Al₉Eu)O₁₇ is 23.05 Å, a 0.4 Å difference from BAM, while EuMgAl₁₁O₁₉ has 1 Å difference from BAM. From the point of view of lattice relaxation, BAM:Eu²⁺ will form BaMg(Al₉Eu)O₁₇ more easily than EuMgAl₁₁O₁₉, after the oxidation at low temperature. But it does not mean EuMgAl₁₁O₁₉ would not occur at higher temperature, since the reaction enthalpy is very small and excess or residual Al₂O₃ may exist in the manufactured BAM product.

The main feature of the magnetoplumbite structure is the three oxygen ions in a mirror plane of a primitive cell. Defect complexes with three interstitial ions have been tested in the previous chapter but they only included configurations with two Eu ions and one oxygen ion. If the defect complex includes one Eu³⁺ and two oxygen ions, a three-oxygen configuration will form. So it is necessary to test this kind of defect complex to

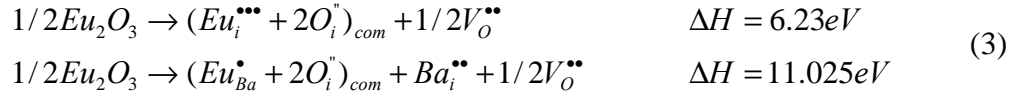
make sure that Eu^{3+} will not be stabilized at a BR site by three oxygen interstitial ions. As there are two possible oxygen locations in the mirror plane, mO and mOB sites, three kinds of defect complex with two oxygen interstitial ions will be created; both oxygens at either mO or mOB sites and a mixture of mO, mOB sites.

Table V.1. Defect Complex with Two Oxygen and One Eu^{3+}

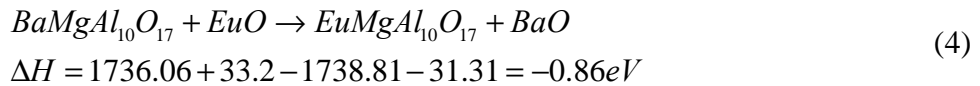
	mO+mOB	mOB+mOB	mO+mO	ΔE^* (eV)
$\text{Eu}_i^{\bullet\bullet\bullet}$	-70.81	-70.78	-	-9.73
$\text{Eu}_{\text{Ba}}^\bullet$	-54.86	-54.86	-	-3.67

* Energy difference between defect complex and the sum of individual defects.

Although the energy of the defect complex is less than the sum of individual defects, in writing down the defect reaction, it is clear that Eu^{3+} ion will not stay inside the mirror plane associated with the three oxygens as shown below.



Because of the high mobility of Eu^{2+} ions in the conduction plane and the fact that the defect complex will lower the total defect energy, Eu^{2+} may be able to come together and form europium β -alumina. The lattice energy of europium β -alumina was calculated and compared with barium β -alumina as follows,



It seems that it would be possible to form europium β -alumina because it should be more stable than the barium phase. However, these two structures are essentially the same except for the cations in the conduction plane. The difference between the cell parameters of these two structures are: $D_{\mathbf{a}} = 0.004\text{\AA}$ and $D_{\mathbf{c}} = 0.24\text{\AA}$ which are very small. Therefore, Eu^{2+} ions may just form a defect-cluster in the barium aluminate matrix, instead of phase separation, because Eu doped in BAM is normally treated as a defect. Actually, the formation of a europium cluster will decrease the luminescent intensity, because the photon released from an Eu^{2+} ion, instead of going out of the material, can be absorbed by a nearby Eu^{2+} . Thus, normally the doping concentration of

Eu is small in commercial materials for optical efficiency.⁶ Heating BAM:Eu²⁺ can create more, or larger, Eu²⁺ clusters, because the Eu²⁺ ion is quite mobile. The effect of the Eu²⁺ cluster is also shown in Oshio's work: the luminescent intensity does not increase linearly with doping concentration but the increase slows down at higher concentration.⁹

5.5 Conclusions

The results have shown that the order of mobility inside the conduction plane is: $\mu_{\text{Eu}^{2+}} \geq \mu_{\text{Ba}} > \mu_{\text{Eu}^{3+}}$. The interstitialcy mechanism dominates the migration of cations in the conduction plane. The valence state of europium determines its migration behavior; Eu³⁺ can migrate into the spinel block at a relatively low temperature, at which no migration of Eu²⁺ and Ba into the spinel block was observed. Eu³⁺ migration to either Al(1) or Al(3) vacancies are both one-step migrations. It requires at least two-steps for Eu³⁺ to occupy either Al(2) or Al(4) vacancies. Mg plays a key role in Eu³⁺ migration into the spinel block. Combined with the earlier study on the europium defect (Chap. 4), it may be concluded that Eu³⁺ ion tends to stay inside the spinel block after its generation above some temperature.

After oxidation, Eu³⁺ in BR sites may migrate to Al(2) sites and form BaMg(Al₉Eu)O₁₇ instead of EuMgAl₁₁O₁₉ at low temperature, because BaMg(Al₉Eu)O₁₇ is more stable than EuMgAl₁₁O₁₉ and its lattice parameters are closer to those of BAM. Eu²⁺ ions tend to come close to each other to form a defect cluster, which will decrease the luminescent intensity of the phosphor. Decreasing the Eu²⁺ mobility in the conduction plane may provide a way to overcome the degradation problem.

References

1. N. Iyi, Z. Inoue, and S. Kimura, "The Crystal Structure and Cation Distribution of Highly Nonstoichiometric Magnesium-Doped Potassium Beta-Alumina," *J. Solid State Chem.*, **61**[2] 236-44 (1986).
2. W.L. Bragg, C. Gottfried, and J. West, "The Structure of Beta Alumina," *Z. Kristallogr.*, **77**[2] 255-74 (1931).
3. C.A. Beevers and M.A.S. Ross, "The Crystal Structure of "Beta Alumina" $\text{Na}_2\text{O} \cdot 11\text{Al}_2\text{O}_3$," *Z. Kristallogr.*, **97**[1] 59-66 (1937).
4. B.G. Dick and A.W. Overhauser, "Theory of the Dielectric Constants of Alkali Halide Crystals," *Phys. Rev.*, **112**[1] 90-103 (1958).
5. T.B. Forester and W. Smith, *DL POLY Reference Manual*, 2.0 ed.; pp. 45-7. CCLRC, Daresbury Laboratory, Warrington, England, 1995.
6. S. Tanaka, I. Ozaki, T. Kunimoto, K. Ohmi, and H. Kobayashi, "Blue emitting CaAl_2O_4 : Eu^{2+} phosphors for PDP application," *J. Lumin.*, **87-89**[1] 1250-3 (2000).
7. W.L. Roth, F. Reidinger, and S.L. Placa, "Studies of Stabilization of Transport Mechanisms in Beta and Beta" Alumina by Neutron Diffraction," pp. 223-41 in *Superionic Conductors*. Edited by G. D. Mahan and W. L. Roth. Plenum, New York, 1976.
8. M.S. Whittingham and R. A. Huggins, "Transport Properties of Silver β -alumina [$\text{Ag}_{1+x}\text{Al}_{11}\text{O}_{17}$]," *J. Electrochem. Soc.*, **118**[1] 1-6 (1971).
9. S. Oshio, K. Kitamura, T. Nishiura, T. Shigeta, S. Horii, and T. Matsuoka, "Analytical Research of Decrease in Luminance Following Annealing of $\text{BaMgAl}_{10}\text{O}_{17}:\text{Eu}^{2+}$ Blue Phosphor for Fluorescent Lamps and Plasma Display Panels," *Natl. Tech. Rep. (Matsushita Electr. Ind. Co.)*, **43**[2] 181-7 (1997).

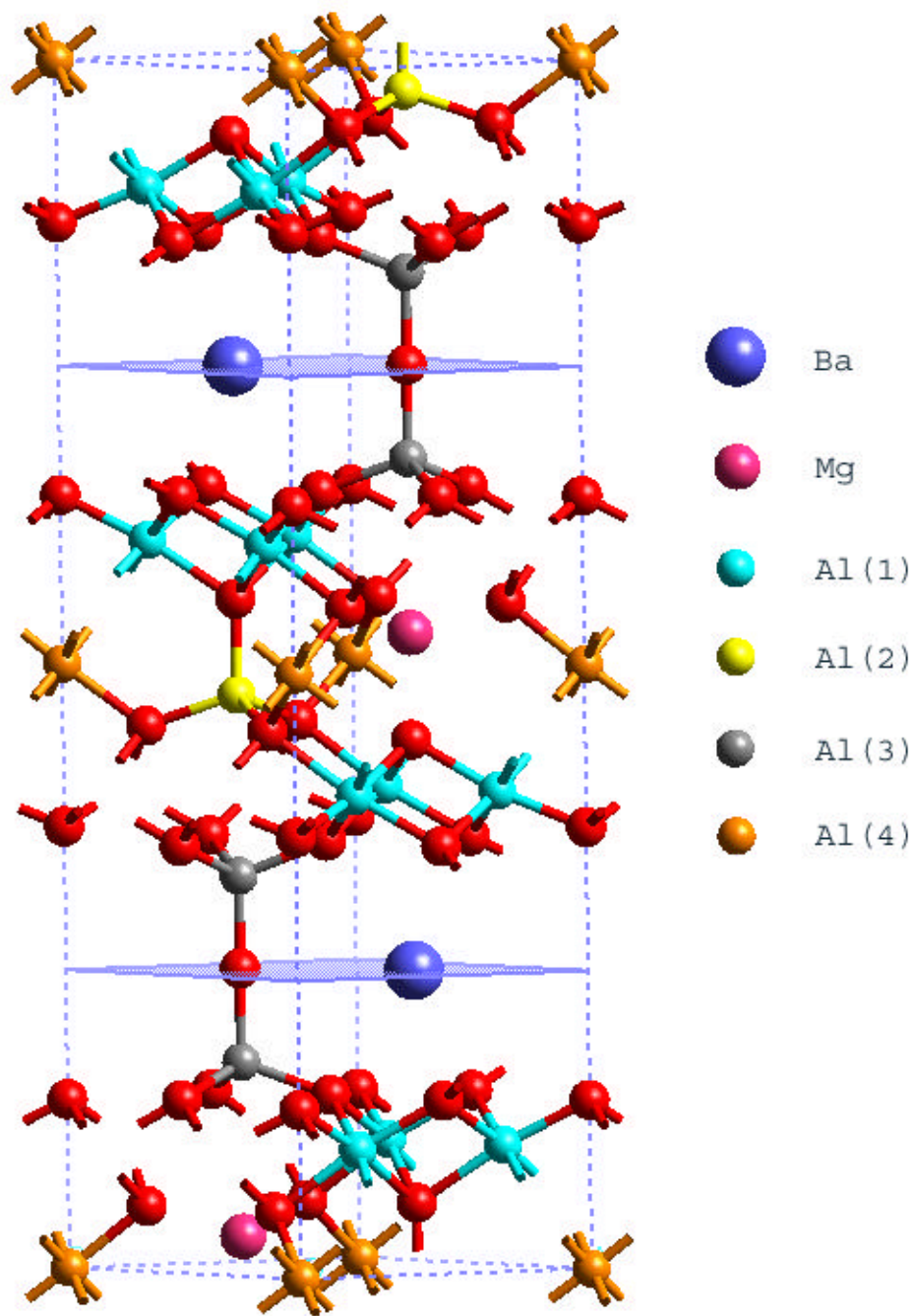


Figure 5.1. Primitive cell of BAM, configuration I.

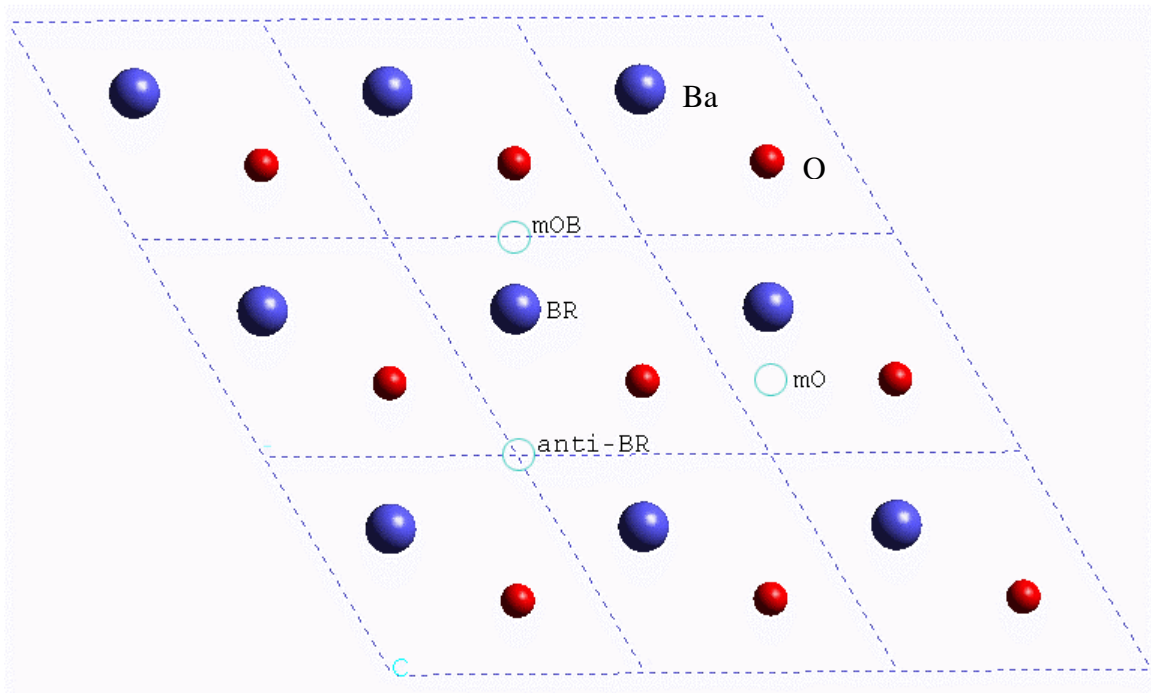


Figure 5.2. Projection of mirror plane of BAM on X-Y plane.

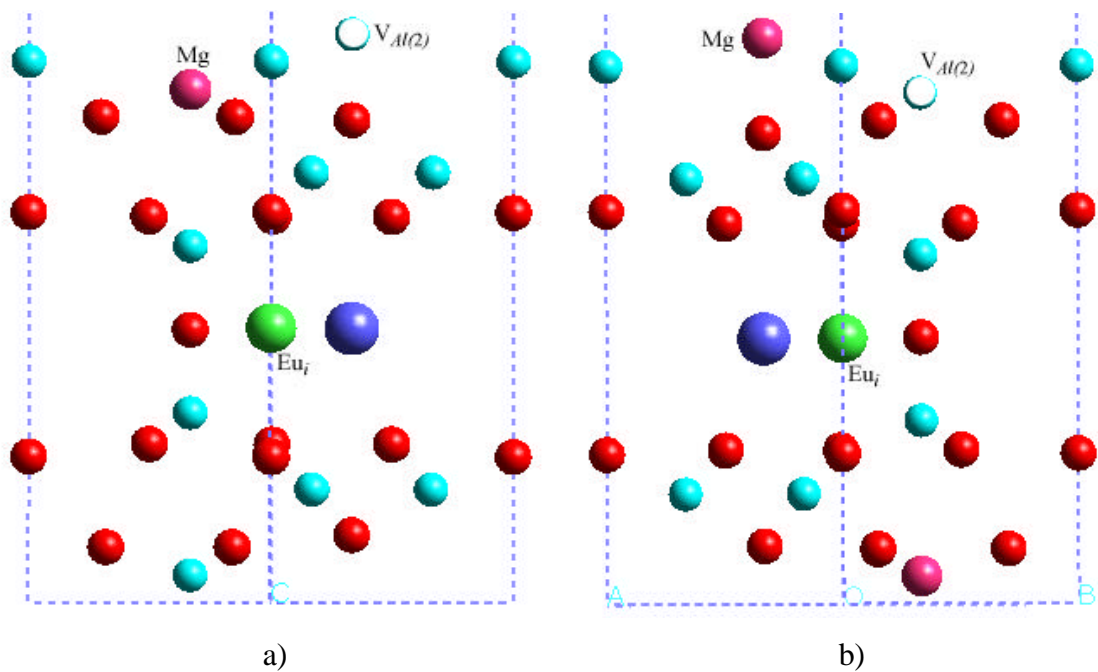


Figure 5.3. Magnesium positions related to $Eu_i^{***} + V_{Al(2)}^m$.
 a) Mg in between two defects. b) Mg not in between two defects.

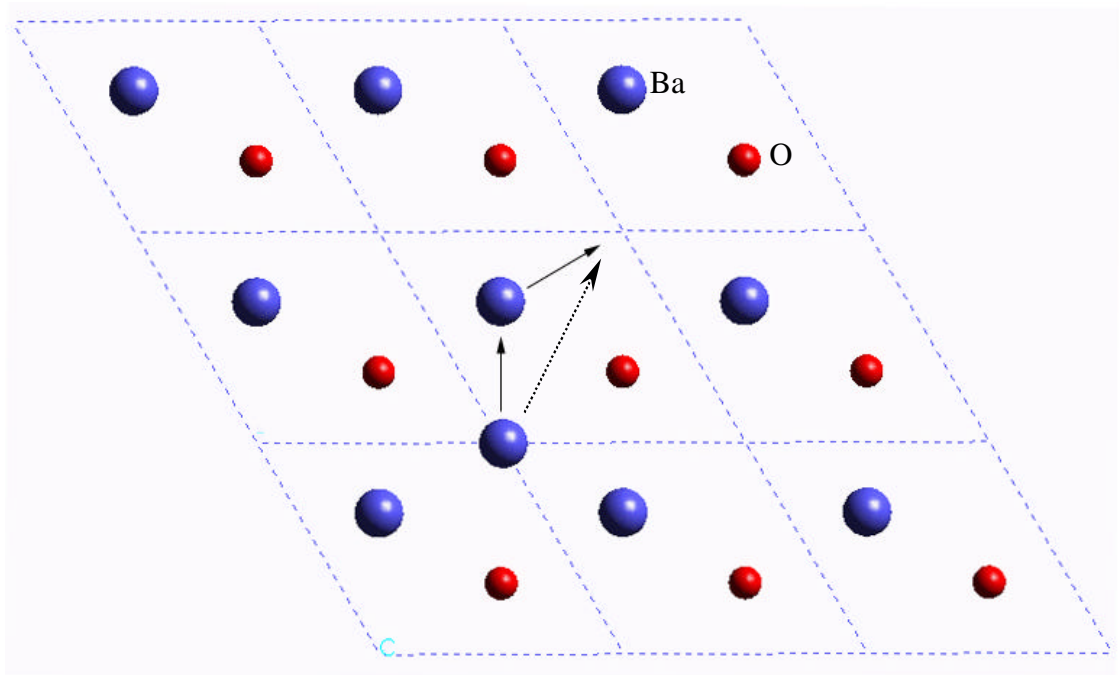


Figure 5.4. Barium interstitialcy migration.

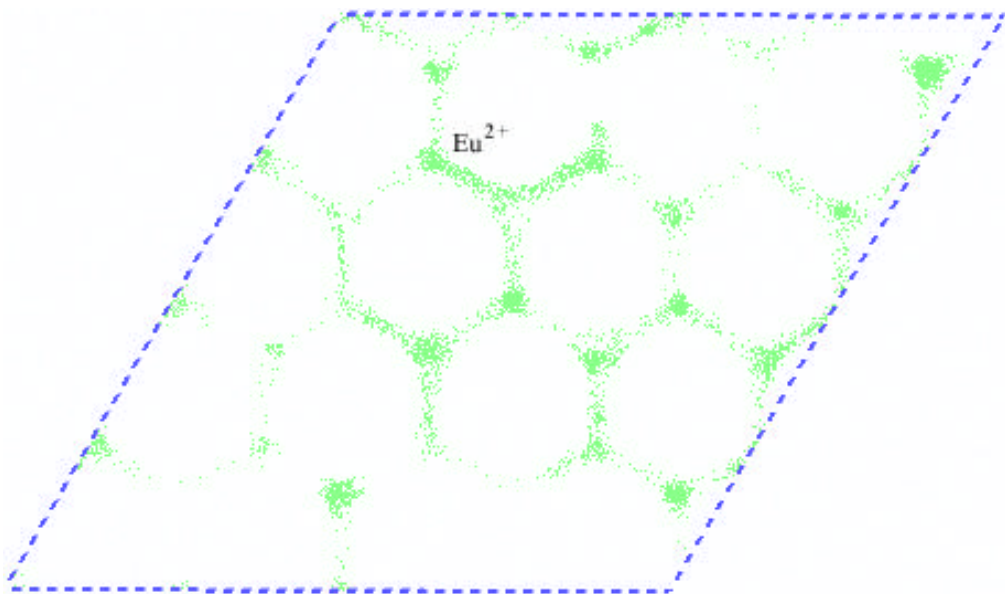


Figure 5.5. Trajectory of Eu^{2+} in the conduction plane.

6. Eu in Barium Hexa-aluminates Containing No Mg

Abstract:

Besides substituting Al with Mg to form BAM, there are two other ways to compensate the charge generated by incorporating Ba in the β -alumina crystal structure. One is to put barium on $\frac{3}{4}$ of the BR sites and oxygen on the remaining $\frac{1}{4}$, which gives the chemical formula of $0.82\text{BaO}\cdot 0.6\text{Al}_2\text{O}_3$, namely a barium-poor phase, because the Ba/Al ratio is far below the ideal value of 1/12. The other is to create aluminum vacancies in the spinel blocks and form $\text{Ba}_3\text{Al}_{32}\text{O}_{51}$, a phase with the Ba/Al ratio larger than 1/12. The structures generated in these two ways were tested for defect properties, intrinsic and extrinsic with Eu. When doped with Eu^{2+} , two emission bands, green and blue, have been observed in the barium-poor phase, which was suggested to come from two different europium positions.¹ Our work has shown that ions in the barium-poor phase, the europium, divalent and trivalent, occupy the Beevers-Ross and Al(3) tetrahedral sites, respectively. However, Eu^{3+} ion prefers to occupy the Al(2) site in $\text{Ba}_3\text{Al}_{32}\text{O}_{51}$, which is the same result found in BAM. The calculations suggest that the expansion of the emission band in the barium-poor phase is due to the fact that the existence of multiple oxygen distributions in the mirror plane varies the local Eu^{2+} environments. Eu^{3+} ions at the tetrahedral sites inside the spinel block may also contribute to the shape of the observed emission band after luminescence degradation.

6.1 Introduction

$\text{BaMgAl}_{10}\text{O}_{17}$ (BAM): Eu^{2+} is a kind of blue phosphor used in lamps and display panels. The drawback of this material is that the luminescence property will degrade with prolonged heating, the blue emission intensity decreasing and a green emission band emerging.¹ It has been shown by Ronda and Smets that another barium hexa-aluminate phase, $\text{Ba}_{0.75}\text{Al}_{11}\text{O}_{17.25}$ (known as a barium-poor phase), has two emission bands when doped with Eu^{2+} .² They suggested that these two bands were due to the Eu^{2+} in two different sites in the crystal. This provided a possible explanation of the degradation of BAM: Eu^{2+} . It is normally believed that the green band observed in the degraded BAM: Eu^{2+} comes from the emission of Eu^{3+} ions, formed by the oxidation of Eu^{2+} ions, but the ligand field acting on Eu^{2+} ions may also shift the emission band. We have carried out a study of europium behavior in the barium-poor phase to compare it with our previous work and to try to understand the differences in the emission bands between the barium-poor phase and BAM. $\text{Ba}_3\text{Al}_{32}\text{O}_{51}$ structure was modeled and compared with the structure of BAM. Its defect properties were also calculated.

The prototype structure of barium hexa-aluminates is β -alumina, $\text{NaAl}_{11}\text{O}_{17}$, which is described as oxygen close-packed spinel blocks separated by sodium-oxygen planes (also called mirror planes or conduction planes). When introducing barium into the structure, there are several ways to compensate the extra positive charge of barium on the Beevers-Ross sites. One is to substitute the same number of aluminum as barium with magnesium to form Mg'_{Al} ; this generates the BAM structure. Another way is to put barium on $\frac{3}{4}$ of the BR sites and oxygen on the remaining $\frac{1}{4}$ (namely O_R), generating the barium-poor phase. The third possible structure has aluminum vacancies inside the spinel block and all BR sites occupied by Ba. These structures are closely related to each other and they can possibly transform from one to the other. A solid solution between BAM and the barium-poor phase has been found to exist with all ratios of these two phases. The introduction of oxygen into the BR site in the barium-poor phase makes the structure more complicated because the BR site is not an anion position and so the oxygen might move away and change the structure of conduction plane. Thus, the defect

properties are hard to analyze by experimental techniques. Computer simulations are a useful tool to attack the problem.

The simulations in this study are based on the Born model description of ionic solid, which treats the solid as a collection of point ions with short-range forces acting between them. The approach has shown success in a lot of simulations, but it has been found that the reliability of the simulations depends strongly on the validity of the potential model used in the calculations. The non-Coulombic potentials can be described in many forms. The Buckingham function is used in this study,

$$V_{ij}(r_{ij}) = A_{ij} \exp(-r_{ij} / r_{ij}) - C_{ij} r_{ij}^{-6} \quad (1)$$

where r_{ij} is the distance between the ions i and j

The polarizability of an individual ion is mimicked through the core-shell model originally developed by Dick and Overhauser, in which the outer valence electron cloud of the ion is simulated by a massless shell of charge Y and the other part of the ion by a core of charge X .³ The total charge of the ion is $X+Y$ and must equal its the oxidation state. The core and shell form a harmonic oscillator with a spring constant k , and the potential energy is given by

$$V_i(r_i) = \frac{1}{2} k_i d_i^2 \quad (2)$$

where d_i is the relative displacement of the core and shell of ion i .

For the shell model, the value of the free-ion electronic polarizability is given by

$$a_i = Y_i^2 / k_i. \quad (3)$$

The potential parameters A , r , and C in Eq. [1], the shell charges Y , and spring constant k associated with the core-shell model description of polarizability, need to be determined for each interaction and ion type in the crystal. In the present study, they were taken from our earlier studies of hexa-aluminates following the original compilation of Lewis and Catlow.⁴⁻⁶

6.1.1 Lattice Energy Calculations

The lattice energy is the binding or cohesive energy of the perfect crystal and is usually defined as the energy that must be released to the crystal to separate its

component ions into free ions at rest at infinite separation. It is the summation of all potentials in the structure:

$$U = 1/2 \sum \sum V_{ij} . \quad (4)$$

The interatomic potential, V_{ij} , includes the long-range Coulombic interaction besides the non-Coulombic potential described above. The Coulombic potential is calculated with the Ewald-sum approach that separates the summation into two sums.⁷ The lattice energy is minimized through a second derivative Newton-like procedure, coded into METAPOCS.⁸ Details of the procedure have been outlined by Cormack.⁹

6.1.2 Defect Energy Calculations

Calculations of defect structures and energies are based on the perfect lattice methods. Additionally, the occurrence of relaxation of lattice atoms around the defect species must be included. The relaxation effect is large because the defect generally provides an extensive perturbation of the surrounding lattice, and, in the case of ionic crystals, the relaxation field is long-range as the perturbation provided by the defect is mainly Coulombic in origin.

The defect calculations are based on the Mott-Littleton theory, which allows one to calculate the defect-induced static polarization of a dielectric continuum.¹⁰ The basic approach is to divide the material into two regions: one is centered at the defect and the other region is outside the first one and is treated as a dielectric continuum. The inner region is treated atomistically within the framework of the Born model described above because the forces and resulting atom displacements are too large to be treated properly using continuum theory in this region, which can, nevertheless, be used to model the outer region of the crystal. CASCADE, coded with this two-region approach, was used in this study to calculate the defect energies.

6.2 The Barium-Poor Phase $\text{Ba}_{0.75}\text{Al}_{11}\text{O}_{17.25}$

6.2.1 Calculated Structure

Since $\frac{1}{4}$ of the BR sites are occupied by oxygen and METAPOCS would not recognize partial occupancy, a super-cell for the barium-poor phase was constructed; it

was two times the size of the β -alumina unit cell, with a composition of $\text{Ba}_3\text{Al}_{44}\text{O}_{69}$. There is no ambiguity in the position of cations (such as the different Mg distributions in BAM structure). As METAPOCS uses periodic boundary condition, the input super-cell with different arrangements of the two primitive cells, such as along **a** or **c** direction, would actually generate different periodic lattices, which leads to a problem: are there any specific arrangements for oxygen in the BR sites? Two types of super-cell have been tested for oxygen distributions, $\text{Ba}_3\text{Al}_{44}\text{O}_{69}$ and a larger super-cell of $\text{Ba}_6\text{Al}_{88}\text{O}_{138}$.

For the $\text{Ba}_3\text{Al}_{44}\text{O}_{69}$ super-cell, only two different arrangements exist. One has two primitive cells along the **a** axis (**a**-structure as a 2x1x1 super-cell) and the other has the primitive cells along the **c** axis (**c**-structure as a 1x1x2 super-cell). After relaxation with METAPOCS, these two structures gave quite different lattice energies. The **a**-structure had a lattice energy of -3588.75eV , lower than -3582.53eV , the lattice energy of the **c**-structure. The 6.22eV difference is very large. When looking at the relaxed structures, the lattice parameter ϑ was no longer 120° in both **a**- and **c**-structures, and whereas the **c** axis was still perpendicular to the **ab** plane in the **a**-structure, it was not in the **c**-structure. It is clear that the **a**-structure is more stable than the **c**-structure.

For the $\text{Ba}_6\text{Al}_{88}\text{O}_{138}$ super-cell, four primitive-cells were arranged as shown in Fig. 6.1. There are totally eight possible BR sites for the two oxygen ions. If the symmetrically similar ones are discounted, only five structures are left to be tested. Based on the locations of the oxygen ions, they were labeled as 1-2, 1-3, 1-5, 1-6 and 1-7; the two digits refer to the regions of the two O_{BR} sites.

From Table VI.1, the 1-3 structure had the lowest lattice energy out of the five structures, but the energy was bigger than twice the lattice energy of the 2x1x1 super-cell. This was surprising because the 1-2 structure is just two 2x1x1 super-cells put together and it was expected that the lattice energy of 1-2 super-cell should be double the lattice energy of 2x1x1 super-cell. On examining the relaxed structure, it could be seen that there was a Reidinger defect formed automatically in the 2x1x1 super-cell but not in the 1-2 structure. The 1-3 structure formed only half a Reidinger defect, which causes its lattice energy to be a lot smaller than that of the 1-2 super-cell. So it was the Reidinger defect that made oxygen more stable in the conduction plane. Then those five structures

and two small super-cells were recalculated. This time, Reidinger defects were constructed at O_{BR} for all super-cells before the structure was relaxed.

Table VI.1. Lattice Energies of Five Structures

Structure	1-2	1-3	1-5	1-6	1-7
E_{latt} (eV)	-7152.54	-7174.89	-7155.51	-7155.51	-7155.29

Table VI.2. Lattice Energies of Five Structures (with Reidinger-Defect)
 2x1x1 super-cell: -3589.44 eV 1x1x2 super-cell: -3577.85 eV

Structure	1-2	1-3	1-5	1-6	1-7
E_{latt} (eV)	-7178.88	-7178.88	-7174.72	-7174.49	-7175.85

After the recalculation, both the 1-2 and 1-3 super-cells (Fig. 6.2,6.3) had lattice energies exactly twice of the 2x1x1 super-cell, which was what was expected. It should be mentioned that when forming the Reidinger defect, two Al(1) ions were displaced toward the mirror plane from the spinel block. The two Al(1) ions with the same x and y coordinates were moved at the same time so that the mirror symmetry was kept. There are three Al(1) ions above and below the mirror plane that can be displaced. Consistent with the work of Park, the lattice energy varied with which Al(1) was displaced, but the lattice energy variance was so small (like BAM) that there is no specific configuration for the barium-poor phase; all structures are likely to coexist at the same time.¹¹ The lattice energy difference in Table VI.2 might seem to be large but the difference per formula unit is small after they are normalized according to the size of the super-cell.

Two O_{BR} ions did not come close to each other to form a three-oxygen arrangement with another oxygen ion at normal site, in a similar way to the magnetoplumbite structure, because no aluminum ions are available to be put in the conduction plane to stabilize them and because barium magnetoplumbite does not exist. The super-cell with a three-oxygen cluster was calculated to have a lattice energy of -7175.82eV, that was, indeed, higher than for the 1-2 structure.

6.2.2 Solid Solution

BAM and the barium-poor phase form a complete solid solution as the X-ray diffraction pattern indicates.¹³ It is of great interest to study this kind of behavior. A 4x4x1 super-cell was constructed to calculate the energy of solid solutions with BAM phase percentages of 100, 75, 50, 25 and 0. The number of primitive cells of the BAM phase in the super-cell was varied according to the ratio. Then the super-cells were relaxed with METAPOCS. All of the tests reached stable structures, whose lattice energies are plotted in Fig. 6.4 with respect to the concentration. The lattice energies listed have been divided by the number of primitive cells in the super-cell.

Although these two phases have different structures, the lattice energy changes linearly with the concentration, which means that there is no preferred composition in between BAM and barium-poor phase, i.e. the solid solution is thermodynamically stable. Since the main difference between these two phases lies in the barium-oxygen plane structure and the lattice mismatch between BAM and barium-poor phase is small (0.02 Å in the *c* axis and 0.03 Å in other two axes), it is no surprise for them to form a complete solid solution across the entire composition range. The small lattice mismatch determines the small relaxation of structure of the solid solution so the lattice energy is just the weighted average of two lattice energies. Actually, the barium-poor phase can be treated just like a defect BAM structure.

6.2.3 Intrinsic Defects

The 2x1x1 super-cell and the 1-3 super-cell were chosen for the calculation of the defect properties of the barium-poor phase, because they have the same lattice energy but different oxygen distributions. As the 2x1x1 super-cell is just half of the 1-2 super-cell, the 2x1x1 super-cell will be referred to as the 1-2 structure in later discussion. The defect properties of the super-cell with the lowest lattice energy of -7182.26eV in Park's work, named the b1 structure (see Fig. 6.5), were also investigated.¹¹ Two O_{BR} were put in the same primitive cell but in different mirror planes in the b1 structure (see Figs. 6.6, 6.7), in contrast to the 1-2 and 1-3 structures, where the two O_{BR} were on the same mirror plane, but in different primitive cells.

Table VI.3 lists the vacancy point defects, for the three super-cells. For simplicity, the classification of ion positions was referenced to β -alumina, although the symmetry will have changed. O_{BR} was labeled as O(6). The point defect energy listed in the table was the lowest one calculated for each type of defect.

Table VI.3. Vacancy Defect Energies of Super-Cells

Defect	Defect Energy (eV) in 1-2 Super-cell	Defect Energy (eV) in 1-3 Super-cell	Defect Energy (eV) in b1 Structure
$V_{Ba}''^*$	15.67	15.49	16.36 ¹
$V_{Ba}''^{**}$	17.89	17.75	16.71 ²
$V_{Al(1)}'''$	55.19	55.19	55.77
$V_{Al(2)}'''$	58.12	57.77	58.55
$V_{Al(3)}'''$	57.67	57.30	58.41
$V_{Al(4)}'''$	55.72	55.37	55.59
$V_{O(1)}''$	23.31	23.15	24.21
$V_{O(2)}''$	23.76	23.60	24.39
$V_{O(3)}''$	23.37	23.22	23.29
$V_{O(4)}''$	22.81	22.65	23.98
$V_{O(5)}''$	24.65	18.20	24.99
$V_{O(6)}''$	18.37	24.50	20.68

* Mirror plane without O_{BR} . ** Mirror plane with O_{BR} .

1 Far away from O_{BR} .

2 Close to O_{BR} .

Defect energies for the first two super-cells were similar, but not the same. Oxygen vacancies occurred at different positions in the mirror plane, because of the different arrangements of the oxygen ions. As two O_{BR} ions were separated in different mirror planes of the b1 super-cell, the defect energy also changed, especially for barium and oxygen vacancies. However, the positions for the oxygen vacancy were in the mirror plane for all structures, which is the result of the high oxygen concentration there. That is

not the case for the BAM structure for which the oxygen vacancy resides inside the spinel block. Vacancies of Al(1) and Al(4) were found to have similar defect energies for all three structures. Al(4) was the energetically favorite vacancy position for the 1-2 and 1-3 super-cells but not for the b1 super-cell, for which vacancy at the Al(1) site had the lowest energy.

The barium vacancy tended to occur far away from O_{BR} . That is because the two defects have the same sign of effective charge. They can not occur together or there will form a negative charge-rich region that will increase the system energy.

Because the super-cells were so large and complicated, a program was designed to scan sites, or interstitial positions, inside the structure and choose those sites with a radius large enough for the interstitial ion, as well as finding positions having special symmetry elements (such as lying on a rotation axis). The size of an interstitial site was defined as the distance to its nearest neighboring ion. Totally, about 400 interstitial positions were calculated for each structure. The energy and position of point defects, for each structure, are shown in Tables 6.4-6. The energy and position of vacancies are also included.

Table VI.4. Point Defects of 1-2 Super-Cell

Defect	Defect Energy (eV)	Defect Position
V_{Al}'''	55.19	Al(1) site
V_{Ba}''	15.67	BR in the mirror plane without O_{BR}
V_O''	18.37	O_{BR}
Al_i'''	-46.84	Between two O_{BR}
Ba_i''	-14.38	Between O(5) and O_{BR}
O_i''	-15.84	Change Al(2) tetrahedron to pentahedron

In the 1-2 super-cell, only one of the two mirror planes contains O_{BR} and is negatively charged. A barium vacancy has an effective negative charge, so that it is not energetically favorable for it to reside in the mirror plane with O_{BR} . For the same reason, an oxygen vacancy tends to lower the negative charge concentration in the O_{BR} plane. Interstitial cations also resided close to O_{BR} to compensate the negative charge. The oxygen interstitial did not stay in the mirror plane; instead it entered into the spinel block and changed the coordination number of one Al(2) ion from 4 to 5. The reason for that is

believed to be the positive charge of the spinel block, $[Al_{11}O_{16}]^{1+}$. The two mirror planes in the super-cell have the chemical formula of $[Ba_4O_4]$ and $[Ba_2O_6]^{8-}$. An oxygen interstitial ion in the mirror plane will increase the local charge more than in the spinel block.

Table VI.5. Point Defects of 1-3 Super-Cell

Defect	Defect Energy (eV)	Defect Position
V_{Al}'''	54.83	Al(1) site
V_{Ba}''	15.49	BR site in the mirror plane without O_{BR}
V_O''	18.20	O(5) in O_{BR} plane
Al_i'''	-47.80	V_{Al} of Reidinger defect
Ba_i''	-14.53	Between two O(5) in O_{BR} plane
O_i''	-16.01	Change Al(2) tetrahedron to pentahedron

Point-defect positions in the 1-3 super-cell were similar to those in the 1-2 super-cell except for the aluminum interstitial ion. All defects with a positive effective charge, other than the Al interstitial were found on the O_{BR} plane. The aluminum interstitial ion occupied the vacant aluminum site formed by the Reidinger defect. An oxygen interstitial ion at the mOB site in the mirror plane, the oxygen interstitial position of the configuration II of BAM, had very small defect energy but was still 0.1eV higher than in the spinel block.

Table VI.6. Point Defects of b1 Super-Cell

Defect	Defect Energy (eV)	Defect Position
V_{Al}'''	55.59	Al(4) site
V_{Ba}''	16.36	BR site far away from O_{BR}
V_O''	20.68	O_{BR}
Al_i'''	-45.64	V_{Al} of Reidinger defect
Ba_i''	-13.06	anti-BR close to O_{BR}
O_i''	-17.09	mOB in mirror plane

Since both mirror planes of the b1 super-cell had an O_{BR} , the oxygen concentration in the mirror plane was less than for the mirror planes of the other two structures. It was possible for the oxygen interstitial ion to reside in the mirror plane and form a defect

configuration like in BAM; the oxygen interstitial ion stayed at the mOB site, a position between a barium and an nearby O(5), and formed a two-bridge configuration as in BAM. The aluminum vacancy changed from the Al(1) site in the 1-2 and 1-3 super-cells to the Al(4) site in the b1 super-cell. The aluminum interstitial ion, like in the 1-3 super-cell, took the vacancy generated by the Al(1) shifting toward the mirror plane in forming a Reidinger defect.

Table VI.7 lists the intrinsic defect energies of the three super-cells. These energies were normalized to energies per point defect in order to be comparable. For all structures, the Barium Frenkel defect held the lowest defect energy, which means the Barium Frenkel defect is expected to be the predominant thermal defect, the same as in BAM. The intrinsic defect with the second lowest defect energy was different for each super-cell.

Table VI.7. Intrinsic Defect Energies of Super-Cells (eV)

Defect	1-2 Super-cell	1-3 Super-cell	b1 Structure
Schottky	1.32	1.08	2.85
Al Frenkel	4.18	3.52	4.98
Ba Frenkel	0.25	0.48	1.65
O Frenkel	1.27	1.10	1.80

It seems that the oxygen distributions changed the defect energies and defect positions, but maintained the lattice energies in a small range for all three structures. The effect of oxygen distribution is long-range; it changes the Madelung potential at each ion. The different charge distributions caused by different O_{BR} distributions changed the locations of defects, which seemed to be a local charge effect. The large number of possible oxygen distributions makes the defect properties of barium-poor phase very complex.

6.2.4 Eu Locations

It has been found from our earlier calculations that europium divalent ions occupy two different positions in the barium-poor phase, with one in the Beevers-Ross site and the other inside the spinel block. The Eu^{2+} ions in BR sites will emit blue light while those inside the spinel block will emit green light.¹ We have calculated the extrinsic defects associated with the europium ions and possible mechanisms for doping. For the doping process, europium ions were assumed to substitute for aluminum or for barium in addition to considering interstitial positions.

Table VI.8. Europium Point Defects in the Three Super-Cells

Defect	1-2 Super-cell		1-3Super-cell		b1 Super-cell	
	Energy (eV)	Position	Energy (eV)	Position	Energy (eV)	Position
Eu_{Ba}	-1.44	BR site in the mirror plane with O_{BR}	-1.42	BR site in the mirror plane with O_{BR}	-1.34	BR site close to O_{BR}
Eu'_{Al}	39.09	Al(2)	39.06	Al(3) beside mirror plane without O_{BR}	38.81	Al(3) in the primitive cell without O_{BR}
$\text{Eu}_i^{\bullet\bullet}$	-16.26	Between two O(5)	-16.41	Between two O(5)	-14.86	anti-BR site close to O_{BR}
$\text{Eu}_{\text{Ba}}^{\bullet}$	-22.76	BR site in the Mirror plane with O_{BR}	-22.78	BR site in the mirror plane with O_{BR}	-22.17	BR site
Eu_{Al}	14.4	Al in Reidinger defect	14.40	Al in Reidinger defect	14.44	Al(3) in the primitive cell with O_{BR}
$\text{Eu}_i^{\bullet\bullet\bullet}$	-37.36	Center of rectangle with $2\text{O}(5)$ and 2O_{BR}	-37.74	Center of rectangle with $2\text{O}(5)$ and 2O_{BR}	-38.81	anti-BR site close to O_{BR}

The preferred positions of europium point defects were similar in each super-cell except for the europium divalent ion substituting for aluminum. For the 1-2 super-cell, the divalent europium ion would substitute on the Al(2) site, the same as in BAM. The Al(1) ion, moving close to the mirror plane to form a Reidinger defect, was substituted in the 1-3 super-cell. Although these two positions are different in space, they are both tetrahedral positions. In the b1 structure, the Al(3) ion was substituted by both divalent

and trivalent Eu. Actually, the Al(3) ion can be considered to be the same as the Al(1) ion in the Reidinger defect, i.e. they both were shifted from octahedral sites to stabilize the oxygen ions in the mirror plane, but the shift of Al(3) becomes part of the structure.

In all three structures, substitutions of aluminum at the edge of spinel block by Eu^{3+} ion had the lowest point defect energy in Eu_{Al} substitution. The mirror plane with O_{BR} has a chemical formula $[\text{Ba}_2\text{O}_6]^{8-}$, so it is no surprise to see point defects with positive net charge prefers to be in or close to it. As seen in Table VI.9, there are many ways for Eu to enter into the structure. As point defect energies are not comparable, defect reactions related to these point defects were written down to obtain the reaction enthalpy in order to find the reaction that will dominate the europium doping process.

Table VI.9. Incorporation of Eu into Super-Cells

Reaction	Defect Energy (eV)		
	1-2 Super-cell	1-3 Super-cell	b1 Super-cell
$\text{EuO} \rightarrow \text{Eu}_i^{\bullet\bullet} + \text{O}_i^{\bullet}$	1.10	0.78	1.25
$\text{EuO} \rightarrow \text{Eu}_{\text{Al}}^{\bullet} + \text{Al}_i^{\bullet\bullet\bullet} + \text{O}_i^{\bullet}$	9.61	8.45	9.28
$\text{EuO} \rightarrow 1/2\text{Al}_2\text{O}_3 + \text{Eu}_{\text{Al}}^{\bullet} + 1/2\text{V}_\text{O}^{\bullet\bullet}$	2.09	1.97	2.96
$\text{EuO} \rightarrow \text{BaO} + \text{Eu}_{\text{Ba}}$	0.45	0.47	0.55
$\text{EuO} \rightarrow \text{Eu}_i^{\bullet\bullet} + \text{V}_{\text{Ba}}^{\bullet} + \text{BaO}$	1.30	0.97	3.39
$1/2\text{Eu}_2\text{O}_3 \rightarrow \text{Eu}_i^{\bullet\bullet\bullet} + 3/2\text{O}_i^{\bullet}$	4.32	3.69	4.57
$1/2\text{Eu}_2\text{O}_3 \rightarrow \text{Eu}_{\text{Al}}^{\bullet} + \text{Al}_i^{\bullet\bullet\bullet} + 3/2\text{O}_i^{\bullet}$	9.24	8.03	8.79
$1/2\text{Eu}_2\text{O}_3 \rightarrow \text{Eu}_{\text{Al}}^{\bullet} + 1/2\text{Al}_2\text{O}_3$	0.45	0.45	0.49
$1/2\text{Eu}_2\text{O}_3 \rightarrow \text{Eu}_{\text{Ba}}^{\bullet} + \text{BaO} + 1/2\text{O}_i^{\bullet}$	3.45	3.35	3.42

As seen in Table VI.9, divalent europium ions substituted for barium ions in BR sites. However, trivalent ions substituted for aluminum in the Reidinger defects instead of Al(2) observed in the BAM structure; the similarity is that both positions are inside oxygen tetrahedra. Based on the work of Ronda and Smets, there may be two positions for europium divalent ions.² They have suggested that one was in the mirror plane and

the other was inside the spinel block. But Eu^{2+} substituting aluminum in the spinel block requires a lot more energy than staying in the mirror plane and the reaction with the second lowest enthalpy is for an Eu^{2+} interstitial ion in the mirror plane.

Actually, there are at least two different BR sites in each structure of the barium-poor phase (see Fig. 6.8); they are different in their distances from O_{BR} . The difference in substitution energy for these two BR sites was 0.14eV (0.01eV for the b1 super-cell). The energy difference was so small (at least for the b1 super-cell) that both barium ions in the two sites could be substituted by Eu^{2+} ions. Figure 6.6 displays the difference between the environments of europium ions in the two sites of the 1-2 super-cell. It is clear that ligand field effects will alter the band structure of the active ion, i.e. the environment will change the emission band of europium ions. The europium ions in different BR sites will definitely emit different wavelengths of luminescence. The structure complexity and large population of different BR sites give a good explanation of the emission band broadening.

6.3 Emission Band Calculations

Two bands have been suggested in the broad emission band of the barium-poor phase containing Eu^{2+} , one is 440nm and the other is about 550nm.^{1,13} The characteristic luminescence originates from the electronic transition $4f^65d^1 \rightarrow 4f^7$. This transition is heavily affected by the interaction between the active ion and its surrounding ions. As reported, the position of the d-band edge in energy (E) for Eu can be estimated by the empirical equation:¹⁴

$$E = Q \left[1 - \left(\frac{V}{4} \right)^{1/V} 10^{-(n \times ea \times r)/80} \right] (\text{cm}^{-1}). \quad (7)$$

V is the charge of the ion being substituted and Q is the energy value of the d-band edge of free ion. The Q value is 34000cm^{-1} for Eu^{2+} and 80800cm^{-1} for Eu^{3+} ions.¹⁵ n is the coordination number of the active ion, ea is the electron affinity of the surrounding ions (1.60 for oxygen ions) and r is the radius of cation replaced by the active ion in the host crystal. If the emission bands are already known, it is possible to estimate the coordination number of the active ion inside the crystal by rewriting equation (7) to:

$$n = -\text{Log} \left[\left(1 - \frac{E}{Q} \right) \cdot \left(\frac{V}{4} \right)^{-1/V} \right] \times 80 / ea / r. \quad (8)$$

Two kinds of cation exist in the barium-poor phase, Ba²⁺ and Al³⁺. Emission bands are calculated for Eu²⁺ and Eu³⁺ ions in these positions.

Table VI.10. Estimated Emission Wavelength of Eu

Eu ²⁺ Position	V	n	r(Å)	E(cm ⁻¹)	Wavelength (nm)
Ba ¹	2	9	1.47	20300	480
Ba ²	2	10	1.52	21100	450
Al(1)	3	6	0.675	8400	1200
Al(2)	3	4	0.53	6000	1670
Eu ³⁺ Position	V	n	r(Å)	E(cm ⁻¹)	Wavelength (nm)
Ba ¹	2	9	1.47	48100	200
Ba ²	2	10	1.52	50100	190
Ba ³	2	12	1.61	53700	170
Al(1)	3	6	0.675	19900	500
Al(2)	3	4	0.53	14200	700

1 Normal BR site

2 BR site with an O_{BR} around

3 BR site in Magnetoplumbite

Since equation 7 is just an empirical function, the calculated emission band would not be precisely the same as the measurement of experiment. But it can give a idea of the change in the emission band of europium in the barium-poor phase compared with BAM:Eu²⁺. A divalent europium ion in the normal BR site is estimated to emit light of 480nm wavelength from the calculation. Although that is different from the measured 440nm, this empirical function can give an idea of how the coordination conditions change emission.

The emission calculation shows that divalent europium substituting for aluminum will emit light with wavelength so much larger than the measured spectrum that the observed broad emission band would not come from the Eu²⁺ ion in the spinel block. Instead, the existence of O_{BR} inside the mirror plane is more likely to change the emission

characteristics of the europium ion. The actual structure of the barium-poor phase will be more complex than this because of multiple O_{BR} -configurations: this is the key to understanding the broadening of the emission band. Because the emission band not only becomes broad but also shifts toward the large wavelengths, two Eu^{2+} positions are suggested.

Actually, the above empirical equation only considered the ligand field generated by the first coordination ions. Although ligand field coming from second or higher order coordination ions might be small, it would also vary the band structure of the center ion; it is the whole structure that determines the band structure of individual ion. Thus, the site energies (potential of the whole structure acting on that site) of BR positions are compared to see whether there is any ‘big’ difference that can explain the emission band shift and broadening.

Table VI.11. Site Energy Comparison of Eu^{2+} Positions

Structure	Site	E_M (eV)	E_S (eV)	E_t (eV)
BAM (Conf. I)	BR	-12.45	1.74	-10.71
BAM(Conf. II)	BR	-12.77 -12.11	1.75 1.73	-11.02 -10.38
BAM-II*	BR	-12.49	1.76	-10.73
1-2 Super-cell	BR	-11.98 -12.97	1.79 1.81	-10.19 -11.16
1-3 Super-cell	BR	-11.98 -12.97	1.79 1.81	-10.19 -11.16
b1 Super-cell	BR	-12.42	1.75	-10.67

E_M : Madelung Energy E_S : Short-range Energy E_t : Total Energy

*: β''' phase with extended spinel blocks

All of the BR site energies in BAM and barium-poor phase are similar, but the site energy varies for different barium-poor structures, which again supports the emission broadening effect of different oxygen distributions. The BR positions on the two different mirror planes of configuration II of BAM have different site energies; the difference is about 0.64eV in total site energy. The small change in their short-range energies is because of the large separation between the Mg position and the conduction plane; relaxation around Mg becomes small at that separation, but the charge effect is a

long-range effect. The site energy difference caused by the Mg-distribution can explain the round-shape of the emission band observed in BAM:Eu²⁺, instead of the sharp-shape.

Since the site energy of the BR position in the b1 super-cell is very close to that of the BR site in BAM, Eu²⁺ in the b1 structure will also show an emission band at around 440nm. The 0.02eV difference of E_t between BAM and BAM-II has shifted the emission band to 467nm.¹⁶ Therefore, it may be said that the 0.35eV difference between the barium-poor phase and BAM will shift the emission band even more in the same direction. Even between the three structures of the barium-poor phase, there is a 0.97eV site-energy difference: no wonder the emission band of the barium-poor phase will become much broader, in considering there are a total of 10 possible structures. Thus the multiple configurations of the barium-poor phase not only broaden the emission band, but also shift it.

It is interesting to see in Table VI.10 that trivalent europium ions in the Al(1) octahedral position will also emit light in the range of observed emission band, but at a wavelength higher than Eu²⁺. It is believed that Eu³⁺ may also contribute to the shape change of the emission band of the barium-poor phase, from the fact that a small amount of Eu³⁺ may occur during the manufacture, coupled with the possibility of Eu³⁺ migrating from mirror plane into the spinel blocks.

As shown above, the barium-poor phase when doped with europium, will have an emission band with a broader range than BAM:Eu²⁺. The variation of the site potential at Eu²⁺ positions will shift the chromaticity from blue to blue-green, similar to the phenomenon of the degradation of BAM:Eu²⁺.¹³ It implies that the degradation mechanism in BAM may include the formation of the barium-poor phase. The suggested formation of EuMgAl₁₁O₁₉ can not explain the shift in emission band. From Table VI.11, if EuMgAl₁₁O₁₉ is formed, the Eu³⁺ ion should emit at a wavelength of 170nm, which is not in the observed emission band. But the Eu³⁺ ion substituting for aluminum shows emission with the right wavelength, so the observed luminescence of Eu³⁺ in the degraded emission band should come from the europium at tetrahedral sites.

6.4 Ba₃Al₃₂O₅₁

6.4.1 Structure

To use an aluminum vacancy as the charge compensation mechanism for barium substituting for sodium, a $\sqrt{3} \times \sqrt{3}$ super-cell was constructed. There was one aluminum vacancy for every three barium ions substituted and then the super-cell must include $3n$ (n is an integer) barium ions in order to generate an integer number of Al vacancies in the super-cell. If one simply expands the primitive cell to a $1 \times 3 \times 1$ super-cell, the structure will lose many symmetry elements and make the defect investigation more complex. In Fig. 6.9, a new unit cell is drawn out of the array of primitive cells. The new unit cell keeps the same symmetry elements while the cell parameter a is $\sqrt{3}$ times that of the primitive cell. Totally six barium ions were in the unit cell with three of them on each mirror plane. Since the origin of the primitive cell was not the same as the new unit cell, the coordinates of ions had to be transformed to the new axes. Two matrix operations were applied to the coordinates:

$$\begin{pmatrix} x' \\ y' \\ z' \end{pmatrix} = \begin{pmatrix} x \\ y \\ z \end{pmatrix} - \begin{pmatrix} a \\ 0 \\ 0 \end{pmatrix} \quad (5)$$

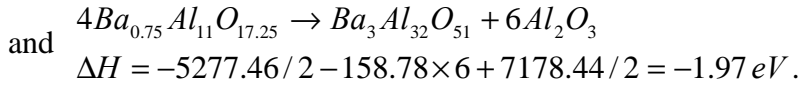
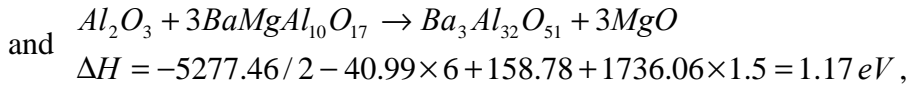
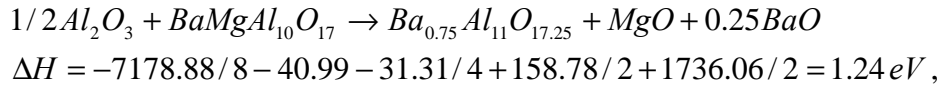
$$\text{and } \begin{pmatrix} x'' \\ y'' \\ z'' \end{pmatrix} = \begin{pmatrix} \cos 150^\circ & \cos 60^\circ & 0 \\ -\cos 60^\circ & \cos 150^\circ & 0 \\ 0 & 0 & 1 \end{pmatrix} \cdot \begin{pmatrix} x' \\ y' \\ z' \end{pmatrix}. \quad (6)$$

The positions of the V_{Al} are the next consideration after the transformation of the coordinates. Since there are six barium ions in the unit cell, two aluminum vacancies must exist in it. To achieve a lower lattice energy, i.e. a more stable structure, two aluminum ions in the same symmetry positions are taken out, so that the loss of symmetry will be minimized. The four symmetrically independent positions of aluminum in the β phase mean that four possible structures exist and their lattice energies are compared in Table VI.12.

Table VI.12. Lattice Energies of Four Possible Structures

Two V_{Al}	Al(1)	Al(2)	Al(3)	Al(4)
E_{latt} (eV)	-5273.82	-5270.12	-5270.53	-5277.46

The Al(4) ion is in the octahedral site of the mid-spinel block, separating two tetrahedral Al(2) ions. The introduction of an Al(4) vacancy made the structure collapse a little along the *c* axis and made the tetrahedra in the middle of the spinel blocks relax from their elongated state. The cell parameter *c* became 22.25 Å, 0.4 Å shorter than that of BAM (see Fig. 6.10). Up to now, three ways of transforming β-alumina to barium hexa-aluminate have been shown. Only BAM and barium-poor phases have been seen by experiments. The existence of the third phase, Ba₃Al₃₂O₅₁, is only a hypothesis. This third phase may be not very stable, might easily transform to other phases or it could be hard to distinguish from other phases. Here, we list the stability comparison of these phases:



Of the three phases, BAM is the most stable and Ba₃Al₃₂O₅₁ is the second most stable. It is interesting that alumina is required for BAM to transform to the other two phases and for Ba₃Al₃₂O₅₁ to transform to the barium-poor phase. It seems that a greater ratio of alumina in the structure will diminish the stability of BAM. It is surprising that the aluminum-vacancy phase is more stable than the barium-poor phase but has not been reported yet. It is generally believed that only two types of barium hexa-aluminates containing no ions other than Ba, Al and O, exist.^{17,18} They are the barium-poor phase (ideal formula of Ba_{0.75}Al₁₁O_{17.25}) and the barium-rich phase (ideal formula of Ba₇Al₆₄O₁₀₃).⁵ Since the aluminum-vacancy phase is more stable than the barium-poor phase, its stability is compared with the barium-rich phase as follows (the lattice energy of barium-rich phase is taken from Park's work¹¹):

$$7Ba_3Al_{32}O_{51} \rightarrow 3Ba_7Al_{64}O_{103} + 16Al_2O_3$$

$$\Delta H = 5277.46 \times 3.5 - 5303.74 \times 3 - 158.78 \times 16 = 19.41 eV.$$

It seems that the hypothetical new phase is also more stable than the barium-rich phase so if the new phase is formed it will not transform to either barium-poor or barium-rich phases. Whether or not this phase exist requires further experimental investigations.

6.4.2 Defect Properties

Routinely, all of the intrinsic and extrinsic defects were investigated and the results are shown in Table VI.13. Within four symmetrically independent aluminum positions, the Al(4) vacancy was easy to form compared to other positions, while the Al interstitial ions also tried to occupy the existing Al(4) vacancy in this defect lattice. In $Ba_3Al_{32}O_{51}$, one third of Al(4) positions were left empty so an Al interstitial at the empty Al(4) would decrease the number of defects in the structure and benefit the system stability. It seems that an existing Al(4) vacancy will not prevent other Al(4) vacancies from occurring nearby. An oxygen interstitial ion can reside in the mOB site and form a two-bridge structure as in BAM, but the defect energy (-13.82eV) is higher than if it resides close to the Al(2) ion inside the spinel block that is also the position for the oxygen interstitial in the barium-poor phase. As for the other phases, the barium Frenkel defect is the predominant thermal defect in the crystal.

Table VI.13. Point Defect in $Ba_3Al_{32}O_{51}$

Defect	Defect Energy (eV)	Defect	Defect Energy (eV)
V_{Ba}''	17.37	$Al_i^{*\bullet\bullet}$	-49.37
$V_{Al(1)}'''$	57.41	$Ba_i^{\bullet\bullet}$	-12.07
$V_{Al(2)}'''$	60.86	O_i''	-15.69
$V_{Al(3)}'''$	58.45	Schottky	4.73
$V_{Al(4)}'''$	56.57	Al Frenkel	3.6
$V_{O(1)}^{\bullet\bullet}$	23.25	Ba Frenkel	2.65
$V_{O(2)}^{\bullet\bullet}$	24.97	O Frenkel	3.76
$V_{O(3)}^{\bullet\bullet}$	26.31		
$V_{O(4)}^{\bullet\bullet}$	23.20		
$V_{O(5)}^{\bullet\bullet}$	23.87		

Table VI.14. Europium Point Defects

Defect	Energy (eV)	Position
Eu_{Ba}	-1.48	BR site
Eu'_{Al}	39.57	Al(3)
$Eu_i^{\bullet\bullet}$	-13.68	anti-BR site
Eu_{Ba}^{\bullet}	-22.51	BR site
Eu_{Al}	14.84	Al(3)
$Eu_i^{\bullet\bullet\bullet}$	-32.88	anti-BR site

As can be seen from Table VI.14, both divalent and trivalent europium defects shared the same locations. In this structure, the large europium ion tended to reside in the anti-BR sites in the mirror plane (which has more open space) than in the spinel block as an interstitial ion. It is surprising to see that the interstitial ions did not take the vacant Al(4) positions. The reason is that the structure had collapsed a little when the structure with the Al(4) vacancy was relaxed. Although there is still a vacancy there, its size is not large enough for europium and the surroundings can not fully relax so the defect energy is higher.

From the reaction enthalpies for the europium doping process, the most energetically favorable processes were for divalent europium ions substituting for barium and for trivalent ions substituting for aluminum. Actually, the defect reactions with the lowest enthalpy are the same for BAM, the barium-poor phase, and $Ba_3Al_{32}O_{51}$, with the only difference being the position of aluminum ion. In BAM, it is the Al(2) site being substituted, in $Ba_3Al_{32}O_{51}$ and barium-poor phase it is the Al(3) site. In total, three positions for europium ions have been found: one for divalent ions and two for trivalent ions.

Table VI.15. Defect Reaction of Eu in $Ba_3Al_{32}O_{51}$

Defect Reaction	Enthalpy (eV)
$EuO \rightarrow Eu_i^{\bullet\bullet} + O_i''$	3.83
$EuO \rightarrow 1/2Al_2O_3 + Eu'_{Al} + 1/2V_O^{\bullet\bullet}$	4.98
$EuO \rightarrow BaO + Eu_{Ba}$	0.41
$1/2Eu_2O_3 \rightarrow Eu_i^{\bullet\bullet\bullet} + 3/2O_i''$	9.03
$1/2Eu_2O_3 \rightarrow Eu_{Al} + 1/2Al_2O_3$	0.89
$1/2Eu_2O_3 \rightarrow Eu_{Ba}^{\bullet} + BaO + 1/2O_i''$	3.78

6.5 Conclusions

The barium-poor phase has no unique structure; instead, many kinds of O_{BR} distribution in the mirror plane will coexist in the material. The oxygen ions in the mirror plane are stabilized by forming Reidinger defects. Lattice energies of these configurations vary only slightly. Basically, the defect properties of the barium-poor phase are similar to BAM, with some exceptions. Eu^{3+} ion tends to occupy the Al(3) sites or the aluminum position in a Reidinger defect, rather than the Al(2) inside the spinel block, because of the effective negative charge on the mirror plane with oxygen interstitials. The barium-poor phase has lattice parameters very close to BAM and they can form solid solutions in any component ratio.

Another possible structure, with V_{Al} as the charge compensation mechanism, was also tested. It shows defect properties similar to BAM and a higher stability than the barium-poor and barium-rich phases. The existence of this phase needs further investigation.

The observed broad emission band of $Ba_{0.75}Al_{11}O_{17.25}:Eu^{2+}$ results from the multiple configurations of the barium-poor phase. The distribution of O_{BR} changes the ligand field acting on the ion in the BR position and hence the emission band of the active ion at that position. Since Eu^{2+} ions seem to only reside in the BR position, the emission band will vary for Eu^{2+} ions in BR positions and the total emission band of the material will become broadened and shifted. The second band suggested by Smet² does not come from the Eu^{2+} inside the spinel block. It is just due to the different ligand field effect of multiple configurations. Possibly, it could also come from Eu^{3+} ions in the tetrahedral sites.

The probability of intergrowth of the barium-poor phase and BAM will deteriorate the luminescent property, even without oxidation. As shown in the phase reaction, excess alumina is needed for the barium-poor phase to form. So control of the alumina component may help to control the degradation. Eu^{3+} ions initially formed at the BR site can migrate into aluminum position in the spinel blocks and this will also shift the emission band. Since we have shown that Mg is needed in this migration, the replacement of Mg with other divalent cations in BAM may also prevent Eu^{3+} ions from entering the spinel block and limiting the emission band shift.

References

1. S. Tanaka, I. Ozaki, T. Kunimoto, K. Ohmi, and H. Kobayashi, "Blue Emitting $\text{CaAl}_2\text{O}_4:\text{Eu}^{2+}$ Phosphors for PDP Application," *J. Lumin.*, **87-89**[1] 1250-3 (2000).
2. C.R. Ronda and B.M.J. Smets, "Chemical Composition of and Eu^{2+} Luminescence in the Barium Hexa-aluminates," *J. Electrochem. Soc.*, **136**[2] 570-3 (1989).
3. B.G. Dick and A.W. Overhauser, "Theory of the Dielectric Constants of Alkali Halide Crystals," *Phys. Rev.*, **112**[1] 90-103 (1958).
4. J.G. Park and A.N. Cormack, "Potential Models for Multicomponent Oxides: Hexa-Aluminates," *Philos. Mag.*, **73**[1] 21-31 (1996).
5. J.G. Park and A.N. Cormack, "Crystal/Defect Structures and Phase Stability in Ba Hexa-aluminates," *J. Solid State Chem.*, **121**[1] 278-90 (1996).
6. G.V. Lewis and C.R.A. Catlow, "Potential Models for Ionic Oxides," *J. Phys. C: Solid State Phys.*, **18**[6] 1149-61 (1985).
7. T.B. Forester and W. Smith, *DL_POLY Reference Manual*, 2.0 ed.; pp. 45-7. CCLRC, Daresbury Laboratory, Warrington, England, 1995.
8. C.R.A. Catlow, A.N. Cormack, and F. Theobald, "Structure Prediction of Transition-Metal Oxides using Energy-Minimization Techniques," *Acta Crystallogr., Sect. B: Struct. Sci.*, **B40**[3] 195-200 (1984).
9. A.N. Cormack, "A Perfect Lattice Approach to Nonstoichiometry," *Solid State Ionics*, **8**[1] 187-92 (1983).
10. N.F. Mott and M.J. Littleton, "Conduction in Polar Crystals. I. Electrolytic Conduction in Solid Salts," *Trans. Faraday Soc.*, **34**[1] 485-99 (1938).
11. J.G. Park, "Structure, Stoichiometry and Stability in Magnetoplumbite and β -Alumina Type Ceramics"; Ph.D. Thesis, Alfred University, Alfred, New York, 1995.
12. W.L. Roth, F. Reidinger, and S.L. Placa, "Studies of Stabilization of Transport Mechanisms in Beta and Beta" Alumina by Neutron Diffraction," pp. 223-41 in *Superionic Conductors*. Edited by G. D. Mahan and W. L. Roth. Plenum, New York, 1976.

13. K. Yokota, S. X. Zhang, K. Kimura, and A. Sakamoto, "Eu²⁺-Activated Barium Magnesium Aluminate Phosphor for Plasma Displays - Phase Relation and Mechanism of Thermal Degradation," *J. Lumin.*, **92**[3] 223-7 (2001).
14. L.G.V. Uitert, "An Empirical Relation Fitting the Position in Energy of the Lower d-Band Edge for Eu²⁺ or Ce³⁺ in Various Compounds," *J. Lumin.*, **29**[1] 1-9 (1984).
15. C.K. Jorgensen, "Partly Filled Shells Constituting Anti-bonding Orbitals with Higher Ionization Energy Than Their Bonding Counterparts," pp. 49-82 in *Structure and Bonding*. Edited by J. D. Dunitz, P. Hemmerich, R. H. Holm, J. A. Ibers, C. K. Jorgensen, J. B. Neilands, D. Reinen, and R. J. P. Williams. Springer-Verlag, Berlin, Germany, 1975.
16. D. Ravichandran, S.T. Johnson, S. Erdei, R. Roy, and W.B. White, "Crystal Chemistry and Luminescence of the Eu²⁺-Activated Alkaline Earth Aluminate Phosphors," *Displays*, **19**[4] 197-203 (1999).
17. F.P.F. van Berkel, H.W. Zandbergen, G.C. Verschoor, and D.J.W. Ijdo, "The Structure of Barium Aluminate, Ba_{0.75}Al₁₁O_{17.25}," *Acta Crystallogr., Sect. C: Cryst. Struct. Commun.*, **C40**[7] 1124-7 (1984).
18. S. Kimura, E. Bannai, and I. Shindo, "Phase Relations Relevant to Hexagonal Barium Aluminates," *Mater. Res. Bull.*, **17**[2] 209-15 (1982).

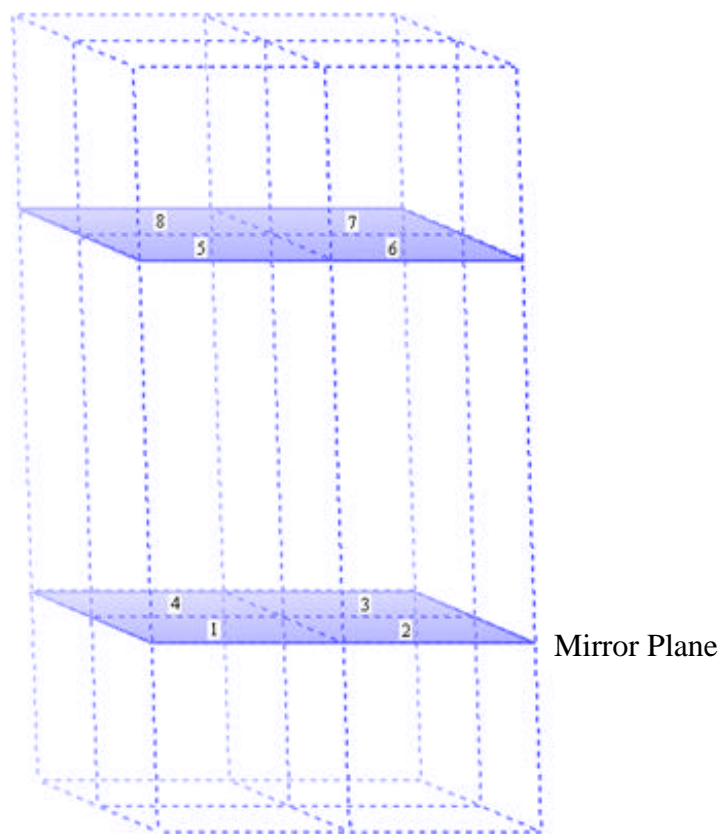


Figure 6.1. $\text{Ba}_6\text{Al}_8\text{O}_{13}$ super-cell.

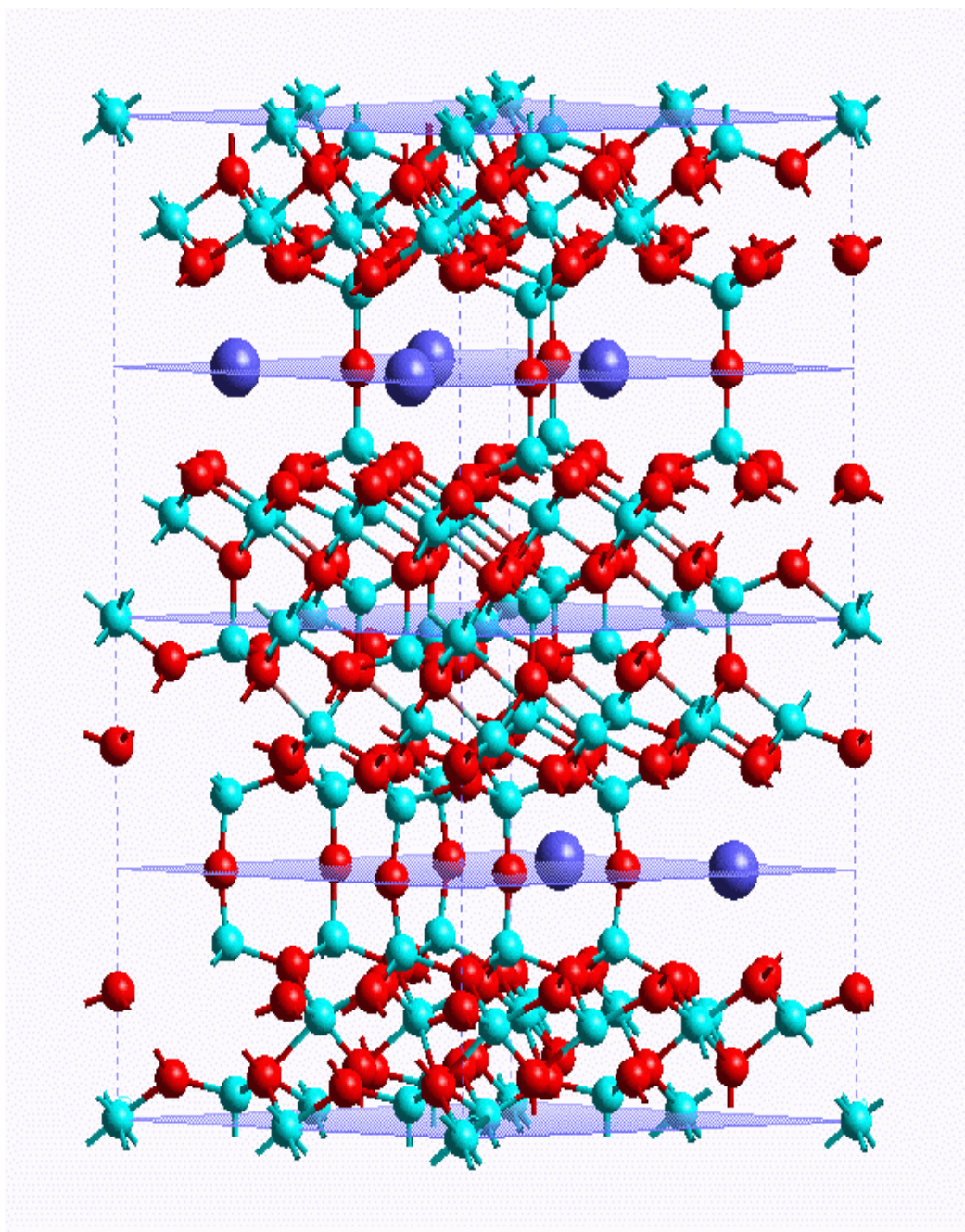


Figure 6.2. Structure of 1-2 super-cell of barium-poor phase.



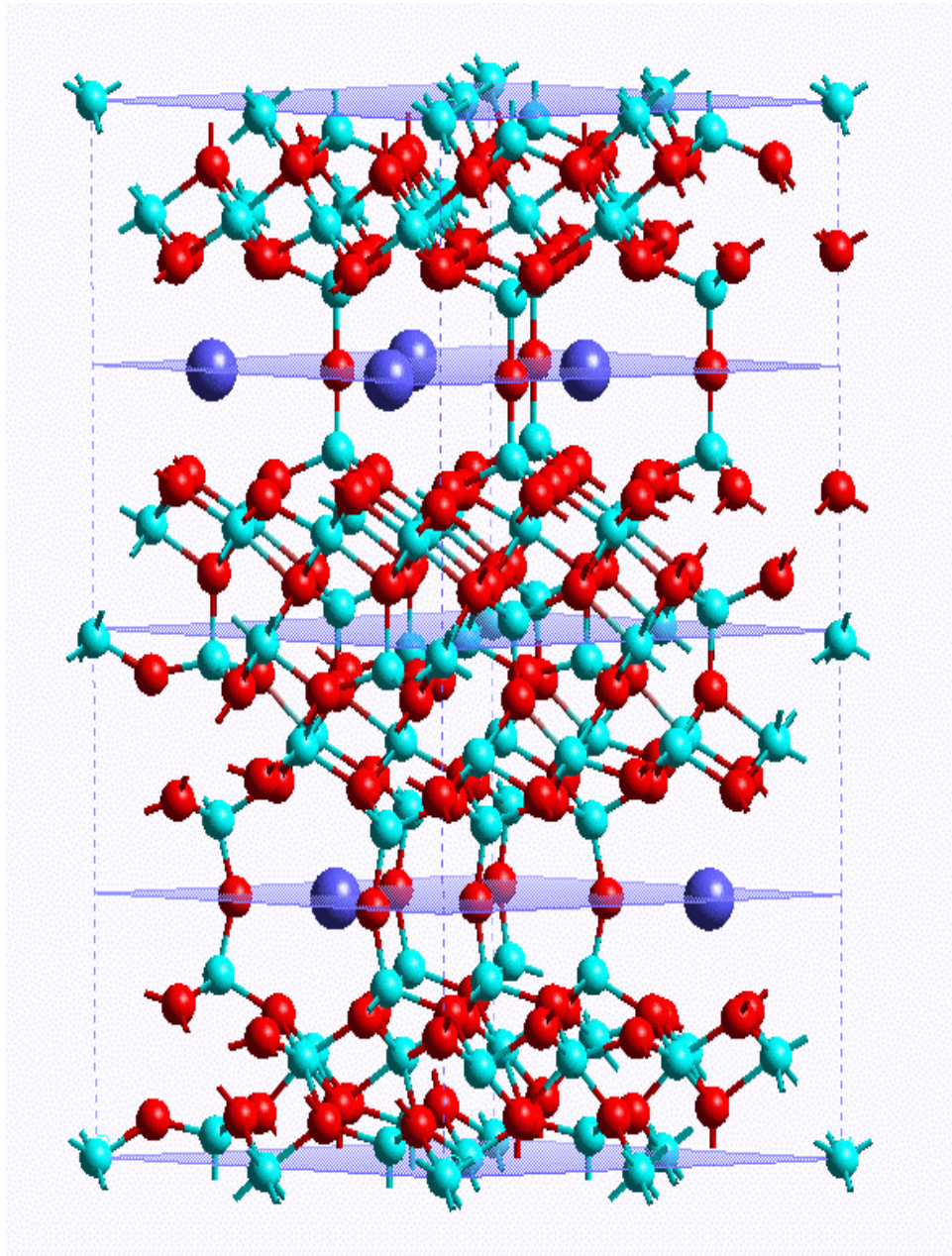


Figure 6.3. Structure of 1-3 super-cell of barium-poor phase.



Lattice Energy of Solid Solution between BAM and Barium Poor Phase

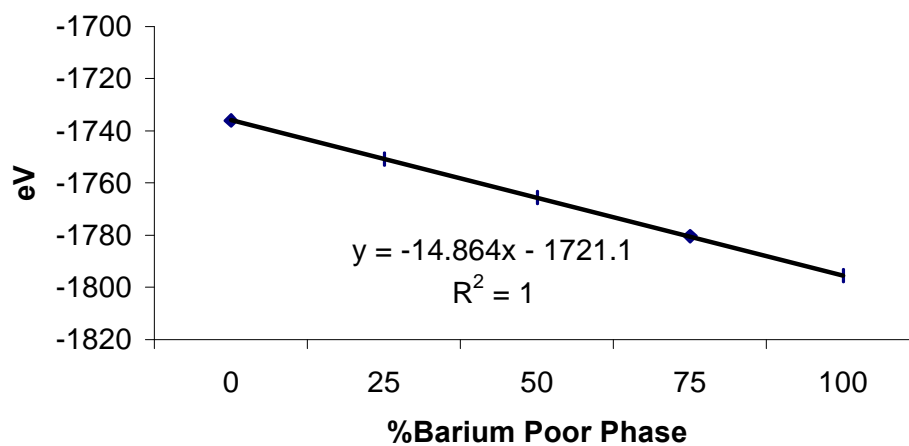


Figure 6.4. Lattice energy of solid solution between BAM and barium-poor phase.

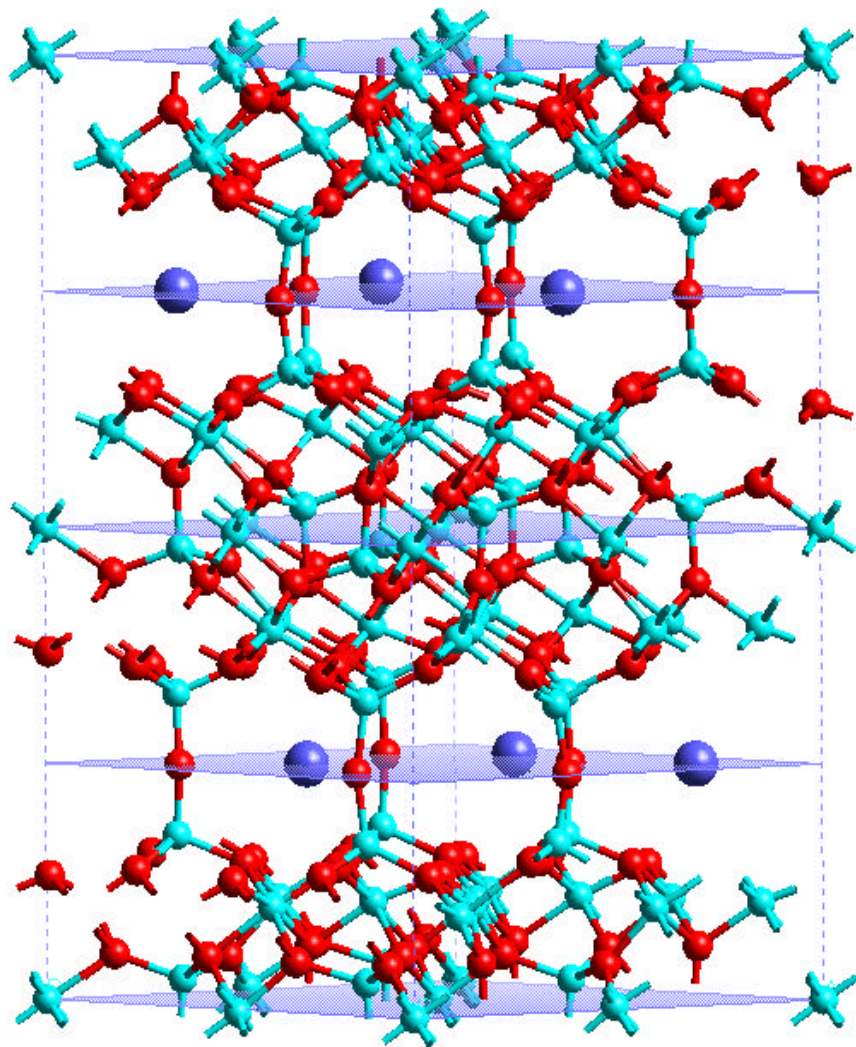


Figure 6.5. Crystal structure of b1 super-cell.



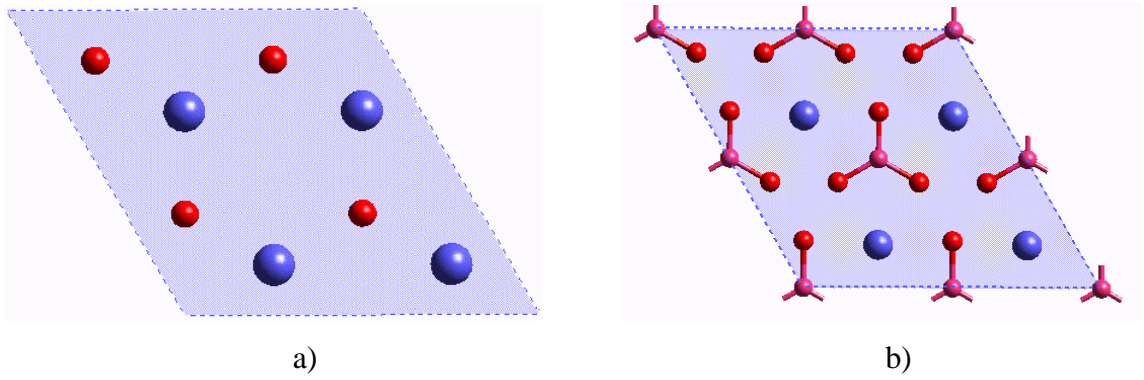


Figure 6.6. Mirror plane structures. a) BAM; b) magnetoplumbite.

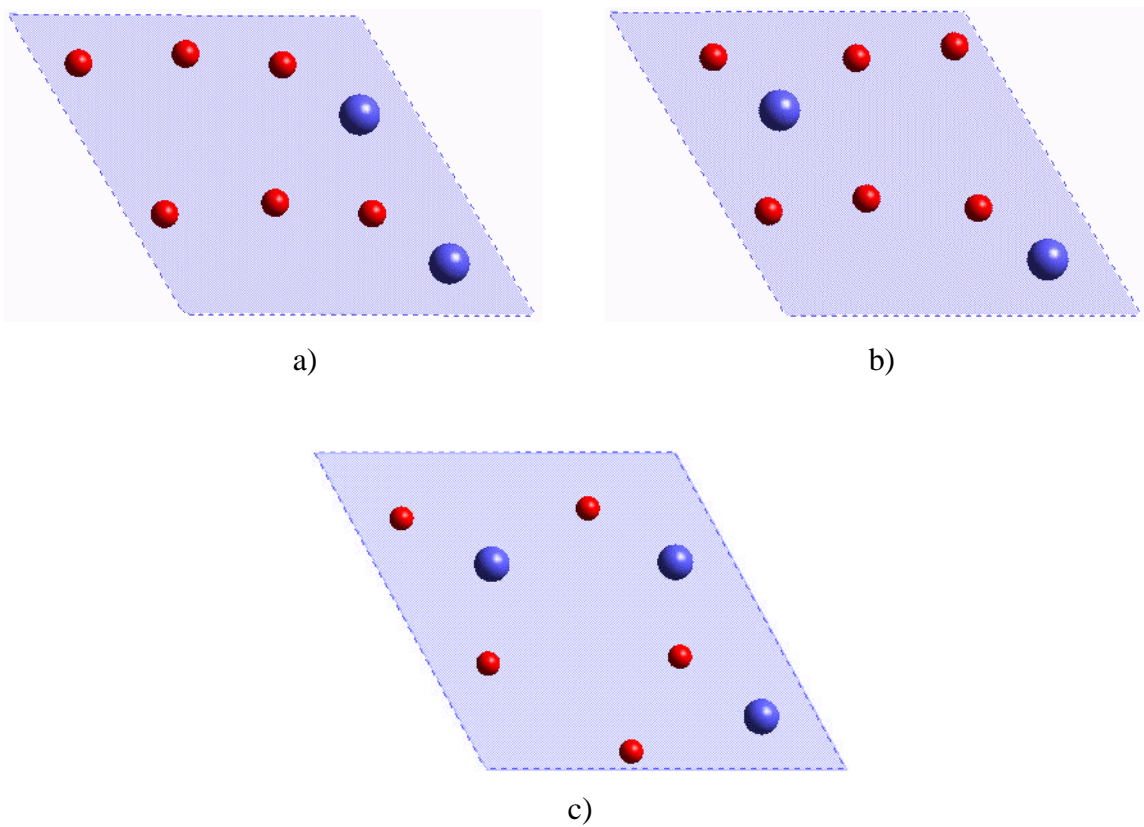
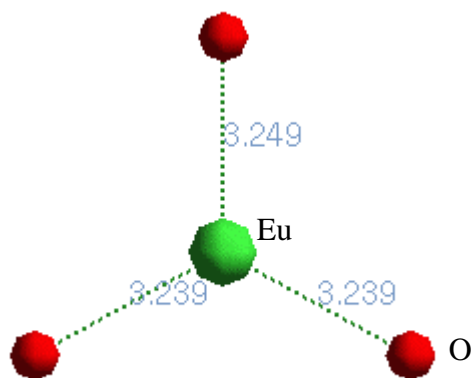
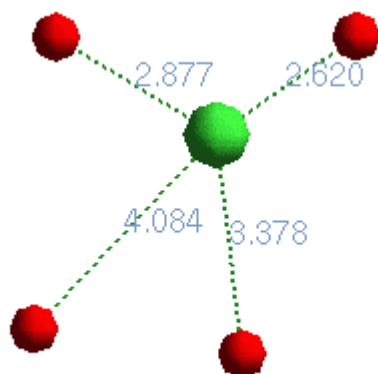


Figure 6.7. a) Mirror plane of 1-2 super-cell; b) Mirror plane of 1-3 super-cell; c) Mirror plane of b1 super-cell.





a)



b)

Figure 6.8. Eu^{2+} environment in mirror plane. a) Associated without O_{BR} ; b) Associated with O_{BR} .

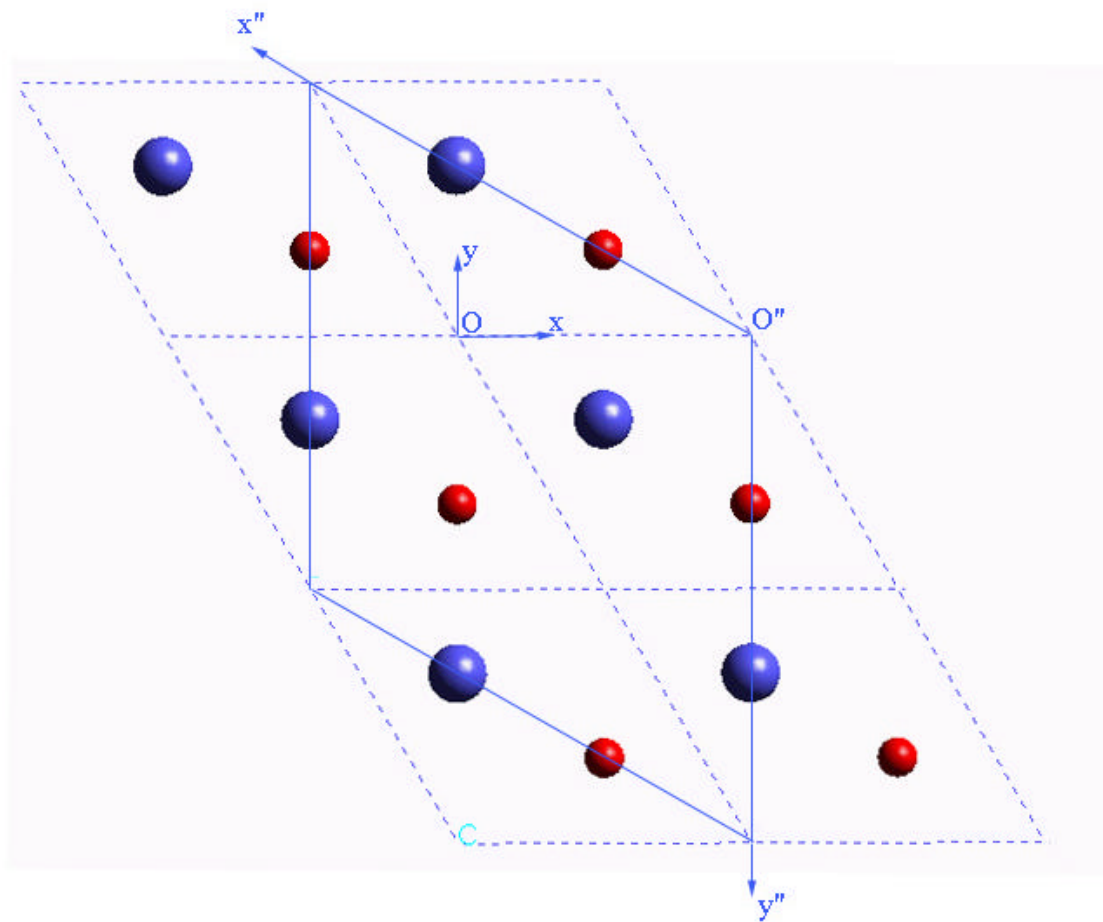


Figure 6.9. Selection of $\sqrt{3} \times \sqrt{3}$ super-cell.

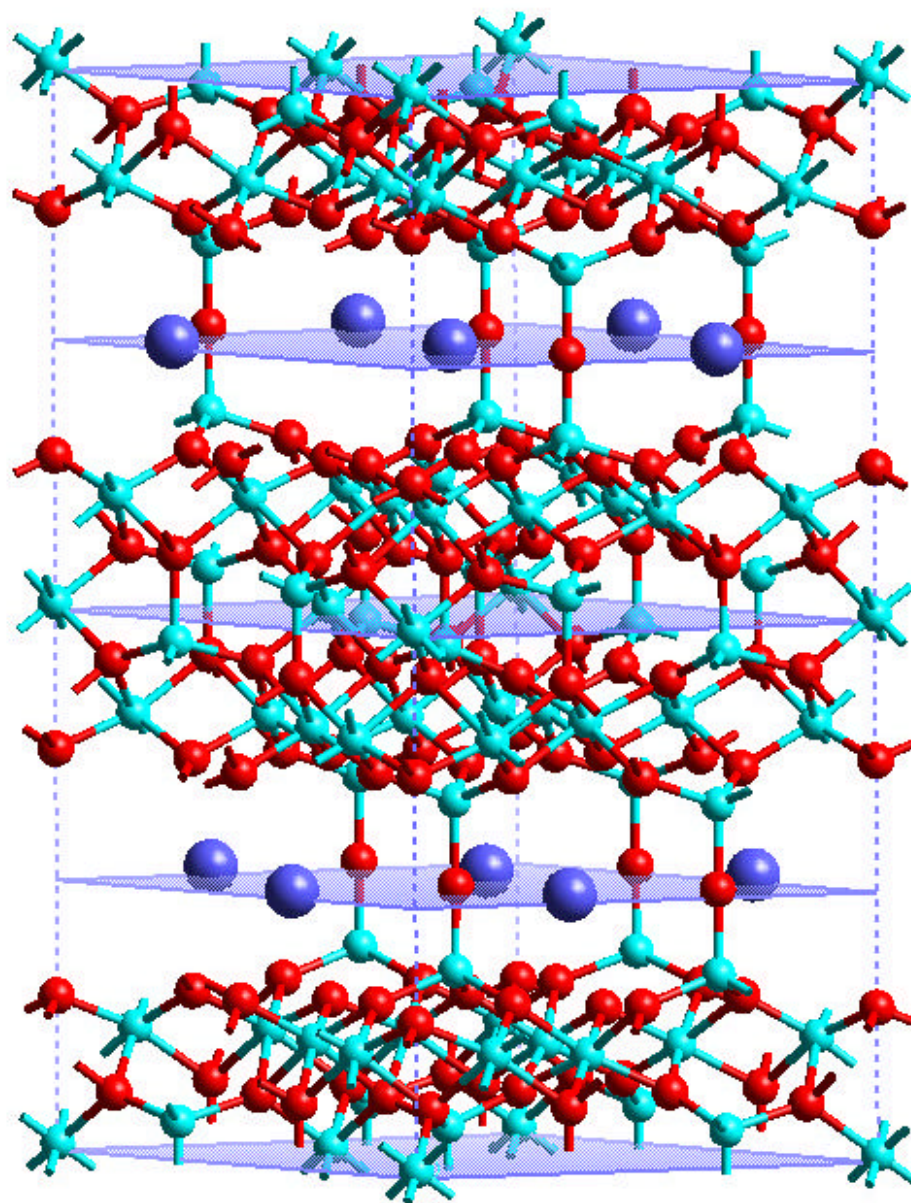


Figure 6.10. $\sqrt{3}\times\sqrt{3}$ unit cell of $\text{Ba}_3\text{Al}_{32}\text{O}_{51}$.



7. Defects in β'' - and β''' - Barium Hexa-aluminates

Abstract:

Lattice and defect properties of barium β'' - and β''' -alumina with structures closely related to $\text{BaMgAl}_{10}\text{O}_{17}$ (BAM, β phase of barium hexa-aluminate), a widely used phosphor host material, have been investigated with computer simulation. Many configurations of the crystal structure have been found to share similar lattice energies. Mg ions are found to distribute inside the structure homogeneously, which stabilizes the lattice more than other Mg distributions. Their intrinsic and Eu extrinsic defects have the same properties as BAM; in particular, Eu^{2+} and Eu^{3+} ions tend to occupy different lattice sites.

Although the β , β'' and β''' phases of barium aluminates doped with Mg have similar chemical formulae and structures, the differences change the emission band of Eu^{2+} ions, providing a possible explanation of the broad emission band observed in BAM:Eu^{2+} . The result also determines the stability order of the three phases. The adjustment of potential for ions in tetrahedral and octahedral sites shows no significant influence on the positions of the europium ion.

7.1 Introduction:

Barium hexa-aluminates are often used as host materials for phosphor applications. They can be doped with Sr, Y or Eu to produce different colors. $\text{BaMgAl}_{10}\text{O}_{17}$ (BAM): Eu^{2+} is widely used as a blue phosphor for lamps and display panels, with its luminescence at around 440nm. Another phase with the same chemical formula as BAM, $\text{Ba}_3\text{Mg}_3\text{Al}_{30}\text{O}_{51}$ (β'' phase), could possibly form during manufacture and exist in the BAM product. The structure of the β'' phase is more complex than BAM, for the unit cell is 50% larger. A barium β''' phase with chemical formula of $\text{BaMg}_3\text{Al}_{14}\text{O}_{25}$ is also being used as a commercial phosphor when doped with europium. Compared to $\text{BaMgAl}_{10}\text{O}_{17}$ (BAM), the emission band is shifted to 467nm.¹ The reason for the band shift will also be studied.

Computer simulations based on classical solid state theory have been proved to be a successful method in the defect studies of complex materials and are adopted in this study. In this paper, possible structures of the β'' and β''' phase are investigated. The intrinsic defects of the most stable structure will also be studied, since they provide compensation mechanisms for introducing europium ions into the structure. The behaviors of the europium ions are compared between the three phases.

7.1.1 Structural Details

β'' -alumina was first discovered by Yamaguchi and Suzuki in 1968 with the formula of $\text{Na}_2\text{O} \cdot 5\text{Al}_2\text{O}_3$.² Later it was found that the structure was metastable without additions of MgO or Li_2O . It was suggested that ions such as Mg and Li with valence less than that of aluminum would stabilize the structure. As in β -alumina, the double prime phase consists of spinel blocks of oxygen close-packed layers with Na-O planes in between the blocks. It can be considered as a rhombohedral variant of the β phase. The space group of the β'' phase is $R\bar{3}m$. Unlike the β phase, in which adjacent spinel blocks in the c direction are mirror images of each other across the Na-O plane, the spinel blocks in β'' -alumina are rotated 120° to the blocks immediately above and below it. So three spinel blocks are required in a primitive cell to generate periodicity and the Na-O plane is

no longer a mirror plane. The stacking order of the oxygen layers in the three spinel blocks are ABCA, CABC and BCAB. Aluminum ions occupy both tetrahedral and octahedral sites between the oxygen close-packed layers.

The number of sodium ions in the conduction plane is normally less than two and the resulting sodium vacancies make β'' -alumina a fast two-dimensional ionic conductor.³ Three positions exist in the conduction plane for cations, BR, anti-BR and mO. Actually, the BR and anti-BR sites in the β'' phase are the same which is not the case for the β phase. Both sites are in the center of an oxygen-tetrahedron, and the only difference is that the two tetrahedra are inverted with respect to each other (see Fig. 7.1). Two thirds of the A sites (between the anti-BR and mO sites), and nearly all the BR sites, are occupied by sodium. When barium is introduced into the structure, the BR and anti-BR positions will be occupied but not the mO position because of the size of barium. Barium ions should fully reside in one set of symmetric positions to maintain high symmetry. The excess charge of Ba_{Na}^{\bullet} can be compensated by a magnesium ion in the aluminum position with a charge of Mg_{Al}' . The chemical formula of the unit cell of barium β'' -alumina, investigated in this work, is $Ba_3Mg_3Al_{30}O_{51}$.

Barium β''' -alumina has the same space group as BAM but has a different size of spinel blocks. There are six oxygen layers in a spinel block in the β''' phase instead of the four in BAM. In a primitive cell of β''' phase, the total number of oxygen layers is the same as in the β'' phase but with one conduction plane less. Thus, the size of the primitive cell of the β''' phase is a little smaller than for the β'' phase. Whether or not the barium-oxygen plane in between the spinel blocks is a mirror plane depends on the Mg distribution, as with BAM. Since the spinel block is extended, there are two more oxygen positions and two more aluminum positions in the structure. However, the structure of the conduction plane is exactly the same as BAM.

7.1.2 Simulation Methodology

A Born model description of solid is used to describe the predominantly ionic materials in this study. This treats the solid as a collection of point ions with Coulombic and non-Coulombic forces acting between them. The approach has enjoyed a wide range

of success, but it has been found that simulation reliability depends on the validity of the potential model used in the calculations. The non-Coulombic potentials are usually described by a simple analytical Buckingham function,

$$V_{ij}(r_{ij}) = A_{ij} \exp(-r_{ij} / r_{ij}) - C_{ij} r_{ij}^{-6} \quad (1)$$

where r_{ij} is the distance between the ions i and j . The long-range potential is just the normal Coulombic interaction with the form of $z_i z_j / r_{ij}$.

The polarizability of individual ions is simulated through the shell model originally developed by Dick and Overhauser, in which the outer valence electron cloud of the ion is simulated by a massless shell of charge Y and the nucleus and inner electrons by a core of charge X .⁴ The total charge of the ion is $X+Y$, equal to the oxidation state of the ion. The interaction between core and shell of any ion is harmonic with a spring constant k , and is given by

$$V_i(r_i) = \frac{1}{2} k_i d_i^2 \quad (2)$$

where d_i is the relative displacement of core and shell of ion i .

For the shell model, the value of the free-ion electronic polarizability is given by

$$a_i = Y_i^2 / k_i. \quad (3)$$

The potential parameters A , r , and C in Eq. [1], the shell charges Y , spring constant k associated with the shell-model description of polarizability, need to be determined for each interaction and ion type in the crystal from experimental data. In the present study, they were taken from our earlier studies of hexa-aluminates following the original compilation of Lewis and Catlow as shown in Table VII.1.⁵⁻⁷

Table VII.1. Potential Parameters Derived by Lewis and Catlow

Interaction	A (eV)	ρ (Å)	C (eV·Å ⁶)
Al(o) – O	1474.40	0.30059	0
Al(t) – O	1334.31	0.30059	0
Ba – O	931.70	0.39490	0
Mg – O	710.50	0.32420	0
O – O	22764.2	0.1491	17.89
Eu(2+) – O	665.20	0.39490	0
Eu(3+) – O	1358.0	0.35560	0
Interaction	Shell charge	K	
Ba (core) – Ba (shell)	1.46	14.78	
O(core) – O(shell)	-2.207	27.29	

7.1.3 Lattice Energy Calculations

The lattice energy is the binding or cohesive energy of the perfect crystal and is usually defined as the energy that must be released to separate its component ions into free ions at rest at infinite separation. It is calculated by the relation:

$$U = 1/2 \sum \sum V_{ij} . \quad (4)$$

The interatomic potential, V_{ij} include both the long-range Coulombic interactions and the short-term potential described above. The lattice energy is minimized through a second derivative Newton-like procedure, coded into METAPOCS.⁸ Details of the procedure have been outlined by Cormack.⁹

In the present work, this perfect lattice approach has been used to establish equilibrated crystal structures for barium β'' - and β''' -alumina, using the previously published potential.⁵ The idea is that equilibrated crystal must have the lowest lattice energy among all possible structures.

7.1.4 Defect Energy Calculations

Calculations of defect structures and energies introduce one vital feature in addition to those for the perfect lattice methods, i.e. relaxation of lattice atoms around the defect species. This effect is large because the defect generally imparts an extensive

perturbation to the surrounding lattice, and, in the case of ionic crystals, the relaxation field is long-range as the perturbation is mainly Coulombic in origin.

The defect calculation is based on the Mott-Littleton theory, which allows one to calculate the defect-induced static polarization of a dielectric continuum.¹⁰ The basic approach is to contain, within the dielectric continuum, a region, immediately surrounding the defect, which is treated atomistically within the framework of the Born model described above. In this region, the forces and resulting atom displacements are too large to be treated properly by continuum theory, which can, nevertheless, be used to model the more distant parts of the crystal. A program, named CASCADE coded this approach, was used to calculate the defect energy in this study.

7.2 Equilibrated Structures

7.2.1 Barium β'' -Alumina

The ambiguity from the β'' structure is the magnesium distribution in the unit cell, as in the BAM structure. As in BAM, Mg ions also occupy the tetrahedral Al(2) position in the β'' structure. Because there are three spinel blocks now in one primitive cell, there is a total of six Al(2) positions available for three Mg ions. The number of possible configuration is $C_6^3 = 20$. The structure prototype used for barium β'' -alumina is the structure of $\text{Na}_2\text{O}\cdot\text{MgO}\cdot 5\text{Al}_2\text{O}_3$ determined by Betterman and Peters.³ Sodium is substituted for barium in a ratio of 2:1 with barium in the BR position but not the mO position. Additionally, barium is not located at BR and anti-BR sites at the same time to keep the symmetry higher. Six Al(2) sites are labeled from 0 to 5 in the ascending order of their z coordinates. The 20 types of Mg distribution are listed in Table VII.2 along with the lattice energies.

Table VII.2. Lattice Energy of Barium β'' -Alumina

Configuration	012	013	023	014	024
Lattice Energy (eV)	-2599.39	-2602.93	-2603.02	-2602.02	-2603.17
Configuration	034	015	025	035	045
Lattice Energy (eV)	-2599.72	-2599.12	-2599.72	-2599.78	-2599.39
Configuration	123	124	134	125	135
Lattice Energy (eV)	-2599.12	-2599.72	-2600.78	-2599.78	-2602.91
Configuration	145	234	235	245	345
Lattice Energy (eV)	-2602.93	-2599.42	-2602.93	-2603.02	-2599.12

The three digits in the “configuration” row refer to the labels of Al(2) positions occupied by Mg. It seems that magnesium ions tend to separate from each other as far as possible. The 024 configuration seemed to have the lowest lattice energy of -2603.17eV because it kept the symmetry of the three-fold screw axis and all Mg ions were distributed homogeneously in the structure (see Fig. 2). At first glance, it seems that the 135 configuration should have the same lattice energy as the 024 configuration. Actually they are different because they have changed the environment of barium ions differently; however, the 0.22eV difference of lattice energy is small. Consider the 0 and 1 positions of Al(2); if Mg is at the 0 site, the ion arrangement from Mg to Ba between the 0 and 1 positions is Mg-O_C-Al-O_A-Ba, but the arrangement becomes Mg-O_A-Al-O_C-Ba if Mg is at the 1 site, because adjacent spinel blocks are rotated 120° to each other. So the 024 and 135 configurations are definitely different from each other.

From Table VII.2, it is easy to notice that many configurations have a lattice energy close to the 024 configuration, which means that the barium β'' -alumina will have no unique structure but has many possible configurations as does the barium-poor phase. A diffraction study will find an average overall these possible structures.

7.2.2 Barium β''' -Alumina

Because of the similarity between β and β''' , Mg ions are likely to reside only in tetrahedral sites inside the spinel blocks and not in the tetrahedral sites at the edge. There are eight such positions and six magnesium ions. It is much easier to consider the

distribution in another way: two aluminum ions distributed in these 8 positions. If the distributions of same symmetry are removed, only 12 possible distributions exist. There are several structures having very close lattice energies and they may exist simultaneously as shown in Table VII.3. This kind of multiple configuration phenomenon has been observed in nearly all barium hexa-aluminates and is the result of the defects included in the structures, i.e. the same symmetry positions occupied by different kinds of ions. Only the structure with the lowest lattice energy was tested for defect properties in which two Al ions at tetrahedral sites are in different spinel blocks distributed homogeneously in a way similar to the Mg distribution in configuration I of BAM (see Fig. 3). The mirror symmetry of the conduction plane is broken by the Mg distribution but the two-fold screw axis is kept.

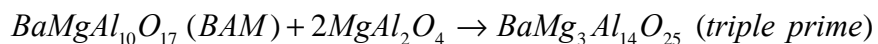
Table VII.3. Lattice Energy of Barium β''' -Alumina

Structure	Lattice Energy (eV)	Structure	Lattice Energy (eV)
b3_1	-2538.12	b3_7	-2538.01
b3_2	-2537.85	b3_8	-2537.48
b3_3	-2538.01	b3_9	-2537.85
b3_4	-2538.57	b3_10	-2535.04
b3_5	-2537.48	b3_11	-2535.26
b3_6	-2537.55	b3_12	-2536.64

Because the stacking order has changed from A-A across the conduction plan in BAM to B-B and C-C in the triple prime phase, the BR site has changed from the 2(d) lattice position to 2(b). Thus the two barium ions in a primitive cell have the same x-y coordinates in the two conduction planes of a primitive cell of the triple prime phase.¹¹ The phase stability is compared below:



$$\Delta H = -2603.17/3 + 1736.06/2 = 0.31eV$$



$$\Delta H = -2538.57/2 + 1736.06/2 + 200.71 \times 2 = 0.17eV.$$

Although their chemical formulae are the same, the BAM structure is more stable than the β'' phase, which also can be seen from the fact that β'' -alumina is metastable without Mg or Li, while β -alumina can exist as its own. The stability of the β''' phase is actually higher than the β'' phase but lower than BAM. Since the difference in reaction enthalpy is not very large, the β'' & β''' phases may intergrow with BAM structure, but β''' phase normally will not exist in the manufactured BAM material, because more magnesia and alumina are needed. The high stability of the BAM phase is the reason it is widely used as the phosphor host material instead of the other phases.

7.3 Intrinsic Defects

Intrinsic defect calculations include the calculation of single point defects such as vacancies and interstitials. It is easy to model the vacancy point defects since there are only four aluminum, five oxygen, one magnesium and one barium position for the 024 configuration of the β'' phase. Only one ion of each ionic class mentioned above needs to be calculated because all ions in the same symmetry class should have the same defect energy. For other configurations that have changed the symmetry group of the structure there should be other sets of symmetry positions. But it is always a good idea to calculate the vacancies of all ions in the unit cell because this guarantees that nothing has been overlooked.

The positions of the interstitial point defects are more complex. In a unit cell, there are positions having more than one symmetry operation and positions having only one point symmetry operation (1-fold rotation). Of course, the former positions must be tested as possible interstitial sites. Some of the other positions may also be possible interstitial sites. In this work, a limitation has been applied to all the possible interstitial sites, which is that the size of the interstitial site must be larger than a given threshold. If the size is small, the introduction of an ion into that position requires larger relaxation, which will increase the defect energy and destabilize the defect. A program was designed to scan all of the possible interstitial positions automatically. The size of a position is defined as the shortest distance between this position and all its neighboring ions. The size threshold was adjusted so that most of the available interstitial positions

were chosen, normally the number of the selected positions was in the range of 100 to 400 depending on the size of the unit cell. All of the special positions need to be considered, but one must check the positions selected by the program to make sure that the special positions are included, by looking at the plot of selected interstitial positions in a unit cell. In this way, all of the positions with only one symmetry operation should have been chosen if their sizes are larger than the threshold.

7.3.1 Intrinsic Defects of Barium β'' -Alumina

Table VII.4 lists the positions and energies of vacancy and interstitial defects. The energies listed are the lowest ones for the defect class. For example, aluminum interstitials can reside at the anti-BR site or in the middle of the spinel block or in many other positions; however, the energy to reside in the middle of the spinel block was the lowest of all. Then this energy was described as the interstitial defect energy of aluminum and the mid-spinel block position was described as the interstitial position of aluminum. The aluminum vacancy tended to occur at the Al(1) position, similar to the configuration II of the BAM structure. The problem is that the 024 configuration seems to be more similar to the configuration I of BAM structure, because they both have lost the mirror symmetry at the barium-oxygen plane whereas configuration II keeps it. It seems that the change from the two-fold screw axis of BAM to the three-fold screw axis of the β'' phase does change the defect properties, although the changes may be small.

The oxygen vacancy occurred at the O(1) position and oxygen interstitial resided at the Al(1) site exactly as in configuration I of BAM. The Reidinger defect is not energetically favorable in the β'' phase which has no mirror symmetry across the barium-oxygen plane. The larger interstitial ions, Ba and Mg, will stay in the anti-BR positions which are associated with more open space. Aluminum entered into the three cation-layers in the middle of spinel block. It can be said that the properties of the intrinsic point defects are almost the same for both BAM and the β'' phase, which is not really a surprise if one takes account of the same chemical formula and their closely related structures. As was found for BAM, the thermally predominant defect in barium β'' -alumina was the Ba Frenkel defect.

Table VII.4. Defect Energy of Barium β'' -Alumina

Point Defect	Defect Energy (eV)	Point Defect	Defect Energy (eV)
V_{Ba}''	16.64	$V_{O(3)}''$	24.90
V_{Mg}''	29.34	$V_{O(4)}''$	24.60
$V_{Al(1)}'''$	56.94	$V_{O(5)}''$	25.06
$V_{Al(2)}'''$	58.68	Ba_i''	-11.81
$V_{Al(3)}'''$	58.62	Mg_i''	-19.39
$V_{Al(4)}'''$	57.43	Al_i'''	-42.98
$V_{O(1)}''$	23.05	O_i''	-14.8
$V_{O(2)}''$	24.63		

Intrinsic Defect	Energy (eV)
Schottky	4.81
Al Frenkel	6.98
Ba Frenkel	2.42
Mg Frenkel	4.98
O Frenkel	4.13

7.3.2 Intrinsic Defects in Barium β''' -Alumina

Because the symmetry of the BR site has changed, the defect properties of β''' also changed. As shown in Table VII.5 the aluminum vacancy was still found to occur at the Al(2) sites in the so-called cation-rich region, where three layers of cations reside in between two close-packed oxygen layers. There are two cation-rich regions in each spinel block of the β''' phase instead of the one in BAM. The middle cation-layer is occupied by the Al(4) ion and the other two cation-layers are occupied by Mg ions or a mix of Mg and Al ions. Thus, there are two types of cation-rich region, with different effective charges caused by the Mg substitution: $[Mg-Al-Mg]^{2-}$ and $[Mg-Al-Al]^{1-}$. A Mg vacancy occurring in $[Mg-Al-Al]^{1-}$ was more energetically favorable than in the other position as a result of the local charge effect. The same effect caused the oxygen vacancy to occur close to the other cation-rich region with the more negative local charge.

Table VII.5. Defect Energies of Barium β''' -Alumina

Point Defect	Defect Energy (eV)	Point Defect	Defect Energy (eV)
V_{Ba}''	16.88	$V_{O(3)}^{\bullet\bullet}$	23.93
V_{Mg}''	27.62	$V_{O(4)}^{\bullet\bullet}$	24.58
$V_{Al(1)}'''$	55.57	$V_{O(5)}^{\bullet\bullet}$	23.80
$V_{Al(2)}'''$	54.83	$V_{O(6)}^{\bullet\bullet}$	22.65
$V_{Al(3)}'''$	-	$V_{O(7)}^{\bullet\bullet}$	25.48
$V_{Al(4)}'''$	58.40	$Ba_i^{\bullet\bullet}$	-11.19
$V_{Al(5)}'''$	-	$Mg_i^{\bullet\bullet}$	-18.53
$V_{Al(6)}'''$	55.70	$Al_i^{\bullet\bullet\bullet}$	-44.21
$V_{O(1)}^{\bullet\bullet}$	24.53	O_i''	-15.91
$V_{O(2)}^{\bullet\bullet}$	22.62		

Intrinsic Defect	Energy (eV)
Schottky	3.80
Al Frenkel	5.31
Ba Frenkel	2.85
Mg Frenkel	4.55
O Frenkel	4.13

Large cations, Mg and Ba, as interstitial ions, occupied the anti-BR position in the conduction plane. The small Al ion stayed inside the spinel block. As in BAM, the aluminum interstitial resided in the octahedral site of the cation-rich region, where oxygen layers were not strictly close-packed. The oxygen interstitial appeared in the Al(1) layer close to a vacant octahedral site. Because the mirror symmetry across the barium-oxygen plane has been destroyed and because of the size of the large barium ion, the oxygen interstitial can not be stabilized by forming a Reidinger defect that is mirror symmetric about the conduction plane. Actually, the calculated intrinsic defect properties are exactly the same for the structure I of BAM, which is not surprising since their structures are very similar, in addition to the similarity of the Mg distribution.

7.4 Extrinsic Defects: Europium

It has been shown above that the properties of intrinsic defects in BAM and the β'' phase are similar to each other except for the aluminum vacancy position. The β''' phase also has the same defect properties as BAM. As these phases may coexist in BAM material, it may also be possible for europium to be found in the β'' and β''' phases after the doping. The properties of europium-related defects have been calculated to investigate the influence of the existence of these phases in the BAM:Eu²⁺ material. Like the intrinsic defects calculation, the single point defects associated with europium were calculated first. They include the europium interstitial and substitution of cations.

Both the divalent and trivalent europium ions in the double and triple prime phases have the same locations for the single point defects as in the BAM structure. Since the size of europium is large, it is more stable for it to reside in the anti-BR site than in the spinel block as an interstitial ion. Table VII.6 shows the lowest defect energy of the point defects associated with europium, and their corresponding positions, but these by themselves do not tell which defect will occur or dominate. Thus, the formation energies of these defects are compared in Table VII.7 and Table VII.8.

The divalent europium ion would prefer to substitute for the barium ion in the conduction plane, because this requires less energy than other defect formation, and is consistent with what is believed.^{1,12} It is the Eu²⁺ ion in the BR site of BAM that emits the observed blue light at around 440nm. Since the coordination number at the BR site has changed from 9 in BAM to 7 in barium β'' -alumina (see Fig. 1c), the estimated emission wavelength changes from 490nm to 550nm, using the d-band edge calculation for Eu²⁺ ion as calculated in Chapter 6.^{13,14} Thus the formation of the β'' phase will shift the emission band. Since Eu²⁺ in the β''' phase shows an emission band at around 467nm from experiments, if it (the β''' phase) exists as a second phase in BAM, and contains Eu²⁺ ions, then a shift in the emission band would be expected.¹ Since the barium β phase is more stable than the β'' and β''' phases, most crystal grains in the material should be the β phase, and the band shift from the double and triple prime phases should be subtle. Other positions for the Eu²⁺ defect are not easy to find because their formation

energies are very large compared to Eu_{Ba} . Unlike the divalent ion, Eu^{3+} did not stay at the BR position, but tried to enter into the spinel block to substitute for the Al(2) ion.

Table VII.6. Point Defect of Europium in Barium β'' -Alumina

Defect	Defect Energy (eV)	Defect Positions
Eu_{Ba}	-1.44	BR
Eu_{Mg}	10.44	Al(2)
Eu'_{Al}	38.58	Al(2)
$Eu_i^{\bullet\bullet}$	-13.33	anti-BR
Eu_{Ba}^{\bullet}	-21.71	BR
Eu_{Mg}^{\bullet}	-13.55	Al(2)
Eu_{Al}	14.5	Al(2)
$Eu_i^{\bullet\bullet\bullet}$	-32.32	anti-BR

Table VII.7. Defect Formation Energies of Eu^{2+} in Barium β'' -Alumina

Defect Formation	Enthalpy (eV)
$EuO \rightarrow Eu_i^{\bullet\bullet} + O_i''$	5.07
$EuO \rightarrow Eu'_{Al} + Al_i^{\bullet\bullet\bullet} + O_i''$	14.0
$EuO \rightarrow 1/2Al_2O_3 + Eu'_{Al} + 1/2V_O^{\bullet\bullet}$	3.92
$EuO \rightarrow Eu_{Mg} + Mg_i^{\bullet\bullet} + O_i''$	9.45
$EuO \rightarrow MgO + Eu_{Mg}$	2.65
$EuO \rightarrow BaO + Eu_{Ba}$	0.45
$EuO \rightarrow Eu_i^{\bullet\bullet} + V_{Ba}'' + BaO$	5.20

Table VII.8. Defect Formation Energies of Eu^{3+} in Barium β'' -Alumina

Defect Formation	Enthalpy (eV)
$1/2Eu_2O_3 \rightarrow Eu_i^{\bullet\bullet\bullet} + 3/2O_i''$	10.92
$1/2Eu_2O_3 \rightarrow Eu_{Al} + Al_i^{\bullet\bullet\bullet} + 3/2O_i''$	14.76
$1/2Eu_2O_3 \rightarrow Eu_{Al} + 1/2Al_2O_3$	0.55
$1/2Eu_2O_3 \rightarrow Eu_{Mg}^{\bullet} + MgO + 1/2O_i''$	3.5
$1/2Eu_2O_3 \rightarrow Eu_{Ba}^{\bullet} + BaO + 1/2O_i''$	5.02

7.5 Potential at Tetrahedral and Octahedral Sites

Since the radius of aluminum varies in different coordination conditions, the potentials for aluminum in tetrahedral and octahedral sites are different. However, since only one potential for europium has been used in these sites in the above calculations, the effect of the potential adjustment will be tested for Eu in the β'' phase. The reason to use a different potential for different conditions is to reflect the radius change of ions in those conditions.

For the Huggins-Mayer relationship,⁹

$$A = b \exp(r / r), \quad (5)$$

the difference between tetrahedral and octahedral positions in radius is

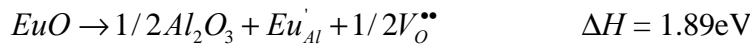
$$\Delta r = r_{oct} - r_{tet} \quad (6)$$

so that the pre-exponential term A of ion in tetrahedral site is given as

$$A_{tet} = A_{oct} \exp(-\Delta r / r) \quad (7)$$

Using Equation (7), the pre-exponential parameter of Eu^{3+} ions in the tetrahedral site is 1130.44eV with the estimation of $r_{tet} = 0.94r_{oct}$. The Eu^{3+} substitution for Al(2) ion was recalculated with the new tetrahedral potential. The defect energy reduced from 14.5eV to 11.82eV in the β'' phase. This means that the reaction enthalpy will become negative so that the Eu^{3+} ion in the Al(2) position will lower the total energy of the system. Overall the potential adjustment did not change the observed Eu defect behavior.

Consider the same thing for Eu^{2+} ion. The substitution defect energy at Al(2) changes from 38.58eV to 36.55eV. Rewrite the reaction for Eu^{2+} substitute for Al(2) as follows:



Although the formation energy is decreased, it is still four times the energy of substituting for barium, so the potential adjustment did not change the behavior of divalent europium defects either.

7.6 Conclusions

The defect properties of both barium β'' - and β''' -alumina are similar to those of $\text{BaMgAl}_{10}\text{O}_{17}$ (BAM). BAM has two possible configurations (different in their Mg

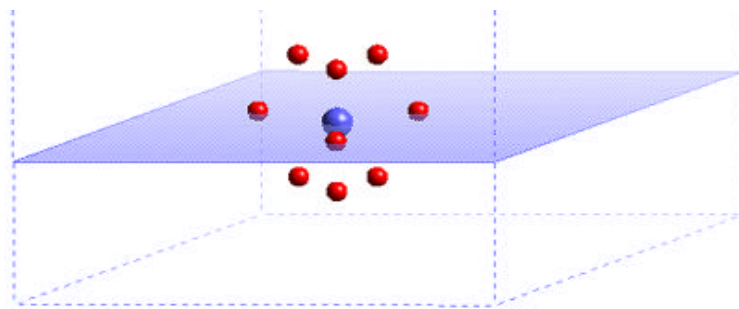
distribution) with the same lattice energy whereas the β'' and β''' phases have more than two such configurations, but also with similar lattice energies. The barium Frenkel defect is the predominant thermal defect of all compounds. Europium ion, the active ion of the phosphor, was found to substitute for the barium ion or the Al(2) ion depending on its valence state, as also found for BAM.

Although correcting the europium potential for tetrahedral condition did change the defect energies, the final results of the europium position did not change. Actually, the potential modification has the effect of enhancing the trend of Eu^{3+} substitution for Al(2). Since the local environment around the BR position has changed in the β'' phase with respect to BAM, the emission wavelength of Eu^{2+} ion has also changed, because Eu^{2+} ions stayed at the BR position. Formation of β'' and β''' phases will shift the emission band but their effect is not really significant because BAM is more stable so that the amount of other phases will be small.

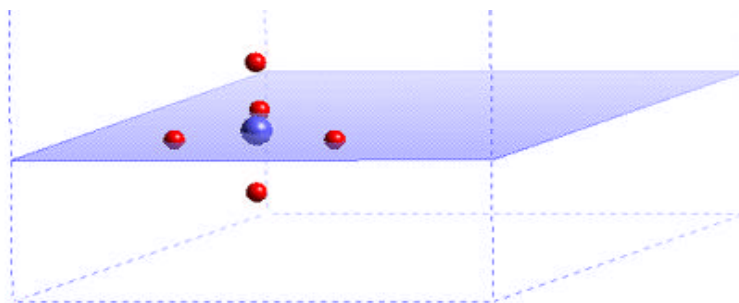
References

1. D. Ravichandran, S.T. Johnson, S. Erdei, R. Roy, and W.B. White, "Crystal Chemistry and Luminescence of the Eu^{2+} -Activated Alkaline Earth Aluminate phosphors," *Displays*, **19**[4] 197-203 (1999).
2. G. Yamaguchi and K. Suzuki, *Bull. Chem. Soc. Jap.*, **41** 93 (1968). As cited in M. Bettman and L.L. Turner, "On the Structure of $\text{Na}_2\text{O}\cdot 4\text{MgO}\cdot 15\text{Al}_2\text{O}_3$, a Variant of Beta-Alumina," *Inorg. Chem.*, **10**[7] 1442-6 (1971).
3. M. Bettman and C.R. Peters, "The Crystal Structure of $\text{Na}_2\text{O}\cdot \text{MgO}\cdot 5\text{Al}_2\text{O}_3$ with Reference to $\text{Na}_2\text{O}\cdot 5\text{Al}_2\text{O}_3$ and Other Isotypal Compounds," *J. Phys. Chem.*, **73**[6] 1774-80 (1969).
4. B.G. Dick and A.W. Overhauser, "Theory of the Dielectric Constants of Alkali Halide Crystals," *Phys. Rev.*, **112**[1] 90-103 (1958).
5. J.G. Park and A.N. Cormack, "Structural Chemistry of Alkaline Earth Hexa-Aluminates," *Mater. Res. Soc. Symp. Proc.*, **369** 457-62 (1995).
6. J.G. Park and A.N. Cormack, "Crystal/Defect Structures and Phase Stability in Ba Hexa-aluminates," *J. Solid State Chem.*, **121**[1] 278-90 (1996).
7. G.V. Lewis and C.R.A. Catlow, "Potential Models for Ionic Oxides," *J. Phys. C: Solid State Phys.*, **18**[6] 1149-61 (1985).
8. C.R.A. Catlow, A.N. Cormack, and F. Theobald, "Structure Prediction of Transition-Metal Oxides using Energy-Minimization Techniques," *Acta Crystallogr., Sect. B: Struct. Sci.*, **B40**[3] 195-200 (1984).
9. A.N. Cormack, G.V. Lewis, S.C. Parker, and C.R.A. Catlow, "On the Cation Distribution of Spinels," *J. Phys. Chem. Solids*, **49**[1] 53-7 (1988).
10. N.F. Mott and M.J. Littleton, "Conduction in Polar Crystals. I. Electrolytic Conduction in Solid Salts," *Trans. Faraday Soc.*, **34**[1] 485-99 (1938).
11. M. Bettman and L.L. Turner, "On the Structure of $\text{Na}_2\text{O}\cdot 4\text{MgO}\cdot 15\text{Al}_2\text{O}_3$, a Variant of Beta-Alumina," *Inorg. Chem.*, **10**[7] 1442-6 (1971).
12. B.M.J. Smets and J.G. Verlijsdonk, "The Luminescence Properties of Eu^{2+} and Mn^{2+} Doped Barium Hexa-aluminates," *Mater. Res. Bull.*, **21**[11] 1305-10 (1986).
13. L.G.V. Uitert, "An Empirical Relation Fitting the Position in Energy of the Lower d-Band Edge for Eu^{2+} or Ce^{3+} in Various Compounds," *J. Lumin.*, **29**[1] 1-9 (1984).

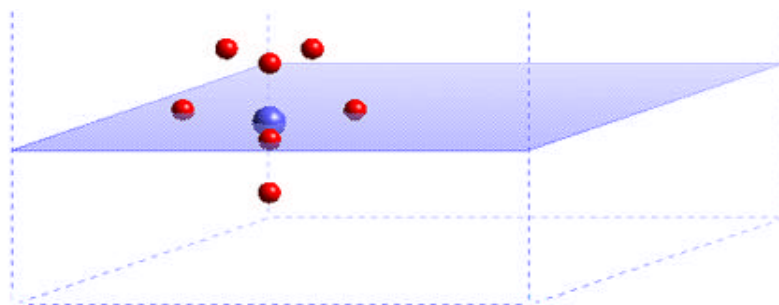
14. C.K. Jorgensen, "Partly Filled Shells Constituting Anti-Bonding Orbitals with Higher Ionization Energy Than Their Bonding Counterparts," pp. 49-82 in *Structure and Bonding*. Edited by J. D. Dunitz, P. Hemmerich, R. H. Holm, J. A. Ibers, C. K. Jorgensen, J. B. Neilands, D. Reinen, and R. J. P. Williams. Springer-Verlag, Berlin, Germany 1975.



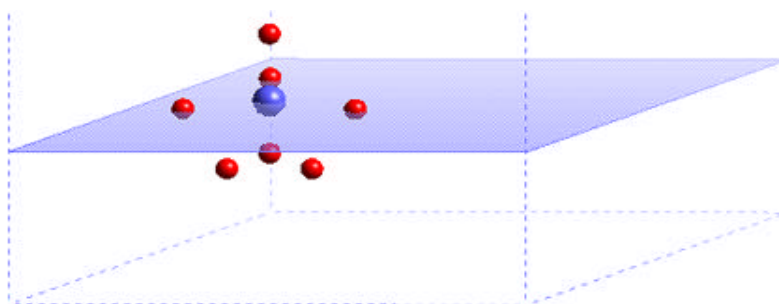
a) BR environment of BAM



b) anti-BR environment of BAM



c) BR environment of barium β'' -alumina



d) anti-BR environment of barium β'' -alumina

Figure 7.1. Comparison of BR and anti-BR positions.



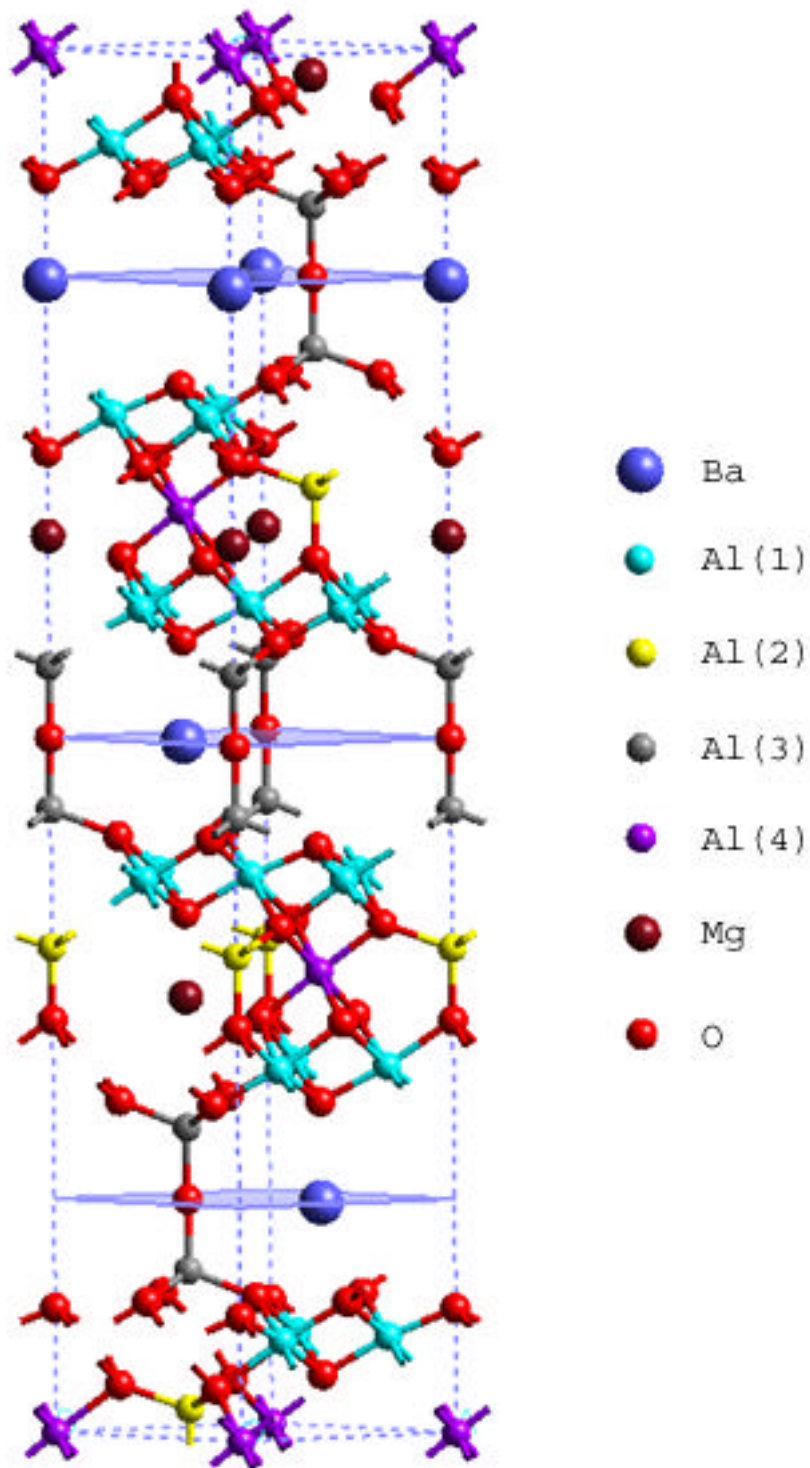


Figure 7.2. Unit cell of barium β'' -alumina.

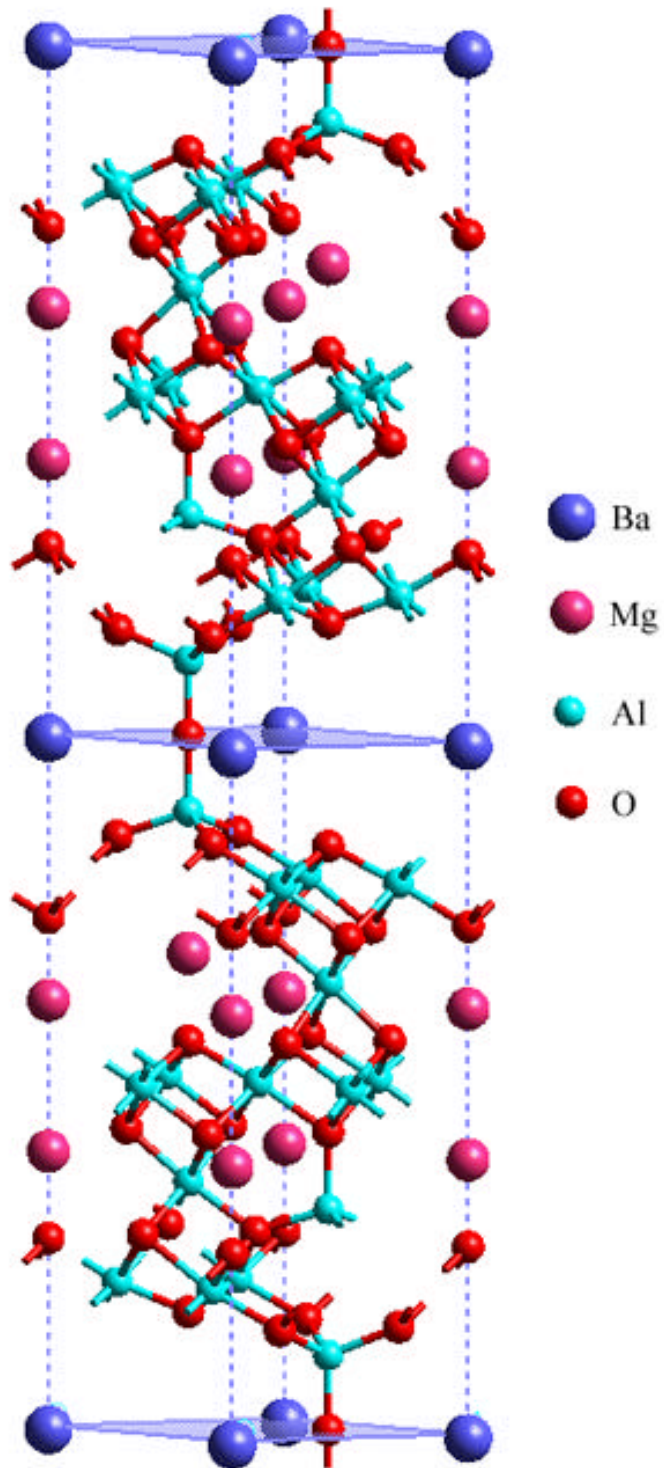


Figure 7.3. Primitive cell of barium β''' -alumina.

8. Summary and Future Work

8.1 Summary

Structural and defect properties of β -alumina-related barium phases have been investigated with the aid of computer simulation. The predicted optical behavior of the barium hexa-aluminates doped with Eu^{2+} ion has been studied and compared. Altogether five structures have been discussed: $\text{BaMgAl}_{10}\text{O}_{17}$ (BAM), $\text{Ba}_{0.75}\text{Al}_{11}\text{O}_{17.25}$ (barium-poor phase), $\text{Ba}_3\text{Mg}_3\text{Al}_{30}\text{O}_{51}$ (β'' phase), $\text{BaMg}_3\text{Al}_{14}\text{O}_{25}$ (β''' phase) and $\text{Ba}_3\text{Al}_{32}\text{O}_{51}$ (a hypothetical phase). Intrinsic and extrinsic defects have been calculated for each structure and compared, along with the Mg ion distributions in the spinel blocks and O ion distributions in the conduction plane. Ion-migration issues associated with Eu ion have also been discussed. The potential dependence of the simulation was also addressed.

Our work has suggested that BAM structures will have two different Mg distributions that will affect the defect properties. The two possible configurations can not be distinguished by the lattice energy. Both configurations will exist in the real material. Although two Mg distributions exist, the thermally predominant defect, a barium Frenkel defect, is the same for both configurations. The most significant change resulting from the Mg distribution is the oxygen interstitial position. The oxygen interstitial ion will reside in the mirror plane to form a two-bridge configuration at the mOB position, if the Mg distribution retains the mirror symmetry. However, if the Mg distribution destroys the mirror symmetry, the oxygen interstitial will stay inside the spinel block, in the half of the spinel block without Mg. It seems that the charge of Mg'_{Al} plays an important role in determining the position of the defect. Calculations of defect complexes and bond valence have verified the results that Eu^{3+} ion prefers Al(2) sites in the spinel block, instead of BR sites in the conduction plane, a result which is potential independent.

Ion migration studies suggest that Eu^{3+} ion can migrate into the spinel block at relatively low temperature with the help of Mg ion, but it will not migrate in the conduction plane, where barium and Eu^{2+} ions show active migration behavior. Oxygen

does not undergo long-range migration in the conduction plane, which implies that the formation of $\text{EuMgAl}_{11}\text{O}_{19}$ as suggested by Shozo et al. would not occur at the temperature when $\text{BaMg}(\text{Al}_9\text{Eu})\text{O}_{17}$ is more likely to be formed instead. Eu^{2+} ion seems to form clusters in the BAM structure, which will deteriorate the luminescent efficiency.

The defect properties of the barium-poor phase are different from BAM, because of the absence of Mg and the presence of oxygen interstitials in the conduction plane. The structural difference changes the location of defects. Eu^{3+} ion is found to occupy the Al(3) site, the other tetrahedral position, instead of the Al(2) site in order to compensate for the effective negative charges of oxygen interstitials in the mirror plane. Multiple configurations with different oxygen interstitial arrangements have been found to have very similar lattice energies. The d-band edge calculation for the europium ion has suggested that the observed broader and shifted emission band of Eu^{2+} ion in the barium-poor phase compared to BAM is the result of the multiple oxygen distributions that will change the ligand field of Eu^{2+} . The change of the ligand field is large enough to broaden and shift the emission band significantly to account for the two-band configuration that is seen in the measured emission spectrum. Eu^{3+} ions in the aluminum positions in the spinel block will also have the effect of shifting the emission band. The calculation also suggests that the two Mg distributions in BAM will change the emission spectrum to a continuously curved peak instead of a sharp peak.

A hypothetical structure $\text{Ba}_3\text{Al}_{32}\text{O}_{51}$ with aluminum vacancies inside the spinel blocks seems to have a lower lattice energy than the barium-poor and barium-rich phases, but its existence has not yet been demonstrated experimentally. Defect calculations on the $\sqrt{3} \times \sqrt{3}$ super-cell of this hypothetical phase show the same defect properties as the barium-poor phase.

Our study has suggested that the barium β'' and β''' phases have defect properties more like BAM than the barium-poor phase, because of similar chemical components and closely related structures. Several structures with different Mg distributions were also found to exist in these two phases. Among all the three phases (β , β'' and β'''), the β phase (BAM) is the most stable one which is the reason why BAM is widely used rather than the other barium hexa-aluminates. Because of the different site environments of BR sites in the β'' phase compared to BAM and because of the possibility of its intergrowth

with BAM, our study suggests that the formation of the β'' phase will shift the emission band significantly and degrade the designed emission properties of BAM:Eu²⁺ material. Europium ion in the β''' phase also shows an emission band shift with respect to BAM but to a small extent so there is no big influence of the formation of the β''' phase in the BAM material. The potential adjustment for different coordinations of Eu was not found to affect the simulation results.

8.2 Suggestions for Future Work

Since there is another phase of barium hexa-aluminate, 1.32BaO6Al₂O₃ (a barium rich phase that can intergrow with the barium-poor phase), the europium ion behavior should be studied further in this phase.

As we have found that Mg plays an important role in the Eu³⁺ migration into the spinel block, which will shift the emission band, other divalent cations should be considered to substitute for Mg to control this migration to hinder the luminescent degradation.

Because the Eu²⁺ cluster in BAM will decrease the luminescent intensity and Eu²⁺ ion migrates with an interstitialcy mechanism, substitution of barium with other ions like Ca may provide a way to separate Eu²⁺ ions so that the luminescent efficiency will be increased.

Many other phases such as CaAl₁₂O₁₉ and SrMgAl₁₀O₁₇ with similar structures to the barium-hexa-aluminates have also been used for Eu²⁺ hosts. And many other active ions of rare-earth elements can be doped in these phases. Our studies can be extended to the studies of active cations in different structures, which will help to design phosphor materials with specific luminescent properties.

Further calculation of the d-band edge of the Eu ion in the three positions, BR, Al(2) and Al(3) sites could be more accurately calculated by ab initio simulation, which would clarify the main reason for the luminescent degradation in BAM:Eu²⁺.

STRUCTURE AND STABILITY OF EUROPIUM DOPED β -ALUMINA
TYPE PHOSPHOR

BY

ZHEHUA WU

B.S. TSINGHUA UNIVERSITY (1998)

SIGNATURE OF AUTHOR _____

APPROVED BY _____ ~~Alastair N. Cormack~~ _____
ADVISOR

ADVISORY COMMITTEE

ADVISORY COMMITTEE

ADVISORY COMMITTEE

CHAIR, ORAL THESIS DEFENSE

ACCEPTED BY _____
DEAN, SCHOOL OF CERAMIC ENGINEERING
AND MATERIALS SCIENCE

ACCEPTED BY _____
DIRECTOR OF GRADUATE STUDIES, ALFRED UNIVERSITY

Acknowledgments

Sincerely, I would like to thank my advisor, Dr. Alastair N. Cormack, who leads me into the world of computer simulation, for his guidance, support and advice during my four-year study at Alfred University. Also I want to express thanks to my thesis advisory committee members, Dr. Robert A. Condrate, Dr. Paul F. Johnson, Dr. Doreen Edwards, for their great help especially in refining my thesis work. I would like to show my gratitude to all my group members, especially Byeongwon Park, JinCheng Du and Darren Stohr, who had helped me with the research difficulties. I am deeply appreciated for Ann Baldwin to help me improve my English skills. I acknowledge the U.S. Department of Energy for financing my Ph.D. thesis and U. C. Berkeley for computational resources.

I would like to show my thank for Dr. YaoZhong Jiang in the Tsinghua University, Beijing, China, who recommended Alfred University for graduate study. My acknowledgements are also given to the past the current Chinese students, especially XiangLong Yuan, ChangQing Shen, who made my life in Alfred much more fun and enjoyable. Special thanks are given to my family and friends in China for their supports and encouragement.

Table of Contents

	Page
Acknowledgments	iii
List of Tables	vi
List of Figures.....	viii
Abstract	x
1. General Introduction	1
References	4
2. The Crystal Structure	6
2.1 Structure of β -Alumina	6
2.2 Beta Triple-Prime Phase	9
2.3 Beta Double-Prime Phase	11
2.4 Barium Magnetoplumbite	13
References	15
3. Atomistic Computer Simulation Techniques	21
3.1 Introduction	21
3.2 Inter Atomic Potentials	22
3.3 Minimization Techniques.....	25
3.4 Defect Energy Calculations.....	27
References	31
4. Defects in $\text{BaMgAl}_{10}\text{O}_{17}:\text{Eu}^{2+}$ Blue Phosphor	34
4.1 Introduction	35
4.2 Results.....	39
4.3 Defect Complexes.....	48
4.4 Europium Ion Size Consideration.....	51
4.5 Calculations with the Bush Potential	53
4.6 Conclusions	55
References	57
5. Ion Migration In BAM.....	64

5.1 Introduction	65
5.2 Experiments.....	68
5.3 Results.....	69
5.4 Related Phases Containing Eu.....	74
5.5 Conclusions	76
References.....	77
6. Eu in Barium Hexa-aluminates Containing No Mg	81
6.1 Introduction	82
6.2 The Barium-Poor Phase $Ba_{0.75}Al_{11}O_{17.25}$	84
6.3 Emission Band Calculations.....	94
6.4 $Ba_3Al_3O_5$	98
6.5 Conclusions	102
References.....	103
7. Defects in β''- and β'''- Barium Hexa-aluminates	114
7.1 Introduction:	115
7.2 Equilibrated Structures	119
7.3 Intrinsic Defects.....	122
7.4 Extrinsic Defects: Europium	126
7.5 Potential at Tetrahedral and Octahedral Sites	128
7.6 Conclusions	128
References.....	130
8. Summary and Future Work	135
8.1 Summary	135
8.2 Suggestions for Future Work	137

List of Tables

	Page
Table II.1. Positional and Occupation Parameters for β -Alumina (I)	8
Table II.2. Positional and Occupation Parameters for β -Alumina (II)	9
Table II.3. Positions of Ions in β''' -Alumina	10
Table II.4. Positions of Ions in β'' -Alumina	11
Table IV.1. Crystallographic Information for the β -Alumina Structure	36
Table IV.2. Potential Parameters Derived by Lewis and Catlow	38
Table IV.3. Potential Models Derived by Bush et al.	38
Table IV.4. Lattice Energies of Mg Distributions in Al(2) and Al(3) Sites	40
Table IV.5. Comparison of Measured and Calculated Structures	41
Table IV.6. Calculated Point Defect Energies (eV)	42
Table IV.7. Calculated Intrinsic Defect Energies (eV)	45
Table IV.8. Europium Point Defect Energies (eV)	46
Table IV.9. Eu^{2+} Ion Incorporation into BAM	47
Table IV.10. Eu^{3+} Ion Incorporation into BAM	48
Table IV.11. Defect Complexes Containing Eu^{3+} and O^{2-}	49
Table IV.12. Defect Complexes with Three Point Defects	50
Table IV.13. Defect Reaction of Defect Complex	50
Table IV.14. Bond Valence of Cations in BAM	52
Table IV.15. Bond Length vs. Coordination Number	52
Table IV.16. Point Defect in Config. I with Bush Potential	53
Table IV.17. Intrinsic Defect Energy of BAM with Bush Potential	54
Table IV.18. Incorporation of Eu into BAM (Bush Potential)	55
Table V.1. Defect Complex with Two Oxygen and One Eu^{3+}	75

Table VI.1. Lattice Energies of Five Structures	86
Table VI.2. Lattice Energies of Five Structures (with Reidinger-Defect)	86
Table VI.3. Vacancy Defect Energies of Super-Cells	88
Table VI.4. Point Defects of 1-2 Super-Cell	89
Table VI.5. Point Defects of 1-3 Super-Cell	90
Table VI.6. Point Defects of b1 Super-Cell	90
Table VI.7. Intrinsic Defect Energies of Super-Cells (eV)	91
Table VI.8. Europium Point Defects in the Three Super-Cells	92
Table VI.9. Incorporation of Eu into Super-Cells	93
Table VI.10. Estimated Emission Wavelength of Eu	95
Table VI.11. Site Energy Comparison of Eu ²⁺ Positions	96
Table VI.12. Lattice Energies of Four Possible Structures	99
Table VI.13. Point Defect in Ba ₃ Al ₃₂ O ₅₁	100
Table VI.14. Europium Point Defects	101
Table VI.15. Defect Reaction of Eu in Ba ₃ Al ₃₂ O ₅₁	101
Table VII.1. Potential Parameters Derived by Lewis and Catlow	118
Table VII.2. Lattice Energy of Barium β"-Alumina	120
Table VII.3. Lattice Energy of Barium β'''-Alumina	121
Table VII.4. Defect Energy of Barium β"-Alumina	124
Table VII.5. Defect Energies of Barium β'''-Alumina	125
Table VII.6. Point Defect of Europium in Barium β"-Alumina	127
Table VII.7. Defect Formation Energies of Eu ²⁺ in Barium β"-Alumina	127
Table VII.8. Defect Formation Energies of Eu ³⁺ in Barium β"-Alumina	127

List of Figures

	Page
Figure 2.1. Structure of ideal β -alumina $\text{NaAl}_{11}\text{O}_{17}$.	17
Figure 2.2. Structure of ideal β''' -alumina $\text{Na}_2\text{O} \cdot \text{MgO} \cdot 15\text{Al}_2\text{O}_3$. All Mg are shown as Al.	18
Figure 2.3. Structure of ideal β'' -alumina.	19
Figure 2.4. Structure of ideal manetoplumbite $\text{MAl}_{12}\text{O}_{19}$.	20
Figure 3.1. Two regions for defect energy calculation. Defect is in the center of region I.	33
Figure 4.1. Primitive cell of β -alumina.	59
Figure 4.2. Two configurations of BAM. a) Configuration I possesses Mg at ab sites; b) Configuration II possesses Mg at ac sites.	60
Figure 4.3. Projection of mirror plane of BAM with ion positions on X-Y plane.	61
Figure 4.4. Three types of oxygen interstitial of BAM.	62
Figure 4.5. Configuration of Reidinger defect.	63
Figure 5.1. Primitive cell of BAM, configuration I.	78
Figure 5.2. Projection of mirror plane of BAM on X-Y plane.	79
Figure 5.3. Magnesium positions related to $\text{Eu}_i^{\bullet\bullet\bullet} + V_{\text{Al}(2)}^{\bullet\bullet}$.	79
Figure 5.4. Barium interstitialcy migration.	80
Figure 5.5. Trajectory of Eu^{2+} in the conduction plane.	80
Figure 6.1. $\text{Ba}_6\text{Al}_{88}\text{O}_{138}$ super-cell.	105
Figure 6.2. Structure of 1-2 super-cell of barium-poor phase.	106
Figure 6.3. Structure of 1-3 super-cell of barium-poor phase.	107
Figure 6.4. Lattice energy of solid solution between BAM and barium-poor phase.	108
Figure 6.5. Crystal structure of b1 super-cell.	109

Figure 6.6. Mirror plane structures. a) BAM; b) magnetoplumbite.	110
Figure 6.7. a) Mirror plane of 1-2 super-cell; b) Mirror plane of 1-3 super-cell; c) Mirror plane of b1 super-cell.	110
Figure 6.8. Eu^{2+} environment in mirror plane. a) Associated without O_{BR} ; b) Associated with O_{BR} .	111
Figure 6.9. Selection of $\sqrt{3} \times \sqrt{3}$ super-cell.	112
Figure 6.10. $\sqrt{3} \times \sqrt{3}$ unit cell of $\text{Ba}_3\text{Al}_{32}\text{O}_{51}$.	113
Figure 7.1. Comparison of BR and anti-BR positions.	132
Figure 7.2. Unit cell of barium β'' -alumina.	133
Figure 7.3. Primitive cell of barium β''' -alumina.	134

Abstract

BaMgAl₁₀O₁₇ (BAM) has been widely used as the host material for Eu-active phosphors for lamps and display panels. It has a luminescent wavelength ranging from 430nm to 450nm, blue in color. However, there is a degradation problem for this phosphor material: the luminescent intensity decreases and the emission band shifts from blue toward green in color with an increase in application period and annealing procedure of manufacture. The suggestion that the luminescent degradation is related to the oxidation of europium from a 2+ to 3+ oxidation state forms the basis for the first part of this thesis. A computer simulation study of the behavior of europium in BAM (based on the classical Born model description the ionic materials) was carried out. Europium ions were found to prefer different lattice positions depending on their valence state: Eu²⁺ prefers the BR site in the mirror plane; Eu³⁺ prefers the Al(2) site in the spinel block.

Because there are many other barium hexa-aluminate phases besides BAM and because they can also be used as the phosphor host materials, the phase relationship between these phases and the properties of the Eu dopant in these phases were also investigated, in particular, for the barium-poor phase, Ba_{0.75}Al₁₁O_{17.25}. The barium-poor phase, after doping with Eu²⁺, shows a broader and shifted emission band compared to BAM. The formation of barium-poor phase has also been proposed as the reason for the observed luminescent degradation in BAM. Calculations on the barium-poor phase were performed to investigate the origin of the emission band differences between it and BAM, and the complete solid solution between them. The coexistence of multiple O_{BR}-distributions in the barium-poor phase was found to be the origin of the observed broader and shifted emission band of Eu²⁺.

Since the hypotheses about luminescent degradation involve phase changes or structural adjustments, molecular dynamics simulations of ion migration were also performed to study the defect and structural changes after the europium oxidation. It was found that Eu³⁺ ions can migrate from the mirror plane to the spinel block at relatively low temperature, and that Eu²⁺ ions have a tendency to congregate in BAM.

1. General Introduction

Barium hexa-aluminates, widely used as host materials for rare-earth elements for optical applications, have many forms with different chemistries but their structures are mainly based on that of β -alumina and are closely related to each other.¹⁻⁴ They are also candidates for gas turbine applications because of their high thermal stability. The structures of barium aluminates are actually nonstoichiometric.⁵⁻⁷ For some phases, additional elements, other than Ba, Al and O, are required in the structure or the structure will not be stable, which adds to the complexity of the material.

β -alumina has the chemical formula of $\text{NaAl}_{11}\text{O}_{17}$, and there are two formula units in a primitive cell. Its structure can be described in terms of oxygen cubic-like closely packed spinel blocks separated by sodium-oxygen planes. In barium aluminates, sodium has been substituted by barium and other structural changes have to be made to compensate for the effective charge of the substitution. The details of the possible forms of barium hexa-aluminates are discussed in Chapter 2.

Experiments to determine these structures have the shortcomings of not being able to determine the detailed local structure and local defect properties. In addition, experimental measurement is always the combination of several factors, and it is hard to differentiate between. For example, the measured unit cell size varies with the temperature, strain, external force field and experimental error. As the material structure gets more complex, there will be too many parameters of structure determination (such as partial occupation and dopant locations) for experiments to handle.

Computer simulation provides a way to overcome these problems and has been used successfully in the study of many aspects of materials science. The structure model in the simulation can be changed systematically so that the effect of any individual parameter can be studied. As computer simulation works on the mathematical description of materials, the detailed arrangement of ions around point defects and the ion distribution are readily obtained. Properties determined by long-range periodicity that are hard to measure can easily be found from super-lattice simulations. Furthermore, computer

simulation can be used to predict material properties and thus, can provide microscopic explanation of macroscopic measurements.

Optically related defect properties are the main concern of this work. When doped with Eu^{2+} ions, barium aluminates become the blue phosphors used for lamps and display panels. There are many phases of barium aluminates that are possible candidates for phosphor host-materials and they show different luminescent properties.⁴ The most widely used phase is $\text{BaMgAl}_{10}\text{O}_{17}$ (BAM). However, there is a problem with this blue phosphor: its luminescent intensity decreases in the annealing step of the manufacturing process, and there is also an emission band shift, which is believed to be the result of Eu oxidation and is thought to be defect or phase-related.⁹⁻¹¹ This problem will shorten the application period of the phosphor material and lower the energy efficiency. Because of the complexity of this structure and of many closely related phases, there is no full understanding of the degradation mechanism from the experiments at this time.

Oshio et al. have suggested that after degradation, an Eu^{3+} magnetoplumbite structure, $\text{EuMgAl}_{11}\text{O}_{19}$, will form inside the barium aluminate.¹¹ But there is another hypothesis for forming a barium-poor phase, $\text{Ba}_{0.75}\text{Al}_{11}\text{O}_{17.25}$, suggested by Yokota et al., because the emission band of the barium-poor phase doped with Eu^{2+} ions is broader than $\text{BAM}:\text{Eu}^{2+}$, and the band also shifts.^{10,12} $\text{EuMgAl}_{11}\text{O}_{19}$ has not been proved to exist yet, and the barium-poor phase is actually a mixture of phases as shown in the work of Park and Cormack.¹³ These two hypotheses are tested in our study.

The goal of this study was to determine the phase relationship between barium hexa-aluminates, and their possible structures. As additional types of cation are required in certain phases, their distribution in the lattice and their effect on defect properties were investigated. Understanding the behavior of europium in different phases is the main objective. The europium related defects and positions were examined and included both divalent and trivalent europium ions to address the degradation issue. From this work, we want to understand the degradation mechanism so that possible adjustments in chemistry or fabrication can be made to solve the problem of luminescent degradation.

Chapter 2 discusses the structural details of barium hexa-aluminates and their basis, β -alumina. Chapter 3 concentrates on the theory of our simulation methodology: its benefits and shortcomings.

Investigation of the structure and defect properties of BAM is discussed in Chapter 4. The potential dependence of the calculations is also discussed to show the results are independent of the potential used, so that it can be applied for further simulation. Positions of europium ions were determined and are discussed.

Chapter 5 focuses on the migration properties of ions in BAM because it shows some kind of two-dimensional ionic conduction. The effect of the structure of the fast-ionic conduction plane on the behavior of europium ion is presented. The temperature dependence of the migration of Eu ions is also described in order to get an idea of what happens at the thermal degradation temperature. The hypothetical of formation of $\text{EuMgAl}_{11}\text{O}_{19}$ is addressed.

In Chapter 6, a phase, known as the barium-poor phase which is possibly formed during degradation of the luminescence, is considered in detail. Several possible structures are calculated and compared. The intrinsic and extrinsic defects in those structures are also compared. The objective is to understand the difference in the observed emission band between BAM and the barium-poor phase.

Chapter 7 discusses the stability and defect properties of other phases closely related to BAM structure. The involvement of these phases in the degradation process is also discussed. Behavior of europium ions is compared between different phases.

These four chapters are written in a way that they can be published easily. Thus, some information is repeated. A summary and suggestions for future work are provided in the last chapter.

References

1. D. Ravichandran, S.T. Johnson, S. Erdei, R. Roy, and W.B. White, "Crystal Chemistry and Luminescence of the Eu^{2+} -Activated Alkaline Earth Aluminate Phosphors," *Displays*, **19**[4] 197-203 (1999).
2. C.R. Ronda and B.M.J. Smets, "Chemical Composition of and Eu^{2+} Luminescence in the Barium Hexa-aluminates," *J. Electrochem. Soc.*, **136**[2] 570-3 (1989).
3. A.L.N. Stevels and J.M.P.J. Verstegen, " Eu^{2+} Luminescence in Hexagonal Aluminates Containing Large Divalent or Trivalent Cations," *J. Electrochem. Soc.*, **123** 691-7 (1976).
4. B. Smets, J. Rutten, G. Hoeks, and J. Verlijsdonk, " $2\text{SrO}\cdot 3\text{Al}_2\text{O}_3\cdot \text{Eu}^{2+}$ and $1.29(\text{Ba},\text{Ca})\text{O}\cdot 6\text{Al}_2\text{O}_3\cdot \text{Eu}^{2+}$," *J. Electrochem. Soc.* **136**[7] 2119-23 (1989).
5. V. Delacarte, A.K. Harari, and J. They, "Barium Hexaaluminoferrites with New Structural Features," *Mater. Res. Bull.*, **28**[5] 435-43 (1993).
6. M. Bettman and L.L. Turner, "On the Structure of $\text{Na}_2\text{O}\cdot 4\text{MgO}\cdot 15\text{Al}_2\text{O}_3$, a Variant of Beta-Alumina," *Inorg. Chem.*, **10**[7] 1442-6 (1971).
7. N. Iyi, Z. Inoue, and S. Kimura, "The Crystal Structure and Cation Distribution of Highly Nonstoichiometric Magnesium-Doped Potassium Beta-Alumina," *J. Solid State Chem.*, **61**[2] 236-44 (1986).
8. D. Ravichandran, R. Roy, W.B. White, and S. Erdei, "Synthesis and Characterization of Sol-Gel Derived Hexa-aluminate Phosphors," *J. Mater. Res.*, **12**[3] 819-24 (1997).
9. S. Tanaka, I. Ozaki, T. Kunimoto, K. Ohmi, and H. Kobayashi, "Blue Emitting $\text{CaAl}_2\text{O}_4\cdot \text{Eu}^{2+}$ Phosphors for PDP Application," *J. Lumin.*, **87-89**[1] 1250-3 (2000).
10. K. Yokota, S.X. Zhang, K. Kimura, and A. Sakamoto, " Eu^{2+} -Activated Barium Magnesium Aluminate Phosphor for Plasma Displays - Phase Relation and Mechanism of Thermal Degradation," *J. Lumin.*, **92**[3] 223-7 (2001).
11. S. Oshio, K. Kitamura, T. Nishiura, T. Shigeta, S. Horii, and T. Matsuoka, "Analytical Research of Decrease in Luminance Following Annealing of $\text{BaMgAl}_{10}\text{O}_{17}\cdot \text{Eu}^{2+}$ Blue Phosphor for Fluorescent Lamps and Plasma Display Panels," *Natl. Tech. Rep. (Matsushita Electr. Ind. Co.)*, **43**[2] 181-7 (1997).
12. B.M.J. Smets and J.G. Verlijsdonk, "The Luminescence Properties of Eu^{2+} and Mn^{2+} -Doped Barium Hexa-aluminates," *Mater. Res. Bull.*, **21**[11] 1305-10 (1986).

13. J.G. Park and A.N. Cormack, "Crystal/Defect Structures and Phase Stability in Ba Hexa-aluminates," *J. Solid State Chem.*, **121**[1] 278-90 (1996).

2. The Crystal Structure

2.1 Structure of β -Alumina

Beta alumina, unlike other phases of alumina (α, γ, δ), is not a pure two-elements crystal with formula of Al_2O_3 . Although, when it was first reported in 1916, β -alumina was thought to contain no other cations except aluminum. It was suggested by Bragg et al. later that the presence of sodium ion was essential for the stability of the structure.¹ They assigned the formula of $\frac{1}{2}\text{Na}_2\text{O} \cdot 11\frac{1}{2}\text{Al}_2\text{O}_3$ to the crystal but they could not devise a satisfactory structure for it. Later Beevers and Ross confirmed the existence of this phase and refined the structure to the chemical formula of $\text{Na}_2\text{O} \cdot 11\text{Al}_2\text{O}_3$.² After that refinement in 1956, Saalfeld suggested that β -alumina is not stoichiometric. Instead there tends to be excess sodium in the phase: it would be more appropriate to write the formula as $(\text{Na}_2\text{O})_{1+x} \cdot 11\text{Al}_2\text{O}_3$.

There is actually a series of sub-structures in the family of β -alumina labeled β' , β'' , β''' and so on. They can be classified into two groups -- one with a two-fold screw axis and the other with a three-fold screw axis. β - and β''' -alumina have the two-fold screw axis while β'' and β'''' have a three-fold axis. Whether or not β' -alumina is a new phase other than non-stoichiometric β -alumina remains unclear.³

As described in the work of Bragg and the work of Beevers and Ross, β -alumina is a column-like structure. It consists of blocks of cubic close-packed oxygen layers with aluminum in the tetrahedral and octahedral positions. A mirror plane that contains same number of sodium and oxygen ions separates adjacent blocks with the bridge-like Al-O-Al structure parallel to the c-axis.¹ In 1967, β -alumina was discovered to be a fast Na^+ ion conductor.⁴ Since then it has been found that the conduction occurs two-dimensionally in the reflection plane via an interstitialcy mechanism. Because of this the mirror plane is also known as the conduction plane.

Because the blocks, with the formula of $[\text{Al}_{11}\text{O}_{16}]^{1+}$, are quite similar to the structure of spinel, MgAl_2O_4 , with Mg substituted by Al, the blocks are also called spinel blocks.

There are four oxygen layers in a block with the oxygen having a cubic-like stacking order of ABCA. Because of the mirror plane between adjacent blocks, two blocks are required to generate periodicity. In a primitive cell there are two stacking orders, ABCA and ACBA along the c direction. The requirement of two spinel blocks in a primitive cell gives the structure space group of $P6_3/mmc$.

There are four crystallographically distinct aluminum ions in the spinel block: Al(1) ion is in the center of an octahedron formed with six oxygen ions not in the middle of the spinel block; Al(2) ion is in a tetrahedral site across the middle of the spinel block; Al(3) ion, also coordinated with four oxygen ions, is found at the edge of the spinel blocks; Al(4), another six coordinated site, is at the central symmetry site in the middle of the spinel blocks (Fig 1).

Sodium ions were thought to occupy two possible sets of positions in Beevers and Ross' study.² One is at $(\frac{2}{3} \frac{1}{3} \frac{1}{4})$ and the other is at $(0 \ 0 \ \frac{1}{4})$. These two positions seem similar to each other if considering their environment only in the mirror plane. Actually the environments are quite different outside the mirror plane. The first coordinating ions of the $(\frac{2}{3} \frac{1}{3} \frac{1}{4})$ site are six oxygen ions, three above and three below the mirror plane. For the $(0 \ 0 \ \frac{1}{4})$ position, there are two oxygens immediately above and below. Beevers and Ross found that having a sodium ion in the $(\frac{2}{3} \frac{1}{3} \frac{1}{4})$ position would provide a more accurate fit to the x-ray intensity, and concluded that Na^+ would stay there. So this position was named after them to be the Beevers-Ross (BR) site, and the other position was called the anti-BR site. In the notation of the $P6_3/mmc$ space group, BR sites are the 2(d) sites and anti-BR sites are the 2(b) sites. After the discovery that β -alumina is rich in sodium relative to the idealized sodium/aluminum ratio of 1:11, many efforts have been put to accommodate excess sodium into the structure.^{4,5} Peters and Bettman found another position for sodium, $(\frac{5}{6} \frac{1}{6} \frac{1}{4})$, that is referred to as the mO position because it is between two oxygen ions in the mirror plane. Actually, the sodium was not exactly located in the mO site but deviates a little away from it toward an anti-BR site namely "A

site”. Three positions have been defined but only two of them are thought to be occupied by sodium. The anti-BR sites are thought to be impossible for sodium ions. Even for the two possible sites, BR and A sites, the occupancy is not the same. Unlike the ideal structure, only about 75% of the BR sites are occupied by sodium in the material. Table II.1 and 2.2 give the crystallographic data of β -alumina based on the work of Peters et al. and the work of Edstrom et al., respectively.^{4,5}

Table II.1. Positional and Occupation Parameters for β -Alumina (I)
From the work of Peters and Bettman⁴

$$a = 5.594 \text{ \AA} \quad c = 22.53 \text{ \AA}$$

Position	Wyck off	Occupancy	X	Z
O(1)	12(k)	0.996	0.15711	0.05011
O(2)	12(k)	0.998	0.50318	0.14678
O(3)	4(f)	0.993	2/3	0.05552
O(4)	4(e)	1.014	0	0.14253
O(5)	2(c)	1.018	1/3	1/4
Al(1)	12(k)	0.989	-0.16775	0.10630
Al(2)	4(f)	1.028	1/3	0.02477
Al(3)	4(f)	1.006	1/3	0.17555
Al(4)	2(a)	1.025	0	0
Na(1)	2(d)	0.750	-0.2938	1/4
Na(2)	6(h)	0.174	-0.1269	1/4

Excess sodium in the conduction plane needs a charge compensation mechanism. This could be achieved by the occurrence of oxygen interstitials or aluminum vacancies. Actually both defects exist in the material. Roth et al., using neutron diffraction analysis, discovered that aluminum vacancy and aluminum interstitial pairs, aluminum Frenkel defects, exist in the spinel blocks.⁶ But as the aluminum vacancy and interstitial exist as pairs, they would not contribute to the charge compensation. It is the oxygen interstitial that compensates the positive charge introduced by excess sodium. The oxygen interstitials are on the mO sites and are stabilized by adjacent aluminum ions in the spinel

blocks displacing toward it from above and below. Then, a $V_{Al}-Al_i-O_i-Al_i-V_{Al}$ defect complex is formed across the mirror plane. After Reidinger published this work in 1979, the idea became widely accepted, and this kind of defect is called a Reidinger Defect.

Table II.2. Positional and Occupation Parameters for β -Alumina (II)
From the work of Edstrom, Thomas and Farrington⁵

$$a = 5.5929 \text{ \AA} \quad c = 22.526 \text{ \AA}$$

Position	Wyck off	Occupancy	x	Z
O(1)	12(k)		0.15712	0.04998
O(2)	12(k)		0.50305	0.14632
O(3)	4(f)		2/3	0.05525
O(4)	4(e)		0	0.14219
O(5)	2(c)		1/3	1/4
Al(1)	12(k)	0.963	-0.16798	0.10610
Al(2)	4(f)		1/3	0.02482
Al(3)	4(f)		1/3	0.17576
Al(4)	2(a)		0	0
Na(1)	2(d)	0.734	2/3	1/4
Na(2)	6(h)	0.162	0.89702	1/4
Al(5)	12(k)	0.037	-0.16045	0.17523
O(6)	6(h)	0.037	5/6	1/4

2.2 Beta Triple-Prime Phase

The first discovery of β''' -alumina was made by Bettman and Turner in 1970 in an attempt to grow β'' -alumina crystals.³ Its ideal chemical formula is $Na_2O \cdot 4MgO \cdot 15Al_2O_3$. Its structure is similar to that of β -alumina with the same space group of $P6_3/mmc$, except that there are six oxygen layers in a spinel block instead of four. The stacking order of oxygen layers in spinel blocks is also cubic close-packed with aluminum and magnesium in the tetrahedral and octahedral positions just like in $MgAl_2O_4$. The stacking order for

two spinel blocks in a unit cell is CAB CAB and BAC BAC, respectively, separated by the Na-O mirror plane. Table II.3 lists the positions of ions in β''' -alumina.

Table II.3. Positions of Ions in β''' -Alumina
 $a = 5.63 \text{ \AA}$ $c = 31.85 \text{ \AA}$

Position	Wyck off	X	Z
O(1)	12(k)	-1/6	0.0334
O(2)	12(k)	1/2	0.1109
O(3)	12(k)	1/6	0.1765
O(4)	4(f)	1/3	0.0334
O(5)	4(e)	0	0.1109
O(6)	4(f)	2/3	0.1765
O(7)	2(c)	1/3	1/4
Al(1)	12(k)	-1/6	0.1474
Al(2)	4(f)	2/3	0.0701
Al(3)	4(f)	1/3	0.0932
Al(4)	4(f)	1/3	0.1972
Al(5)	4(e)	0	0.0577
Al(6)	6(g)	1/2	0
Na(1)	2(b)	0	1/4
Na(2)	2(d)	2/3	1/4
Na(3)	6(h)	-1/6	1/4

Another mismatch between the β and β''' phases lies in the positions of sodium ions. It was suggested that in β''' phase all three positions, 2(b), 2(d) and 6(h) could be occupied by sodium ions, with different occupancy. Sodium most commonly occurs on the 2(b) sites. Since the two oxygen layers immediately above and below the conduction plane have changed from the A-A stacking in the β phase to B-B and C-C stacking in the β''' phase, the BR site has changed from 2(d) to 2(b) in the symmetric notation, if considering the surroundings.

2.3 Beta Double-Prime Phase

In 1968 Yamaguchi and Suzuki reported a compound namely β' -alumina which was unusually rich in sodium oxide.⁸ Because there is normally excess sodium oxide in β -alumina, whether it was a new phase or just a nonstoichiometric β alumina is doubtful. In the same paper, they also described a new crystal structure, $\text{Na}_2\text{O} \cdot 5\text{Al}_2\text{O}_3$, β'' -alumina. Later Bettman and Peters found a compound, β'' -alumina, containing MgO and analyzed the single crystal using X-ray diffraction.⁹ The ideal chemical formula of the compound was found to be $\text{Na}_2\text{O} \cdot \text{MgO} \cdot 5\text{Al}_2\text{O}_3$. It was suggested that small quantities of Mg or Li stabilize the structure because the β'' -alumina containing no MgO or Li_2O is not stable. Table II.4 shows the crystallographic information of β'' -alumina.

Table II.4. Positions of Ions in β'' -Alumina
 $a = 5.614 \text{ \AA}$ $c = 33.85 \text{ \AA}$

Position	Wyck off	X	Z
O(1)	18(h)	0.156	0.0339
O(2)	18(h)	0.1657	0.2357
O(3)	6(c)	0	0.0961
O(4)	6(c)	0	0.2955
O(5)	3(b)	0	$\frac{1}{4}$
Al(1)	18(h)	0.336	0.0708
Al(2)	6(c)*	0	0.3501
Al(3)	6(c)	0	0.4498
Al(4)	3(a)	0	0
Na(1)	6(c) ¹	$\frac{2}{3}$	$\frac{1}{4}$
Na(2)	18(h) ²	$\frac{1}{2}$	$\frac{1}{4}$

* share with Mg

1 nearly full occupancy

2 two thirds occupancy

Like the β phase, β'' -alumina consists of oxygen close-packed spinel blocks separated by sodium-oxygen planes. Instead of two spinel blocks as in the primitive cell of the β

phase, there are three spinel blocks in a primitive cell of β'' -alumina. β'' -alumina can be seen as a rhombohedral variant of β -alumina. Three spinel blocks are stacked along the three-fold screw axis. Adjacent spinel blocks are no longer mirror symmetric to each other across the sodium-oxygen plane; instead they rotate 120° to each other so the sodium-oxygen plane is no longer a mirror plane. As the screw axis is three-fold, the stacking orders of oxygen close-packed layers in the three spinel blocks are ABCA, CABC and BCAB. The space group of β'' -alumina becomes $R\bar{3}m$.

The actual spinel blocks are distorted (i.e. the oxygen layers are not strictly two-dimensional). They are affected by the distribution of magnesium ions and partial occupancy of sodium ions in the conduction plane, as in the β phase. But in a spinel block, the upper half is centrosymmetric with the lower half at the aluminum ion in the middle of the spinel block.

The conduction plane of β'' -alumina is similar to the β phase but is not exactly the same and the terms “BR, anti-BR and mO” also apply to it. However, now the coordination of BR and anti-BR sites are the same in the β'' phase because of the change in oxygen stacking order. The BR and anti-BR sites are shifted to the centers of elongated tetrahedra rather than octahedra. Sodium ions occupy two thirds of the A sites and nearly fully occupy the BR positions. Bettman and Peters have suggested that the number of sodium ions per conduction plane is less than 2 so that sodium vacancies in the conduction plane make it a fast ion conductor. There is no need for oxygen interstitials in the conduction plane because the charge compensation can be achieved by ions with valence charge less than the $3+$ of aluminum. Therefore, Reidinger defects do not exist in β'' -alumina.

Both β'' and β''' phases have 12 oxygen close-packed layers in one primitive cell but the β''' phase has only two conduction planes instead of three, so the β''' phase is more dense in the c direction than β'' -alumina. The corresponding rhombohedral structure of the β''' phase, known as the β'''' phase, was discovered by Weber and Venro in 1970. It has six oxygen close-packed layers in a spinel block as in the β''' phase and a three-fold screw axis as in β'' phase.

2.4 Barium Magnetoplumbite

Many analogous and similar structures related to β -alumina have been found and studied after the discovery of β -alumina. They are based on Ga_2O_3 or Fe_2O_3 in place of Al_2O_3 such as $\text{K}_2\text{O}\cdot 11\text{Fe}_2\text{O}_3$ and $\text{K}_2\text{O}\cdot 5\text{Fe}_2\text{O}_3$.¹¹ Later a similar compound, $\text{PbO}\cdot 6\text{Fe}_2\text{O}_3$ was determined by Adelsköld and named magnetoplumbite (MP).¹⁰ It has nearly the same structure as β -alumina, except for the mirror plane. Its mirror plane is fully packed with three oxygen ions, one aluminum and one lead ion. Oxygen positions in the mirror plane have changed from 2(c) in the β phase to 6(h) in MP. 6(h) is the mO site in β -alumina in which an oxygen ion in the mirror plane connects with three other oxygen ions in the same plane. So there are three 6(h) sites (mO sites) per mirror plane in a primitive cell, all of them are occupied in MP structure. The aluminum in the mirror plane is at the center of a trigonal bipyramid consisting of five oxygen ions. Three out of the five oxygen ions are at 6(h) sites in the mirror plane; the other two are immediately above and below the mirror plane at the edge of spinel blocks.

MP structures have also been found in the $\text{BaO}\text{-FeO}\text{-Fe}_2\text{O}_3$ ternary system. $\text{BaFe}_{12}\text{O}_{19}$ has been widely investigated to improve the magnetic properties of barium ferrite. During a study of aluminum-substituted barium ferrite, Batti et al. discovered a miscibility gap between barium ferrite and barium aluminate, which led to the reclassification of the structure of barium aluminate from MP to β -alumina. Since then a lot of effort has been put into the investigation of barium aluminates.¹²⁻¹⁶ Two structures are believed to exist in the phase diagram of barium aluminates. One is a barium-poor phase with the 'ideal' formula of $\text{Ba}_{0.75}\text{Al}_{11}\text{O}_{17.25}$ and the other is a barium rich phase that is not fully determined yet.

The barium-poor phase has the same structure as β -alumina but with 75% barium vacancies in the two BR sites in the primitive cell. There is a Reidinger defect, $\text{V}_{\text{Al}}\text{-Al}_i\text{-O}_i\text{-Al}_i\text{-V}_{\text{Al}}$, close to the vacant BR site to compensate the charge. Normally it is described in a 2×2 super-cell, a four primitive-cell superstructure. Three of the four primitive cells are the ideal β -alumina structures with barium in BR sites. One of them is a defect cell without barium ion but with two Reidinger defects. Actually, there are many possible configurations for the barium-poor phase, with different distributions of two

Reidinger defects in the super-cell. Park and Cormack have shown that although the lattice energies of these configurations vary, the differences are small.¹⁷

The barium-poor phase can be considered in this way: taking β -alumina, $\text{Na}_2\text{O}\cdot 11\text{Al}_2\text{O}_3$, as the prototype, 75% of sodium are changed to barium and the effective positive charge generated is compensated by substituting the other 25% sodium with oxygen. It is the uncertainty of the locations of barium or substituted oxygen that makes the barium-poor phase uncertain. $\text{BaMgAl}_{10}\text{O}_{17}$ (BAM) can be described in a similar way but this time all the sodium become barium and the same number of aluminum change to magnesium. When applying the same kind of change to β'' -alumina, one will get barium β'' -alumina. Structures obtained in this way are used as the starting structures for our simulations, but they are surely not in equilibrium and may be heavily strained. In this work, these derived structures will be equilibrated by METAPOCS, using lattice energy minimization technique; the unit cell strain is also minimized¹⁸. Defect calculations are performed after the lattice relaxation.

References

1. W.L. Bragg, C. Gottfried, and J. West, "The Structure of Beta Alumina," *Z. Kristallogr.*, **77**[2] 255-74 (1931).
2. C.A. Beevers and M.A.S. Ross, "The Crystal Structure of "Beta Alumina" $\text{Na}_2\text{O}\cdot 11\text{Al}_2\text{O}_3$," *Z. Kristallogr.*, **97**[1] 59-66 (1937).
3. M. Bettman and L.L. Ternier, "On the Structure of $\text{Na}_2\text{O}\cdot 4\text{MgO}\cdot 15\text{Al}_2\text{O}_3$, a Variant of Beta-Alumina," *Inorg. Chem.*, **10**[7] 1442-6 (1971).
4. C.R. Peters and M. Bettman, "Refinement of the Structure of Sodium β -Alumina," *Acta Crystallogr., Sect. B: Struct. Crystallogr. Cryst. Chem.*, **B27**[9] 1826-34 (1971).
5. K. Edstrom and J.O. Thomas, "Sodium-Ion Distribution in Na^+ Beta-Alumina: Crystallographic Challenge," *Acta Crystallogr., Sect. B: Struct. Sci.*, **B47**[2] 210-6 (1991).
6. W.L. Roth, F. Reidinger, and S.L. Placa, "Studies of Stabilization of Transport Mechanisms in Beta and Beta" Alumina by Neutron Diffraction," pp. 223-41 in *Superionic Conductors*. Edited by G. D. Mahan and W. L. Roth. Plenum, New York, 1976.
7. M. Bettman and L.L. Ternier, "On the Structure of $\text{Na}_2\text{O}\cdot 4\text{MgO}\cdot 15\text{Al}_2\text{O}_3$, a Variant of Beta-Alumina," *Inorg. Chem.*, **10**[7] 1442-6 (1971).
8. G. Yamaguchi and K. Suzuki, *Bull. Chem. Soc. Jap.*, **41** 93 (1968). As cited in M. Bettman and L.L. Ternier, "On the Structure of $\text{Na}_2\text{O}\cdot 4\text{MgO}\cdot 15\text{Al}_2\text{O}_3$, a Variant of Beta-Alumina," *Inorg. Chem.*, **10**[7] 1442-6 (1971).
9. M. Bettman and C.R. Peters, "The Crystal Structure of $\text{Na}_2\text{O}\cdot \text{MgO}\cdot 5\text{Al}_2\text{O}_3$ with Reference to $\text{Na}_2\text{O}\cdot 5\text{Al}_2\text{O}_3$ and Other Isotypal Compounds," *J. Phys. Chem.*, **73**[6] 1774-80 (1969).
10. V. Adelskold, "X-Ray Studies on Magnetoplumbite, $\text{PbO}\cdot 6\text{Fe}_2\text{O}_3$ and Other Substances Resembling β -Alumina, $\text{Na}_2\text{O}\cdot 11\text{Al}_2\text{O}_3$," *Ark. Kemi, Mineral. Geol.*, **12A** 1-9 (1938).
11. C.J.M. Rooymans, C. Langereis, and J.A. Schulkes, " KFe_5O_8 , a New Phase in the $\text{K}_2\text{O}\text{-Fe}_2\text{O}_3$ System," *Solid State Commun.*, **4**[3] 85-7 (1965).
12. H.W. Zandbergen, F.C. Mijlhoff, D.J.W. Ijdo, and G.V. Tendeloo, "A Model for the Structure of $1.31\text{BaO}\cdot 6\text{M}_2\text{O}_3$; M = Al, Ga; An Electron Microscopy Study," *Mater. Res. Bull.*, **19**[11] 1443-50 (1984).

13. S. Kimura, E. Bannai, and I. Shindo, "Phase Relations Relevant to Hexagonal Barium Aluminates," *Mater. Res. Bull.*, **17**[2] 209-15 (1982).
14. N. Iyi, S. Takekawa, Y. Bando, and S. Kimura, "Electron Microscopic Study of Barium Hexa-aluminates," *J. Solid State Chem.*, **47**[1] 34-40 (1983).
15. F.P.F. van Berkel, H.W. Zandbergen, G.C. Verschoor, and D.J.W. Ijdo, "The Structure of Barium Aluminate, $Ba_{0.75}Al_{11}O_{17.25}$ " *Acta Crystallogr., Sect. C: Cryst. Struct. Commun.*, **C40**[7] 1124-7 (1984).
16. N. Yamamoto and M. O'Keefe, "Electron Microscopy and Diffraction of Phases in the Al_2O_3 - $BaAl_2O_4$ System," *Acta Crystallogr., Sect. B: Struct. Sci.*, **B40**[1] 21-6 (1984).
17. J.G. Park and A.N. Cormack, "Crystal/Defect Structures and Phase Stability in Ba Hexa-aluminates," *J. Solid State Chem.*, **121**[1] 278-90 (1996).
18. C.R.A. Catlow, A.N. Cormack, and F. Theobald, "Structure Prediction of Transition-Metal Oxides Using Energy-Minimization Techniques," *Acta Crystallogr., Sect. B: Struct. Sci.*, **B40**[3] 195-200 (1984).

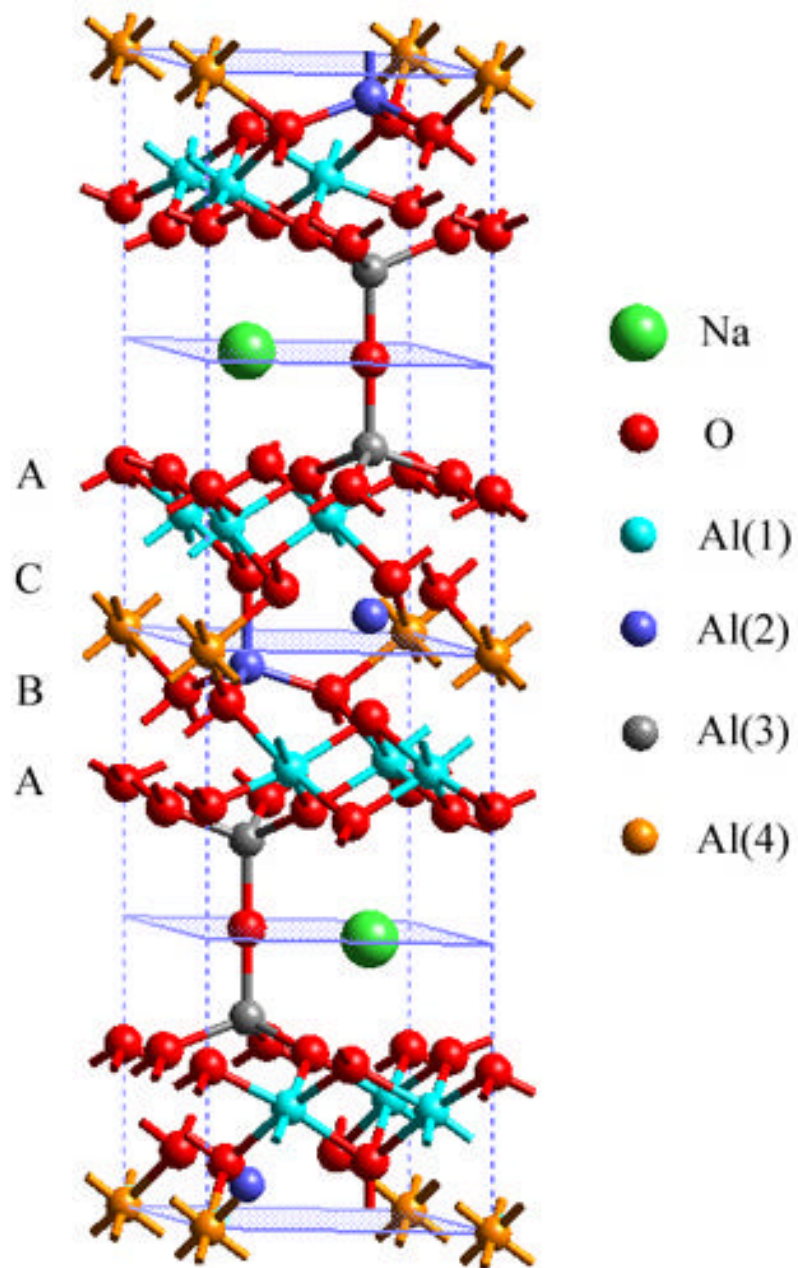


Figure 2.1. Structure of ideal β -alumina $\text{NaAl}_{11}\text{O}_{17}$.

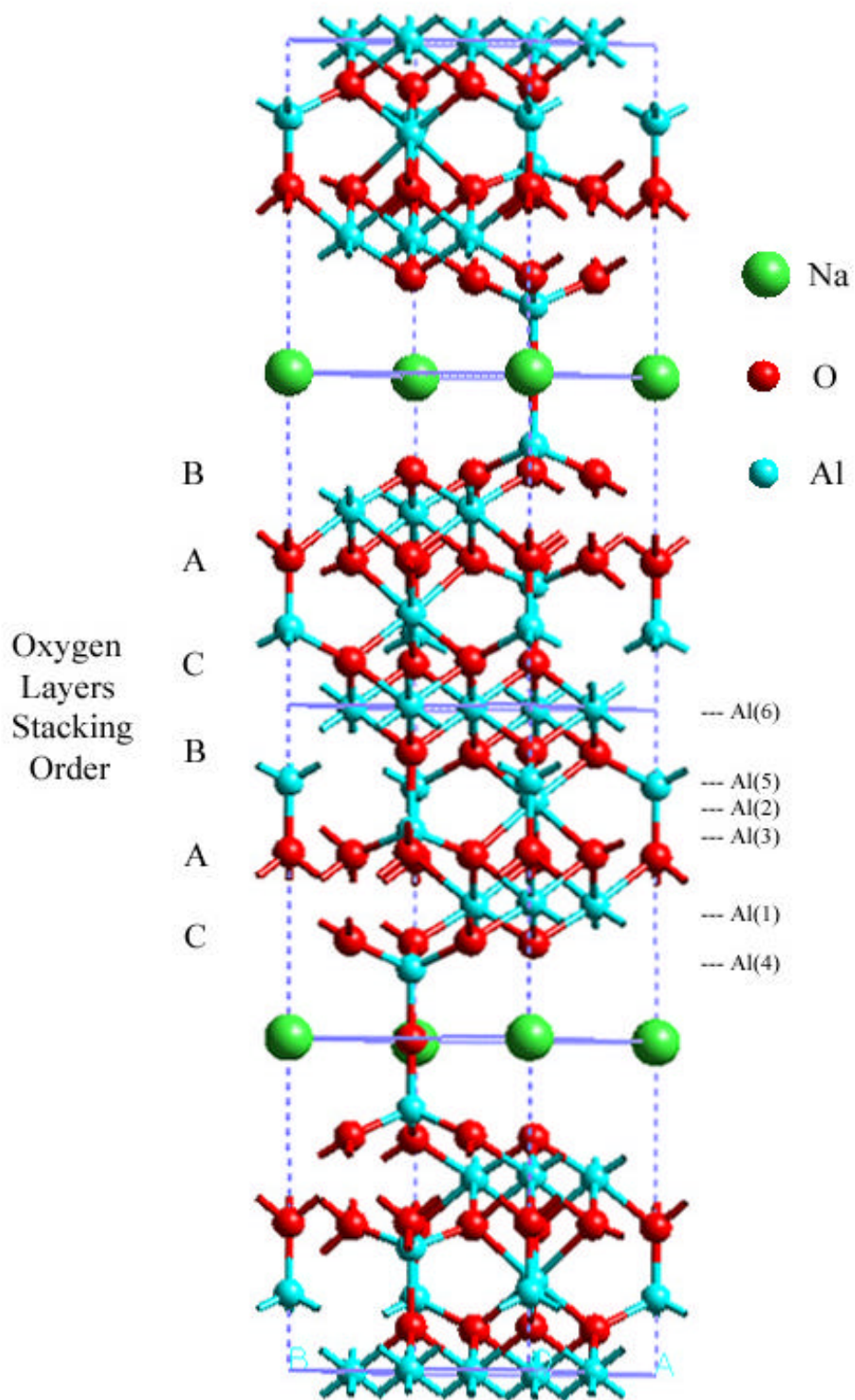


Figure 2.2. Structure of ideal β''' -alumina $\text{Na}_2\text{O}\cdot\text{MgO}\cdot 15\text{Al}_2\text{O}_3$. All Mg are shown as Al.

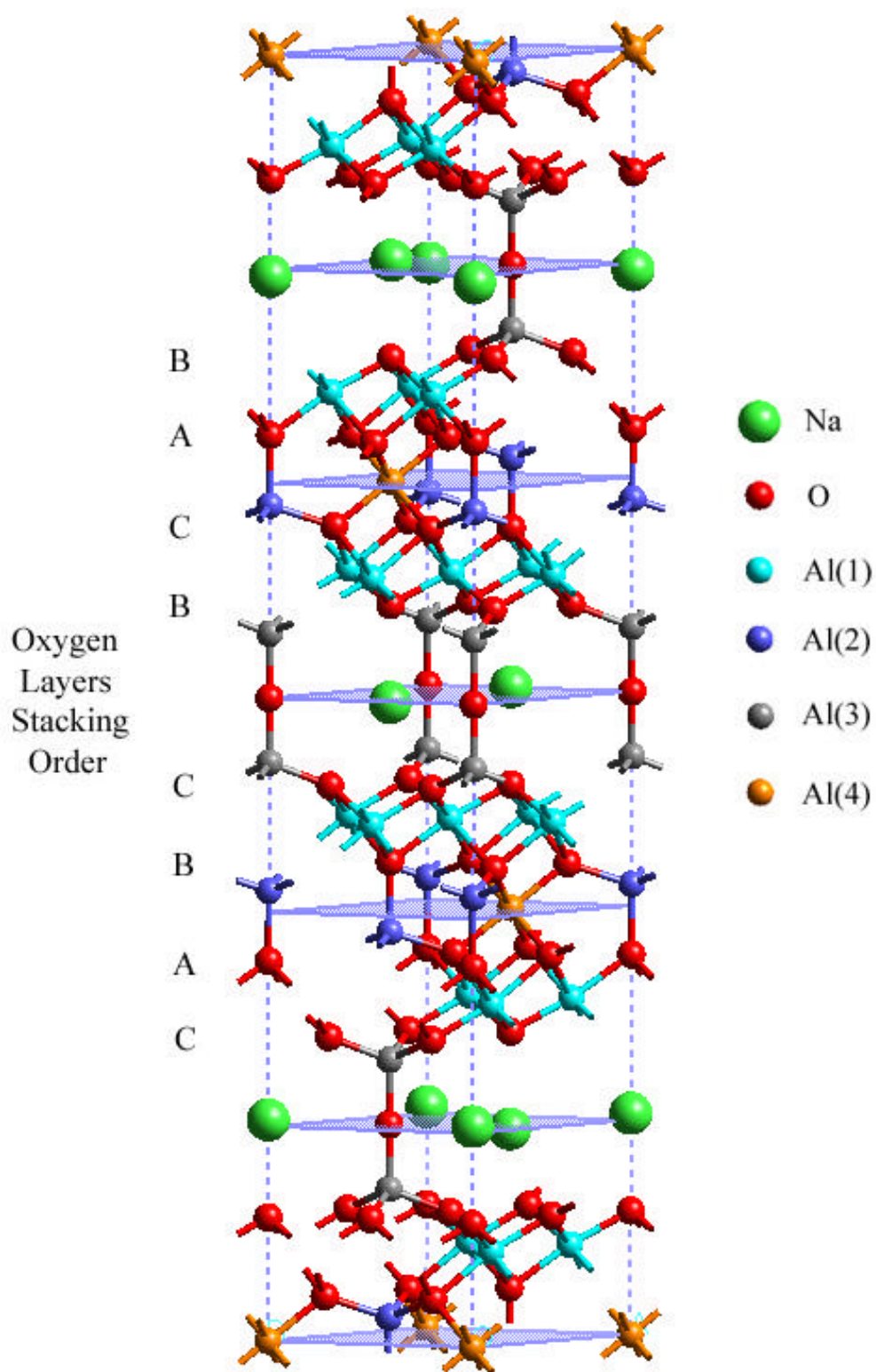


Figure 2.3. Structure of ideal β'' -alumina.

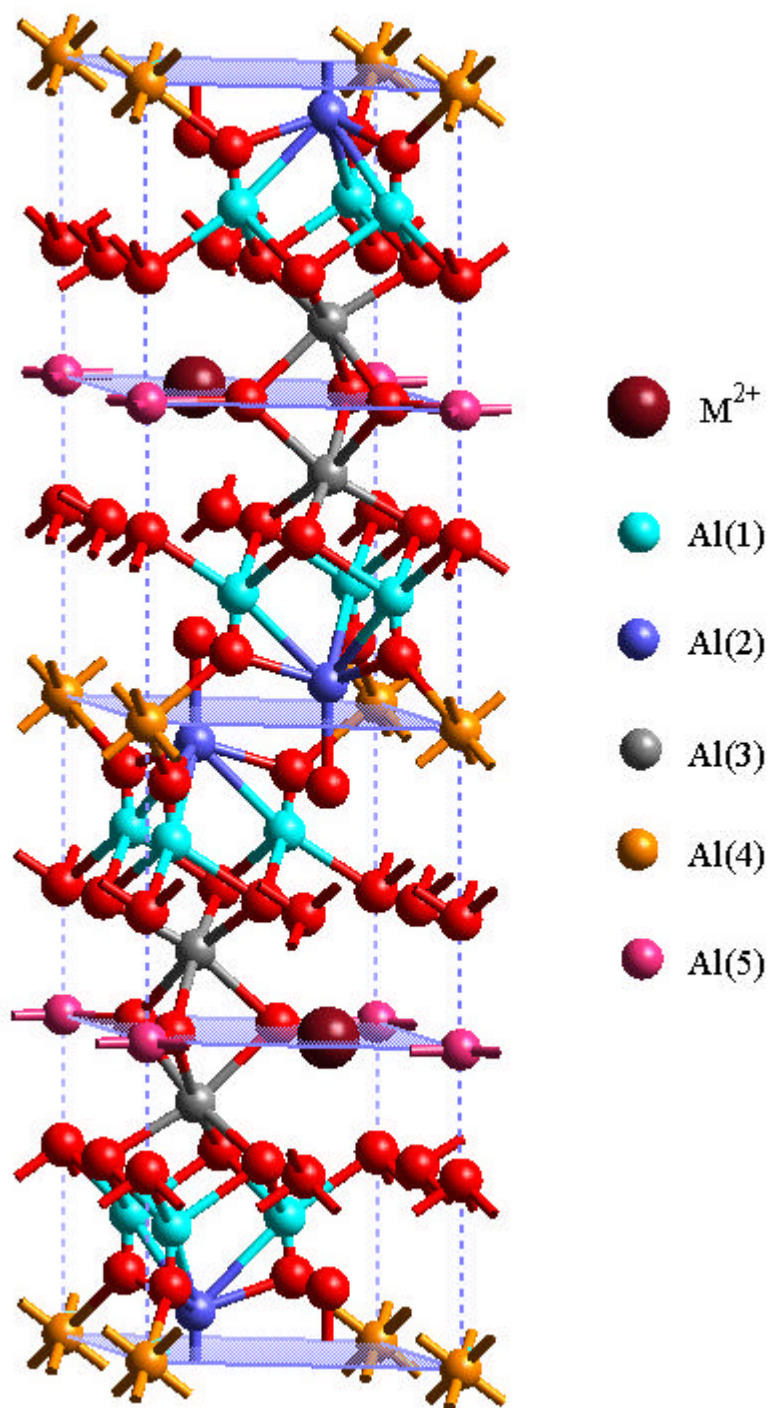


Figure 2.4. Structure of ideal manetoplumbite $MA_{12}O_{19}$.

3. Atomistic Computer Simulation Techniques

3.1 Introduction

With expansion of the region of human life, materials become more and more important to society. Ceramic materials, an important class of materials, have found applications in nearly all advanced technologies. Ceramic science was studied empirically initially. Later, as the characterization techniques, such as X-Ray diffraction and transmission electron microscopy, were developed, more and more principles and theories were suggested by experience. Now, computer simulation has assumed importance in the study of materials science.

Compared to computer simulation, traditional experimental studies have some shortcomings in studying the disorder and complex materials. First of all, a lot of parameters need to be determined for complex systems: not only the unit cell dimensions but also the coordinates of asymmetric ions. One would not be surprised to see that long periods of experiment time and intense arguments occur before general acceptance of some hypotheses. Secondly, detailed local information such as defect structure and ion distribution in non-stoichiometric phases is difficult to determine experimentally. Thirdly, the measurement of a specific property may be the combination of effects of several factors, and it may not be easy to differentiate between them. According to Moore's law, the power of computer doubles every eighteen months, which is unimaginable for experimental techniques. So, computer simulation has become more and more widely adopted in scientific research. The validity of many simulation studies has been demonstrated by later experiments.¹⁻³ Right now, computer simulation has covered many scales, electronic scale for superconductivity, atomistic scale for crystal structure and larger scale for finite element study of mechanical properties. In the present work, atomistic scale of simulation has been practiced and compared to the experiment results. This chapter briefly describes the atomistic simulation methodology.

Simulation speed is an important issue that needs to be addressed. Practically, simulation time should not last too long or the benefits of computer simulation will be lost. A compromise between the time consumed and the calculation algorithm must be made. Even today, the speed of computer does not quite match the need for many simulations such as first-principle simulations and large-size molecular dynamics simulations (more than ten thousand atoms). Many algorithms with approximations have been applied to calculations in order to shorten the simulation time, and therefore, some precision will be lost in this process. So, the properties calculated are sometimes more qualitative than quantitative.

Simulations in this study are based on inter atomic potentials (i.e. the description of interactions between particles in a numerical way). The extent to which the potential model represents the reality affects the accuracy of calculated results, and thus the potential model is the key factor in the simulation.

3.2 Inter Atomic Potentials

The materials being studied in this work are mainly ionic materials. For ionic materials, the interatomic potentials can be divided into two parts, Coulombic and non-Coulombic terms.⁴

$$V_{ij} = Z_i Z_j / r_{ij} + U_{ij}(r). \quad (1)$$

The first term in the above equation is the long-range Coulombic interaction. Normally, integer charges are assigned to each species of ion. But it is possible to assign to them an effective partial charge. It all depends on the actual determination process of the potential model. It has been found for most systems, including oxides, that integral ionic charges are adequate.^{3,5}

The second term on the right side in Eqn.1, $U_{ij}(r)$, represents both short-range (overlap of electronic clouds) and long-range (dispersion) interactions. An assumption has been made about the potential model of ionic materials that the covalent distortion of the electron cloud is so small that it can be treated as polarization perturbation. This assumption limits the potential model to ionic, or mainly ionic, materials.⁴ Then $U_{ij}(r)$ is separated into two terms, one with and one without polarization contributions.

$$V_{ij} = Z_i Z_j / r_{ij} + U_{ij}^N(r) + U_{ij}^P(r, F_i, F_j). \quad (2)$$

The polarizative contribution not only depends on the separation of ions but also on the electronic static field (F_i and F_j).

Many methods have been proposed to address the simulation of polarization in ionic materials. Among them, the core-shell model introduced by Dick and Overhauser is widely used, and it is also the mechanism used in the present work.⁶ In the core-shell model, ions are treated as atomic cores associated with a massless shell by a harmonic spring. Normally, the massless shell possesses a charge Y calculated by the ion polarizability, but the sum of charges on the core and shell must be equal to the total ionic charge. The polarization of ions is modeled by the contraction and expansion of the spring between the core and shell, with spring constant K . The polarizability of the free ion is described as

$$a = Y^2 / K. \quad (3)$$

The values; Y and K can be fitted by ab-initio (quantum mechanical) methods. Since ab-initio calculations take a very long time to run and the results are not very satisfactory, Y and K parameters are often fitted to elastic, dielectric, phonon frequencies and crystal data. It is not easy to get a single set of parameters to make calculation of all these properties agree with the observed value. Normally, the crystal data are considered the most important factor compared to other properties; the principal criterion of an adequate potential model is the extent of similarity between calculated and measured crystal structures.

A lot of forms have been suggested for the non-polarization potential term such as the 12-6 potential, Lennard-Jones potential and Buckingham potential.⁷ The model established by Fumi and Tosi, a Buckingham potential model, is used in this work; it has the following functional form:⁸

$$U_{ij}^N(r) = A_{ij} \exp(-r_{ij} / r) - C_{ij} / r^6. \quad (4)$$

Sometimes an additional term D_{ij}/r^8 is also included in the model.⁴ Like the parameters in the shell model, the parameters A , r and C are determined by least squares fitting to lattice properties. The calculated structure must be strain-free as in the real material in its thermally equilibrated state; this must be able to be achieved by a proper potential model.

Another problem may arise in fitting the potential: so many constants need to be determined at the same time that the existing lattice properties are not sufficient. For example, in the simple binary compound, three interactions exist: cation-cation, anion-anion and cation-anion. If all five constants (A , r , C , Y and K) are to be determined for each interaction, thirteen constants are necessary to be determined (there is no Y and K for cation-anion interaction). Things will become worse for more complex compounds. So additional approximations have been made to limit the number of parameters. First, as the polarisabilities of cations, especially those with charges greater than 2, are low, it is quite reasonable to assume that cations are non-polarisable. Second, because the cation-cation separations are large enough and because of the anion screening effect, the short-range interactions between cations are so small that they may be neglected. Third, it has been found that a common anion-anion interaction can be used for a series of materials such as alkaline-earth oxides.⁹ For example, the O-O potential derived from MgO can be applied to much more complex structures like MgAl₂O₄.

Because of the above assumptions, the generated potential will not be perfect, and it has limitations in application. If two ions are far away from each other, the short-range interaction becomes so small that it can be treated as zero without problem. A distance cutoff is used to define the range beyond which short-range interaction is zero. The use of a short-range potential cutoff also improves the calculation speed.

Another thing to which attention should be paid is that the potential may be coordination dependent. There is no doubt that cation-anion distances are different for different numbers of anions around the cation, so the cation radius differs in tetrahedral and octahedral sites. To take into account of the effect of coordination number, a modification of the potential model may be necessary. Cormack et al. used an approach of adjusting the pre-exponential term, A , to represent the change in radius.¹⁰

For the Huggins-Mayer relationship

$$A = b \exp(r / r) \quad (5)$$

the difference between tetrahedral and octahedral positions in radius is

$$\Delta r = r_{oct} - r_{tet} \quad (6)$$

so the pre-exponential term A of ion in tetrahedral site is given by

$$A_{tet} = A_{oct} \exp(-\Delta r / r). \quad (7)$$

This kind of potential adjustment has been applied to the aluminum-oxygen potential for the different aluminum sites in our study.

3.3 Minimization Techniques

A lattice simulation consists of two parts, calculation of the lattice energy and the minimization of the lattice energy. The perfect lattice energy calculation sums all of the interaction potentials, both Coulombic and non-Coulombic. As the long-range Coulombic potential does not converge quickly, a technique developed by Ewald is normally used, in which the point charge is replaced by an electron cloud with a Gaussian distribution and then, the whole system is translated into reciprocal space.⁷ Summation of the Fourier series in reciprocal space converges quickly, and the overlap between electron clouds is subtracted in real space, a procedure that also converges quickly.

The concept of energy minimization is simple; lattice parameters and the ion coordinates are adjusted toward the direction that will lower the lattice energy. The equilibrated structure is considered as an equilibrium state between structure and lattice energy (i.e. the equilibrated lattice structure has the lowest lattice energy compared to any other lattice structures with small perturbation to it). If the potential model precisely described the crystal, one would reach the observed structure from a closely related structure by energy minimization with the assumption that there is no other energy minimum between the starting structure and equilibrated structure. That is, the basis used to estimate structure from a similar crystal but with different chemical composition. The lattice energy minimization technique can also be used to test the credibility of a potential model by comparing the calculated structure with the observed one.

Similar to experiments, the simulation conditions also affect the minimization process. A minimum lattice energy can be achieved by adjusting the coordinates only, or by adjusting both lattice parameters and coordinates at the same time. The former condition is called Constant Volume, and the latter is called Constant Pressure. As indicated earlier, the thermally equilibrated observed structure is strain free so that the minimization process must also maintain structure in this situation. The internal strain on an ion can be calculated by the differentiation of the sum of the potential on this ion with respect to its coordinates.

Here, the lattice energy minimization discussed by Catlow and Norgett is described under the constant pressure condition. For a unit cell with N ions, the increase in the lattice energy with the displacement of one ion can be written as

$$U(r') = U(r) + g^T \cdot d + (1/2)d^T \cdot w \cdot d \quad (8)$$

where the new ion position r' is displaced from r by the strain vector d . d has $N+6$ dimensions for the whole structure: three dimensions x , y and z for each ion and 6 independent bulk strain terms for the unit cell. For ions, $d = r' - r = dr$ and $g = \nabla U / \nabla dr$, the first derivative of U with respect to displacement. For the other six bulk strains, $d = de$. e is a component of the reduced strain matrix Δe .

$$\Delta e = d \begin{vmatrix} e_1 & (1/2)e_6 & (1/2)e_5 \\ (1/2)e_6 & e_2 & (1/2)e_4 \\ (1/2)e_5 & (1/2)e_4 & e_3 \end{vmatrix} \quad (9)$$

and the related $g = \nabla U / \nabla de$. W is the second derivative of lattice energy given by the relations,

$$W = \begin{vmatrix} \frac{\partial^2 U}{\partial dr \partial dr} & \frac{\partial^2 U}{\partial dr \partial de} \\ \frac{\partial^2 U}{\partial de \partial dr} & \frac{\partial^2 U}{\partial de \partial de} \end{vmatrix} = \begin{vmatrix} W_{rr} & W_{re} \\ W_{er} & W_{ee} \end{vmatrix} \quad (10)$$

Applying the equilibrium condition

$$\nabla U / \nabla dr = 0 \quad (11)$$

to differentiate equation (8) will generate

$$0 = g + W_{rr} \cdot dr \rightarrow g = -W_{rr} \cdot dr \quad (12)$$

which determines the condition for the minimum $U(r)$. Rewriting equation (12) in order to get the function of displacement of ions,

$$dr = -W_{rr}^{-1} \cdot g. \quad (13)$$

If only one ion is allowed to move, equation (13) gives the optimum displacement of the ion. Since every ion is allowed to relax (i.e. the strain field varies after the minimization), energy minimization must be done by iteration, updating the coordinates with equation (13). In this process, the most time-consuming step is to calculate the inverse matrix of W_{rr} for each ion because it must be recalculated at each iteration.

The simulation time can be dramatically reduced if the fast matrix method used by Norgett and Fletcher is adopted.¹¹ W_{rr}^{-1} is not calculated at each iteration, instead it will be estimated from the value of last iteration. The inverse matrix at iteration $n+1$ can be estimated from the matrix at iteration n as:

$$W_{rr}^{-1}(n+1) = W_{rr}^{-1}(n) + \frac{\mathbf{dr} \cdot \mathbf{dr}^T}{\mathbf{dr}^T \cdot \mathbf{dg}} - \frac{W_{rr}^{-1}(n) \cdot \mathbf{dg} \cdot \mathbf{dg}^T \cdot W_{rr}^{-1}(n)}{\mathbf{dg}^T \cdot W_{rr}^{-1}(n) \cdot \mathbf{dg}} \quad (14)$$

where $\mathbf{dr} = r_{n+1} - r_n$ and $\mathbf{dg} = g_{n+1} - g_n$. In this way, not only has the time to invert the matrix been shortened but also the time spent on the calculation of the W_{rr} matrix. Its limitation is that the error in the estimation process is cumulative so that the matrix must be recalculated after every 10 to 30 iterations.

Constant Volume minimization is simpler than Constant Pressure for it does not need to consider the change of lattice parameters (i.e. d has only 3N dimension and W has only one term W_{rr}).

3.4 Defect Energy Calculations

After introducing a defect into structure, the defective lattice is relaxed to minimize the energy, to make the system stable. Thus, the defect energy calculation is also known as a lattice relaxation process. In defect energy calculations, the internal energy of the perfect lattice is set to zero. Since energy is required to move an ion from the lattice to infinity, the vacancy defect energy is always positive. The introduction of an additional ion into the crystal is not the same; normally, the interstitial defect energy is negative, but if it causes too large a stress in the lattice, it can be positive.

Since the relaxation of the structure closest to the defect is greatest and decreases with distance from the defect, Lidiard and Norgett have developed a two-region strategy.¹² As shown in Fig. 3.1, an inner region immediately surrounding the defect is simulated on the atomic scale by solving the equation (13) as in the perfect lattice simulation; and an outer region which is slightly disturbed is approximately treated as a dielectric continuum inside which ions are displaced according to the electric field of the defect. The boundary between these two regions must be addressed explicitly.

The total energy of a defect system is written as

$$E = E_I(X) + E_{II}(Y) + E_{I,II}(X, Y). \quad (15)$$

$E_I(X)$ is the energy of inner region I and X are the vectors describing ions' positions in region I. $E_{II}(Y)$ is the energy of outer region II and Y is the corresponding vector for the displacement of ions in region II which is determined by the detailed X configuration in region I. $E_{I,II}(X, Y)$ is the interaction energy between region I and region II.

The energy of region is assumed to be a quadratic function of Y ,

$$E_{II}(Y) = \frac{1}{2} Y^T \cdot A \cdot Y, \quad (16)$$

and the equilibrium condition for displacements in region II is

$$\frac{\partial E}{\partial Y} = 0 = A \cdot Y + \frac{1}{2} \frac{\partial E_{I,II}(X, Y)}{\partial Y} \Big|_{Y=Y'}. \quad (17)$$

Y' is the equilibrium value of Y corresponding to arbitrary X . The energy of region II can be rewritten as

$$E_{II}(Y) = -\frac{1}{2} \frac{\partial E_{I,II}(X, Y)}{\partial Y} \Big|_{Y=Y'} \cdot Y \quad (18)$$

and the total energy changes to

$$E = E_I(X) + E_{I,II}(X, Y) - \frac{1}{2} \frac{\partial E_{I,II}(X, Y)}{\partial Y} \Big|_{Y=Y'} \cdot Y. \quad (19)$$

X can be determined now by applying the equilibrium condition for X

$$\frac{dE}{dX} = \frac{\partial E}{\partial X} \Big|_{Y=Y'} + \frac{\partial E}{\partial Y} \Big|_{X'} \cdot \frac{\partial Y}{\partial X} = 0 \quad (20)$$

since Y is in equilibrium with respect to arbitrary X' , $\frac{\partial E}{\partial Y} = 0$, we can rewrite Eqn. (20) as

$$\frac{\partial E}{\partial X} \Big|_{Y=Y'} = \frac{\partial E_I(X)}{\partial X} + \frac{\partial E_{I,II}(X, Y)}{\partial X} \Big|_{Y=Y} - \frac{1}{2} \frac{\partial^2 E_{I,II}(X, Y)}{\partial X \partial Y} \Big|_{Y=Y'} \cdot Y = 0. \quad (21)$$

The position of the ions can be calculated from equation (21) and the lattice relaxation is solved. In order to get a self-consistent solution, equations (18) and (21) must be calculated iteratively until no further changes in X and Y are seen.

The above process is theoretically deduced from the pure energy and equilibrium condition. In order to include the potential model, the energy terms must be expanded in terms of the potential model. For a perfect lattice, the energy is summed as

$$E = \sum_{ij} U_{ij} (|R_i - R_j|) \quad (22)$$

where R is the vector position of the ion. In the same way, the defect lattice energy is written as

$$E = \sum_{ij} U_{ij} (|r_i - r_j|) \quad (23)$$

where r is the vector describing the relaxed ion's position. The defect energy is the difference between these two energies:

$$E = \sum_{ij} U_{ij} (|r_i - r_j|) - \sum_{ij} U_{ij} (|R_i - R_j|) \quad (24)$$

Considering the separation of the summation into sums within regions and sums between two regions, there are an infinite number of ions in region II so that it will take a long time for the sum to converge. Further simplification has been made. The defect energy can be rewritten in the following way:

$$\begin{aligned} E &= \sum_{ij(I)} [U_{ij} (|r_i - r_j|) - U_{ij} (|R_i - R_j|)] \\ &+ \sum_{\substack{i(I) \\ j(II)}} [U_{ij} (|r_i - r_j|) - U_{ij} (|R_i - R_j|)] \\ &+ \sum_{\substack{i(I) \\ j(II)}} [\partial U_{ij} (|r_i - r_j|) / \partial r_{ij} - \partial U_{ij} (|R_i - R_j|)] \cdot (r_j - R_j). \end{aligned} \quad (25)$$

here the summation in region II has been transformed into a summation between region I and region II, but there are still an infinite number of interactions. Mott and Littleton have defined two parts in the outer region to get over this problem.¹³ Part IIa has the size of at least the short-range potential cutoff outside region I. Ions in IIa interact with ions in region I with the full potential model, while region IIb only interacts with the effective defect charge in region I by Coulombic force. Hence, the energy of region IIb is

$$E_{I,II}^b(X, Y) = -Q^2 \sum_{j(IIb)} \frac{q_j M_j}{|R_j|^4} \quad (26)$$

where Q is the effective charge of region I, $q_j M_j$ and R_j are the charge, Mott-Littleton parameter and position vector, respectively, of the ion j in region IIb.

As long as the region I size is large enough so that the assumption of the two-region technique is valid, the defect energy will converge quickly to some value and not depend

on the region size any more. Normally, region I will contains more than one hundred ions. The software used in this work is METAPOCS and CASCADE:¹⁴ the former is for lattice relaxation, and the later is for defect calculation.

References

1. A.S. Nowick and B.S. Lim, "Electrical Relaxations: Simple Versus Complex Ionic Systems," *Phys. Rev.*, **B63**[18] 184115-22 (2001).
2. A.N. Cormack, C.R.A. Catlow, and A.S. Nowick, "Theoretical Studies of Off-Center Sc^{3+} Impurities in CeO_2 ," *J. Phys. Chem. Solids*, **50**[2] 177-81 (1989).
3. G.V. Lewis and C.R.A. Catlow, "Defect Studies of Doped and Undoped Barium Titanate Using Computer Simulation Techniques," *J. Phys. Chem. Solids*, **47**[1] 89-97 (1986).
4. W.C. Mackrodt, "Theory of Defect Calculations for Ionic And Semi-Ionic Materials," pp. 107-30 in NATO ASI Series: *Mass Transport in Solids*. Edited by F. Beniere and C. R. A. Catlow. Plenum Press, New York and London, 1983.
5. T.S. Bush, J.D. Gale, C.R.A. Catlow, and P.D. Battle, "Self-Consistent Interatomic Potentials for the Simulation of Binary and Ternary Oxides," *J. Mater. Chem.*, **4**[6] 831-7 (1994).
6. B.G. Dick and A.W. Overhauser, "Theory of the Dielectric Constants of Alkali Halide Crystals," *Phys. Rev.*, **112**[1] 90-103 (1958).
7. T.B. Forester and W. Smith, *DL_POLY Reference Manual*, 2.0 ed.; pp. 45-7. CCLRC, Daresbury Laboratory, Warrington, UK., 1995.
8. F.G. Fumi and M.P. Tosi, "Ionic Sizes and Born Repulsive Parameters in the NaCl-Type Alkali Halides-I," *J. Phys. Chem. Solids*, **25**[1] 31-43 (1964).
9. G.V. Lewis and C.R.A. Catlow, "Potential Models for Ionic Oxides," *J. Phys. C: Solid State Phys.*, **18**[6] 1149-61 (1985).
10. A.N. Cormack, G.V. Lewis, S.C. Parker, and C.R.A. Catlow, "On the Cation Distribution of Spinels," *J. Phys. Chem. Solids*, **49**[1] 53-7 (1988).
11. M.J. Norgett and R. Fletcher, "Fast Matrix Methods for Calculating the Relaxation about Defects in Crystals," *J. Phys. C: Solid State Phys.*, **3**[11] L190-2 (1970).
12. A.B. Lidiard and M.J. Norgett, "Point Defects in Ionic Crystals," pp. 385-412 in *Computational Solid State Physics*. Edited by F. Herman, N. W. Dalton, and T. R. Koehler. Plenum, New York, 1972.
13. N.F. Mott and M.J. Littleton, "Conduction in Polar Crystals. I. Electrolytic Conduction in Solid Salts," *Trans. Faraday Soc.*, **34**[1] 485-99 (1938).

14. C.R.A. Catlow, A.N. Cormack, and F. Theobald, "Structure Prediction of Transition-Metal Oxides using Energy-Minimization Techniques," *Acta Crystallogr., Sect. B: Struct. Sci.*, **B40**[3] 195-200 (1984).

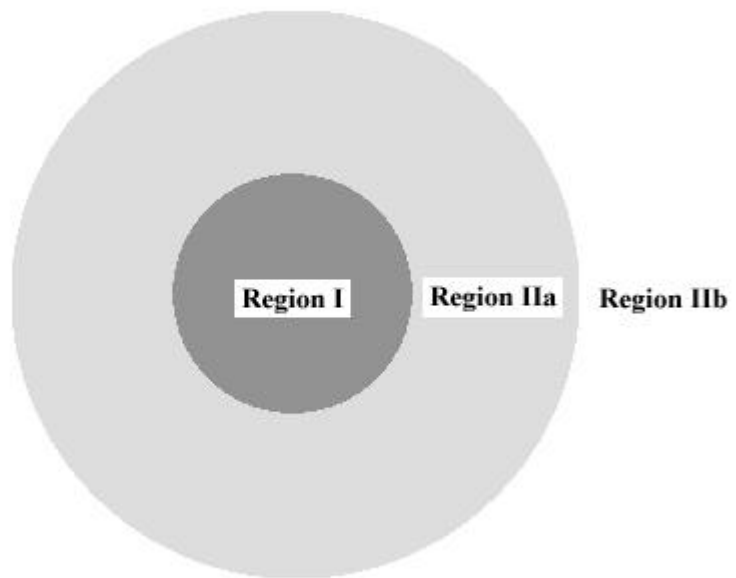


Figure 3.1. Two regions for defect energy calculation. Defect is in the center of region I.

4. Defects in BaMgAl₁₀O₁₇: Eu²⁺ Blue Phosphor

Abstract:

The luminescent properties of BaMgAl₁₀O₁₇: Eu²⁺ blue phosphor are closely related to the valence state of europium inside the crystal and its defect structure. Because of the complexity of the BAM structure, research was carried out to study the europium-related defects by computer simulation. Two lattices with different Mg distributions were found to have the same lattice energy, but the arrangement of Mg affects the defect energy and position. Eu³⁺ behavior was also discussed to address the oxidation-induced luminescent degradation. Two energetically most-favorable positions were found for europium, one is the Beavers-Ross site on the conduction plane for Eu²⁺, and the other is the Al(2) site in the middle of the spinel block for Eu³⁺. Results of defect complex and bond-valence calculations have suggested that the large europium ion can reside in the oxygen close-packed spinel blocks. A comparison of europium defect properties calculated with two different potential models suggests that results of the simulations are potential independent.

4.1 Introduction

The optical properties of phosphor materials depend not only on the active elements but also on the host materials. The active ions, typically rare-earth ions, are introduced into the host material as dopants. The local environment of the active element will change the emission spectrum of the final phosphor material. In an increasing number of cases, host compounds have somewhat complex crystal structures, which provide several possible sites for the active ion.

$\text{BaMgAl}_{10}\text{O}_{17}$ (BAM): Eu^{2+} is widely used as a blue phosphor for lamp and display panels. It is not clear where the exact positions of europium ions are in the structure, from experiment because of the complex crystal chemistry of BAM structure. Computer simulation based on the classical Born model has been found to be a successful method in the defect studies.

In this paper, various aspects of barium β -aluminates (BAM) have been investigated with the aid of computer simulation; these include the BAM structure itself, magnesium distributions and defect properties. The intrinsic defects, besides the europium extrinsic defects, have also been studied because they affect charge compensating mechanisms when europium ions are introduced into the structure. The potential dependence of the results has also been investigated.

4.1.1 Detail of Structure

The BAM structure was derived from that of β -alumina ($\text{NaAl}_{11}\text{O}_{17}$) and the β -alumina was first discovered by Rankin and Merwin.¹⁻³ Bragg, and Beevers and Ross have refined the β -alumina structure with x-ray diffraction; the atom positions are summarized in Table IV.1.^{4,5} The structure has a space group of $\text{P6}_3/\text{mmc}$ and can be described as consisting of oxygen close-packed spinel blocks of composition $[\text{Al}_{11}\text{O}_{16}]^{+1}$ separated by mirror planes of composition $[\text{NaO}]^{-1}$ (Fig. 4.1). The stacking order of oxygen close-packed layers in one spinel block is ABCA. Sodium occupies the Beevers-Ross (BR) site in the mirror plane. Aluminum ions partially occupy octahedral

and tetrahedral sites. Based on the symmetry, there are four aluminums, five oxygens and one sodium in symmetrically independent positions. In forming BAM, sodium is replaced by barium and the same number of aluminum ions is replaced by magnesium in order to keep the unit cell charge neutral. Thus the chemical formula of the spinel blocks becomes $[\text{MgAl}_{10}\text{O}_{16}]$ and the mirror plane changes to $[\text{BaO}]$; both are charge neutral. Magnesium may substitute in any of the four aluminum sites in the crystal but the structure will be more stable if the original symmetry is kept as far as possible after the substitution as shown in our simulations. Because the spinel blocks are similar to the structure of MgAl_2O_4 and Mg occupies the tetrahedral positions in spinel, the possible positions of Mg in the spinel blocks are most likely also the tetrahedral sites: Al(2) and Al(3).

Table IV.1. Crystallographic Information for the β -Alumina Structure
 $a=5.594 \text{ \AA}$ $c=22.53 \text{ \AA}$

Atom	Wyckoff position	Type of Site	x	y	z
Na(1)	2c	BR	2/3	1/3	1/4
Al(1)	12k	Octahedral	0.832	-x	0.106
Al(2)	4f	Tetrahedral	1/3	2/3	0.025
Al(3)	4f	Tetrahedral	1/3	2/3	0.176
Al(4)	2a	Octahedral	0	0	0
O(1)	12k	Tetrahedral	0.157	-x	0.05
O(2)	12k	Tetrahedral	0.503	-x	0
O(3)	4f	Tetrahedral	1/3	2/3	0.056
O(4)	4e	Tetrahedral	0	0	0.143
O(5)	2c	Tetrahedral	1/3	2/3	1/4

The simulations in this study are based on the Born model description of a solid, which treats the solid as a collection of point ions with long-range and short-range forces acting between them. This approach has enjoyed a wide range of success, but it has been found that the reliability of the simulations depends on the validity of the potential model

used in the calculations. The non-Coulombic potentials are usually described by a simple analytical Buckingham function,

$$V_{ij}(r_{ij}) = A_{ij} \exp(-r_{ij} / r_{ij}) - C_{ij} r_{ij}^{-6} \quad (1)$$

where r_{ij} is the distance between the ions i and j .

The polarizability of individual ion is included through the core-shell model originally developed by Dick and Overhauser, in which the outer valence electron cloud of the ion is simulated by a massless shell of charge Y and the nucleus and inner electrons by a core of charge X .⁶ The total charge of the ion ($X+Y$) is equal to the oxidation state of the ion. The interaction between core and shell of any ion is harmonic with a spring constant k , and is given by

$$V_i(r_i) = \frac{1}{2} k_i d_i^2 \quad (2)$$

where d_i is the relative displacement of core and shell of ion i .

For the core-shell model, the value of the free-ion electronic polarizability is given by

$$a_i = Y_i^2 / k_i. \quad (3)$$

The potential parameters (A , r , and C in Eq. (1)), the shell charges Y , and the spring constant k associated with the shell-model description of polarizability need to be determined for the interactions between each ion pair in the crystal. In the present study, they were taken from our earlier studies of hexa-aluminates following the original compilation of Lewis and Catlow⁷⁻⁹. Another set of potentials derived independently by Bush et al. was also tested.¹⁰

4.1.2 Lattice Energy Calculations

The lattice energy is the binding or cohesive energy of the perfect crystal and is usually defined as the energy that must be released to the crystal to separate its component ions into free ions at rest at infinite separation. It is calculated by the relation:

$$U = 1/2 \sum \sum V_{ij}. \quad (4)$$

The interatomic potential, V_{ij} , includes the long-range Coulombic interactions and the non-Coulombic potential described above. The lattice energy is minimized through a

second derivative Newton-like procedure, coded into METAPOCS.¹¹ Details of the procedure have been outlined by Cormack and outlined in the previous chapter.¹²

In the present work, this perfect lattice approach has been used to establish an equilibrated crystal structure for BAM using the previously published potential summarized in Table IV.2.⁷ In addition, Bush potentials, shown in Table IV.3 were used to justify whether the results are potential independent.

Table IV.2. Potential Parameters Derived by Lewis and Catlow

Interaction	A (eV)	ρ (Å)	C (eV·Å ⁶)
Al(o) – O	1474.40	0.30059	0
Al(t) – O	1334.31	0.30059	0
Ba – O	931.70	0.39490	0
Mg – O	710.50	0.32420	0
O – O	22764.2	0.14910	17.89
Eu(2+) – O	665.20	0.39490	0
Eu(3+) – O	1358.0	0.35560	0
Interaction	Shell charge	K	
Ba (core) – Ba (shell)	1.46	14.78	
O(core) – O(shell)	-2.207	27.29	

Table IV.3. Potential Models Derived by Bush et al.

Interaction	A (eV)	ρ (Å)	C (eV·Å ⁶)
Al – O	2409.505	0.2649	0
Ba – O	4818.416	0.3067	0
Mg – O	2457.243	0.2610	0
O – O	25.41	0.6937	32.32
Eu(2+) – O	6212.907	0.27948	0
Eu(3+) – O	847.868	0.3791	0
Interaction	Shell charge	Spring constant	
Al(core) – Al(shell)	2.957	403.98	
Ba(core) – Ba(shell)	1.831	34.05	
O(core) – O(shell)	-2.513	20.53	
Eu(3+ core) – Eu(3+ shell)	3.991	304.92	

4.1.3 Defect Energy Calculations

Calculations of defect structure and energy introduce one vital feature in addition to those for the perfect lattice methods. That is, the occurrence of relaxation of lattice atoms around the defect species. The effect is large because the defect generally provides an extensive perturbation of the surrounding lattice, and, in the case of ionic crystals, the relaxation field is long-range as the perturbation provided by the defect is mainly Coulombic in origin.

The defect calculation is based on the Mott-Littleton theory, which allows one to calculate the defect-induced static polarization of a dielectric continuum.¹³ The basic approach is to contain, within the dielectric continuum, a region, immediately surrounding the defect, which is treated atomistically within the framework of the Born model described above. In this region, the forces and resulting atom displacements are too large to be treated properly using continuum theory, which can, nevertheless, be used to model the more distant parts of the crystal. This two-region approach is coded in CASCADE that was the program used in this work.

4.2 Results

4.2.1 Structures of BAM

Using β -alumina as a prototype, the BAM structure was obtained by substituting all Na with Ba and two Al with Mg in a primitive cell; the structure was then put into METAPOCS to relax it to a minimum energy configuration. Mg ions were put in Al(2) or Al(3) positions (four Al(2) positions are labeled as a-d and four Al(3) positions are labeled as a'-d' along c axis in Fig. 4.2). It was determined that the lattice energy of the unit cell with all Mg in Al(2) site was lower than for the other Mg distributions (Table IV.4). Furthermore, there are three possible ways to put two magnesium ions in four Al(2) sites.

After checking all the possibilities, in which magnesium ions are in ab, ac and bc sites respectively, we have found two types of Mg distribution having nearly the same lattice energy (a 0.06eV difference). This suggests that there will be a variety of Mg distributions in BAM crystals, since apart from the preference for the Al(2) site there is no driving force for Mg ordering in the equivalent sites. We have defined these two

possible structures of BAM as configuration I and II. Configuration I has Mg in a and c sites, and configuration II has Mg in a and b sites (Fig. 4.2). In configuration II, the two mirror planes in the unit cell are now different from each other because of the Mg distribution and then the defect properties may vary in different regions. In configuration II, all Mg are located in the lower half of the unit cell (IIM) and no Mg is in the upper half (IIA). Actually, configuration I has lost the mirror symmetry but kept the 2-fold screw axis, whereas configuration II has kept the mirror symmetry but lost the 2-fold screw axis. For convenience, the phrase “mirror plane” is generally used to refer to the barium-oxygen plane in both configurations.

Table IV.4. Lattice Energies of Mg Distributions in Al(2) and Al(3) Sites

Configuration with Al(2) and Al(3) mix	aa'	ab'	ac'	ad'
Lattice Energy (eV)	-1733.27	-1734.91	-1735.09	-1733.60
Configuration with only Al(2)	ab	ac	bc	
Lattice Energy (eV)	-1736	-1736.06	-1733.83	
Configuration with only Al(3)	a'b'	a'c'	b'c'	
Lattice Energy (eV)	-1733.32	-1734.42	-1733.71	

The calculated crystal structure parameters for BAM (configuration I) are given in Table IV.5, in which they are compared with the experimental data of Iyi et al.² Because the structure has been changed after the substitution of Mg, the coordinates are averaged for each symmetrically independent position. In addition, the Mg in the spinel block was introduced as a defect, and the lattice must relax in some way to allocate the defect. This relaxation changes the size and shape of the spinel block slightly; that is the reason for the fact that Ba and O(5) ions did not remain exactly on the mirror plane ($z=0.25, 0.75$). Having magnesium and barium in the structure has expanded the unit cell and the cell parameters become $a=5.72 \text{ \AA}$ and $c=22.65 \text{ \AA}$. Although the calculated structure is slightly different from the β -alumina structure, the agreement between our modeled structure and

the experiment data of BAM is very good, as can be seen from the Δx and Δz columns in Table IV.5, which represents the difference between calculation and experiment.

Table IV.5. Comparison of Measured and Calculated Structures

Atom type	$X_{\text{obs.}}$	$X_{\text{calc.}}$	ΔX	$Z_{\text{obs.}}$	$Z_{\text{calc.}}$	ΔZ
Ba	0.6678	0.6667	0.0011	0.2500	0.24662	0.00338
Al(1)	0.8343	0.8338	0.0005	0.10544	0.10268	0.00276
Al(2)	0.3333	0.3333	0	0.02400	0.01848	0.00552
Al(3)	0.3333	0.3333	0	0.17416	0.17052	0.00364
Al(4)	0.0000	0.0000	0	0.00000	0.00000	0
O(1)	0.1534	0.1488	0.0046	0.05152	0.05130	0.00022
O(2)	0.5042	0.5040	0.0002	0.14799	0.14333	0.00466
O(3)	0.6667	0.6667	0	0.05901	0.05409	0.00492
O(4)	0.0000	0.0000	0	0.14437	0.139590	0.00478
O(5)	0.3333	0.3333	0	0.25000	0.24789	0.00211

Because of the good agreement between calculated and measured structural data, the potential was ready for further defect simulations. Although the Mg distribution does not affect the lattice energies significantly for configurations I and II, they may be expected to have a significant effect on the energies of point defects.

4.2.2 Intrinsic Disorder

Point defect energies of all ion species in the two configurations and the two regions of configuration II have been calculated with CASCADE and are compared in Table IV.6. These are energies associated with bringing the defects into the crystal from infinity. No ionization processes have been included. As the introduction of Mg into the structure has changed the symmetry, defect energies in BAM are not necessarily the same for the originally symmetry-similar positions of β -alumina. It is appropriate to calculate defects on all possible lattice sites as well as sites that are normally symmetrically equivalent. For example, all aluminum vacancies of Al(2) in β -alumina should have the same defect energy. But in BAM, the aluminum ions in the Al(2) position have different

environments compared to each other; i.e. one Al(2) would have a magnesium close to it but the other has magnesium further away. Although their environments, or site symmetries, are different, they are still described as being in the Al(2) position, as classified in β -alumina, to keep the problem simple. Thus all aluminums in the Al(2) sites must be calculated individually. When looking at the Table IV.6, it must be kept in mind that the defect energy listed was the lowest one for that class of positions.

Table IV.6. Calculated Point Defect Energies (eV)

Defect	Config. I	Config IIM	Config. IIA
V_{Ba}^{\bullet}	17.01	17.70	16.16
V_{Mg}^{\bullet}	29.30	29.39	29.39
$V_{Al(1)}^{\bullet\bullet}$	58.34	58.66	56.78
$V_{Al(2)}^{\bullet\bullet}$	58.52	-	58.31
$V_{Al(3)}^{\bullet\bullet}$	59.39	59.78	58.92
$V_{Al(4)}^{\bullet\bullet}$	57.08	57.07	57.07
$V_{O(1)}^{\bullet\bullet}$	23.31	23.18	24.90
$V_{O(2)}^{\bullet\bullet}$	24.92	24.62	26.00
$V_{O(3)}^{\bullet\bullet}$	25.44	25.47	25.62
$V_{O(4)}^{\bullet\bullet}$	23.33	23.13	25.79
$V_{O(5)}^{\bullet\bullet}$	25.16	24.02	26.23
$Ba_i^{\bullet\bullet}$	-11.21	-12.19	-10.25
$Mg_i^{\bullet\bullet}$	-18.22	-18.91	-16.94
$Al_i^{\bullet\bullet}$	-42.51	-42.86	-42.57
O_i^{\bullet}	-14.76	-15.52	-15.24

When considering the interstitial defect, one will wonder where are the possible interstitial positions for ions. Since the mirror plane region is quite open in β -alumina and symmetry has been impaired, it is not so straightforward to select all the possible positions beside the special sites such as unoccupied octahedral sites and the anti-BR site. In order to consider all of the possibilities, a computer program was designed to find the possible positions automatically. The basic idea of the program is that as long as the site is large enough (i.e. the distance from this site to its nearest ion is larger than a prescribed threshold), it can be a candidate to hold an interstitial ion. The smaller is the size of the

interstitial position is, the bigger the relaxation is needed to accommodate the interstitial ion, and the higher the defect energy may be, and the more sites are selected. No distance between two interstitial positions is shorter than the threshold to limit the number of selected sites. Another criterion is that no two sites have the same environment surrounding them. Even though many limitations have been applied to the structure, the program still generated around 200 candidates. The lower the symmetry is, the more candidates are generated. All of the generated interstitial sites have been tested for each ion species and the position with the lowest point defect energy has been considered as the interstitial position for that ion species. However, that does not mean interstitials only occur at that position; it merely means that the probability of finding an interstitial of that ion at that position is the greatest.

In configuration I, the aluminum vacancy seems most likely to occur at Al(4) in the middle of spinel block, but it was the Al(1) site that became vacant in configuration II. Other vacancy positions were the same for the two Mg distributions.

The barium interstitial prefers to occupy the anti-BR site in the mirror plane and was the same for both configurations. Since the divalent barium ion is quite large relative to other ions (its radius is 1.5 Å, which is nearly double the size of an aluminum ion), it is not surprising that barium can not reside inside the spinel block since it is oxygen close-packed. Magnesium was also found to occupy the anti-BR site, but with a little deviation toward a nearby O(5) ion. Aluminum behaves differently from other cations because its size is so small that it can enter into the spinel block. Aluminum ion prefers to take the octahedral sites across the middle of the spinel block. Since there are three cation layers in the middle of a spinel block, Mg-Al(4)-Al(2), two oxygen layers at the edge of this region have been separated further away from each other, and they are no longer strictly close-packed. The octahedron formed by these two oxygen layers has become distorted and longer in the *c* direction. The aluminum interstitial was not found in the center of the octahedron but closer to the Al(2) layer, because of the relaxation around magnesium ion. The fact that aluminum interstitial ions are inside the spinel blocks is consistent with the observation of neutron diffraction by Roth et al.¹⁴ Oxygen interstitials in configuration I sit in the Al(1) layer and close to the unoccupied octahedral site; this is different from the observation in β -alumina.¹⁵

For oxygen in β -alumina, the favorite interstitial position is the mO site in the conduction plane, between two adjacent O(5) ions. After relaxation, two Al(1) ions above and below the mO site move automatically toward the conduction plane to stabilize the interstitial ion. This creates a $V_{Al}-Al_i-O_i-Al_i-V_{Al}$ defect cluster, called a Reidinger defect, across the mirror plane (see Fig. 4.4a). The interstitial oxygen stayed strictly on the mirror plane. After its migration, the coordination number of the aluminum in the Reidinger defect changes from six to four. However, for configuration I of BAM, only one aluminum ion moved toward the O_i , forming a $V_{Al}-Al_i-O_i$ defect cluster (Fig. 4.4c) if the oxygen interstitial ion was put into the mO position. In this case the interstitial oxygen no longer stayed on the mO site but relaxed away from the nearby barium and the mirror plane. The reason is because the size of barium is larger than sodium so that the oxygen interstitial is pushed away and the two corner-shared tetrahedra of the Reidinger defect become bent and stretched. Then, the Reidinger defect was no longer stable, and it broke. However oxygen can still be stabilized by a single aluminum ion moving toward it. Therefore, the defect energy for the oxygen interstitial in the mirror plane is no longer the lowest one, even if we forced the structure to form a Reidinger defect before the defect relaxation.

Another kind of defect cluster of oxygen interstitials has been found in configuration II. The oxygen interstitial ion tends to stay between the barium and a nearby O(5) ion that normally associates with two Al(3) ions to form a bridge perpendicular to the mirror plane; we define this position as the mOB site. The O(5) ion shared the aluminum ions with the interstitial oxygen and formed a two-bridge configuration. The Al(3)-O(5)-Al(3)- O_i defect cluster forms a parallelogram (see Fig. 4.4b). It should be mentioned that this parallelogram is mirror symmetric across the conduction plane. That is the reason why this defect has the lowest defect energy for it keeps the symmetry of the configuration II structure. While testing this two-bridge configuration in configuration I, the defect energy was -14.23eV , a little higher than the lowest one found earlier. It is not surprising to see this because the structure of configuration I has no mirror symmetry so the two-bridge defect-cluster with mirror symmetry has no benefit over other defects.

The chemical formula of region IIM is $[\text{BaMg}_2\text{Al}_9\text{O}_{17}]^{-1}$ while the formula of region IIA is $[\text{BaAl}_{11}\text{O}_{17}]^{+1}$. It is reasonable to say that a net-positive-charged point defect should prefer the IIM region and vice versa; this proves to be true in the calculation.

Energies of Schottky and Frenkel defects have been calculated from the point defect energies.¹⁶ These intrinsic defect energies have been normalized (per defect) for comparison. A Frenkel defect consists of one vacancy and one interstitial point defect while the Schottky defect consists of a formula unit of vacancies. The intrinsic defect energies are actually defect formation enthalpies.

Frenkel defect energy calculation involve

$$A_A \rightarrow A_i + V_A$$

$$\Delta E_{FA} = E_{Ai} + E_{VA} .$$

Schottky defect energy calculation involve

$$\text{null} \rightarrow \text{BaMgAl}_{10}\text{O}_{17} + V_{Ba}'' + V_{Mg}'' + 10V_{Al}''' + 17V_O^{\bullet\bullet}$$

$$\Delta E_S = E_{VBa} + E_{VMg} + 10E_{VAl} + 17E_{VO} + E_{latt} .$$

In order to compare different defects, the intrinsic defect energy was calculated per single point defect. Table IV.7 lists the final comparable defect energies. The barium Frenkel defect has the lowest defect energy, and therefore, it will be predominant in thermally generated defects. The energetically favorable barium interstitial position is the anti-BR site on the mirror plane. In addition, point defects will be created for charge compensation after the introduction of europium or other optically active ions.

Table IV.7. Calculated Intrinsic Defect Energies (eV)

Disorder	Config. I	Config. IIM	Config. IIA	Lowest
Schottky	5.01	4.93	5.82	4.93
Frenkel: O	4.28	3.81	4.83	3.81
Frenkel: Ba	2.90	2.76	2.96	2.76
Frenkel: Mg	5.54	5.24	6.23	5.24
Frenkel: Al	7.29	7.11	7.11	7.11

4.2.3 Europium Incorporation

It is important to determine the sites of europium ion to understand the luminescent behavior of BAM phosphor. There are many processes available for Eu to enter into the structure, and the way to distinguish between them lies in the heat of solution; the incorporation process with the lowest heat of solution will be the one that dominates. The Eu ion may substitute for cations or enter into interstitial sites. First, the sites with lowest defect energy were found (see Table IV.8) while allocating Eu to where it could possibly reside. The second step was to write down the solution reaction.

Table IV.8. Europium Point Defect Energies (eV)

Defect	Config. I	Config. II
Eu_{Ba}	-1.34	-1.47
Eu_{Mg}	10.59	10.59
Eu'_{Al}	38.47	38.34
$Eu_i^{\bullet\bullet}$	-12.88	-14.00
Eu_{Ba}^{\bullet}	-21.67	-22.22
Eu_{Mg}^{\bullet}	-13.23	-13.29
Eu_{Al}	14.44	14.37
$Eu_i^{\bullet\bullet\bullet}$	-31.56	-33.32

The defect energies in Table IV.8 are the lowest one for each kind of defect. For example, Eu^{2+} ions can substitute for four different Al ions in different symmetry locations. There is no doubt that we will get four different defect energies. Here the defect energy of Eu_{Al}' corresponds to the one of Eu^{2+} ions substituting for the Al(2) ion since it has the lowest point defect energy. There was no difference in the positions of the europium defect for the two structural configurations. Interstitial ions were located on the anti-BR site. The Al(2) ion was easy to be substituted by the europium ions. Since there is only one kind of position each for Ba and Mg, there is no ambiguity in the europium substitution of them.

The absolute value of the point defect energy is itself meaningless except for the comparison between the same kind of defects (such as interstitials). There is no way to tell which kind of defect will occur more easily than the others from the point defect energy alone unless they are put into a defect reaction and reaction enthalpies are calculated. The quasi-defect reactions, along with the corresponding reaction energies, or heats of solution, are shown in Table IV.9 and 4.10.

Table IV.9. Eu^{2+} Ion Incorporation into BAM

Defect Reaction	Enthalpy (eV)	
	Conf. I	Conf. II
$\text{EuO} \rightarrow \text{Eu}_i^{\bullet\bullet} + \text{O}_i''$	5.56	3.68
$\text{EuO} \rightarrow \text{Eu}'_{\text{Al}} + \text{Al}_i^{\bullet\bullet\bullet} + \text{O}_i''$	14.4	13.16
$\text{EuO} \rightarrow 1/2\text{Al}_2\text{O}_3 + \text{Eu}'_{\text{Al}} + 1/2\text{V}_\text{O}^{\bullet\bullet}$	3.94	3.72
$\text{EuO} \rightarrow \text{Eu}_{\text{Mg}} + \text{Mg}_i^{\bullet\bullet} + \text{O}_i''$	10.81	9.36
$\text{EuO} \rightarrow \text{MgO} + \text{Eu}_{\text{Mg}}$	3.35	2.35
$\text{EuO} \rightarrow \text{BaO} + \text{Eu}_{\text{Ba}}$	0.55	0.42
$\text{EuO} \rightarrow \text{Eu}_i^{\bullet\bullet} + \text{V}_{\text{Ba}}'' + \text{BaO}$	6.02	4.05

It has been shown that the barium Beavers-Ross site is the most energetically favorable site for Eu^{2+} ion. This is most likely because mirror plane is more open than inside the spinel block and the doping process requires only a straight swap of barium for europium. The other possible mechanisms require a compensating defect, which will raise the overall energy of the defect reaction. Note that for interstitial Eu^{2+} , a barium vacancy could be an alternative compensating defect. If Eu_i and V_{Ba} are close to each other, the Eu_i will relax into the adjacent vacancy, which gives a simple swap process. Otherwise, the overall energy is somewhat higher.

Table IV.10. Eu³⁺ Ion Incorporation into BAM

Defect Reaction	Enthalpy (eV)	
	Conf. I	Conf. II
$1/2Eu_2O_3 \rightarrow Eu_i^{\bullet\bullet\bullet} + 3/2O_i''$	11.74	8.84
$1/2Eu_2O_3 \rightarrow Eu_{Al} + Al_i^{\bullet\bullet\bullet} + 3/2O_i''$	15.23	13.66
$1/2Eu_2O_3 \rightarrow Eu_{Al} + 1/2Al_2O_3$	0.49	0.42
$1/2Eu_2O_3 \rightarrow Eu_{Mg}^{\bullet} + MgO + 1/2O_i''$	4.39	3.95
$1/2Eu_2O_3 \rightarrow Eu_{Ba}^{\bullet} + BaO + 1/2O_i''$	5.08	4.15

Lattice Energy (eV): E_{BaO} = -31.31 E_{MgO} = -40.99 E_{EuO} = -33.2

E_{Al₂O₃} = -158.78 E_{Eu₂O₃} = -130.88

Oxidation, a detrimental process for BAM phosphors, changes the valence of europium from 2 to 3. It is important to understand whether (or to what extent) the behavior of trivalent europium differs from divalent Eu. In a similar way, we can write incorporation reactions for Eu³⁺ as shown in Table IV.10.

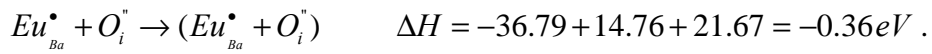
The important thing that should be mentioned is that the trivalent europium ion no longer prefers to substitute for the barium ion, as the divalent europium ion did. Instead we found that it would prefer to substitute for an aluminum ion in the Al(2) position, that is, a tetrahedral site. This raises a problem: Is it possible for the large Eu³⁺ ion to sit between close-packed oxygen layers? As can be seen in Table IV.10, the substitution of barium by Eu³⁺ ions needs half the amount of oxygen interstitials to compensate the charge generated. What would happen if the europium and oxygen ions associated with each other? Would the association of O ions stabilize the Eu³⁺ ions at BR site? Further simulations have been done to investigate this kind of interaction between point defects.

4.3 Defect Complexes

When two defects are close to each other, they interact and may decrease or increase the total defect energy. There is a limit of defect separation in a defect complex, beyond which there is no discernable interaction. Actually, the closer the defects are, the bigger is the interaction. We were interested in defect complexes in the mirror plane containing

europium ions. It has been shown above that the divalent europium ion stayed in the mirror plane and trivalent ion stayed close to the middle of spinel block. In the mirror plane, two positions were available for europium ions: Beevers-Ross and anti-Beevers-Ross sites. Also, two positions have been found for oxygen interstitial ions: mO and mOB sites. Defect complexes with two point defects were calculated first (Table IV.11). The two point defects were placed as close as possible to get the maximum interaction.

The formation of defect complex did lower the defect energy. For example in configuration I,



The Eu^{3+} and O interstitials came close to each other and that lowered the defect energy by 0.36eV. If the decrease in the defect energy is large enough, it may be possible for Eu^{3+} ions to stay in the mirror plane.

Table IV.11. Defect Complexes Containing Eu^{3+} and O^{2-}

Oxygen position	Europium position	Config. I (eV)	Config. II (eV)
mO	BR	-36.79	-
mO	Anti-BR	-50.38	-50.25
mOB	BR	-39.06	-39.47
mOB	Anti-BR	-51.96	-52.92

Defect complexes with three point defects have also been considered. BR and anti-BR sites were occupied by europium at the same time while oxygen interstitials were put into mO or mOB sites. The association of divalent and trivalent europium ions was also calculated in Table IV.12.

The more complicated defect complexes were energetically unfavorable because they generated big dipole moments in a small region that resulted in a large stress of their surroundings. For example, a $O_i^{\bullet}(\text{mOB}) - Eu_{Ba}^{\bullet} - Eu_i^{\bullet\bullet\bullet} - O_i^{\bullet}(\text{mOB})$ had a defect energy of -90.82eV that was bigger than -91.02eV, the sum of energies of two separated defect complexes, $O_i^{\bullet}(\text{mOB}) - Eu_{Ba}^{\bullet}$ and $Eu_i^{\bullet\bullet\bullet} - O_i^{\bullet}(\text{mOB})$. And, the association between

defects in a big defect complex would become weaker because of the larger separation of point defects from one end to the other.

Table IV.12. Defect Complexes with Three Point Defects

Defect complex	Config. I (eV)	Config. II (eV)
$Eu_{Ba}^{\bullet} - O_i'' (\text{mO}) - Eu_i^{\bullet\bullet\bullet}$	-73.83	-75.03
$O_i'' (\text{mOB}) - Eu_{Ba}^{\bullet} - Eu_i^{\bullet\bullet\bullet}$	-70.54	-71.92
$Eu_{Ba}^{\bullet} - Eu_i^{\bullet\bullet\bullet} - O_i'' (\text{mOB})$	-73.12	-74.47
$Eu_{Ba} - O_i'' (\text{mO}) - Eu_i^{\bullet\bullet\bullet}$	-52.23	-52.28
$O_i (\text{mOB}) - Eu_{Ba} - Eu_i^{\bullet\bullet\bullet}$	-49.00	-50.00
$Eu_{Ba} - Eu_i^{\bullet\bullet\bullet} - O_i'' (\text{mOB})$	-53.44	-54.39
$Eu_{Ba}^{\bullet} - O_i'' (\text{mO}) - Eu_i^{\bullet\bullet}$	-53.12	-52.93
$O_i'' (\text{mOB}) - Eu_{Ba}^{\bullet} - Eu_i^{\bullet\bullet}$	-51.76	-52.52
$Eu_{Ba}^{\bullet} - Eu_i^{\bullet\bullet} - O_i'' (\text{mOB})$	-52.07	-52.82

Based on the defect reaction enthalpies in Table IV.13, defect complexes can not limit the trivalent europium ion to the mirror plane for either structural configuration. Although forming defect complexes sometimes lowers the reaction enthalpy, the decrease is not big enough: the enthalpy of forming the defect complex is still much larger than for europium substituting for Al(2). Thus, the defect complex can not prevent the trivalent europium ion from entering into the tetrahedral Al(2) sites in the spinel block.

Table IV.13. Defect Reaction of Defect Complex

Defect reaction	Enthalpy (eV)	
	Config. I	Config. II
$1/2Eu_2O_3 \rightarrow (Eu_i^{\bullet\bullet\bullet} + O_i'')_{com} + 1/2O_i''$	6.10	4.76
$1/2Eu_2O_3 \rightarrow (Eu_{Ba}^{\bullet} + O_i'')_{com} + BaO + 1/2V_O^{\bullet\bullet}$	6.72	6.22
$1/2Eu_2O_3 \rightarrow 1/2(Eu_i^{\bullet\bullet\bullet} + O_i'' + Eu_{Ba}^{\bullet})_{com} + 1/2BaO + 1/2O_i''$	5.49	4.51
$1/2Eu_2O_3 + EuO \rightarrow (Eu_i^{\bullet\bullet\bullet} + O_i'' + Eu_{Ba}^{\bullet})_{com} + BaO + 1/2O_i''$	6.51	5.18
$1/2Eu_2O_3 + EuO \rightarrow (Eu_i^{\bullet\bullet} + O_i'' + Eu_{Ba}^{\bullet})_{com} + BaO + 1/2O_i''$	6.83	6.64

com: Defect complex

4.4 Europium Ion Size Consideration

Although it seems that the large Eu^{3+} ion should not reside in the spinel block because the spinel block is oxygen close-packed, the distance between two oxygen layers across the middle of spinel block (2.431 Å) is larger than distance between other neighboring oxygen layers (2.016 Å) in the spinel block. Therefore, the mid-region of spinel block is not strictly close-packed. There are three cation-layers, Mg-Al(4)-Al(2), in the middle of the spinel block. Normally, the coordination number of rare-earth elements is equal to or larger than six because they are large in size and they prefer to reside in the larger octahedral sites. Thus, there is not much information about the Eu^{3+} radius in tetrahedral sites in the literature. However, it can be calculated from bond-valence theory and then can be compared with the distances in the calculated structure. Based on the bond valence theory, the valence of an ion is related to its bond lengths with the form¹⁷

$$V_i = \sum_j v_j = \sum_j \exp\left(\frac{R_{ij} - d_{ij}}{b}\right) \quad (5)$$

where V_i , the valence of ion i , is the summation of bond valences v_i between the central ion and its neighbors. d_{ij} is the bond length, R_{ij} is the bond valence parameter for the ion pair (i,j) and b is a constant equal to 0.37.¹⁸ The Eu^{3+} -O distances were 2.144 Å x 3 and 2.111 Å when Eu^{3+} ion was in the preferred position, the Al(2) tetrahedral site of BAM. The bond valence sum for that position is calculated to be 3.389 (see Table IV.14) and is close to the europium oxidation state of 3 and the 13% difference is in reasonable range compared to other ions. It seems that the Eu^{3+} ion just has a bond valence higher than the theoretical value, which means that Eu^{3+} ions will be tightly pinned by the environment and will hardly move. In contrast, those ions in the mirror plane, which can move easily, have bond valences far below their ideal values.

Table IV.14. Bond Valence of Cations in BAM

Ion	V_i	n	V_i/V_0 (%)
Al(1)	2.966	6	98.9
Al(2)	2.564	4	85.5
Al(3)	2.827	4	94.2
Al(4)	2.624	6	87.5
Ba	1.413	9	70.7
Mg	1.955	4	97.8
Eu ²⁺ (BR)	1.071	9	53.6
Eu ³⁺ (Al2)	3.389	4	113

V_0 : theoretical valence

If we assume that all Eu³⁺ - O lengths are the same in a tetrahedron, we can rewrite equation [5] as:

$$d_{ij} = R_{ij} + b \ln \left(\frac{n}{V_i} \right) \quad (6)$$

where n is the coordination number. This gives the predicted bond length for different coordination conditions.

Table IV.15. Bond Length vs. Coordination Number

n (Eu-O)	4	5	6
d (Eu-O) Å	2.1804	2.263	2.3305

The bond length of Eu³⁺ - O in BAM is smaller than the predicted value from bond valence theory. This may be related to the cation rich environment in the mid-spinel region. The oxygen ions around Eu³⁺ can not relax too much. Before the substitution, the Al-O bond lengths for Al(2) are 1.797 Å and 1.822 Å x 3. The substitution did relax the surrounding oxygen ions to a suitable distance to accommodate the large Eu³⁺ ion. The shortened Eu³⁺-O bond length is the compromise between normal bond length and the actual surroundings.

4.5 Calculations with the Bush Potential

The potentials used to generate the above results were taken from the work of Lewis and Catlow and adjusted from our earlier studies.³ It is important for the results to be the same using different potential models to confirm the results. It has been shown above that the calculated structure fits the experimental data well. Further verification of the potential model has been done. Another set of totally different potentials (derived by Bush et al.¹⁰) deduced independently was used to calculate the structure. Bush et al. used core-shell models for all cations, and the potential model might be considered to be more accurate. However, they did not define the $\text{Eu}^{2+}\text{-O}$ potential in their work, so the potential was fitted to the properties of EuO later using the new oxygen-oxygen potential. Because of the lack of physical data for fitting, i.e. it did not reproduce well all of the physical data, the fitted potential was not very satisfactory. As with the earlier potential, we found two Mg distributions with the new potential. Since we only want to test the potential dependence of calculations, only the data for configuration I calculated by the Bush potential are listed (see Table IV.16).

Table IV.16. Point Defect in Config. I with Bush Potential

Intrinsic Point Defect	Defect Energy (eV)	Extrinsic Point Defect	Defect Energy (eV)
V_{Ba}''	19.06	Eu_{Ba}	-1.58
V_{Mg}''	27.90	Eu_{Mg}	8.53
$V_{Al(1)}'''$	58.88	Eu_{Al}'	35.88
$V_{Al(2)}'''$	56.34	Eu_i''	-14.64
$V_{Al(3)}'''$	59.60	Eu_{Ba}^\bullet	-19.65
$V_{Al(4)}'''$	60.24	Eu_{Mg}^\bullet	-12.99
$V_{O(1)}''$	18.54	Eu_{Al}	14.53
$V_{O(2)}''$	20.83	Eu_i'''	-31.28
$V_{O(3)}''$	19.96		
$V_{O(4)}''$	19.14		
$V_{O(5)}''$	25.16		
Ba_i''	-12.84		
Mg_i''	-19.34		
Al_i''	-47.31		
O_i''	-11.61		

On substituting for aluminum, europium ions preferred the Al(2) sites which is the same as the results with Lewis potential. The preferred positions of the defect are the same except for the aluminum vacancy. Using the Bush potentials, it is the Al(2) position that has the lowest vacancy energy. The europium point defects occur at exactly the same places with both two sets of potentials.

Table IV.17. Intrinsic Defect Energy of BAM with Bush Potential

Disorder	Energy (eV)
Schottky	1.87
Frenkel: O	4.28
Frenkel: Ba	3.11
Frenkel: Mg	4.28
Frenkel: Al	4.52

The predominant intrinsic defect was the barium Frenkel defect for the Lewis and Catlow potential, which was expected, but the Schottky defect has the lowest reaction enthalpy for the Bush potential.

Although the absolute values of reaction energies show small differences, Eu^{3+} ions entering into the Al(2) site and Eu^{2+} ions substituting for barium still consumes the lowest energy (Table IV.18). Another interesting thing is that Eu^{2+} ions substituting Al(2), the favorite site for Eu^{3+} , has a dramatically decreased heat of solution and comes close to that of Eu^{2+} ions sitting in the BR site. It seems that Eu^{2+} may occur inside the spinel block; this is contrary to the previous results with the Lewis and Catlow potential. Since the fitting of Eu^{2+} -O potential was not satisfactory, the results obtained from the Lewis & Catlow potentials may be considered to be more reliable: only one Eu^{2+} position exists.

The environment of the Eu^{3+} ion on the Al(2) site consists of three Eu^{3+} - O bonds with a bond-length equal to 2.102 Å and one Eu^{3+} - O bond-length equal to 2.098 Å. This is close to the configuration obtained with Lewis and Catlow potential, but the size is a little smaller. From this comparison, it is clear that the europium ion positions are insensitive to the potentials.

Table IV.18. Incorporation of Eu into BAM (Bush Potential)

Defect Reaction	Enthalpy (eV)
$EuO \rightarrow Eu_i^{\bullet\bullet} + O_i^{\prime\prime}$	8.28
$EuO \rightarrow 1/2Al_2O_3 + Eu_{Al}^{\prime} + 1/2V_O^{\bullet\bullet}$	0.93
$EuO \rightarrow MgO + Eu_{Mg}$	2.18
$EuO \rightarrow BaO + Eu_{Ba}$	0.54
$1/2Eu_2O_3 \rightarrow Eu_i^{\bullet\bullet\bullet} + 3/2O_i^{\prime\prime}$	15.87
$1/2Eu_2O_3 \rightarrow Eu_{Al} + 1/2Al_2O_3$	0.37
$1/2Eu_2O_3 \rightarrow Eu_{Mg}^{\bullet} + MgO + 1/2O_i^{\prime\prime}$	4.83
$1/2Eu_2O_3 \rightarrow Eu_{Ba}^{\bullet} + BaO + 1/2O_i^{\prime\prime}$	6.7

Lattice Energy (eV): $E_{BaO} = -32.46$ $E_{MgO} = -40.99$ $E_{EuO} = -34.58$
 $E_{Al_2O_3} = -157.6$ $E_{Eu_2O_3} = -129.28$

4.6 Conclusions

Based on our calculations, the BAM structure may accommodate two Mg distributions that can not be distinguished by their lattice energies. We think both configurations will exist in the real material, which makes the defect structures much more complicated. Although two Mg distributions exist, the predominant defect is the same for both configurations, namely the Barium Frenkel defect. The distribution of Mg changes the defect properties and the most significant change in the defect properties is the oxygen interstitial position. The Mg distribution that retains the mirror symmetry at the barium-oxygen plane constrains the oxygen interstitial ion in the mirror plane to form a two-bridge configuration instead of a Reidinger defect as in β -alumina. However, if the Mg distribution destroys the mirror symmetry, the oxygen will stay inside the spinel block in the half unit cell without Mg. It seems that the relative charge of Mg_{Al}^{\prime} plays an important role in determining the positions of defects.

Two sets of potential models have been tested. The results show a difference in the predominant thermal defect, but the europium defects had the same properties. Two europium sites were found: divalent ions prefer to occupy the Beevers-Ross site in the

mirror plane while trivalent europium ions prefer the Al(2) tetrahedral position in the spinel block. Although the calculated Eu^{3+} -O bond length is smaller than the expected value, the difference is small and the bond length is in the reasonable range.

Defect complexes with two and three defects, at least one of which is Eu^{3+} , have been calculated and compared. The defect complexes did show smaller defect energies than the sum of individual defects, but the amount of energy decrease was not big enough to stabilize the Eu^{3+} ion in the mirror plane.

Although Eu^{3+} was predicted to prefer the Al site, this was a thermodynamic conclusion, and kinetic factor was not considered. For example, if Eu^{3+} was formed during application by oxidation from Eu^{2+} , it would not be necessary for it to be at the Al(2) site. As the Eu^{2+} ion resides at the BR position in the conduction plane, Eu^{3+} could be formed at that position. There is about 5 Å distance between the BR and Al(2) sites. Whether Eu^{3+} ions can migrate such a distance is a kinetic problem that will be investigated later.

References

1. M. Bettman and L.L. Terner, "On the Structure of $\text{Na}_2\text{O}\cdot 4\text{MgO}\cdot 15\text{Al}_2\text{O}_3$, a Variant of Beta-Alumina," *Inorg. Chem.*, **10**[7] 1442-6 (1971).
2. N. Iyi, Z. Inoue, and S. Kimura, "The Crystal Structure and Cation Distribution of Highly Nonstoichiometric Magnesium-Doped Potassium Beta-Alumina," *J. Solid State Chem.*, **61**[2] 236-44 (1986).
3. G.A. Rankin and H.E. Merwin, "The Ternary System $\text{CaO}\text{-}\text{Al}_2\text{O}_3\text{-}\text{MgO}$," *J. Am. Chem. Soc.*, **38**[3] 568 (1916).
4. W.L. Bragg, C. Gottfried, and J. West, "The Structure of Beta Alumina," *Z. Kristallogr.*, **77**[2] 255-74 (1931).
5. C.A. Beevers and M.A.S. Ross, "The Crystal Structure of "Beta Alumina" $\text{Na}_2\text{O}\cdot 11\text{Al}_2\text{O}_3$," *Z. Kristallogr.*, **97**[1] 59-66 (1937).
6. B.G. Dick and A.W. Overhauser, "Theory of the Dielectric Constants of Alkali Halide Crystals," *Phys. Rev.*, **112**[1] 90-103 (1958).
7. J.G. Park and A.N. Cormack, "Potential Models for Multicomponent Oxides: Hexa-Aluminates," *Philos. Mag.*, **73**[1] 21-31 (1996).
8. J.G. Park and A.N. Cormack, "Crystal/Defect Structures and Phase Stability in Ba Hexa-aluminates," *J. Solid State Chem.*, **121**[1] 278-90 (1996).
9. G.V. Lewis and C.R.A. Catlow, "Potential Models for Ionic Oxides," *J. Phys. C: Solid State Phys.*, **18**[6] 1149-61 (1985).
10. T.S. Bush, J.D. Gale, C.R.A. Catlow, and P.D. Battle, "Self-Consistent Interatomic Potentials for the Simulation of Binary and Ternary Oxides," *J. Mater. Chem.*, **4**[6] 831-7 (1994).
11. C.R.A. Catlow, A.N. Cormack, and F. Theobald, "Structure Prediction of Transition-Metal Oxides Using Energy-Minimization Techniques," *Acta Crystallogr., Sect. B: Struct. Sci.*, **B40**[3] 195-200 (1984).
12. A.N. Cormack, "A Perfect Lattice Approach to Nonstoichiometry," *Solid State Ionics*, **8**[1] 187-92 (1983).
13. N.F. Mott and M.J. Littleton, "Conduction in Polar Crystals. I. Electrolytic Conduction in Solid Salts," *Trans. Faraday Soc.*, **34**[1] (1938).

14. W.L. Roth, F. Reidinger, and S.L. Placa, "Studies of Stabilization of Transport Mechanisms in Beta and Beta" Alumina by Neutron Diffraction," pp. 223-41 in *Superionic Conductors*. Edited by G. D. Mahan and W. L. Roth. Plenum, New York, 1976.
15. K. Edstrom and J.O. Thomas, "Sodium-Ion Distribution in Na⁺ Beta-Alumina: Crystallographic Challenge," *Acta Crystallogr., Sect. B: Struct. Sci.*, **B47**[2] 210-6 (1991).
16. A.N. Cormack, "Defect Processes in Ceramics," pp. 63-98 in *Advances in Solid-State Chemistry*. Edited by C. R. A. Catlow. Jai Press, Greenwich, Connecticut, 1993.
17. I.D. Brown, "The Bond-Valence Method: An Empirical Approach to Chemical Structure and Bonding," pp. 1-30 in *Structure and Bonding in Crystals*. Edited by M. O'Keeffe and A. Navrotsky. Academic Press, New York, 1981.
18. N.E. Brese and M. O'Keeffe, "Bond-Valence Parameters for Solids," *Acta Crystallogr., Sect. B: Struct. Sci.*, **B47**[1] 192-7 (1991).

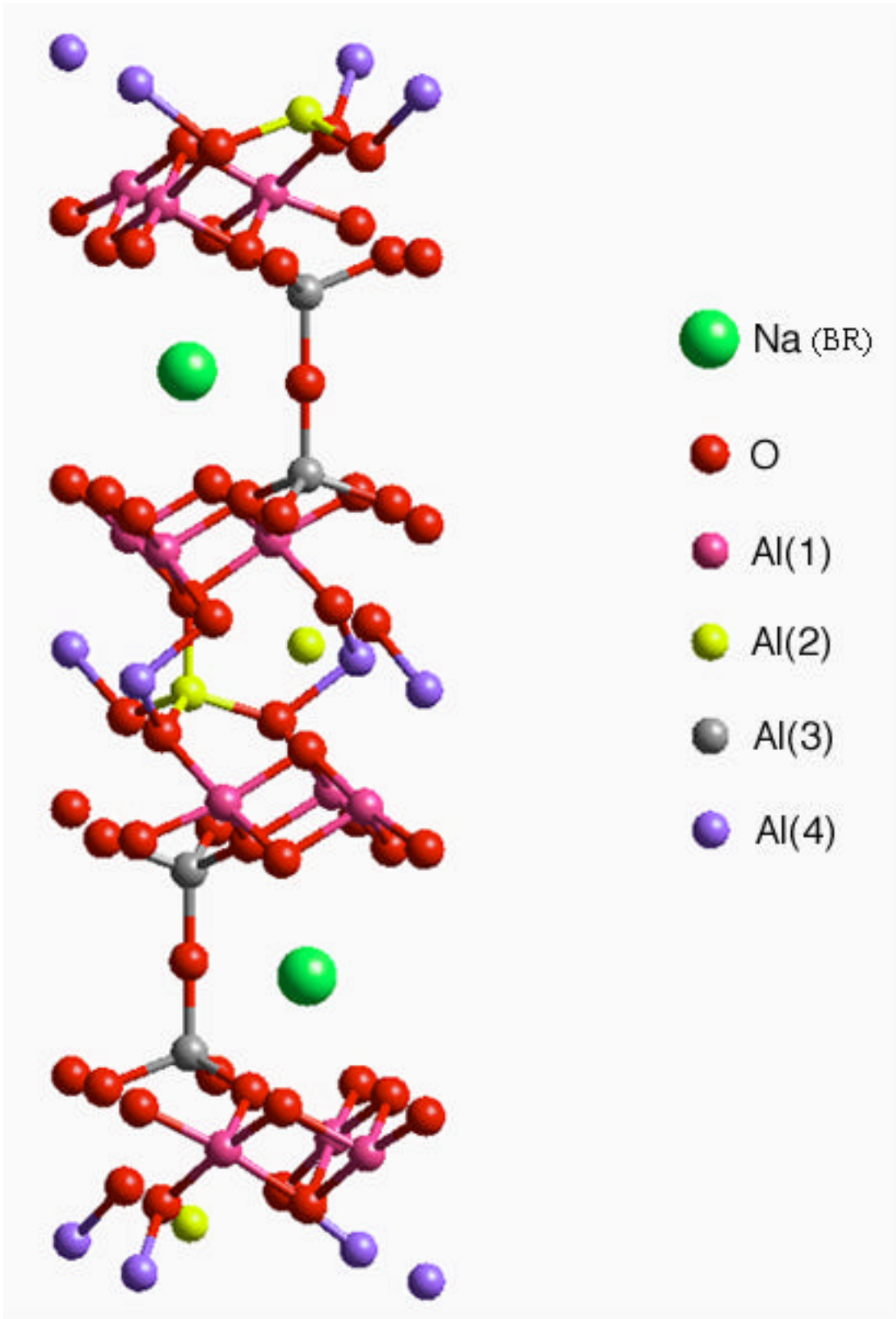


Figure 4.1. Primitive cell of β -alumina.

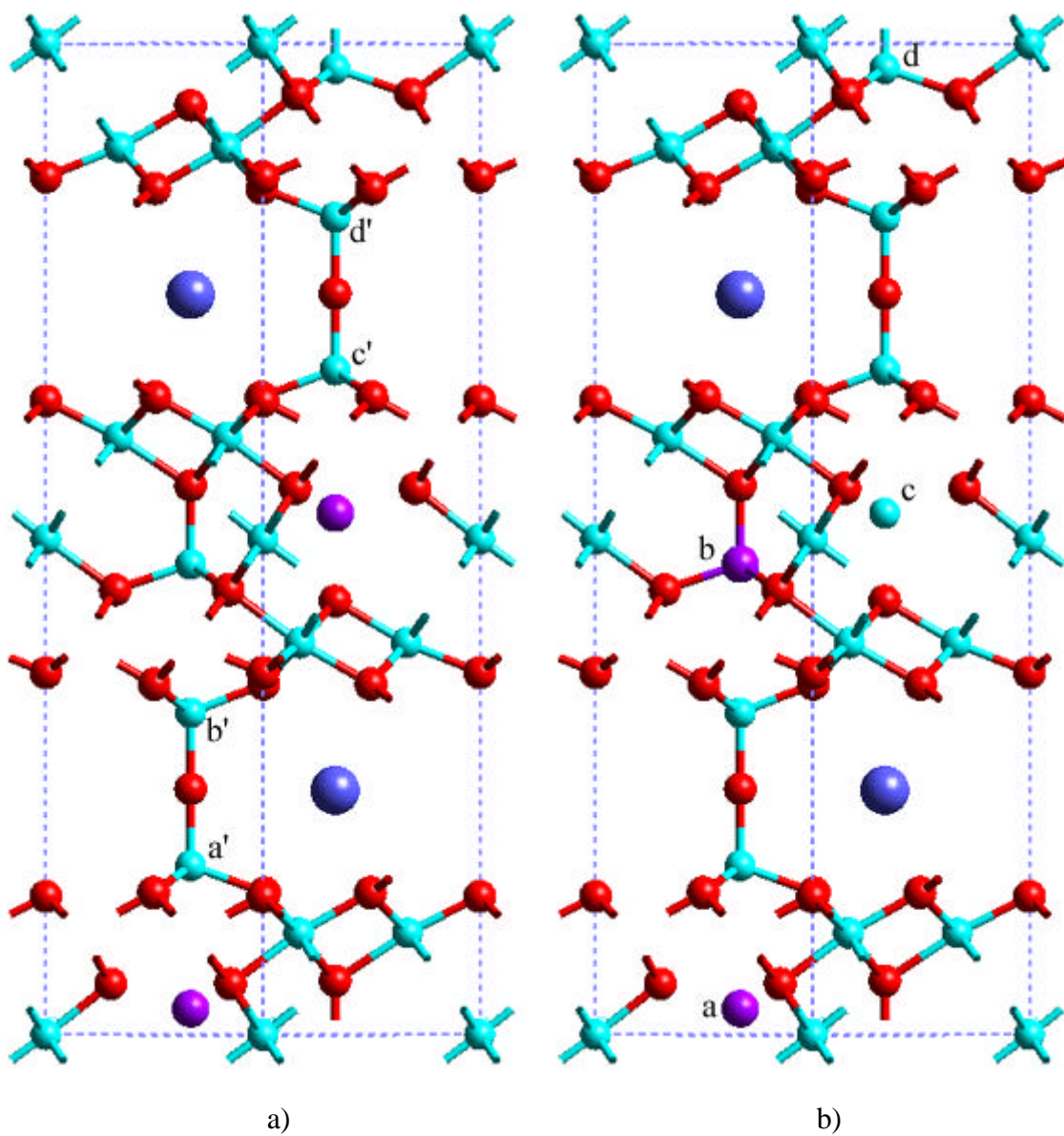


Figure 4.2. Two configurations of BAM. a) Configuration I possesses Mg at ab sites; b) Configuration II possesses Mg at ac sites.



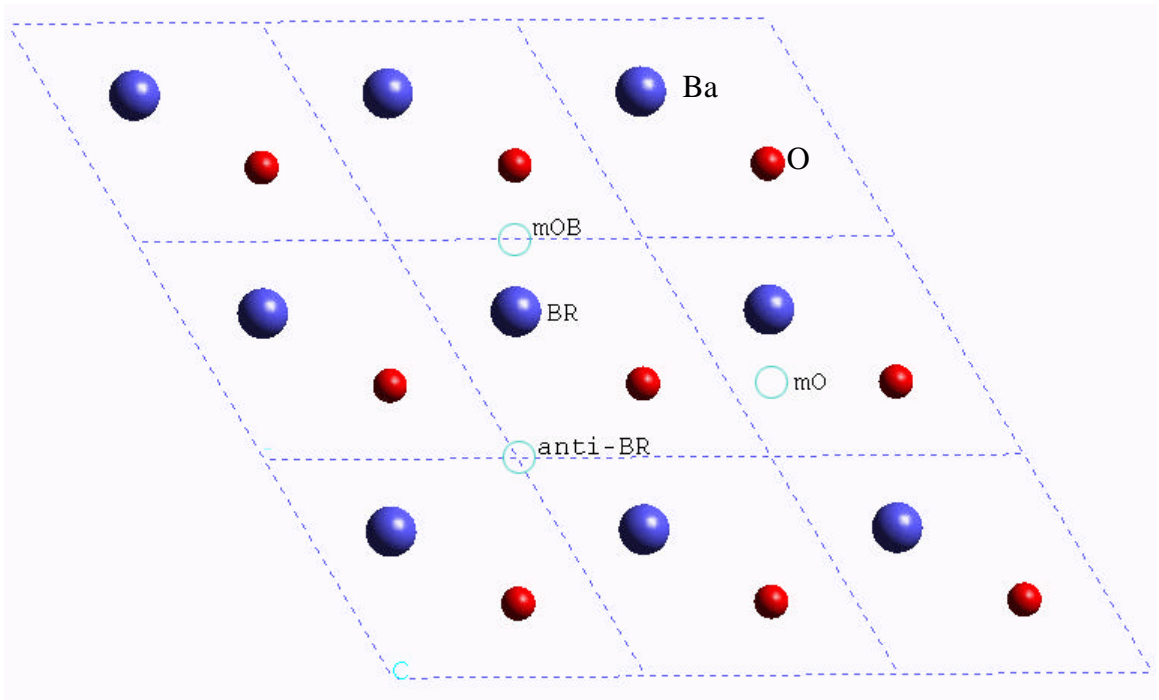
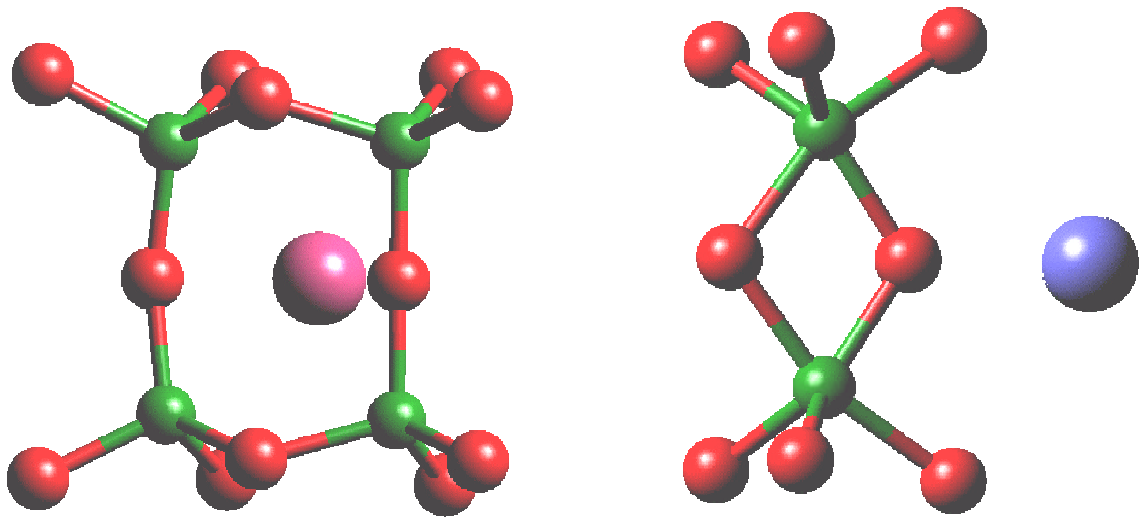
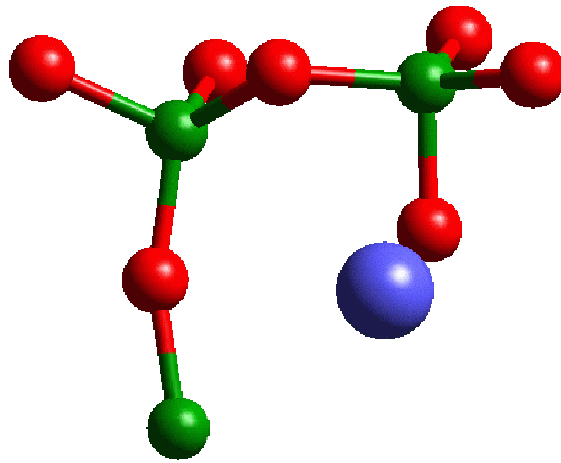


Figure 4.3. Projection of mirror plane of BAM with ion positions on X-Y plane.



a)

b)



c)

Figure 4.4. Three types of oxygen interstitial of BAM.

 Ba

 O

 Al

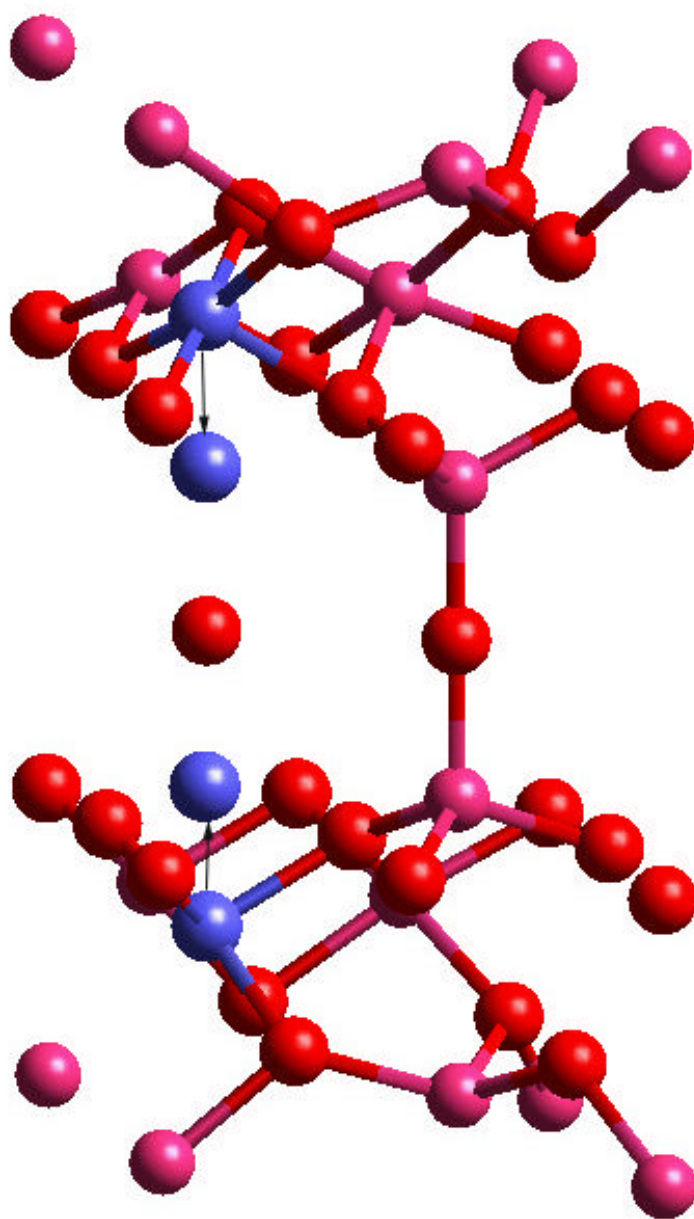


Figure 4.5. Configuration of Reidinger defect.

● Ba ● O ● Al

5. Ion Migration In BAM

Abstract:

$\text{BaMgAl}_{10}\text{O}_{17}:\text{Eu}^{2+}$, a blue phosphor material, has a luminescent property degradation problem, in which the emission intensity decreases with time and heating process. It is believed that the degradation process is related to the oxidation of europium from the divalent state to the trivalent state. Earlier simulation work has shown that the europium ion prefers to occupy two different positions in the BAM lattice, in different oxidation states. The two positions are about 5 \AA away from each other. In this work, molecular dynamics simulation was adopted to investigate the migration of ions in BAM, particularly the Eu ions.

Our results suggest that regardless of the position of Eu^{3+} in the conduction plane (BR or anti-BR), it can migrate into the spinel block at relatively low temperature, under certain conditions, such as the presence of a nearby Mg ion. The probability of migration increases with the temperature. Eu^{2+} ion migrates very differently from the trivalent ion; instead of entering into the spinel block, it migrates inside the conduction plane with a mobility close to or larger than the mobility of Ba ion. The hypothesis of forming $\text{EuMgAl}_{11}\text{O}_{19}$ after degradation is discussed from the aspect of ionic migration.

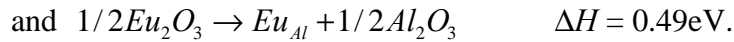
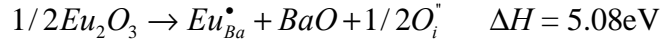
5.1 Introduction

The structure prototype of BAM ($\text{BaMgAl}_{10}\text{O}_{17}$) is β -alumina ($\text{NaAl}_{11}\text{O}_{17}$).¹ The structure of β -alumina can be described as oxygen close-packed spinel blocks separated by sodium-oxygen planes.² It has the space group symmetry of $P6_3/mmc$ that requires two spinel blocks and two Na-O planes in one primitive cell. On changing the material from β -alumina to BAM, magnesium ions are substituted for two aluminum ions on tetrahedral sites in order to compensate the charge generated by the $\text{Ba}_{\text{Na}}^{\bullet}$ substitution. Although it has been found that there are two structures, with different Mg distributions, having nearly the same lattice energy, only the structure with the lower lattice energy (configuration I) was investigated in this chapter to check the migration property of europium ions (see Fig. 5.1).

The aluminum sites in BAM can be classified into four asymmetric positions labeled as Al(1)-Al(4), in which Al(1) and Al(4) are octahedral positions and the other two are tetrahedral positions. Magnesium has been found to occupy the Al(2) position. The Mg distribution of the structure investigated here has the two Mg ions in different spinel blocks and retains the 2-fold screw axis symmetry. This kind of distribution destroys the mirror symmetry at the barium-oxygen plane in between the two adjacent spinel blocks along the *c*-axis. The barium-oxygen plane is referred to as a conduction plane instead of a mirror plane because of the above reason, and because of the high mobility of barium in this plane.

In the conduction plane (Fig. 5.2) there are three different positions, labeled as BR, anti-BR and mO sites, named after the work of Beevers and Ross.³ Although BR and anti-BR sites are both surrounded by three oxygen ions in the conduction plane, their neighboring ions above and below them in the *c* direction are different. The BR site is in the center of an octahedron with three oxygen ions above and another three below. For the anti-BR site, there are oxygen ions immediately above and below it, and the three ions form a straight line parallel to the *c*-axis.

It has been found that Eu^{2+} ion is incorporated into the structure at the BR site, while Eu^{3+} ion prefers to substitute on the Al(2) site in the middle of spinel block from our earlier work (Chapter 4). As one would imagine, Eu^{3+} ion is quite likely to form at the BR site, through oxidation of the Eu^{2+} at that site. It has been found that there is about 4.5eV difference in the defect reaction enthalpy for Eu^{3+} entering into these two positions.



Although the enthalpy difference is quite large, it is not clear whether it is large enough for the Eu^{3+} ion to move through the oxygen close-packed layers. Therefore, it is necessary to investigate the possibility of europium migration. Molecular dynamics (MD) simulation provides a useful tool to study the migration of ions at different temperature, and was used to investigate the migration of Eu in our study.

5.1.1 Molecular Dynamics Simulation

As its name implies, molecular dynamics simulation models the movement of particles: ions, atoms and molecules. In ionic crystals, ions are under the influence of all the other ions, long-range and short-range. They will move according to the summation of all the influences. Normally, ions just oscillate at their equilibrium position in an equilibrated material, and jump randomly with small jump frequency unless a gradient is established somehow (thermal, electrical, chemical etc.). If the temperature of the material is high enough, the frequency of an ion obtaining a kinetic energy large enough to overcome the migration obstacle formed by all other ions becomes larger. Actually, any kind of migration can occur at any temperature above 0K, but with different probability. The higher the temperature is, the larger the probability.

The first thing in setting up a MD simulation is to describe the system. For the ionic material of BAM, the system consists of many individual ions with charges determined by their valence state. Boundary conditions can be periodical or restrictive (nonperiodic in any of the x, y and z directions), depending on the simulation requirement. Periodic boundary conditions are used frequently to simulate bulk materials. The system size can be altered to adjust some species' concentration, such as dopants and defects. Normally,

the core-shell model used in energy minimization simulations would not be adopted in a MD simulation, because the frequency of the core-shell vibration is very high which requires the simulation to work at that infinitesimal time-step and the time of the simulation becomes unacceptably long.⁴

Secondly, the interaction between ions in the system is defined. The interaction includes long-range Coulombic and short-range non-Coulombic interactions. The potential energy of one pair of ions is described as

$$V_{ij}(r_{ij}) = z_i z_j / r_{ij} + A_{ij} \exp(-r_{ij} / r_{ij}) - C_{ij} r_{ij}^{-6}. \quad (1)$$

In the above equation, the non-Coulombic potential is in Buckingham form for the consistency with earlier work.

For summation of the long-range potentials, the Ewald approach is used for periodic systems; the direct Coulombic sum can be used for periodic or non-periodic systems, but with long calculation time. The Ewald sum calculates the long-range potential in two steps. First, a spherical Gaussian cloud of opposite charge centered on each ion is superimposed on the system; this changes the long-range interaction to short-range and then the summation converges quickly. Second, another set of Gaussian clouds of the same charge as each ion is superimposed, so that the total effect of the two superimpositions is zero. The second set of Gaussian clouds can be summed quickly in reciprocal space. Therefore, the Ewald sum replaces an infinite sum in real space into two infinite sums: one in real space and the other in reciprocal space, but both converge quickly.⁵

The force acting on each ion can be calculated by differentiating the potential at that ion with respect to its coordinates. Ions will move under those forces for an infinitesimal period of time and then the forces have to be recalculated because the potential at each ion has changed after the ions' positions have changed. Normally, the scale of the time-step is about 10^{-3} picosecond. It can not be too large or the calculation will become unrealistic; because the frequency of phonon motion is about 10^{13} Hz, and thus, the simulation time-step must be far smaller than 10^{-13} s. The small scale of the time-step limits the capability of MD simulation because it can not simulate in real time scale; one-second simulation requires about 10^{14} time-steps for which the calculation will last "forever". For example, the calculation of one time-step for a one-thousand-atom

system lasts 0.1 second (based on our calculation), a simulation of 10^{14} time-steps will last 10^{13} seconds which is definitely unacceptable.

Normally MD simulations use the Verlet leapfrog scheme as standard to calculate the positions and velocities of ions in a system at each time-step, in the microcanonical (NVE) ensemble in which the total energy of the system is conserved.⁵ The temperature of the system may vary in a small range. This kind of algorithm is also used in our studies. Constant temperature MD simulation uses other algorithms to calculate the trajectories; the system energy may be conservative or not depending on the actual algorithm used.⁵

5.2 Experiments

As the possibility to observe migration is dependent on the temperature, it is necessary to find the effective temperature at which Eu^{3+} migration occurs frequently, if Eu^{3+} does migrate into the spinel block. To control the concentration of europium ions, the size of the super-cell used in the simulation contains about 1000 ions. Only one europium ion is incorporated into the structure and the europium defect concentration is about 3% of total number of Ba ions, which is inside the range of the commercial phosphor product⁶.

In the beginning, the simplest defect configuration was tested: an Eu^{3+} interstitial and an Al(4) vacancy. The Al vacancy acted as the charge compensation mechanism and the possible destination of the Eu migration. The reason to choose the Al(4) vacancy instead of the Al(2) vacancy where Eu^{3+} prefers to reside, is that the Al(4) vacancy has a lower defect energy than the Al(2) vacancy in the tested BAM structure based on our earlier study. The defect energy difference is about 1.26eV. Neutron diffraction analysis of Roth et al. has shown a large number of aluminum Frenkel defects of aluminum ions in the spinel block so this kind of set-up is reasonable.⁷ The europium interstitial and aluminum vacancy were put in the same primitive cell to increase the possibility of migration occurrence. They were separated in distance by 6.6 Å. The simulation was run, beginning from 550K and the temperature increased in 100K intervals until migration was observed.

After the determination of the temperature at which the probability of observing migration was high, other aluminum vacancies, including the Al(2) (the favored position

of Eu^{3+} ions), as the Eu^{3+} migration destinations, were tested at that temperature or at temperatures a little higher. Migration properties of Eu^{2+} , Ba and O ions were also investigated.

5.3 Results

5.3.1 Europium Migration for Configurations of Eu Interstitial + Al Vacancy

5.3.1.1 $\text{Eu}_i^{\bullet\bullet\bullet} + V_{\text{Al}(4)}^{\bullet\bullet\bullet}$

The first observation of migration occurred at 850K, in which one Al(1) ion moved up to the middle region of the spinel block to occupy the vacant Al(4) position and then the Eu^{3+} interstitial migrated from the conduction plane to the nearby vacant Al(1) position. These two migrations seem to occur continuously, Al(1) migrating first and then the Eu^{3+} . The simulation was rerun several times to test the probability of the migration occurring. None of the later runs showed the migration. This implies that Eu^{3+} migration can occur at 850K but with very small probability. After increasing the temperature to 950K, all of the tested runs showed the same kind of migration that occurred at 850K. Thus a temperature of 950K was used as the starting temperature in later simulations. Actually, the temperature in the simulation does not correspond to the real temperature. The simulation temperature is normally higher than the real temperature because the integer charges have been assigned to each ion (because of the assumption of fully ionic material) and then the Coulombic binding energy is bigger than in the real case.

Although Eu migration had been observed, it needed to be investigated further. As seen in the BAM structure (see Fig. 5.1), an ion in the conduction plane will experience different environments when moving up or down. Moving up, it will encounter an Al(2) ion earlier than an Mg ion (substituting at Al(2) site) but it will see Mg ion earlier when moving down; this is because only one Al at the two Al(2) sites in a spinel block is substituted by Mg. As the Al(4) vacancy can occur above or below the europium interstitial, these two situations must be investigated individually. Another thing that needs to be considered is that the two defects can reside in different primitive cells and that the migration path and mechanism may change for different kinds of defect

arrangement. More simulations were carried out at three different temperatures, 950K, 1050K and 1150K for each defect arrangement.

When the two defects were in the same primitive cell, migration of an Al(1) to the vacant Al(4) occurred. Whether or not the migration of Eu^{3+} to the vacant Al(1) would occur was dependent on the presence of magnesium in the migration path. Migration would happen when there was an Mg in between the Eu^{3+} interstitial and the vacant Al(4) position initially, but not in the case when an Al(2) ion was in between them. In the case of an Al ion in between, the Eu^{3+} ion did move above the conduction plane and appeared to try to enter the spinel block but it just stayed there, even with extended simulation time.

When the two defects were not in the same primitive cell, no Eu^{3+} migration into the spinel block was observed. Instead, the Eu^{3+} ion moved to a nearby BR position and stayed there by displacing the Ba ion in the BR position to an interstitial position. That is because BR site is larger than the anti-BR site; i.e. the distance from a BR site to its nearest neighboring ion is larger than for an anti-BR site. The barium ion pushed into the interstitial position by the Eu^{3+} ion migrated inside the conduction plane toward the vacant aluminum site. The migration of an Al(1) ion to the vacant Al(4) position did not occur in all simulations; it showed up at high temperature, but not at lower temperature, which is reasonable because the Al(4) vacancy is more energetically favorable and the change from Al(4) vacancy to Al(1) vacancy increases the system energy.

5.3.1.2 $\text{Eu}_i^{\bullet\bullet\bullet} + V_{\text{Al}(2)}^{\text{m}}$

Al(2) is a tetrahedral position close to the middle of spinel block. It is a little closer to the conduction plane than Al(4). Many defect arrangements were tested to find the possibility and mechanism of migration. No direct migration of Eu^{3+} ion into the Al(2) position was observed. Instead when the two defects were in the same primitive cell with no Mg in between them, the Eu^{3+} moved into a vacant Al(3) position generated by the Al(3) ion migrating to the vacant Al(2) position. The europium ion just stayed at the edge of the spinel block and did not migrate any further because there is no longer an available position in the spinel block. This migration is not contrary to the magnesium effect shown in the previous results because this time the vacancy is further away from

the interstitial and their correlation is weakened by the cation-rich region in the middle of spinel block, as well as the large separation, if the Mg ion is in between (see Fig. 5.3).

For all of the other arrangements of these two defects, Eu^{3+} ion occupied a nearby BR position and the generated barium interstitial moved inside the conduction plane to a position close to the vacancy. But no migration of barium into the spinel block was observed. Al(3) was found sometimes to migrate to the vacant Al(2) in the spinel block at higher temperature.

5.3.1.3 $\text{Eu}_i^{\bullet\bullet\bullet} + V_{\text{Al}(1)}^{\prime\prime}$ and $\text{Eu}_i^{\bullet\bullet\bullet} + V_{\text{Al}(3)}^{\prime\prime}$

As Eu^{3+} occupation of the Al(1) and Al(3) positions was observed in the previous migration study, it is not surprising to see the direct migration of Eu^{3+} ion into these two aluminum positions if they are vacant at the beginning of simulations. But the limitation was that the aluminum vacancy must be in the same primitive cell as the europium or the migration did not occur. And, if in the migration direction, Al(2) was closer to Eu than the Mg, Eu^{3+} did not pass through the oxygen close-packed layer. However it did jump to the vacant Al(3) at the edge of spinel block easily, no matter the position of the magnesium ion. For simulations of both defect configurations without Eu^{3+} long-range migration, it was the barium ion that moved close to the vacancy and stabilized the system. Eu^{3+} ion just underwent a short-range displacement to a nearby BR position.

The above results imply that Mg plays a key role in the migration of europium into the spinel block. The reason could be the relaxation caused by local strain field around Mg ion whose radius is larger than Al and so the substitution of Al with Mg opens up the spinel block. Or it could be the effective local charge of -1 associated with the substitution; the local charge would attract the Eu^{3+} and help its migration. The Mg influence could also be the combination of these two issues.

No Eu^{3+} long-range migration inside the conduction plane was observed in all defect configurations and at all three temperatures. It was the barium long-range migration that occurred when the europium interstitial and aluminum vacancy were not in the same primitive cell. The Ba interstitial migrated in the conduction plane to a position close to the vacancy, which also stabilized the system, but to a smaller extent than when Eu^{3+} was inside the spinel block.

Since Eu^{3+} ion is supposed to form at the BR position, migration from the BR position also needs to be considered. Besides the aluminum vacancy acting as the destination of migration, a barium interstitial ion is also required to keep the whole system charge neutral (which is the requirement of the MD program, DLPOLY). So the defect configuration becomes $\text{Eu}_{\text{Ba}}^{\bullet} + V_{\text{Al}}^{\text{m}} + \text{Ba}_i^{\bullet\bullet}$. When the barium interstitial was in the same conduction plane as the europium ion, the europium behaved as the same as when it was in the interstitial position. It should be noted that when $\text{Eu}_{\text{Ba}}^{\bullet}$ and $\text{Ba}_i^{\bullet\bullet}$ were the same distance away from the V_{Al}^{m} , it was the europium ion that migrated to the vacancy, otherwise the vacancy remained unoccupied. In the conduction plane, Ba ion migrated much more easily than Eu^{3+} but it never went into the spinel block. If $\text{Eu}_{\text{Ba}}^{\bullet}$ and $\text{Ba}_i^{\bullet\bullet}$ were in different conduction planes, the europium remained where it was but deviated a small distance toward the vacancy. In this case, if the europium began to migrate towards the aluminum vacancy, another vacancy would be generated in the conduction plane at the BR site, and this seemed to hinder the Eu^{3+} migration toward the aluminum vacancy.

5.3.2 Migration of Other Ions

Barium migration in the conduction plane occurred by an interstitialcy mechanism, in which a barium interstitial pushed another barium in a normal BR position into an adjacent interstitial position (see Fig. 5.4) and then occupied the normal lattice position. The final configuration after an interstitialcy migration looks like the interstitial ion migration to a nearby interstitial position. This result is consistent with the experimental observations.⁸

The migration properties of divalent europium ion were also investigated. Eu^{2+} ion was put at a BR position with a barium interstitial in the same conduction plane and a barium vacancy in the other to test the mobility of Eu^{2+} inside the conduction plane. The trajectory plot of Eu^{2+} in the conduction plane shows that the europium almost moved through all the BR positions (see Fig. 5.5). Thus the mobility of Eu^{2+} ion must be the same as barium, or larger. The hexagonal shape in the trajectory map implies an interstitialcy migration mechanism; otherwise the shape should be triangular.

The defect set up to test the possibility of Eu^{2+} migration into the spinel block was the following: an Eu^{2+} was placed in its favorite BR position, an aluminum vacancy was placed inside the spinel block in the same primitive cell as the Eu^{2+} ion, and an Eu^{3+} interstitial was placed in the other conduction plane (without Eu^{2+}) and in a different primitive cell away from the Eu^{2+} . As shown above, when the Eu^{3+} ion was not in the same primitive cell as the Al vacancy, it did not migrate and thus would not disturb the migration of Eu^{2+} ion. Although a barium interstitial would form close to the aluminum vacancy, it is in the conduction plane where it would not seriously affect the Eu^{2+} migration. In all simulations with different aluminum vacancies, no long-range migration of Eu^{2+} ions was observed, although there was a little relaxation off the conduction plane. It seems that the divalent and trivalent europium ions behave quite differently in the migration process, although they are only different in the electronic charge they possess and in their size.

The migration of the only anion, O^{2-} , in the material has also been tested. There are three oxygen positions of interest: the position inside the spinel block, where it is the favorite oxygen interstitial position for configuration I of BAM; the mO site where is the oxygen interstitial position in β -alumina, and the mOB site which oxygen will occupy in configuration II of BAM. An Eu^{2+} interstitial in the conduction plane will be the compensating defect.

When inside the spinel block according to the interstitial position of configuration I of BAM, the oxygen migrated to the conduction plane, only if there was an Eu^{2+} interstitial in the same unit cell. Otherwise, the oxygen remained in place. When the oxygen migrated to the conduction plane, it formed a defect complex with the Eu^{2+} .

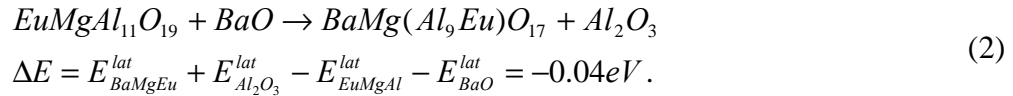
If the oxygen interstitial at the mOB site formed a two-bridge configuration with an O(5) in the conduction plane, it did not migrate at all. Instead the two oxygen ions rotated around the Al(3)-Al(3) axis, with a trajectory of a circle. When put in the third position, the mO site at the conduction plane, the oxygen did not stay there; instead it moved close to a nearby O(5) ion and formed a two-bridge configuration, as it did in the mOB site. There was no observation of Al(1) moving toward conduction plane to form a Reidinger defect, which is consistent with the previous defect energy calculations. In a

word, there was no long-range oxygen migration in the conduction plane at the tested temperatures.

5.4 Related Phases Containing Eu

Shozo et al. have proposed that oxidation converts the BAM:Eu²⁺ phosphor into a mixture of two compounds, BaMgAl₁₀O₁₇ and EuMgAl₁₁O₁₉ which was proposed to have a magnetoplumbite (MP) structure with three oxygen ions in the mirror plane.⁹ But in this migration study, oxygen and Eu³⁺ did not migrate inside the conduction plane, at the temperature at which Eu³⁺ can migrate into the spinel block easily. Thus the Eu³⁺ MP structure can not form, at least at that temperature where luminescent degradation begins to occur. Instead, based on our earlier result that Eu³⁺ prefers to substitute for Al in the spinel blocks of BAM, the phase after oxidation should be BaMg(Al₉Eu)O₁₇ keeping the β -alumina type structure.

These two structures were modeled and their lattice energies are compared below:



The negative reaction enthalpy means that the reaction will process toward right side of the reaction automatically, in other words, BaMg(Al₉Eu)O₁₇ is thermodynamically more stable, although the difference is small. Another thing that should be noted is that the unit cell parameter along 2-fold screw axis for BaMg(Al₉Eu)O₁₇ is 23.05 Å, a 0.4 Å difference from BAM, while EuMgAl₁₁O₁₉ has 1 Å difference from BAM. From the point of view of lattice relaxation, BAM:Eu²⁺ will form BaMg(Al₉Eu)O₁₇ more easily than EuMgAl₁₁O₁₉, after the oxidation at low temperature. But it does not mean EuMgAl₁₁O₁₉ would not occur at higher temperature, since the reaction enthalpy is very small and excess or residual Al₂O₃ may exist in the manufactured BAM product.

The main feature of the magnetoplumbite structure is the three oxygen ions in a mirror plane of a primitive cell. Defect complexes with three interstitial ions have been tested in the previous chapter but they only included configurations with two Eu ions and one oxygen ion. If the defect complex includes one Eu³⁺ and two oxygen ions, a three-oxygen configuration will form. So it is necessary to test this kind of defect complex to

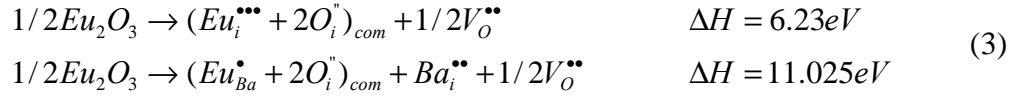
make sure that Eu^{3+} will not be stabilized at a BR site by three oxygen interstitial ions. As there are two possible oxygen locations in the mirror plane, mO and mOB sites, three kinds of defect complex with two oxygen interstitial ions will be created; both oxygens at either mO or mOB sites and a mixture of mO, mOB sites.

Table V.1. Defect Complex with Two Oxygen and One Eu^{3+}

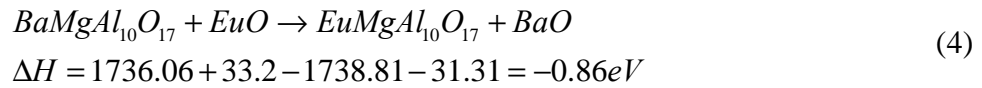
	mO+mOB	mOB+mOB	mO+mO	ΔE^* (eV)
$\text{Eu}_i^{\bullet\bullet\bullet}$	-70.81	-70.78	-	-9.73
$\text{Eu}_{\text{Ba}}^\bullet$	-54.86	-54.86	-	-3.67

* Energy difference between defect complex and the sum of individual defects.

Although the energy of the defect complex is less than the sum of individual defects, in writing down the defect reaction, it is clear that Eu^{3+} ion will not stay inside the mirror plane associated with the three oxygens as shown below.



Because of the high mobility of Eu^{2+} ions in the conduction plane and the fact that the defect complex will lower the total defect energy, Eu^{2+} may be able to come together and form europium β -alumina. The lattice energy of europium β -alumina was calculated and compared with barium β -alumina as follows,



It seems that it would be possible to form europium β -alumina because it should be more stable than the barium phase. However, these two structures are essentially the same except for the cations in the conduction plane. The difference between the cell parameters of these two structures are: $D\mathbf{a} = 0.004\text{\AA}$ and $D\mathbf{c} = 0.24\text{\AA}$ which are very small. Therefore, Eu^{2+} ions may just form a defect-cluster in the barium aluminate matrix, instead of phase separation, because Eu doped in BAM is normally treated as a defect. Actually, the formation of a europium cluster will decrease the luminescent intensity, because the photon released from an Eu^{2+} ion, instead of going out of the material, can be absorbed by a nearby Eu^{2+} . Thus, normally the doping concentration of

Eu is small in commercial materials for optical efficiency.⁶ Heating BAM:Eu²⁺ can create more, or larger, Eu²⁺ clusters, because the Eu²⁺ ion is quite mobile. The effect of the Eu²⁺ cluster is also shown in Oshio's work: the luminescent intensity does not increase linearly with doping concentration but the increase slows down at higher concentration.⁹

5.5 Conclusions

The results have shown that the order of mobility inside the conduction plane is: $\mu_{\text{Eu}^{2+}} \geq \mu_{\text{Ba}} > \mu_{\text{Eu}^{3+}}$. The interstitialcy mechanism dominates the migration of cations in the conduction plane. The valence state of europium determines its migration behavior; Eu³⁺ can migrate into the spinel block at a relatively low temperature, at which no migration of Eu²⁺ and Ba into the spinel block was observed. Eu³⁺ migration to either Al(1) or Al(3) vacancies are both one-step migrations. It requires at least two-steps for Eu³⁺ to occupy either Al(2) or Al(4) vacancies. Mg plays a key role in Eu³⁺ migration into the spinel block. Combined with the earlier study on the europium defect (Chap. 4), it may be concluded that Eu³⁺ ion tends to stay inside the spinel block after its generation above some temperature.

After oxidation, Eu³⁺ in BR sites may migrate to Al(2) sites and form BaMg(Al₉Eu)O₁₇ instead of EuMgAl₁₁O₁₉ at low temperature, because BaMg(Al₉Eu)O₁₇ is more stable than EuMgAl₁₁O₁₉ and its lattice parameters are closer to those of BAM. Eu²⁺ ions tend to come close to each other to form a defect cluster, which will decrease the luminescent intensity of the phosphor. Decreasing the Eu²⁺ mobility in the conduction plane may provide a way to overcome the degradation problem.

References

1. N. Iyi, Z. Inoue, and S. Kimura, "The Crystal Structure and Cation Distribution of Highly Nonstoichiometric Magnesium-Doped Potassium Beta-Alumina," *J. Solid State Chem.*, **61**[2] 236-44 (1986).
2. W.L. Bragg, C. Gottfried, and J. West, "The Structure of Beta Alumina," *Z. Kristallogr.*, **77**[2] 255-74 (1931).
3. C.A. Beevers and M.A.S. Ross, "The Crystal Structure of "Beta Alumina" $\text{Na}_2\text{O} \cdot 11\text{Al}_2\text{O}_3$," *Z. Kristallogr.*, **97**[1] 59-66 (1937).
4. B.G. Dick and A.W. Overhauser, "Theory of the Dielectric Constants of Alkali Halide Crystals," *Phys. Rev.*, **112**[1] 90-103 (1958).
5. T.B. Forester and W. Smith, *DL POLY Reference Manual*, 2.0 ed.; pp. 45-7. CCLRC, Daresbury Laboratory, Warrington, England, 1995.
6. S. Tanaka, I. Ozaki, T. Kunimoto, K. Ohmi, and H. Kobayashi, "Blue emitting CaAl_2O_4 : Eu^{2+} phosphors for PDP application," *J. Lumin.*, **87-89**[1] 1250-3 (2000).
7. W.L. Roth, F. Reidinger, and S.L. Placa, "Studies of Stabilization of Transport Mechanisms in Beta and Beta" Alumina by Neutron Diffraction," pp. 223-41 in *Superionic Conductors*. Edited by G. D. Mahan and W. L. Roth. Plenum, New York, 1976.
8. M.S. Whittingham and R. A. Huggins, "Transport Properties of Silver β -alumina [$\text{Ag}_{1+x}\text{Al}_{11}\text{O}_{17}$]," *J. Electrochem. Soc.*, **118**[1] 1-6 (1971).
9. S. Oshio, K. Kitamura, T. Nishiura, T. Shigeta, S. Horii, and T. Matsuoka, "Analytical Research of Decrease in Luminance Following Annealing of $\text{BaMgAl}_{10}\text{O}_{17}:\text{Eu}^{2+}$ Blue Phosphor for Fluorescent Lamps and Plasma Display Panels," *Natl. Tech. Rep. (Matsushita Electr. Ind. Co.)*, **43**[2] 181-7 (1997).

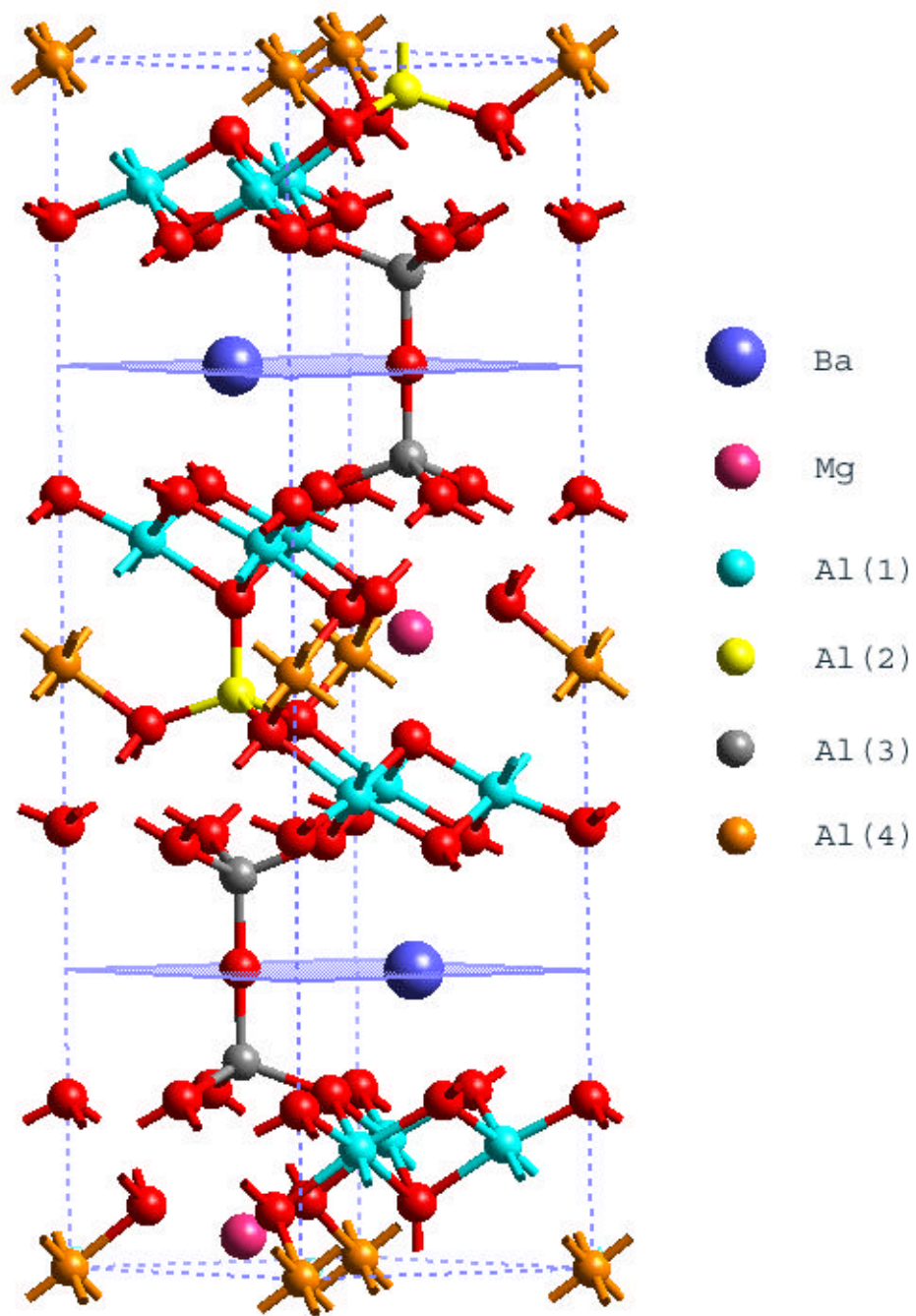


Figure 5.1. Primitive cell of BAM, configuration I.

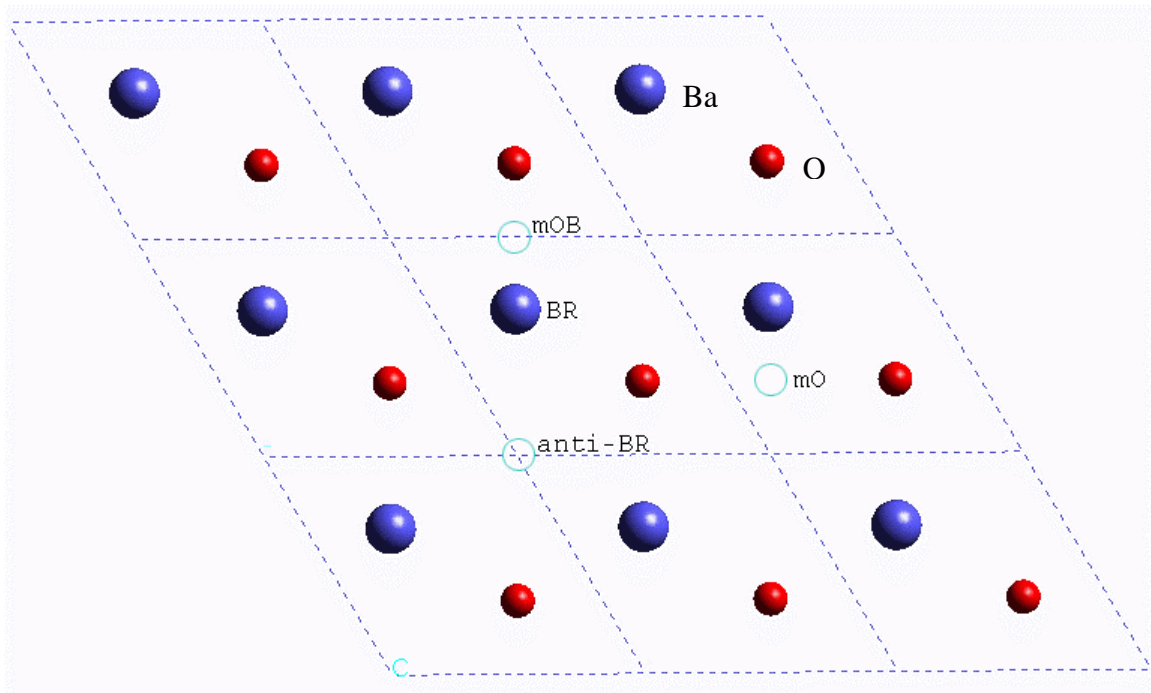


Figure 5.2. Projection of mirror plane of BAM on X-Y plane.

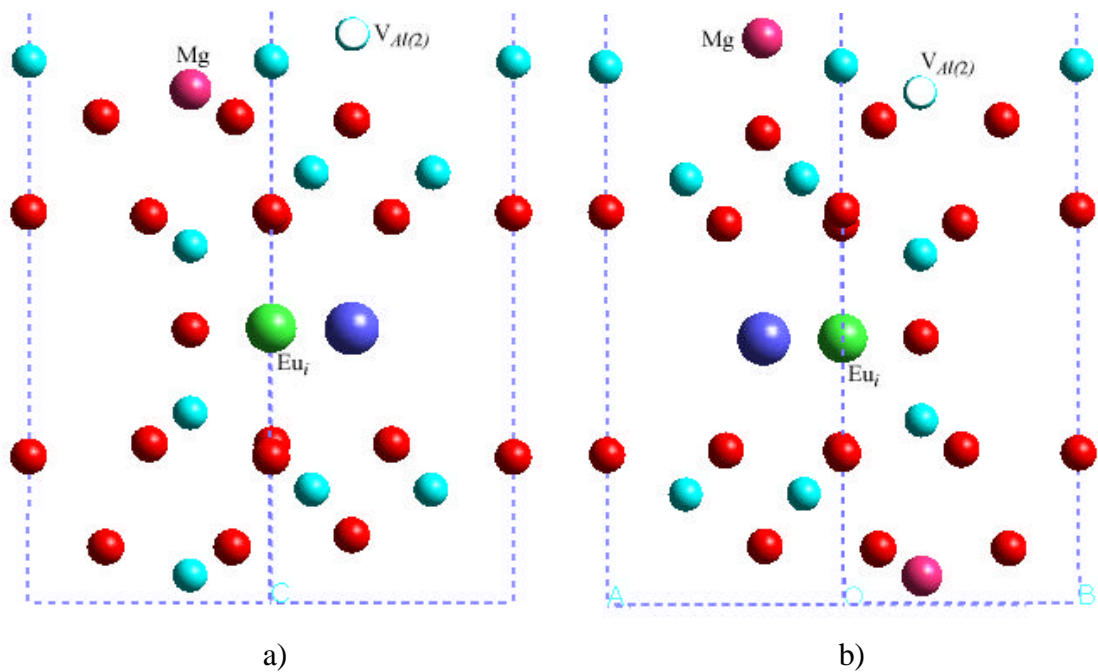


Figure 5.3. Magnesium positions related to $Eu_i^{3+} + V_{Al(2)}^{3-}$.
 a) Mg in between two defects. b) Mg not in between two defects.

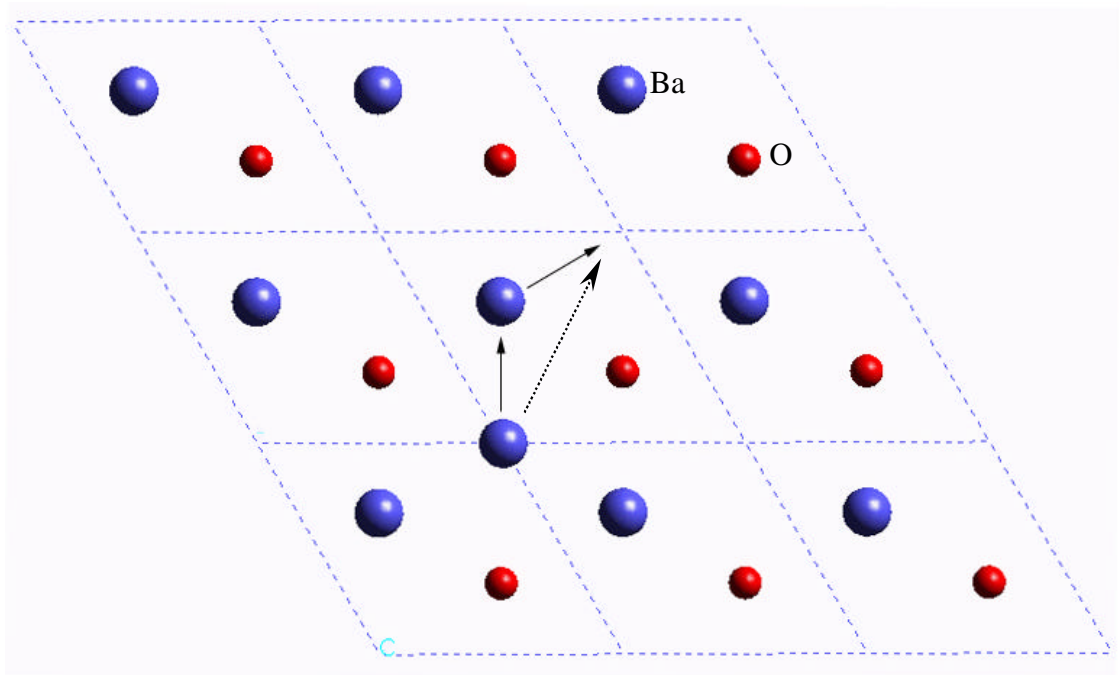


Figure 5.4. Barium interstitialcy migration.

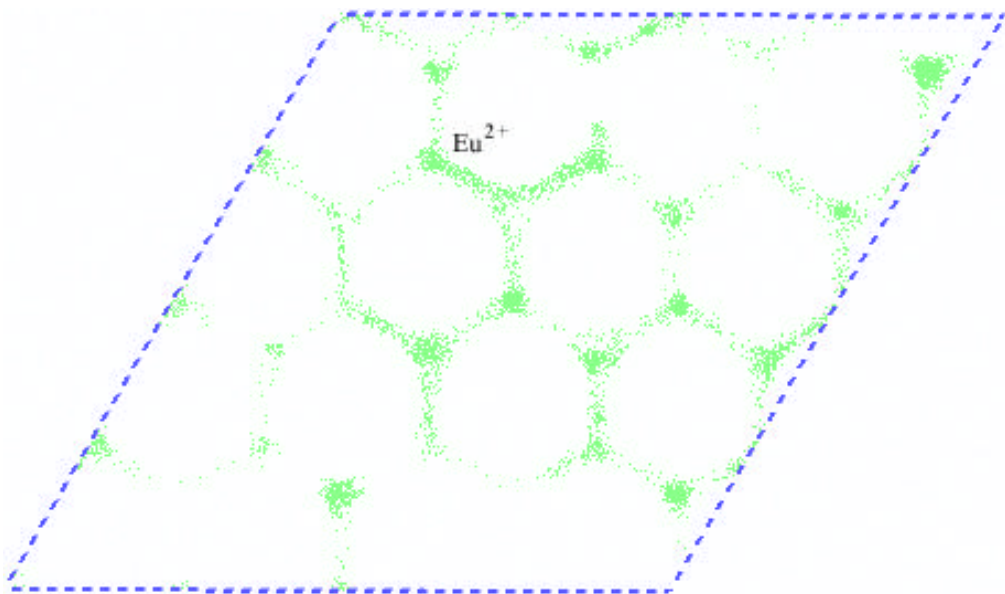


Figure 5.5. Trajectory of Eu^{2+} in the conduction plane.

6. Eu in Barium Hexa-aluminates Containing No Mg

Abstract:

Besides substituting Al with Mg to form BAM, there are two other ways to compensate the charge generated by incorporating Ba in the β -alumina crystal structure. One is to put barium on $\frac{3}{4}$ of the BR sites and oxygen on the remaining $\frac{1}{4}$, which gives the chemical formula of $0.82\text{BaO}\cdot 0.6\text{Al}_2\text{O}_3$, namely a barium-poor phase, because the Ba/Al ratio is far below the ideal value of 1/12. The other is to create aluminum vacancies in the spinel blocks and form $\text{Ba}_3\text{Al}_{32}\text{O}_{51}$, a phase with the Ba/Al ratio larger than 1/12. The structures generated in these two ways were tested for defect properties, intrinsic and extrinsic with Eu. When doped with Eu^{2+} , two emission bands, green and blue, have been observed in the barium-poor phase, which was suggested to come from two different europium positions.¹ Our work has shown that ions in the barium-poor phase, the europium, divalent and trivalent, occupy the Beevers-Ross and Al(3) tetrahedral sites, respectively. However, Eu^{3+} ion prefers to occupy the Al(2) site in $\text{Ba}_3\text{Al}_{32}\text{O}_{51}$, which is the same result found in BAM. The calculations suggest that the expansion of the emission band in the barium-poor phase is due to the fact that the existence of multiple oxygen distributions in the mirror plane varies the local Eu^{2+} environments. Eu^{3+} ions at the tetrahedral sites inside the spinel block may also contribute to the shape of the observed emission band after luminescence degradation.

6.1 Introduction

$\text{BaMgAl}_{10}\text{O}_{17}$ (BAM): Eu^{2+} is a kind of blue phosphor used in lamps and display panels. The drawback of this material is that the luminescence property will degrade with prolonged heating, the blue emission intensity decreasing and a green emission band emerging.¹ It has been shown by Ronda and Smets that another barium hexa-aluminate phase, $\text{Ba}_{0.75}\text{Al}_{11}\text{O}_{17.25}$ (known as a barium-poor phase), has two emission bands when doped with Eu^{2+} .² They suggested that these two bands were due to the Eu^{2+} in two different sites in the crystal. This provided a possible explanation of the degradation of BAM: Eu^{2+} . It is normally believed that the green band observed in the degraded BAM: Eu^{2+} comes from the emission of Eu^{3+} ions, formed by the oxidation of Eu^{2+} ions, but the ligand field acting on Eu^{2+} ions may also shift the emission band. We have carried out a study of europium behavior in the barium-poor phase to compare it with our previous work and to try to understand the differences in the emission bands between the barium-poor phase and BAM. $\text{Ba}_3\text{Al}_{32}\text{O}_{51}$ structure was modeled and compared with the structure of BAM. Its defect properties were also calculated.

The prototype structure of barium hexa-aluminates is β -alumina, $\text{NaAl}_{11}\text{O}_{17}$, which is described as oxygen close-packed spinel blocks separated by sodium-oxygen planes (also called mirror planes or conduction planes). When introducing barium into the structure, there are several ways to compensate the extra positive charge of barium on the Beevers-Ross sites. One is to substitute the same number of aluminum as barium with magnesium to form Mg'_{Al} ; this generates the BAM structure. Another way is to put barium on $\frac{3}{4}$ of the BR sites and oxygen on the remaining $\frac{1}{4}$ (namely O_R), generating the barium-poor phase. The third possible structure has aluminum vacancies inside the spinel block and all BR sites occupied by Ba. These structures are closely related to each other and they can possibly transform from one to the other. A solid solution between BAM and the barium-poor phase has been found to exist with all ratios of these two phases. The introduction of oxygen into the BR site in the barium-poor phase makes the structure more complicated because the BR site is not an anion position and so the oxygen might move away and change the structure of conduction plane. Thus, the defect

properties are hard to analyze by experimental techniques. Computer simulations are a useful tool to attack the problem.

The simulations in this study are based on the Born model description of ionic solid, which treats the solid as a collection of point ions with short-range forces acting between them. The approach has shown success in a lot of simulations, but it has been found that the reliability of the simulations depends strongly on the validity of the potential model used in the calculations. The non-Coulombic potentials can be described in many forms. The Buckingham function is used in this study,

$$V_{ij}(r_{ij}) = A_{ij} \exp(-r_{ij} / r_{ij}) - C_{ij} r_{ij}^{-6} \quad (1)$$

where r_{ij} is the distance between the ions i and j

The polarizability of an individual ion is mimicked through the core-shell model originally developed by Dick and Overhauser, in which the outer valence electron cloud of the ion is simulated by a massless shell of charge Y and the other part of the ion by a core of charge X .³ The total charge of the ion is $X+Y$ and must equal its the oxidation state. The core and shell form a harmonic oscillator with a spring constant k , and the potential energy is given by

$$V_i(r_i) = \frac{1}{2} k_i d_i^2 \quad (2)$$

where d_i is the relative displacement of the core and shell of ion i .

For the shell model, the value of the free-ion electronic polarizability is given by

$$a_i = Y_i^2 / k_i. \quad (3)$$

The potential parameters A , r , and C in Eq. [1], the shell charges Y , and spring constant k associated with the core-shell model description of polarizability, need to be determined for each interaction and ion type in the crystal. In the present study, they were taken from our earlier studies of hexa-aluminates following the original compilation of Lewis and Catlow.⁴⁻⁶

6.1.1 Lattice Energy Calculations

The lattice energy is the binding or cohesive energy of the perfect crystal and is usually defined as the energy that must be released to the crystal to separate its

component ions into free ions at rest at infinite separation. It is the summation of all potentials in the structure:

$$U = 1/2 \sum \sum V_{ij} . \quad (4)$$

The interatomic potential, V_{ij} , includes the long-range Coulombic interaction besides the non-Coulombic potential described above. The Coulombic potential is calculated with the Ewald-sum approach that separates the summation into two sums.⁷ The lattice energy is minimized through a second derivative Newton-like procedure, coded into METAPOCS.⁸ Details of the procedure have been outlined by Cormack.⁹

6.1.2 Defect Energy Calculations

Calculations of defect structures and energies are based on the perfect lattice methods. Additionally, the occurrence of relaxation of lattice atoms around the defect species must be included. The relaxation effect is large because the defect generally provides an extensive perturbation of the surrounding lattice, and, in the case of ionic crystals, the relaxation field is long-range as the perturbation provided by the defect is mainly Coulombic in origin.

The defect calculations are based on the Mott-Littleton theory, which allows one to calculate the defect-induced static polarization of a dielectric continuum.¹⁰ The basic approach is to divide the material into two regions: one is centered at the defect and the other region is outside the first one and is treated as a dielectric continuum. The inner region is treated atomistically within the framework of the Born model described above because the forces and resulting atom displacements are too large to be treated properly using continuum theory in this region, which can, nevertheless, be used to model the outer region of the crystal. CASCADE, coded with this two-region approach, was used in this study to calculate the defect energies.

6.2 The Barium-Poor Phase $\text{Ba}_{0.75}\text{Al}_{11}\text{O}_{17.25}$

6.2.1 Calculated Structure

Since $\frac{1}{4}$ of the BR sites are occupied by oxygen and METAPOCS would not recognize partial occupancy, a super-cell for the barium-poor phase was constructed; it

was two times the size of the β -alumina unit cell, with a composition of $\text{Ba}_3\text{Al}_{44}\text{O}_{69}$. There is no ambiguity in the position of cations (such as the different Mg distributions in BAM structure). As METAPOCS uses periodic boundary condition, the input super-cell with different arrangements of the two primitive cells, such as along **a** or **c** direction, would actually generate different periodic lattices, which leads to a problem: are there any specific arrangements for oxygen in the BR sites? Two types of super-cell have been tested for oxygen distributions, $\text{Ba}_3\text{Al}_{44}\text{O}_{69}$ and a larger super-cell of $\text{Ba}_6\text{Al}_{88}\text{O}_{138}$.

For the $\text{Ba}_3\text{Al}_{44}\text{O}_{69}$ super-cell, only two different arrangements exist. One has two primitive cells along the **a** axis (**a**-structure as a 2x1x1 super-cell) and the other has the primitive cells along the **c** axis (**c**-structure as a 1x1x2 super-cell). After relaxation with METAPOCS, these two structures gave quite different lattice energies. The **a**-structure had a lattice energy of -3588.75eV , lower than -3582.53eV , the lattice energy of the **c**-structure. The 6.22eV difference is very large. When looking at the relaxed structures, the lattice parameter γ was no longer 120° in both **a**- and **c**-structures, and whereas the **c** axis was still perpendicular to the **ab** plane in the **a**-structure, it was not in the **c**-structure. It is clear that the **a**-structure is more stable than the **c**-structure.

For the $\text{Ba}_6\text{Al}_{88}\text{O}_{138}$ super-cell, four primitive-cells were arranged as shown in Fig. 6.1. There are totally eight possible BR sites for the two oxygen ions. If the symmetrically similar ones are discounted, only five structures are left to be tested. Based on the locations of the oxygen ions, they were labeled as 1-2, 1-3, 1-5, 1-6 and 1-7; the two digits refer to the regions of the two O_{BR} sites.

From Table VI.1, the 1-3 structure had the lowest lattice energy out of the five structures, but the energy was bigger than twice the lattice energy of the 2x1x1 super-cell. This was surprising because the 1-2 structure is just two 2x1x1 super-cells put together and it was expected that the lattice energy of 1-2 super-cell should be double the lattice energy of 2x1x1 super-cell. On examining the relaxed structure, it could be seen that there was a Reidinger defect formed automatically in the 2x1x1 super-cell but not in the 1-2 structure. The 1-3 structure formed only half a Reidinger defect, which causes its lattice energy to be a lot smaller than that of the 1-2 super-cell. So it was the Reidinger defect that made oxygen more stable in the conduction plane. Then those five structures

and two small super-cells were recalculated. This time, Reidinger defects were constructed at O_{BR} for all super-cells before the structure was relaxed.

Table VI.1. Lattice Energies of Five Structures

Structure	1-2	1-3	1-5	1-6	1-7
E_{latt} (eV)	-7152.54	-7174.89	-7155.51	-7155.51	-7155.29

Table VI.2. Lattice Energies of Five Structures (with Reidinger-Defect)
 2x1x1 super-cell: -3589.44 eV 1x1x2 super-cell: -3577.85 eV

Structure	1-2	1-3	1-5	1-6	1-7
E_{latt} (eV)	-7178.88	-7178.88	-7174.72	-7174.49	-7175.85

After the recalculation, both the 1-2 and 1-3 super-cells (Fig. 6.2,6.3) had lattice energies exactly twice of the 2x1x1 super-cell, which was what was expected. It should be mentioned that when forming the Reidinger defect, two Al(1) ions were displaced toward the mirror plane from the spinel block. The two Al(1) ions with the same x and y coordinates were moved at the same time so that the mirror symmetry was kept. There are three Al(1) ions above and below the mirror plane that can be displaced. Consistent with the work of Park, the lattice energy varied with which Al(1) was displaced, but the lattice energy variance was so small (like BAM) that there is no specific configuration for the barium-poor phase; all structures are likely to coexist at the same time.¹¹ The lattice energy difference in Table VI.2 might seem to be large but the difference per formula unit is small after they are normalized according to the size of the super-cell.

Two O_{BR} ions did not come close to each other to form a three-oxygen arrangement with another oxygen ion at normal site, in a similar way to the magnetoplumbite structure, because no aluminum ions are available to be put in the conduction plane to stabilize them and because barium magnetoplumbite does not exist. The super-cell with a three-oxygen cluster was calculated to have a lattice energy of -7175.82eV, that was, indeed, higher than for the 1-2 structure.

6.2.2 Solid Solution

BAM and the barium-poor phase form a complete solid solution as the X-ray diffraction pattern indicates.¹³ It is of great interest to study this kind of behavior. A 4x4x1 super-cell was constructed to calculate the energy of solid solutions with BAM phase percentages of 100, 75, 50, 25 and 0. The number of primitive cells of the BAM phase in the super-cell was varied according to the ratio. Then the super-cells were relaxed with METAPOCS. All of the tests reached stable structures, whose lattice energies are plotted in Fig. 6.4 with respect to the concentration. The lattice energies listed have been divided by the number of primitive cells in the super-cell.

Although these two phases have different structures, the lattice energy changes linearly with the concentration, which means that there is no preferred composition in between BAM and barium-poor phase, i.e. the solid solution is thermodynamically stable. Since the main difference between these two phases lies in the barium-oxygen plane structure and the lattice mismatch between BAM and barium-poor phase is small (0.02 Å in the *c* axis and 0.03 Å in other two axes), it is no surprise for them to form a complete solid solution across the entire composition range. The small lattice mismatch determines the small relaxation of structure of the solid solution so the lattice energy is just the weighted average of two lattice energies. Actually, the barium-poor phase can be treated just like a defect BAM structure.

6.2.3 Intrinsic Defects

The 2x1x1 super-cell and the 1-3 super-cell were chosen for the calculation of the defect properties of the barium-poor phase, because they have the same lattice energy but different oxygen distributions. As the 2x1x1 super-cell is just half of the 1-2 super-cell, the 2x1x1 super-cell will be referred to as the 1-2 structure in later discussion. The defect properties of the super-cell with the lowest lattice energy of -7182.26eV in Park's work, named the b1 structure (see Fig. 6.5), were also investigated.¹¹ Two O_{BR} were put in the same primitive cell but in different mirror planes in the b1 structure (see Figs. 6.6, 6.7), in contrast to the 1-2 and 1-3 structures, where the two O_{BR} were on the same mirror plane, but in different primitive cells.

Table VI.3 lists the vacancy point defects, for the three super-cells. For simplicity, the classification of ion positions was referenced to β -alumina, although the symmetry will have changed. O_{BR} was labeled as O(6). The point defect energy listed in the table was the lowest one calculated for each type of defect.

Table VI.3. Vacancy Defect Energies of Super-Cells

Defect	Defect Energy (eV) in 1-2 Super-cell	Defect Energy (eV) in 1-3 Super-cell	Defect Energy (eV) in b1 Structure
$V_{Ba}''^*$	15.67	15.49	16.36 ¹
$V_{Ba}''^{**}$	17.89	17.75	16.71 ²
$V_{Al(1)}'''$	55.19	55.19	55.77
$V_{Al(2)}'''$	58.12	57.77	58.55
$V_{Al(3)}'''$	57.67	57.30	58.41
$V_{Al(4)}'''$	55.72	55.37	55.59
$V_{O(1)}''$	23.31	23.15	24.21
$V_{O(2)}''$	23.76	23.60	24.39
$V_{O(3)}''$	23.37	23.22	23.29
$V_{O(4)}''$	22.81	22.65	23.98
$V_{O(5)}''$	24.65	18.20	24.99
$V_{O(6)}''$	18.37	24.50	20.68

* Mirror plane without O_{BR} . ** Mirror plane with O_{BR} .

1 Far away from O_{BR} .

2 Close to O_{BR} .

Defect energies for the first two super-cells were similar, but not the same. Oxygen vacancies occurred at different positions in the mirror plane, because of the different arrangements of the oxygen ions. As two O_{BR} ions were separated in different mirror planes of the b1 super-cell, the defect energy also changed, especially for barium and oxygen vacancies. However, the positions for the oxygen vacancy were in the mirror plane for all structures, which is the result of the high oxygen concentration there. That is

not the case for the BAM structure for which the oxygen vacancy resides inside the spinel block. Vacancies of Al(1) and Al(4) were found to have similar defect energies for all three structures. Al(4) was the energetically favorite vacancy position for the 1-2 and 1-3 super-cells but not for the b1 super-cell, for which vacancy at the Al(1) site had the lowest energy.

The barium vacancy tended to occur far away from O_{BR} . That is because the two defects have the same sign of effective charge. They can not occur together or there will form a negative charge-rich region that will increase the system energy.

Because the super-cells were so large and complicated, a program was designed to scan sites, or interstitial positions, inside the structure and choose those sites with a radius large enough for the interstitial ion, as well as finding positions having special symmetry elements (such as lying on a rotation axis). The size of an interstitial site was defined as the distance to its nearest neighboring ion. Totally, about 400 interstitial positions were calculated for each structure. The energy and position of point defects, for each structure, are shown in Tables 6.4-6. The energy and position of vacancies are also included.

Table VI.4. Point Defects of 1-2 Super-Cell

Defect	Defect Energy (eV)	Defect Position
V_{Al}'''	55.19	Al(1) site
V_{Ba}''	15.67	BR in the mirror plane without O_{BR}
V_O''	18.37	O_{BR}
Al_i'''	-46.84	Between two O_{BR}
Ba_i''	-14.38	Between O(5) and O_{BR}
O_i''	-15.84	Change Al(2) tetrahedron to pentahedron

In the 1-2 super-cell, only one of the two mirror planes contains O_{BR} and is negatively charged. A barium vacancy has an effective negative charge, so that it is not energetically favorable for it to reside in the mirror plane with O_{BR} . For the same reason, an oxygen vacancy tends to lower the negative charge concentration in the O_{BR} plane. Interstitial cations also resided close to O_{BR} to compensate the negative charge. The oxygen interstitial did not stay in the mirror plane; instead it entered into the spinel block and changed the coordination number of one Al(2) ion from 4 to 5. The reason for that is

believed to be the positive charge of the spinel block, $[Al_{11}O_{16}]^{1+}$. The two mirror planes in the super-cell have the chemical formula of $[Ba_4O_4]$ and $[Ba_2O_6]^{8-}$. An oxygen interstitial ion in the mirror plane will increase the local charge more than in the spinel block.

Table VI.5. Point Defects of 1-3 Super-Cell

Defect	Defect Energy (eV)	Defect Position
V_{Al}'''	54.83	Al(1) site
V_{Ba}''	15.49	BR site in the mirror plane without O_{BR}
V_O''	18.20	O(5) in O_{BR} plane
Al_i'''	-47.80	V_{Al} of Reidinger defect
Ba_i''	-14.53	Between two O(5) in O_{BR} plane
O_i''	-16.01	Change Al(2) tetrahedron to pentahedron

Point-defect positions in the 1-3 super-cell were similar to those in the 1-2 super-cell except for the aluminum interstitial ion. All defects with a positive effective charge, other than the Al interstitial were found on the O_{BR} plane. The aluminum interstitial ion occupied the vacant aluminum site formed by the Reidinger defect. An oxygen interstitial ion at the mOB site in the mirror plane, the oxygen interstitial position of the configuration II of BAM, had very small defect energy but was still 0.1eV higher than in the spinel block.

Table VI.6. Point Defects of b1 Super-Cell

Defect	Defect Energy (eV)	Defect Position
V_{Al}'''	55.59	Al(4) site
V_{Ba}''	16.36	BR site far away from O_{BR}
V_O''	20.68	O_{BR}
Al_i'''	-45.64	V_{Al} of Reidinger defect
Ba_i''	-13.06	anti-BR close to O_{BR}
O_i''	-17.09	mOB in mirror plane

Since both mirror planes of the b1 super-cell had an O_{BR} , the oxygen concentration in the mirror plane was less than for the mirror planes of the other two structures. It was possible for the oxygen interstitial ion to reside in the mirror plane and form a defect

configuration like in BAM; the oxygen interstitial ion stayed at the mOB site, a position between a barium and an nearby O(5), and formed a two-bridge configuration as in BAM. The aluminum vacancy changed from the Al(1) site in the 1-2 and 1-3 super-cells to the Al(4) site in the b1 super-cell. The aluminum interstitial ion, like in the 1-3 super-cell, took the vacancy generated by the Al(1) shifting toward the mirror plane in forming a Reidinger defect.

Table VI.7 lists the intrinsic defect energies of the three super-cells. These energies were normalized to energies per point defect in order to be comparable. For all structures, the Barium Frenkel defect held the lowest defect energy, which means the Barium Frenkel defect is expected to be the predominant thermal defect, the same as in BAM. The intrinsic defect with the second lowest defect energy was different for each super-cell.

Table VI.7. Intrinsic Defect Energies of Super-Cells (eV)

Defect	1-2 Super-cell	1-3 Super-cell	b1 Structure
Schottky	1.32	1.08	2.85
Al Frenkel	4.18	3.52	4.98
Ba Frenkel	0.25	0.48	1.65
O Frenkel	1.27	1.10	1.80

It seems that the oxygen distributions changed the defect energies and defect positions, but maintained the lattice energies in a small range for all three structures. The effect of oxygen distribution is long-range; it changes the Madelung potential at each ion. The different charge distributions caused by different O_{BR} distributions changed the locations of defects, which seemed to be a local charge effect. The large number of possible oxygen distributions makes the defect properties of barium-poor phase very complex.

6.2.4 Eu Locations

It has been found from our earlier calculations that europium divalent ions occupy two different positions in the barium-poor phase, with one in the Beevers-Ross site and the other inside the spinel block. The Eu^{2+} ions in BR sites will emit blue light while those inside the spinel block will emit green light.¹ We have calculated the extrinsic defects associated with the europium ions and possible mechanisms for doping. For the doping process, europium ions were assumed to substitute for aluminum or for barium in addition to considering interstitial positions.

Table VI.8. Europium Point Defects in the Three Super-Cells

Defect	1-2 Super-cell		1-3Super-cell		b1 Super-cell	
	Energy (eV)	Position	Energy (eV)	Position	Energy (eV)	Position
Eu_{Ba}	-1.44	BR site in the mirror plane with O_{BR}	-1.42	BR site in the mirror plane with O_{BR}	-1.34	BR site close to O_{BR}
Eu'_{Al}	39.09	Al(2)	39.06	Al(3) beside mirror plane without O_{BR}	38.81	Al(3) in the primitive cell without O_{BR}
$\text{Eu}_i^{\bullet\bullet}$	-16.26	Between two O(5)	-16.41	Between two O(5)	-14.86	anti-BR site close to O_{BR}
$\text{Eu}_{\text{Ba}}^{\bullet}$	-22.76	BR site in the Mirror plane with O_{BR}	-22.78	BR site in the mirror plane with O_{BR}	-22.17	BR site
Eu_{Al}	14.4	Al in Reidinger defect	14.40	Al in Reidinger defect	14.44	Al(3) in the primitive cell with O_{BR}
$\text{Eu}_i^{\bullet\bullet\bullet}$	-37.36	Center of rectangle with $2\text{O}(5)$ and 2O_{BR}	-37.74	Center of rectangle with $2\text{O}(5)$ and 2O_{BR}	-38.81	anti-BR site close to O_{BR}

The preferred positions of europium point defects were similar in each super-cell except for the europium divalent ion substituting for aluminum. For the 1-2 super-cell, the divalent europium ion would substitute on the Al(2) site, the same as in BAM. The Al(1) ion, moving close to the mirror plane to form a Reidinger defect, was substituted in the 1-3 super-cell. Although these two positions are different in space, they are both tetrahedral positions. In the b1 structure, the Al(3) ion was substituted by both divalent

and trivalent Eu. Actually, the Al(3) ion can be considered to be the same as the Al(1) ion in the Reidinger defect, i.e. they both were shifted from octahedral sites to stabilize the oxygen ions in the mirror plane, but the shift of Al(3) becomes part of the structure.

In all three structures, substitutions of aluminum at the edge of spinel block by Eu^{3+} ion had the lowest point defect energy in Eu_{Al} substitution. The mirror plane with O_{BR} has a chemical formula $[\text{Ba}_2\text{O}_6]^{8-}$, so it is no surprise to see point defects with positive net charge prefers to be in or close to it. As seen in Table VI.9, there are many ways for Eu to enter into the structure. As point defect energies are not comparable, defect reactions related to these point defects were written down to obtain the reaction enthalpy in order to find the reaction that will dominate the europium doping process.

Table VI.9. Incorporation of Eu into Super-Cells

Reaction	Defect Energy (eV)		
	1-2 Super-cell	1-3 Super-cell	b1 Super-cell
$\text{EuO} \rightarrow \text{Eu}_i^{\bullet\bullet} + \text{O}_i^{\bullet}$	1.10	0.78	1.25
$\text{EuO} \rightarrow \text{Eu}_{\text{Al}}^{\bullet} + \text{Al}_i^{\bullet\bullet\bullet} + \text{O}_i^{\bullet}$	9.61	8.45	9.28
$\text{EuO} \rightarrow 1/2\text{Al}_2\text{O}_3 + \text{Eu}_{\text{Al}}^{\bullet} + 1/2\text{V}_\text{O}^{\bullet\bullet}$	2.09	1.97	2.96
$\text{EuO} \rightarrow \text{BaO} + \text{Eu}_{\text{Ba}}$	0.45	0.47	0.55
$\text{EuO} \rightarrow \text{Eu}_i^{\bullet\bullet} + \text{V}_{\text{Ba}}^{\bullet} + \text{BaO}$	1.30	0.97	3.39
$1/2\text{Eu}_2\text{O}_3 \rightarrow \text{Eu}_i^{\bullet\bullet\bullet} + 3/2\text{O}_i^{\bullet}$	4.32	3.69	4.57
$1/2\text{Eu}_2\text{O}_3 \rightarrow \text{Eu}_{\text{Al}}^{\bullet} + \text{Al}_i^{\bullet\bullet\bullet} + 3/2\text{O}_i^{\bullet}$	9.24	8.03	8.79
$1/2\text{Eu}_2\text{O}_3 \rightarrow \text{Eu}_{\text{Al}}^{\bullet} + 1/2\text{Al}_2\text{O}_3$	0.45	0.45	0.49
$1/2\text{Eu}_2\text{O}_3 \rightarrow \text{Eu}_{\text{Ba}}^{\bullet} + \text{BaO} + 1/2\text{O}_i^{\bullet}$	3.45	3.35	3.42

As seen in Table VI.9, divalent europium ions substituted for barium ions in BR sites. However, trivalent ions substituted for aluminum in the Reidinger defects instead of Al(2) observed in the BAM structure; the similarity is that both positions are inside oxygen tetrahedra. Based on the work of Ronda and Smets, there may be two positions for europium divalent ions.² They have suggested that one was in the mirror plane and

the other was inside the spinel block. But Eu^{2+} substituting aluminum in the spinel block requires a lot more energy than staying in the mirror plane and the reaction with the second lowest enthalpy is for an Eu^{2+} interstitial ion in the mirror plane.

Actually, there are at least two different BR sites in each structure of the barium-poor phase (see Fig. 6.8); they are different in their distances from O_{BR} . The difference in substitution energy for these two BR sites was 0.14eV (0.01eV for the b1 super-cell). The energy difference was so small (at least for the b1 super-cell) that both barium ions in the two sites could be substituted by Eu^{2+} ions. Figure 6.6 displays the difference between the environments of europium ions in the two sites of the 1-2 super-cell. It is clear that ligand field effects will alter the band structure of the active ion, i.e. the environment will change the emission band of europium ions. The europium ions in different BR sites will definitely emit different wavelengths of luminescence. The structure complexity and large population of different BR sites give a good explanation of the emission band broadening.

6.3 Emission Band Calculations

Two bands have been suggested in the broad emission band of the barium-poor phase containing Eu^{2+} , one is 440nm and the other is about 550nm.^{1,13} The characteristic luminescence originates from the electronic transition $4f^65d^1 \rightarrow 4f^7$. This transition is heavily affected by the interaction between the active ion and its surrounding ions. As reported, the position of the d-band edge in energy (E) for Eu can be estimated by the empirical equation:¹⁴

$$E = Q \left[1 - \left(\frac{V}{4} \right)^{1/V} 10^{-(n \times ea \times r)/80} \right] (\text{cm}^{-1}). \quad (7)$$

V is the charge of the ion being substituted and Q is the energy value of the d-band edge of free ion. The Q value is 34000cm^{-1} for Eu^{2+} and 80800cm^{-1} for Eu^{3+} ions.¹⁵ n is the coordination number of the active ion, ea is the electron affinity of the surrounding ions (1.60 for oxygen ions) and r is the radius of cation replaced by the active ion in the host crystal. If the emission bands are already known, it is possible to estimate the coordination number of the active ion inside the crystal by rewriting equation (7) to:

$$n = -\text{Log} \left[\left(1 - \frac{E}{Q} \right) \cdot \left(\frac{V}{4} \right)^{-1/V} \right] \times 80 / ea / r. \quad (8)$$

Two kinds of cation exist in the barium-poor phase, Ba²⁺ and Al³⁺. Emission bands are calculated for Eu²⁺ and Eu³⁺ ions in these positions.

Table VI.10. Estimated Emission Wavelength of Eu

Eu ²⁺ Position	V	n	r(Å)	E(cm ⁻¹)	Wavelength (nm)
Ba ¹	2	9	1.47	20300	480
Ba ²	2	10	1.52	21100	450
Al(1)	3	6	0.675	8400	1200
Al(2)	3	4	0.53	6000	1670
Eu ³⁺ Position	V	n	r(Å)	E(cm ⁻¹)	Wavelength (nm)
Ba ¹	2	9	1.47	48100	200
Ba ²	2	10	1.52	50100	190
Ba ³	2	12	1.61	53700	170
Al(1)	3	6	0.675	19900	500
Al(2)	3	4	0.53	14200	700

1 Normal BR site

2 BR site with an O_{BR} around

3 BR site in Magnetoplumbite

Since equation 7 is just an empirical function, the calculated emission band would not be precisely the same as the measurement of experiment. But it can give a idea of the change in the emission band of europium in the barium-poor phase compared with BAM:Eu²⁺. A divalent europium ion in the normal BR site is estimated to emit light of 480nm wavelength from the calculation. Although that is different from the measured 440nm, this empirical function can give an idea of how the coordination conditions change emission.

The emission calculation shows that divalent europium substituting for aluminum will emit light with wavelength so much larger than the measured spectrum that the observed broad emission band would not come from the Eu²⁺ ion in the spinel block. Instead, the existence of O_{BR} inside the mirror plane is more likely to change the emission

characteristics of the europium ion. The actual structure of the barium-poor phase will be more complex than this because of multiple O_{BR} -configurations: this is the key to understanding the broadening of the emission band. Because the emission band not only becomes broad but also shifts toward the large wavelengths, two Eu^{2+} positions are suggested.

Actually, the above empirical equation only considered the ligand field generated by the first coordination ions. Although ligand field coming from second or higher order coordination ions might be small, it would also vary the band structure of the center ion; it is the whole structure that determines the band structure of individual ion. Thus, the site energies (potential of the whole structure acting on that site) of BR positions are compared to see whether there is any ‘big’ difference that can explain the emission band shift and broadening.

Table VI.11. Site Energy Comparison of Eu^{2+} Positions

Structure	Site	E_M (eV)	E_S (eV)	E_t (eV)
BAM (Conf. I)	BR	-12.45	1.74	-10.71
BAM(Conf. II)	BR	-12.77 -12.11	1.75 1.73	-11.02 -10.38
BAM-II*	BR	-12.49	1.76	-10.73
1-2 Super-cell	BR	-11.98 -12.97	1.79 1.81	-10.19 -11.16
1-3 Super-cell	BR	-11.98 -12.97	1.79 1.81	-10.19 -11.16
b1 Super-cell	BR	-12.42	1.75	-10.67

E_M : Madelung Energy E_S : Short-range Energy E_t : Total Energy

*: β''' phase with extended spinel blocks

All of the BR site energies in BAM and barium-poor phase are similar, but the site energy varies for different barium-poor structures, which again supports the emission broadening effect of different oxygen distributions. The BR positions on the two different mirror planes of configuration II of BAM have different site energies; the difference is about 0.64eV in total site energy. The small change in their short-range energies is because of the large separation between the Mg position and the conduction plane; relaxation around Mg becomes small at that separation, but the charge effect is a

long-range effect. The site energy difference caused by the Mg-distribution can explain the round-shape of the emission band observed in BAM:Eu²⁺, instead of the sharp-shape.

Since the site energy of the BR position in the b1 super-cell is very close to that of the BR site in BAM, Eu²⁺ in the b1 structure will also show an emission band at around 440nm. The 0.02eV difference of E_t between BAM and BAM-II has shifted the emission band to 467nm.¹⁶ Therefore, it may be said that the 0.35eV difference between the barium-poor phase and BAM will shift the emission band even more in the same direction. Even between the three structures of the barium-poor phase, there is a 0.97eV site-energy difference: no wonder the emission band of the barium-poor phase will become much broader, in considering there are a total of 10 possible structures. Thus the multiple configurations of the barium-poor phase not only broaden the emission band, but also shift it.

It is interesting to see in Table VI.10 that trivalent europium ions in the Al(1) octahedral position will also emit light in the range of observed emission band, but at a wavelength higher than Eu²⁺. It is believed that Eu³⁺ may also contribute to the shape change of the emission band of the barium-poor phase, from the fact that a small amount of Eu³⁺ may occur during the manufacture, coupled with the possibility of Eu³⁺ migrating from mirror plane into the spinel blocks.

As shown above, the barium-poor phase when doped with europium, will have an emission band with a broader range than BAM:Eu²⁺. The variation of the site potential at Eu²⁺ positions will shift the chromaticity from blue to blue-green, similar to the phenomenon of the degradation of BAM:Eu²⁺.¹³ It implies that the degradation mechanism in BAM may include the formation of the barium-poor phase. The suggested formation of EuMgAl₁₁O₁₉ can not explain the shift in emission band. From Table VI.11, if EuMgAl₁₁O₁₉ is formed, the Eu³⁺ ion should emit at a wavelength of 170nm, which is not in the observed emission band. But the Eu³⁺ ion substituting for aluminum shows emission with the right wavelength, so the observed luminescence of Eu³⁺ in the degraded emission band should come from the europium at tetrahedral sites.

6.4 Ba₃Al₃₂O₅₁

6.4.1 Structure

To use an aluminum vacancy as the charge compensation mechanism for barium substituting for sodium, a $\sqrt{3} \times \sqrt{3}$ super-cell was constructed. There was one aluminum vacancy for every three barium ions substituted and then the super-cell must include $3n$ (n is an integer) barium ions in order to generate an integer number of Al vacancies in the super-cell. If one simply expands the primitive cell to a $1 \times 3 \times 1$ super-cell, the structure will lose many symmetry elements and make the defect investigation more complex. In Fig. 6.9, a new unit cell is drawn out of the array of primitive cells. The new unit cell keeps the same symmetry elements while the cell parameter a is $\sqrt{3}$ times that of the primitive cell. Totally six barium ions were in the unit cell with three of them on each mirror plane. Since the origin of the primitive cell was not the same as the new unit cell, the coordinates of ions had to be transformed to the new axes. Two matrix operations were applied to the coordinates:

$$\begin{pmatrix} x' \\ y' \\ z' \end{pmatrix} = \begin{pmatrix} x \\ y \\ z \end{pmatrix} - \begin{pmatrix} a \\ 0 \\ 0 \end{pmatrix} \quad (5)$$

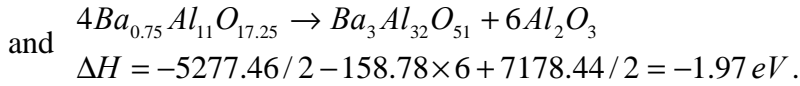
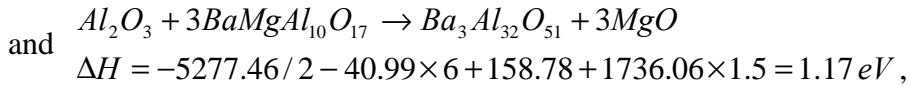
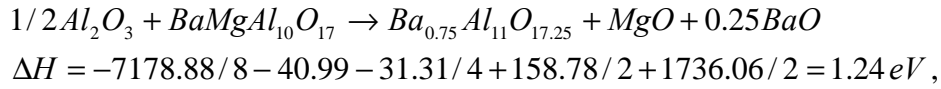
$$\text{and } \begin{pmatrix} x'' \\ y'' \\ z'' \end{pmatrix} = \begin{pmatrix} \cos 150 & \cos 60 & 0 \\ -\cos 60 & \cos 150 & 0 \\ 0 & 0 & 1 \end{pmatrix} \cdot \begin{pmatrix} x' \\ y' \\ z' \end{pmatrix}. \quad (6)$$

The positions of the V_{Al} are the next consideration after the transformation of the coordinates. Since there are six barium ions in the unit cell, two aluminum vacancies must exist in it. To achieve a lower lattice energy, i.e. a more stable structure, two aluminum ions in the same symmetry positions are taken out, so that the loss of symmetry will be minimized. The four symmetrically independent positions of aluminum in the β phase mean that four possible structures exist and their lattice energies are compared in Table VI.12.

Table VI.12. Lattice Energies of Four Possible Structures

Two V_{Al}	Al(1)	Al(2)	Al(3)	Al(4)
E_{latt} (eV)	-5273.82	-5270.12	-5270.53	-5277.46

The Al(4) ion is in the octahedral site of the mid-spinel block, separating two tetrahedral Al(2) ions. The introduction of an Al(4) vacancy made the structure collapse a little along the *c* axis and made the tetrahedra in the middle of the spinel blocks relax from their elongated state. The cell parameter *c* became 22.25 Å, 0.4 Å shorter than that of BAM (see Fig. 6.10). Up to now, three ways of transforming β-alumina to barium hexa-aluminate have been shown. Only BAM and barium-poor phases have been seen by experiments. The existence of the third phase, Ba₃Al₃₂O₅₁, is only a hypothesis. This third phase may be not very stable, might easily transform to other phases or it could be hard to distinguish from other phases. Here, we list the stability comparison of these phases:



Of the three phases, BAM is the most stable and Ba₃Al₃₂O₅₁ is the second most stable. It is interesting that alumina is required for BAM to transform to the other two phases and for Ba₃Al₃₂O₅₁ to transform to the barium-poor phase. It seems that a greater ratio of alumina in the structure will diminish the stability of BAM. It is surprising that the aluminum-vacancy phase is more stable than the barium-poor phase but has not been reported yet. It is generally believed that only two types of barium hexa-aluminates containing no ions other than Ba, Al and O, exist.^{17,18} They are the barium-poor phase (ideal formula of Ba_{0.75}Al₁₁O_{17.25}) and the barium-rich phase (ideal formula of Ba₇Al₆₄O₁₀₃).⁵ Since the aluminum-vacancy phase is more stable than the barium-poor phase, its stability is compared with the barium-rich phase as follows (the lattice energy of barium-rich phase is taken from Park's work¹¹):

$$7Ba_3Al_{32}O_{51} \rightarrow 3Ba_7Al_{64}O_{103} + 16Al_2O_3$$

$$\Delta H = 5277.46 \times 3.5 - 5303.74 \times 3 - 158.78 \times 16 = 19.41 eV.$$

It seems that the hypothetical new phase is also more stable than the barium-rich phase so if the new phase is formed it will not transform to either barium-poor or barium-rich phases. Whether or not this phase exist requires further experimental investigations.

6.4.2 Defect Properties

Routinely, all of the intrinsic and extrinsic defects were investigated and the results are shown in Table VI.13. Within four symmetrically independent aluminum positions, the Al(4) vacancy was easy to form compared to other positions, while the Al interstitial ions also tried to occupy the existing Al(4) vacancy in this defect lattice. In $Ba_3Al_{32}O_{51}$, one third of Al(4) positions were left empty so an Al interstitial at the empty Al(4) would decrease the number of defects in the structure and benefit the system stability. It seems that an existing Al(4) vacancy will not prevent other Al(4) vacancies from occurring nearby. An oxygen interstitial ion can reside in the mOB site and form a two-bridge structure as in BAM, but the defect energy (-13.82eV) is higher than if it resides close to the Al(2) ion inside the spinel block that is also the position for the oxygen interstitial in the barium-poor phase. As for the other phases, the barium Frenkel defect is the predominant thermal defect in the crystal.

Table VI.13. Point Defect in $Ba_3Al_{32}O_{51}$

Defect	Defect Energy (eV)	Defect	Defect Energy (eV)
V_{Ba}''	17.37	$Al_i^{*\bullet\bullet}$	-49.37
$V_{Al(1)}'''$	57.41	$Ba_i^{\bullet\bullet}$	-12.07
$V_{Al(2)}'''$	60.86	O_i''	-15.69
$V_{Al(3)}'''$	58.45	Schottky	4.73
$V_{Al(4)}'''$	56.57	Al Frenkel	3.6
$V_{O(1)}^{\bullet\bullet}$	23.25	Ba Frenkel	2.65
$V_{O(2)}^{\bullet\bullet}$	24.97	O Frenkel	3.76
$V_{O(3)}^{\bullet\bullet}$	26.31		
$V_{O(4)}^{\bullet\bullet}$	23.20		
$V_{O(5)}^{\bullet\bullet}$	23.87		

Table VI.14. Europium Point Defects

Defect	Energy (eV)	Position
Eu_{Ba}	-1.48	BR site
Eu'_{Al}	39.57	Al(3)
$Eu_i^{\bullet\bullet}$	-13.68	anti-BR site
Eu_{Ba}^{\bullet}	-22.51	BR site
Eu_{Al}	14.84	Al(3)
$Eu_i^{\bullet\bullet\bullet}$	-32.88	anti-BR site

As can be seen from Table VI.14, both divalent and trivalent europium defects shared the same locations. In this structure, the large europium ion tended to reside in the anti-BR sites in the mirror plane (which has more open space) than in the spinel block as an interstitial ion. It is surprising to see that the interstitial ions did not take the vacant Al(4) positions. The reason is that the structure had collapsed a little when the structure with the Al(4) vacancy was relaxed. Although there is still a vacancy there, its size is not large enough for europium and the surroundings can not fully relax so the defect energy is higher.

From the reaction enthalpies for the europium doping process, the most energetically favorable processes were for divalent europium ions substituting for barium and for trivalent ions substituting for aluminum. Actually, the defect reactions with the lowest enthalpy are the same for BAM, the barium-poor phase, and $Ba_3Al_{32}O_{51}$, with the only difference being the position of aluminum ion. In BAM, it is the Al(2) site being substituted, in $Ba_3Al_{32}O_{51}$ and barium-poor phase it is the Al(3) site. In total, three positions for europium ions have been found: one for divalent ions and two for trivalent ions.

Table VI.15. Defect Reaction of Eu in $Ba_3Al_{32}O_{51}$

Defect Reaction	Enthalpy (eV)
$EuO \rightarrow Eu_i^{\bullet\bullet} + O_i''$	3.83
$EuO \rightarrow 1/2Al_2O_3 + Eu'_{Al} + 1/2V_O^{\bullet\bullet}$	4.98
$EuO \rightarrow BaO + Eu_{Ba}$	0.41
$1/2Eu_2O_3 \rightarrow Eu_i^{\bullet\bullet\bullet} + 3/2O_i''$	9.03
$1/2Eu_2O_3 \rightarrow Eu_{Al} + 1/2Al_2O_3$	0.89
$1/2Eu_2O_3 \rightarrow Eu_{Ba}^{\bullet} + BaO + 1/2O_i''$	3.78

6.5 Conclusions

The barium-poor phase has no unique structure; instead, many kinds of O_{BR} distribution in the mirror plane will coexist in the material. The oxygen ions in the mirror plane are stabilized by forming Reidinger defects. Lattice energies of these configurations vary only slightly. Basically, the defect properties of the barium-poor phase are similar to BAM, with some exceptions. Eu^{3+} ion tends to occupy the Al(3) sites or the aluminum position in a Reidinger defect, rather than the Al(2) inside the spinel block, because of the effective negative charge on the mirror plane with oxygen interstitials. The barium-poor phase has lattice parameters very close to BAM and they can form solid solutions in any component ratio.

Another possible structure, with V_{Al} as the charge compensation mechanism, was also tested. It shows defect properties similar to BAM and a higher stability than the barium-poor and barium-rich phases. The existence of this phase needs further investigation.

The observed broad emission band of $Ba_{0.75}Al_{11}O_{17.25}:Eu^{2+}$ results from the multiple configurations of the barium-poor phase. The distribution of O_{BR} changes the ligand field acting on the ion in the BR position and hence the emission band of the active ion at that position. Since Eu^{2+} ions seem to only reside in the BR position, the emission band will vary for Eu^{2+} ions in BR positions and the total emission band of the material will become broadened and shifted. The second band suggested by Smet² does not come from the Eu^{2+} inside the spinel block. It is just due to the different ligand field effect of multiple configurations. Possibly, it could also come from Eu^{3+} ions in the tetrahedral sites.

The probability of intergrowth of the barium-poor phase and BAM will deteriorate the luminescent property, even without oxidation. As shown in the phase reaction, excess alumina is needed for the barium-poor phase to form. So control of the alumina component may help to control the degradation. Eu^{3+} ions initially formed at the BR site can migrate into aluminum position in the spinel blocks and this will also shift the emission band. Since we have shown that Mg is needed in this migration, the replacement of Mg with other divalent cations in BAM may also prevent Eu^{3+} ions from entering the spinel block and limiting the emission band shift.

References

1. S. Tanaka, I. Ozaki, T. Kunimoto, K. Ohmi, and H. Kobayashi, "Blue Emitting $\text{CaAl}_2\text{O}_4:\text{Eu}^{2+}$ Phosphors for PDP Application," *J. Lumin.*, **87-89**[1] 1250-3 (2000).
2. C.R. Ronda and B.M.J. Smets, "Chemical Composition of and Eu^{2+} Luminescence in the Barium Hexa-aluminates," *J. Electrochem. Soc.*, **136**[2] 570-3 (1989).
3. B.G. Dick and A.W. Overhauser, "Theory of the Dielectric Constants of Alkali Halide Crystals," *Phys. Rev.*, **112**[1] 90-103 (1958).
4. J.G. Park and A.N. Cormack, "Potential Models for Multicomponent Oxides: Hexa-Aluminates," *Philos. Mag.*, **73**[1] 21-31 (1996).
5. J.G. Park and A.N. Cormack, "Crystal/Defect Structures and Phase Stability in Ba Hexa-aluminates," *J. Solid State Chem.*, **121**[1] 278-90 (1996).
6. G.V. Lewis and C.R.A. Catlow, "Potential Models for Ionic Oxides," *J. Phys. C: Solid State Phys.*, **18**[6] 1149-61 (1985).
7. T.B. Forester and W. Smith, *DL_POLY Reference Manual*, 2.0 ed.; pp. 45-7. CCLRC, Daresbury Laboratory, Warrington, England, 1995.
8. C.R.A. Catlow, A.N. Cormack, and F. Theobald, "Structure Prediction of Transition-Metal Oxides using Energy-Minimization Techniques," *Acta Crystallogr., Sect. B: Struct. Sci.*, **B40**[3] 195-200 (1984).
9. A.N. Cormack, "A Perfect Lattice Approach to Nonstoichiometry," *Solid State Ionics*, **8**[1] 187-92 (1983).
10. N.F. Mott and M.J. Littleton, "Conduction in Polar Crystals. I. Electrolytic Conduction in Solid Salts," *Trans. Faraday Soc.*, **34**[1] 485-99 (1938).
11. J.G. Park, "Structure, Stoichiometry and Stability in Magnetoplumbite and β -Alumina Type Ceramics"; Ph.D. Thesis, Alfred University, Alfred, New York, 1995.
12. W.L. Roth, F. Reidinger, and S.L. Placa, "Studies of Stabilization of Transport Mechanisms in Beta and Beta" Alumina by Neutron Diffraction," pp. 223-41 in *Superionic Conductors*. Edited by G. D. Mahan and W. L. Roth. Plenum, New York, 1976.

13. K. Yokota, S. X. Zhang, K. Kimura, and A. Sakamoto, "Eu²⁺-Activated Barium Magnesium Aluminate Phosphor for Plasma Displays - Phase Relation and Mechanism of Thermal Degradation," *J. Lumin.*, **92**[3] 223-7 (2001).
14. L.G.V. Uitert, "An Empirical Relation Fitting the Position in Energy of the Lower d-Band Edge for Eu²⁺ or Ce³⁺ in Various Compounds," *J. Lumin.*, **29**[1] 1-9 (1984).
15. C.K. Jorgensen, "Partly Filled Shells Constituting Anti-bonding Orbitals with Higher Ionization Energy Than Their Bonding Counterparts," pp. 49-82 in *Structure and Bonding*. Edited by J. D. Dunitz, P. Hemmerich, R. H. Holm, J. A. Ibers, C. K. Jorgensen, J. B. Neilands, D. Reinen, and R. J. P. Williams. Springer-Verlag, Berlin, Germany, 1975.
16. D. Ravichandran, S.T. Johnson, S. Erdei, R. Roy, and W.B. White, "Crystal Chemistry and Luminescence of the Eu²⁺-Activated Alkaline Earth Aluminate Phosphors," *Displays*, **19**[4] 197-203 (1999).
17. F.P.F. van Berkel, H.W. Zandbergen, G.C. Verschoor, and D.J.W. Ijdo, "The Structure of Barium Aluminate, Ba_{0.75}Al₁₁O_{17.25}," *Acta Crystallogr., Sect. C: Cryst. Struct. Commun.*, **C40**[7] 1124-7 (1984).
18. S. Kimura, E. Bannai, and I. Shindo, "Phase Relations Relevant to Hexagonal Barium Aluminates," *Mater. Res. Bull.*, **17**[2] 209-15 (1982).

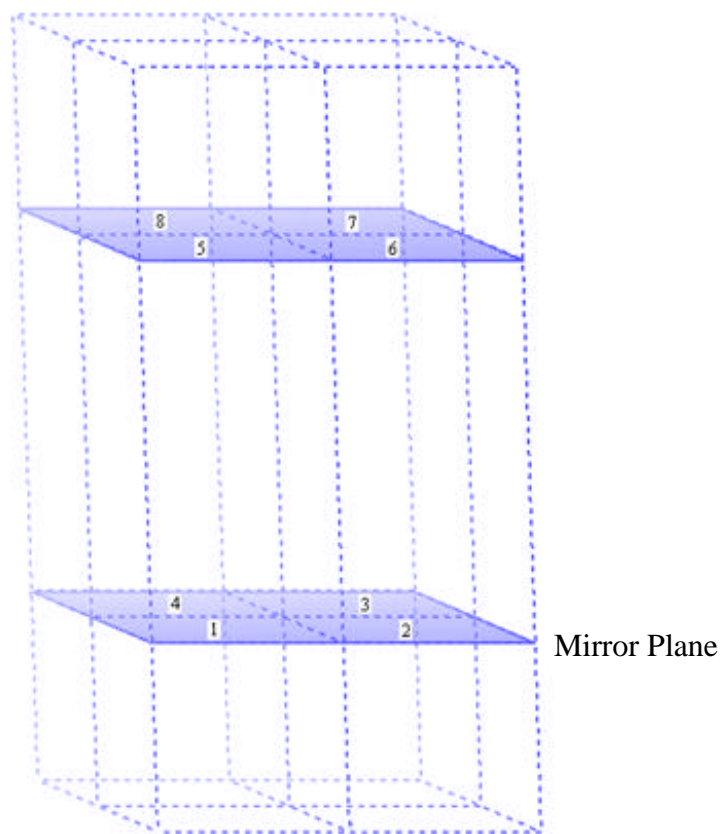


Figure 6.1. $\text{Ba}_6\text{Al}_8\text{O}_{13}$ super-cell.

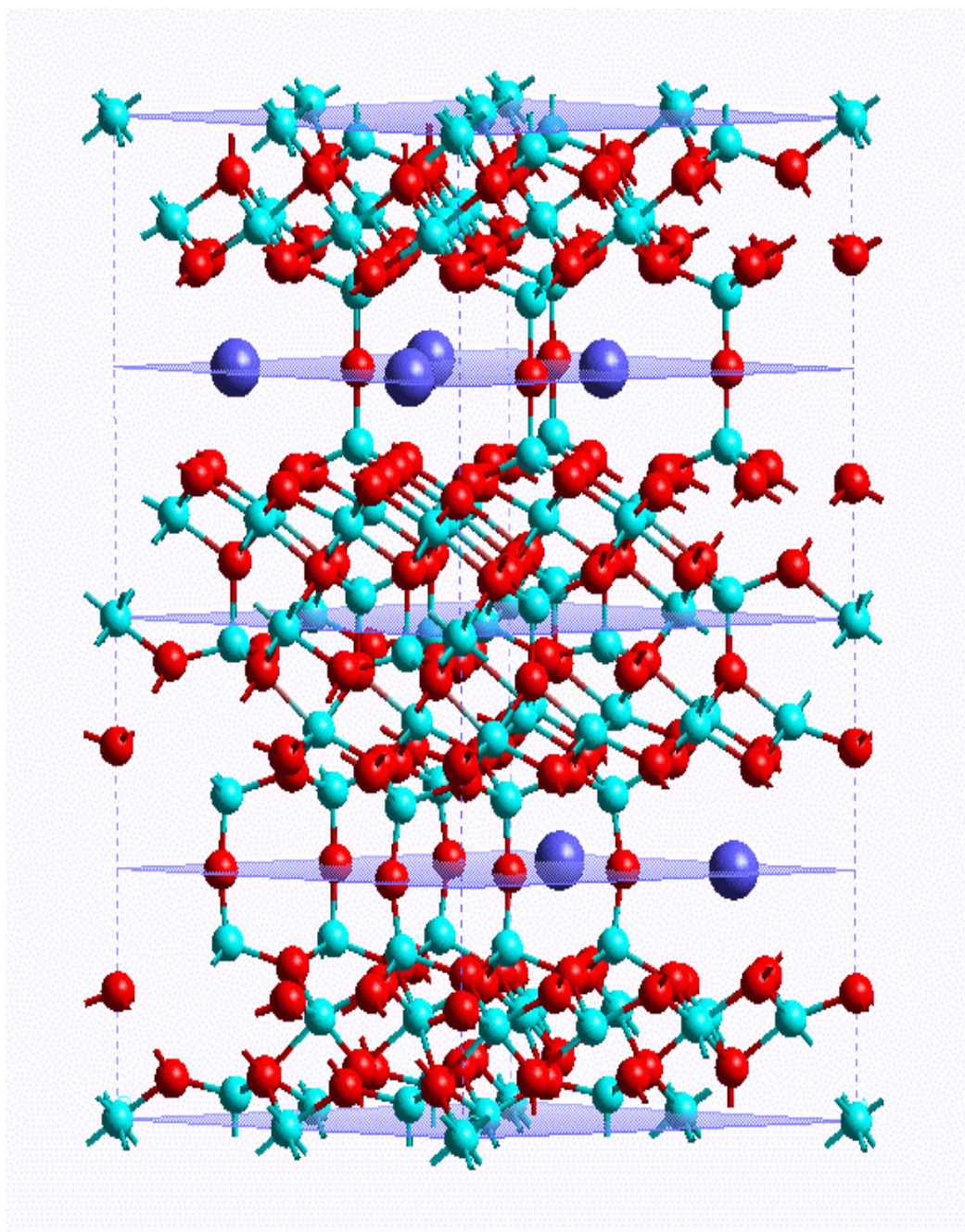


Figure 6.2. Structure of 1-2 super-cell of barium-poor phase.



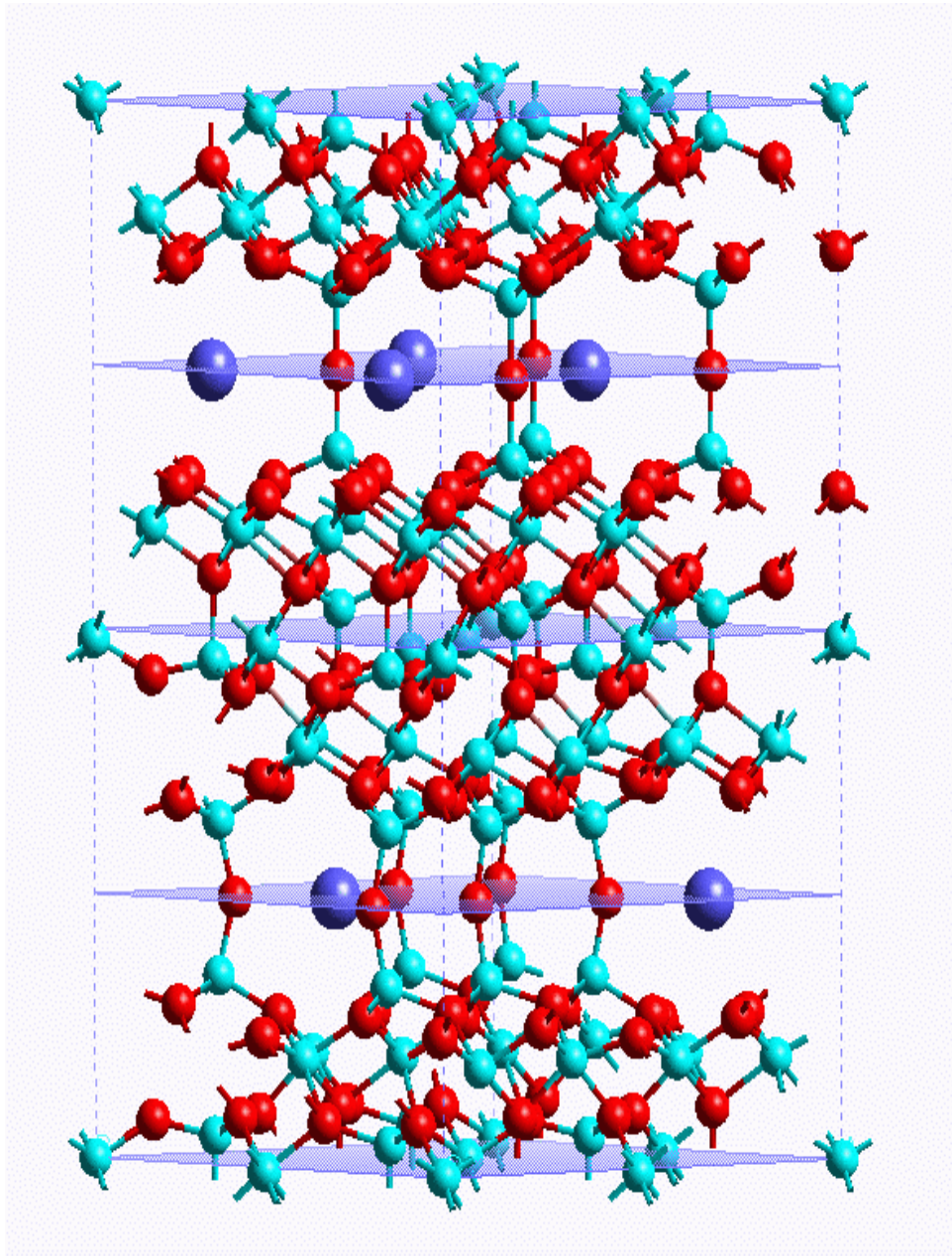


Figure 6.3. Structure of 1-3 super-cell of barium-poor phase.



Lattice Energy of Solid Solution between BAM and Barium Poor Phase

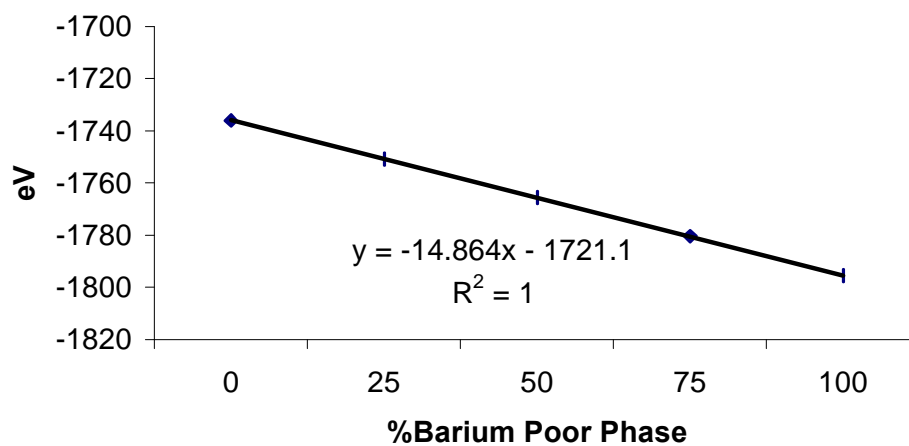


Figure 6.4. Lattice energy of solid solution between BAM and barium-poor phase.

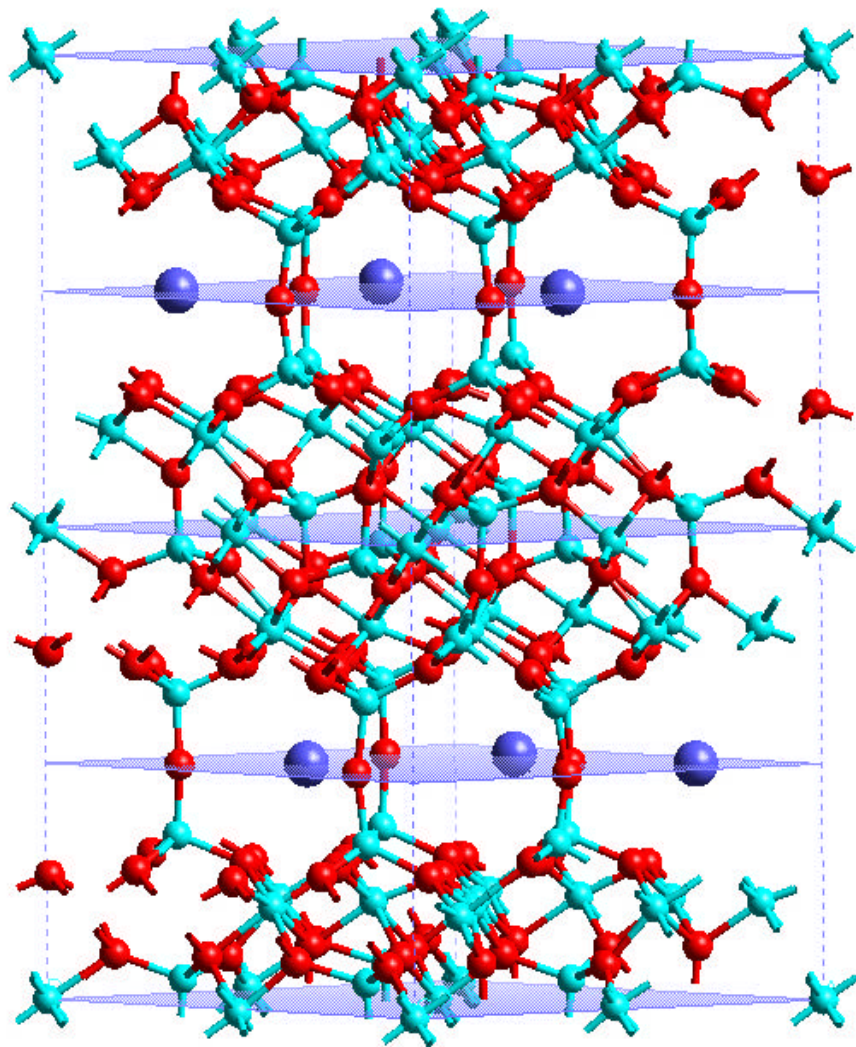


Figure 6.5. Crystal structure of b1 super-cell.



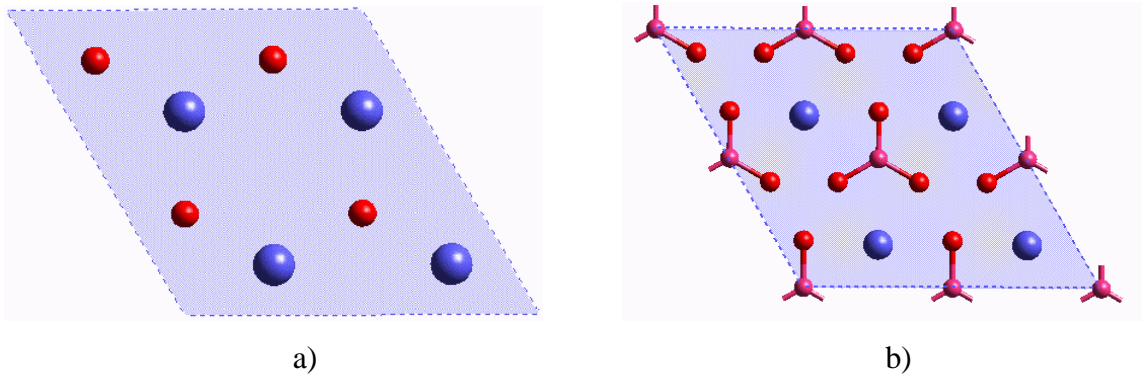


Figure 6.6. Mirror plane structures. a) BAM; b) magnetoplumbite.

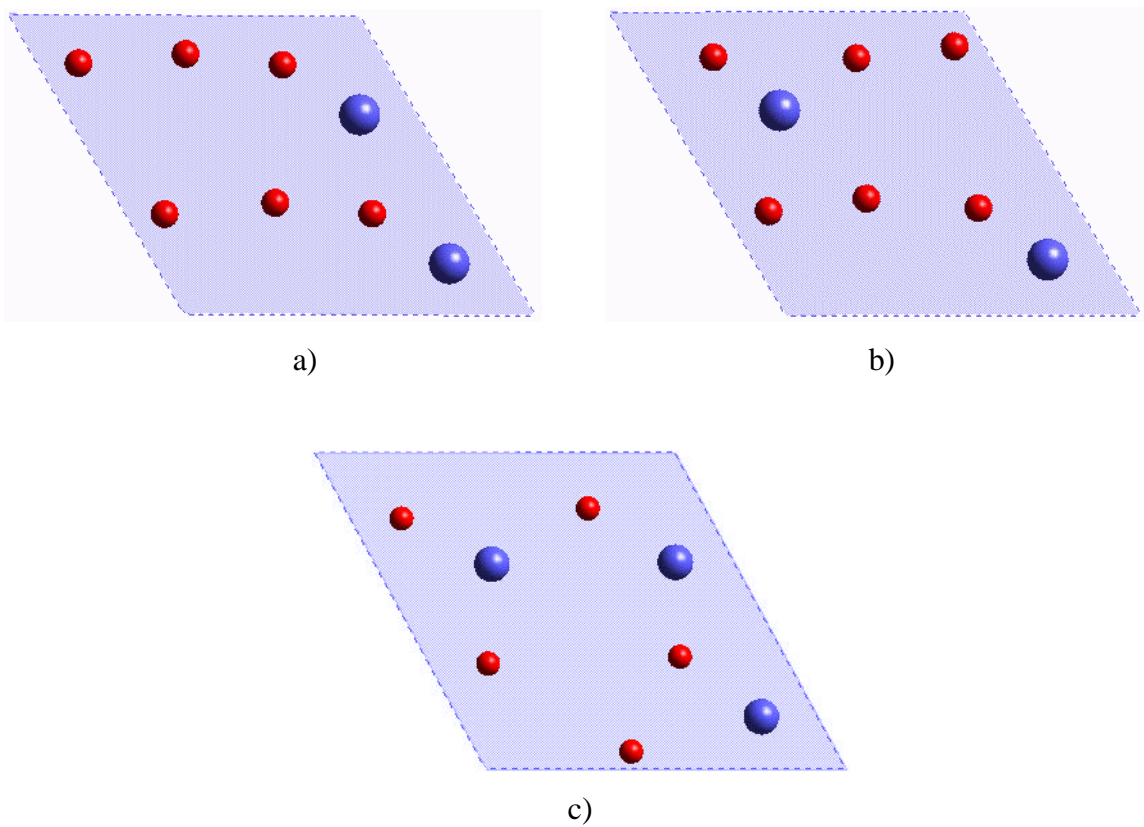
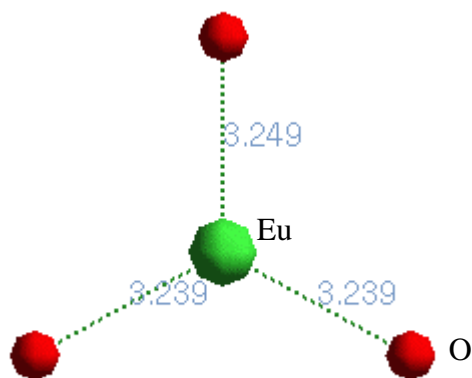
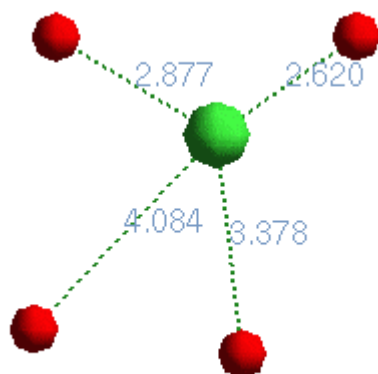


Figure 6.7. a) Mirror plane of 1-2 super-cell; b) Mirror plane of 1-3 super-cell; c) Mirror plane of b1 super-cell.





a)



b)

Figure 6.8. Eu^{2+} environment in mirror plane. a) Associated without O_{BR} ; b) Associated with O_{BR} .

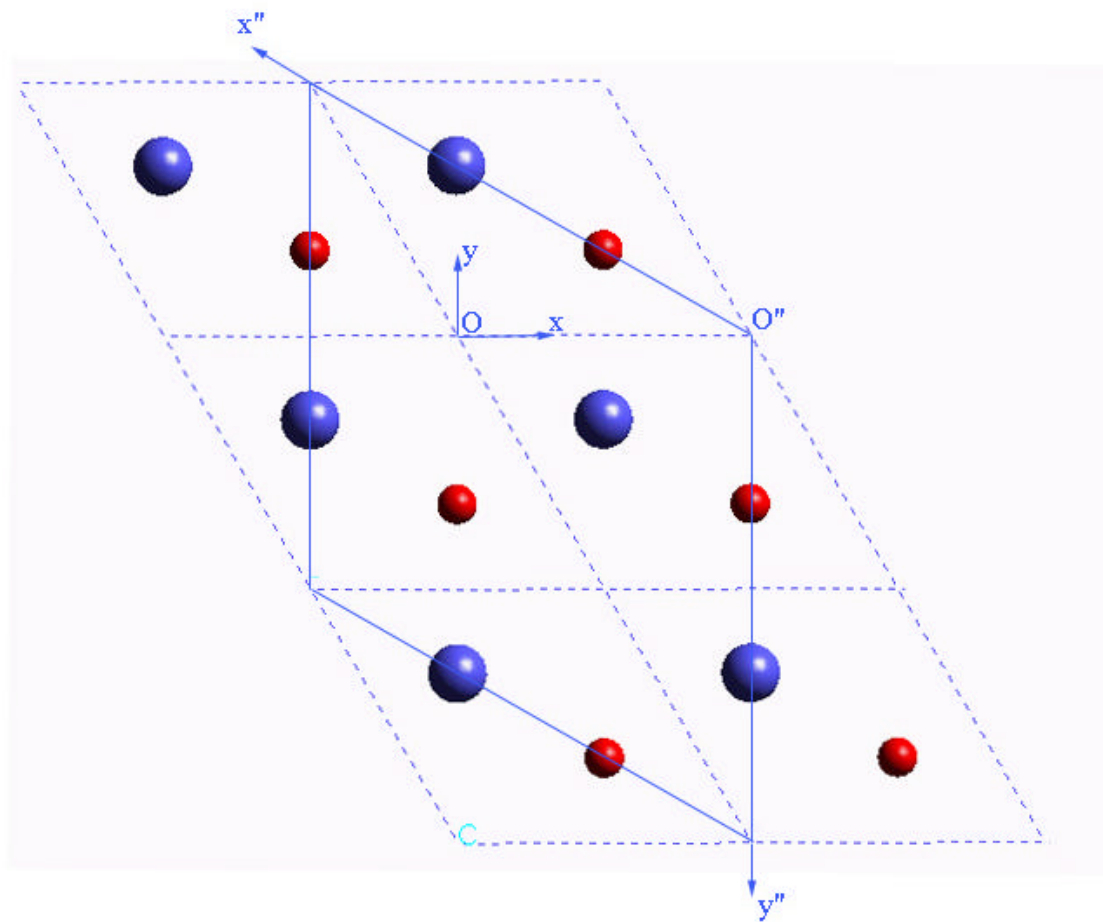


Figure 6.9. Selection of $\sqrt{3} \times \sqrt{3}$ super-cell.

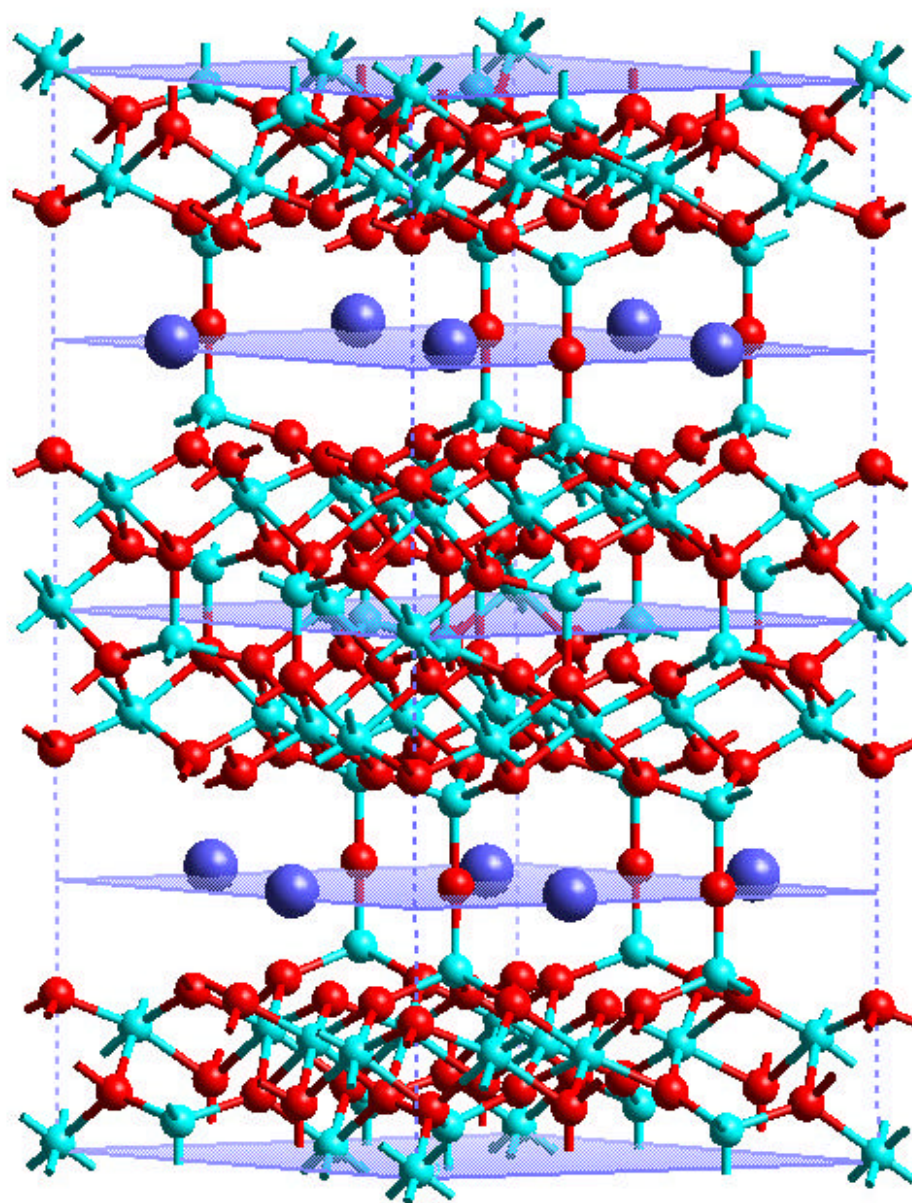


Figure 6.10. $\sqrt{3}\times\sqrt{3}$ unit cell of $\text{Ba}_3\text{Al}_{32}\text{O}_{51}$.



7. Defects in β'' - and β''' - Barium Hexa-aluminates

Abstract:

Lattice and defect properties of barium β'' - and β''' -alumina with structures closely related to $\text{BaMgAl}_{10}\text{O}_{17}$ (BAM, β phase of barium hexa-aluminate), a widely used phosphor host material, have been investigated with computer simulation. Many configurations of the crystal structure have been found to share similar lattice energies. Mg ions are found to distribute inside the structure homogeneously, which stabilizes the lattice more than other Mg distributions. Their intrinsic and Eu extrinsic defects have the same properties as BAM; in particular, Eu^{2+} and Eu^{3+} ions tend to occupy different lattice sites.

Although the β , β'' and β''' phases of barium aluminates doped with Mg have similar chemical formulae and structures, the differences change the emission band of Eu^{2+} ions, providing a possible explanation of the broad emission band observed in BAM:Eu^{2+} . The result also determines the stability order of the three phases. The adjustment of potential for ions in tetrahedral and octahedral sites shows no significant influence on the positions of the europium ion.

7.1 Introduction:

Barium hexa-aluminates are often used as host materials for phosphor applications. They can be doped with Sr, Y or Eu to produce different colors. $\text{BaMgAl}_{10}\text{O}_{17}$ (BAM): Eu^{2+} is widely used as a blue phosphor for lamps and display panels, with its luminescence at around 440nm. Another phase with the same chemical formula as BAM, $\text{Ba}_3\text{Mg}_3\text{Al}_{30}\text{O}_{51}$ (β'' phase), could possibly form during manufacture and exist in the BAM product. The structure of the β'' phase is more complex than BAM, for the unit cell is 50% larger. A barium β''' phase with chemical formula of $\text{BaMg}_3\text{Al}_{14}\text{O}_{25}$ is also being used as a commercial phosphor when doped with europium. Compared to $\text{BaMgAl}_{10}\text{O}_{17}$ (BAM), the emission band is shifted to 467nm.¹ The reason for the band shift will also be studied.

Computer simulations based on classical solid state theory have been proved to be a successful method in the defect studies of complex materials and are adopted in this study. In this paper, possible structures of the β'' and β''' phase are investigated. The intrinsic defects of the most stable structure will also be studied, since they provide compensation mechanisms for introducing europium ions into the structure. The behaviors of the europium ions are compared between the three phases.

7.1.1 Structural Details

β'' -alumina was first discovered by Yamaguchi and Suzuki in 1968 with the formula of $\text{Na}_2\text{O} \cdot 5\text{Al}_2\text{O}_3$.² Later it was found that the structure was metastable without additions of MgO or Li_2O . It was suggested that ions such as Mg and Li with valence less than that of aluminum would stabilize the structure. As in β -alumina, the double prime phase consists of spinel blocks of oxygen close-packed layers with Na-O planes in between the blocks. It can be considered as a rhombohedral variant of the β phase. The space group of the β'' phase is $R\bar{3}m$. Unlike the β phase, in which adjacent spinel blocks in the c direction are mirror images of each other across the Na-O plane, the spinel blocks in β'' -alumina are rotated 120° to the blocks immediately above and below it. So three spinel blocks are required in a primitive cell to generate periodicity and the Na-O plane is

no longer a mirror plane. The stacking order of the oxygen layers in the three spinel blocks are ABCA, CABC and BCAB. Aluminum ions occupy both tetrahedral and octahedral sites between the oxygen close-packed layers.

The number of sodium ions in the conduction plane is normally less than two and the resulting sodium vacancies make β'' -alumina a fast two-dimensional ionic conductor.³ Three positions exist in the conduction plane for cations, BR, anti-BR and mO. Actually, the BR and anti-BR sites in the β'' phase are the same which is not the case for the β phase. Both sites are in the center of an oxygen-tetrahedron, and the only difference is that the two tetrahedra are inverted with respect to each other (see Fig. 7.1). Two thirds of the A sites (between the anti-BR and mO sites), and nearly all the BR sites, are occupied by sodium. When barium is introduced into the structure, the BR and anti-BR positions will be occupied but not the mO position because of the size of barium. Barium ions should fully reside in one set of symmetric positions to maintain high symmetry. The excess charge of Ba_{Na}^{\bullet} can be compensated by a magnesium ion in the aluminum position with a charge of Mg_{Al}' . The chemical formula of the unit cell of barium β'' -alumina, investigated in this work, is $Ba_3Mg_3Al_{30}O_{51}$.

Barium β''' -alumina has the same space group as BAM but has a different size of spinel blocks. There are six oxygen layers in a spinel block in the β''' phase instead of the four in BAM. In a primitive cell of β''' phase, the total number of oxygen layers is the same as in the β'' phase but with one conduction plane less. Thus, the size of the primitive cell of the β''' phase is a little smaller than for the β'' phase. Whether or not the barium-oxygen plane in between the spinel blocks is a mirror plane depends on the Mg distribution, as with BAM. Since the spinel block is extended, there are two more oxygen positions and two more aluminum positions in the structure. However, the structure of the conduction plane is exactly the same as BAM.

7.1.2 Simulation Methodology

A Born model description of solid is used to describe the predominantly ionic materials in this study. This treats the solid as a collection of point ions with Coulombic and non-Coulombic forces acting between them. The approach has enjoyed a wide range

of success, but it has been found that simulation reliability depends on the validity of the potential model used in the calculations. The non-Coulombic potentials are usually described by a simple analytical Buckingham function,

$$V_{ij}(r_{ij}) = A_{ij} \exp(-r_{ij} / r_{ij}) - C_{ij} r_{ij}^{-6} \quad (1)$$

where r_{ij} is the distance between the ions i and j . The long-range potential is just the normal Coulombic interaction with the form of $z_i z_j / r_{ij}$.

The polarizability of individual ions is simulated through the shell model originally developed by Dick and Overhauser, in which the outer valence electron cloud of the ion is simulated by a massless shell of charge Y and the nucleus and inner electrons by a core of charge X .⁴ The total charge of the ion is $X+Y$, equal to the oxidation state of the ion. The interaction between core and shell of any ion is harmonic with a spring constant k , and is given by

$$V_i(r_i) = \frac{1}{2} k_i d_i^2 \quad (2)$$

where d_i is the relative displacement of core and shell of ion i .

For the shell model, the value of the free-ion electronic polarizability is given by

$$a_i = Y_i^2 / k_i. \quad (3)$$

The potential parameters A , r , and C in Eq. [1], the shell charges Y , spring constant k associated with the shell-model description of polarizability, need to be determined for each interaction and ion type in the crystal from experimental data. In the present study, they were taken from our earlier studies of hexa-aluminates following the original compilation of Lewis and Catlow as shown in Table VII.1.⁵⁻⁷

Table VII.1. Potential Parameters Derived by Lewis and Catlow

Interaction	A (eV)	ρ (Å)	C (eV·Å ⁶)
Al(o) – O	1474.40	0.30059	0
Al(t) – O	1334.31	0.30059	0
Ba – O	931.70	0.39490	0
Mg – O	710.50	0.32420	0
O – O	22764.2	0.1491	17.89
Eu(2+) – O	665.20	0.39490	0
Eu(3+) – O	1358.0	0.35560	0

Interaction	Shell charge	K
Ba (core) – Ba (shell)	1.46	14.78
O(core) – O(shell)	-2.207	27.29

7.1.3 Lattice Energy Calculations

The lattice energy is the binding or cohesive energy of the perfect crystal and is usually defined as the energy that must be released to separate its component ions into free ions at rest at infinite separation. It is calculated by the relation:

$$U = 1/2 \sum \sum V_{ij} . \quad (4)$$

The interatomic potential, V_{ij} include both the long-range Coulombic interactions and the short-term potential described above. The lattice energy is minimized through a second derivative Newton-like procedure, coded into METAPOCS.⁸ Details of the procedure have been outlined by Cormack.⁹

In the present work, this perfect lattice approach has been used to establish equilibrated crystal structures for barium β'' - and β''' -alumina, using the previously published potential.⁵ The idea is that equilibrated crystal must have the lowest lattice energy among all possible structures.

7.1.4 Defect Energy Calculations

Calculations of defect structures and energies introduce one vital feature in addition to those for the perfect lattice methods, i.e. relaxation of lattice atoms around the defect species. This effect is large because the defect generally imparts an extensive

perturbation to the surrounding lattice, and, in the case of ionic crystals, the relaxation field is long-range as the perturbation is mainly Coulombic in origin.

The defect calculation is based on the Mott-Littleton theory, which allows one to calculate the defect-induced static polarization of a dielectric continuum.¹⁰ The basic approach is to contain, within the dielectric continuum, a region, immediately surrounding the defect, which is treated atomistically within the framework of the Born model described above. In this region, the forces and resulting atom displacements are too large to be treated properly by continuum theory, which can, nevertheless, be used to model the more distant parts of the crystal. A program, named CASCADE coded this approach, was used to calculate the defect energy in this study.

7.2 Equilibrated Structures

7.2.1 Barium β'' -Alumina

The ambiguity from the β'' structure is the magnesium distribution in the unit cell, as in the BAM structure. As in BAM, Mg ions also occupy the tetrahedral Al(2) position in the β'' structure. Because there are three spinel blocks now in one primitive cell, there is a total of six Al(2) positions available for three Mg ions. The number of possible configuration is $C_6^3 = 20$. The structure prototype used for barium β'' -alumina is the structure of $\text{Na}_2\text{O}\cdot\text{MgO}\cdot 5\text{Al}_2\text{O}_3$ determined by Betterman and Peters.³ Sodium is substituted for barium in a ratio of 2:1 with barium in the BR position but not the mO position. Additionally, barium is not located at BR and anti-BR sites at the same time to keep the symmetry higher. Six Al(2) sites are labeled from 0 to 5 in the ascending order of their z coordinates. The 20 types of Mg distribution are listed in Table VII.2 along with the lattice energies.

Table VII.2. Lattice Energy of Barium β'' -Alumina

Configuration	012	013	023	014	024
Lattice Energy (eV)	-2599.39	-2602.93	-2603.02	-2602.02	-2603.17
Configuration	034	015	025	035	045
Lattice Energy (eV)	-2599.72	-2599.12	-2599.72	-2599.78	-2599.39
Configuration	123	124	134	125	135
Lattice Energy (eV)	-2599.12	-2599.72	-2600.78	-2599.78	-2602.91
Configuration	145	234	235	245	345
Lattice Energy (eV)	-2602.93	-2599.42	-2602.93	-2603.02	-2599.12

The three digits in the “configuration” row refer to the labels of Al(2) positions occupied by Mg. It seems that magnesium ions tend to separate from each other as far as possible. The 024 configuration seemed to have the lowest lattice energy of -2603.17eV because it kept the symmetry of the three-fold screw axis and all Mg ions were distributed homogeneously in the structure (see Fig. 2). At first glance, it seems that the 135 configuration should have the same lattice energy as the 024 configuration. Actually they are different because they have changed the environment of barium ions differently; however, the 0.22eV difference of lattice energy is small. Consider the 0 and 1 positions of Al(2); if Mg is at the 0 site, the ion arrangement from Mg to Ba between the 0 and 1 positions is Mg-O_C-Al-O_A-Ba, but the arrangement becomes Mg-O_A-Al-O_C-Ba if Mg is at the 1 site, because adjacent spinel blocks are rotated 120° to each other. So the 024 and 135 configurations are definitely different from each other.

From Table VII.2, it is easy to notice that many configurations have a lattice energy close to the 024 configuration, which means that the barium β'' -alumina will have no unique structure but has many possible configurations as does the barium-poor phase. A diffraction study will find an average overall these possible structures.

7.2.2 Barium β''' -Alumina

Because of the similarity between β and β''' , Mg ions are likely to reside only in tetrahedral sites inside the spinel blocks and not in the tetrahedral sites at the edge. There are eight such positions and six magnesium ions. It is much easier to consider the

distribution in another way: two aluminum ions distributed in these 8 positions. If the distributions of same symmetry are removed, only 12 possible distributions exist. There are several structures having very close lattice energies and they may exist simultaneously as shown in Table VII.3. This kind of multiple configuration phenomenon has been observed in nearly all barium hexa-aluminates and is the result of the defects included in the structures, i.e. the same symmetry positions occupied by different kinds of ions. Only the structure with the lowest lattice energy was tested for defect properties in which two Al ions at tetrahedral sites are in different spinel blocks distributed homogeneously in a way similar to the Mg distribution in configuration I of BAM (see Fig. 3). The mirror symmetry of the conduction plane is broken by the Mg distribution but the two-fold screw axis is kept.

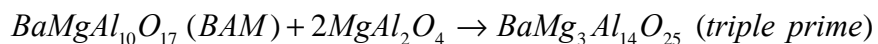
Table VII.3. Lattice Energy of Barium β''' -Alumina

Structure	Lattice Energy (eV)	Structure	Lattice Energy (eV)
b3_1	-2538.12	b3_7	-2538.01
b3_2	-2537.85	b3_8	-2537.48
b3_3	-2538.01	b3_9	-2537.85
b3_4	-2538.57	b3_10	-2535.04
b3_5	-2537.48	b3_11	-2535.26
b3_6	-2537.55	b3_12	-2536.64

Because the stacking order has changed from A-A across the conduction plan in BAM to B-B and C-C in the triple prime phase, the BR site has changed from the 2(d) lattice position to 2(b). Thus the two barium ions in a primitive cell have the same x-y coordinates in the two conduction planes of a primitive cell of the triple prime phase.¹¹ The phase stability is compared below:



$$\Delta H = -2603.17/3 + 1736.06/2 = 0.31eV$$



$$\Delta H = -2538.57/2 + 1736.06/2 + 200.71 \times 2 = 0.17eV.$$

Although their chemical formulae are the same, the BAM structure is more stable than the β'' phase, which also can be seen from the fact that β'' -alumina is metastable without Mg or Li, while β -alumina can exist as its own. The stability of the β''' phase is actually higher than the β'' phase but lower than BAM. Since the difference in reaction enthalpy is not very large, the β'' & β''' phases may intergrow with BAM structure, but β''' phase normally will not exist in the manufactured BAM material, because more magnesia and alumina are needed. The high stability of the BAM phase is the reason it is widely used as the phosphor host material instead of the other phases.

7.3 Intrinsic Defects

Intrinsic defect calculations include the calculation of single point defects such as vacancies and interstitials. It is easy to model the vacancy point defects since there are only four aluminum, five oxygen, one magnesium and one barium position for the 024 configuration of the β'' phase. Only one ion of each ionic class mentioned above needs to be calculated because all ions in the same symmetry class should have the same defect energy. For other configurations that have changed the symmetry group of the structure there should be other sets of symmetry positions. But it is always a good idea to calculate the vacancies of all ions in the unit cell because this guarantees that nothing has been overlooked.

The positions of the interstitial point defects are more complex. In a unit cell, there are positions having more than one symmetry operation and positions having only one point symmetry operation (1-fold rotation). Of course, the former positions must be tested as possible interstitial sites. Some of the other positions may also be possible interstitial sites. In this work, a limitation has been applied to all the possible interstitial sites, which is that the size of the interstitial site must be larger than a given threshold. If the size is small, the introduction of an ion into that position requires larger relaxation, which will increase the defect energy and destabilize the defect. A program was designed to scan all of the possible interstitial positions automatically. The size of a position is defined as the shortest distance between this position and all its neighboring ions. The size threshold was adjusted so that most of the available interstitial positions

were chosen, normally the number of the selected positions was in the range of 100 to 400 depending on the size of the unit cell. All of the special positions need to be considered, but one must check the positions selected by the program to make sure that the special positions are included, by looking at the plot of selected interstitial positions in a unit cell. In this way, all of the positions with only one symmetry operation should have been chosen if their sizes are larger than the threshold.

7.3.1 Intrinsic Defects of Barium β'' -Alumina

Table VII.4 lists the positions and energies of vacancy and interstitial defects. The energies listed are the lowest ones for the defect class. For example, aluminum interstitials can reside at the anti-BR site or in the middle of the spinel block or in many other positions; however, the energy to reside in the middle of the spinel block was the lowest of all. Then this energy was described as the interstitial defect energy of aluminum and the mid-spinel block position was described as the interstitial position of aluminum. The aluminum vacancy tended to occur at the Al(1) position, similar to the configuration II of the BAM structure. The problem is that the 024 configuration seems to be more similar to the configuration I of BAM structure, because they both have lost the mirror symmetry at the barium-oxygen plane whereas configuration II keeps it. It seems that the change from the two-fold screw axis of BAM to the three-fold screw axis of the β'' phase does change the defect properties, although the changes may be small.

The oxygen vacancy occurred at the O(1) position and oxygen interstitial resided at the Al(1) site exactly as in configuration I of BAM. The Reidinger defect is not energetically favorable in the β'' phase which has no mirror symmetry across the barium-oxygen plane. The larger interstitial ions, Ba and Mg, will stay in the anti-BR positions which are associated with more open space. Aluminum entered into the three cation-layers in the middle of spinel block. It can be said that the properties of the intrinsic point defects are almost the same for both BAM and the β'' phase, which is not really a surprise if one takes account of the same chemical formula and their closely related structures. As was found for BAM, the thermally predominant defect in barium β'' -alumina was the Ba Frenkel defect.

Table VII.4. Defect Energy of Barium β'' -Alumina

Point Defect	Defect Energy (eV)	Point Defect	Defect Energy (eV)
V_{Ba}''	16.64	$V_{O(3)}''$	24.90
V_{Mg}''	29.34	$V_{O(4)}''$	24.60
$V_{Al(1)}'''$	56.94	$V_{O(5)}''$	25.06
$V_{Al(2)}'''$	58.68	Ba_i''	-11.81
$V_{Al(3)}'''$	58.62	Mg_i''	-19.39
$V_{Al(4)}'''$	57.43	Al_i'''	-42.98
$V_{O(1)}''$	23.05	O_i''	-14.8
$V_{O(2)}''$	24.63		

Intrinsic Defect	Energy (eV)
Schottky	4.81
Al Frenkel	6.98
Ba Frenkel	2.42
Mg Frenkel	4.98
O Frenkel	4.13

7.3.2 Intrinsic Defects in Barium β''' -Alumina

Because the symmetry of the BR site has changed, the defect properties of β''' also changed. As shown in Table VII.5 the aluminum vacancy was still found to occur at the Al(2) sites in the so-called cation-rich region, where three layers of cations reside in between two close-packed oxygen layers. There are two cation-rich regions in each spinel block of the β''' phase instead of the one in BAM. The middle cation-layer is occupied by the Al(4) ion and the other two cation-layers are occupied by Mg ions or a mix of Mg and Al ions. Thus, there are two types of cation-rich region, with different effective charges caused by the Mg substitution: $[Mg-Al-Mg]^{2-}$ and $[Mg-Al-Al]^{1-}$. A Mg vacancy occurring in $[Mg-Al-Al]^{1-}$ was more energetically favorable than in the other position as a result of the local charge effect. The same effect caused the oxygen vacancy to occur close to the other cation-rich region with the more negative local charge.

Table VII.5. Defect Energies of Barium β''' -Alumina

Point Defect	Defect Energy (eV)	Point Defect	Defect Energy (eV)
V_{Ba}''	16.88	$V_{O(3)}^{\bullet\bullet}$	23.93
V_{Mg}''	27.62	$V_{O(4)}^{\bullet\bullet}$	24.58
$V_{Al(1)}'''$	55.57	$V_{O(5)}^{\bullet\bullet}$	23.80
$V_{Al(2)}'''$	54.83	$V_{O(6)}^{\bullet\bullet}$	22.65
$V_{Al(3)}'''$	-	$V_{O(7)}^{\bullet\bullet}$	25.48
$V_{Al(4)}'''$	58.40	$Ba_i^{\bullet\bullet}$	-11.19
$V_{Al(5)}'''$	-	$Mg_i^{\bullet\bullet}$	-18.53
$V_{Al(6)}'''$	55.70	$Al_i^{\bullet\bullet\bullet}$	-44.21
$V_{O(1)}^{\bullet\bullet}$	24.53	O_i''	-15.91
$V_{O(2)}^{\bullet\bullet}$	22.62		

Intrinsic Defect	Energy (eV)
Schottky	3.80
Al Frenkel	5.31
Ba Frenkel	2.85
Mg Frenkel	4.55
O Frenkel	4.13

Large cations, Mg and Ba, as interstitial ions, occupied the anti-BR position in the conduction plane. The small Al ion stayed inside the spinel block. As in BAM, the aluminum interstitial resided in the octahedral site of the cation-rich region, where oxygen layers were not strictly close-packed. The oxygen interstitial appeared in the Al(1) layer close to a vacant octahedral site. Because the mirror symmetry across the barium-oxygen plane has been destroyed and because of the size of the large barium ion, the oxygen interstitial can not be stabilized by forming a Reidinger defect that is mirror symmetric about the conduction plane. Actually, the calculated intrinsic defect properties are exactly the same for the structure I of BAM, which is not surprising since their structures are very similar, in addition to the similarity of the Mg distribution.

7.4 Extrinsic Defects: Europium

It has been shown above that the properties of intrinsic defects in BAM and the β'' phase are similar to each other except for the aluminum vacancy position. The β''' phase also has the same defect properties as BAM. As these phases may coexist in BAM material, it may also be possible for europium to be found in the β'' and β''' phases after the doping. The properties of europium-related defects have been calculated to investigate the influence of the existence of these phases in the BAM:Eu²⁺ material. Like the intrinsic defects calculation, the single point defects associated with europium were calculated first. They include the europium interstitial and substitution of cations.

Both the divalent and trivalent europium ions in the double and triple prime phases have the same locations for the single point defects as in the BAM structure. Since the size of europium is large, it is more stable for it to reside in the anti-BR site than in the spinel block as an interstitial ion. Table VII.6 shows the lowest defect energy of the point defects associated with europium, and their corresponding positions, but these by themselves do not tell which defect will occur or dominate. Thus, the formation energies of these defects are compared in Table VII.7 and Table VII.8.

The divalent europium ion would prefer to substitute for the barium ion in the conduction plane, because this requires less energy than other defect formation, and is consistent with what is believed.^{1,12} It is the Eu²⁺ ion in the BR site of BAM that emits the observed blue light at around 440nm. Since the coordination number at the BR site has changed from 9 in BAM to 7 in barium β'' -alumina (see Fig. 1c), the estimated emission wavelength changes from 490nm to 550nm, using the d-band edge calculation for Eu²⁺ ion as calculated in Chapter 6.^{13,14} Thus the formation of the β'' phase will shift the emission band. Since Eu²⁺ in the β''' phase shows an emission band at around 467nm from experiments, if it (the β''' phase) exists as a second phase in BAM, and contains Eu²⁺ ions, then a shift in the emission band would be expected.¹ Since the barium β phase is more stable than the β'' and β''' phases, most crystal grains in the material should be the β phase, and the band shift from the double and triple prime phases should be subtle. Other positions for the Eu²⁺ defect are not easy to find because their formation

energies are very large compared to Eu_{Ba} . Unlike the divalent ion, Eu^{3+} did not stay at the BR position, but tried to enter into the spinel block to substitute for the Al(2) ion.

Table VII.6. Point Defect of Europium in Barium β'' -Alumina

Defect	Defect Energy (eV)	Defect Positions
Eu_{Ba}	-1.44	BR
Eu_{Mg}	10.44	Al(2)
Eu'_{Al}	38.58	Al(2)
$Eu_i^{\bullet\bullet}$	-13.33	anti-BR
Eu_{Ba}^{\bullet}	-21.71	BR
Eu_{Mg}^{\bullet}	-13.55	Al(2)
Eu_{Al}	14.5	Al(2)
$Eu_i^{\bullet\bullet\bullet}$	-32.32	anti-BR

Table VII.7. Defect Formation Energies of Eu^{2+} in Barium β'' -Alumina

Defect Formation	Enthalpy (eV)
$EuO \rightarrow Eu_i^{\bullet\bullet} + O_i''$	5.07
$EuO \rightarrow Eu'_{Al} + Al_i^{\bullet\bullet\bullet} + O_i''$	14.0
$EuO \rightarrow 1/2Al_2O_3 + Eu'_{Al} + 1/2V_O^{\bullet\bullet}$	3.92
$EuO \rightarrow Eu_{Mg} + Mg_i^{\bullet\bullet} + O_i''$	9.45
$EuO \rightarrow MgO + Eu_{Mg}$	2.65
$EuO \rightarrow BaO + Eu_{Ba}$	0.45
$EuO \rightarrow Eu_i^{\bullet\bullet} + V_{Ba}'' + BaO$	5.20

Table VII.8. Defect Formation Energies of Eu^{3+} in Barium β'' -Alumina

Defect Formation	Enthalpy (eV)
$1/2Eu_2O_3 \rightarrow Eu_i^{\bullet\bullet\bullet} + 3/2O_i''$	10.92
$1/2Eu_2O_3 \rightarrow Eu_{Al} + Al_i^{\bullet\bullet\bullet} + 3/2O_i''$	14.76
$1/2Eu_2O_3 \rightarrow Eu_{Al} + 1/2Al_2O_3$	0.55
$1/2Eu_2O_3 \rightarrow Eu_{Mg}^{\bullet} + MgO + 1/2O_i''$	3.5
$1/2Eu_2O_3 \rightarrow Eu_{Ba}^{\bullet} + BaO + 1/2O_i''$	5.02

7.5 Potential at Tetrahedral and Octahedral Sites

Since the radius of aluminum varies in different coordination conditions, the potentials for aluminum in tetrahedral and octahedral sites are different. However, since only one potential for europium has been used in these sites in the above calculations, the effect of the potential adjustment will be tested for Eu in the β'' phase. The reason to use a different potential for different conditions is to reflect the radius change of ions in those conditions.

For the Huggins-Mayer relationship,⁹

$$A = b \exp(r / r), \quad (5)$$

the difference between tetrahedral and octahedral positions in radius is

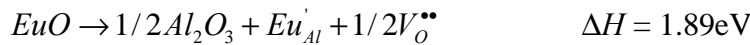
$$\Delta r = r_{oct} - r_{tet} \quad (6)$$

so that the pre-exponential term A of ion in tetrahedral site is given as

$$A_{tet} = A_{oct} \exp(-\Delta r / r) \quad (7)$$

Using Equation (7), the pre-exponential parameter of Eu^{3+} ions in the tetrahedral site is 1130.44eV with the estimation of $r_{tet} = 0.94r_{oct}$. The Eu^{3+} substitution for Al(2) ion was recalculated with the new tetrahedral potential. The defect energy reduced from 14.5eV to 11.82eV in the β'' phase. This means that the reaction enthalpy will become negative so that the Eu^{3+} ion in the Al(2) position will lower the total energy of the system. Overall the potential adjustment did not change the observed Eu defect behavior.

Consider the same thing for Eu^{2+} ion. The substitution defect energy at Al(2) changes from 38.58eV to 36.55eV. Rewrite the reaction for Eu^{2+} substitute for Al(2) as follows:



Although the formation energy is decreased, it is still four times the energy of substituting for barium, so the potential adjustment did not change the behavior of divalent europium defects either.

7.6 Conclusions

The defect properties of both barium β'' - and β''' -alumina are similar to those of $\text{BaMgAl}_{10}\text{O}_{17}$ (BAM). BAM has two possible configurations (different in their Mg

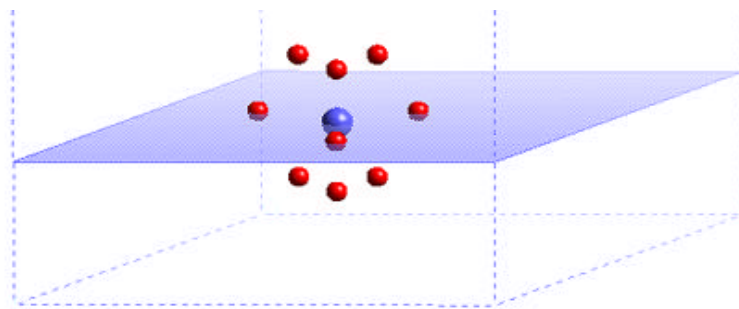
distribution) with the same lattice energy whereas the β'' and β''' phases have more than two such configurations, but also with similar lattice energies. The barium Frenkel defect is the predominant thermal defect of all compounds. Europium ion, the active ion of the phosphor, was found to substitute for the barium ion or the Al(2) ion depending on its valence state, as also found for BAM.

Although correcting the europium potential for tetrahedral condition did change the defect energies, the final results of the europium position did not change. Actually, the potential modification has the effect of enhancing the trend of Eu^{3+} substitution for Al(2). Since the local environment around the BR position has changed in the β'' phase with respect to BAM, the emission wavelength of Eu^{2+} ion has also changed, because Eu^{2+} ions stayed at the BR position. Formation of β'' and β''' phases will shift the emission band but their effect is not really significant because BAM is more stable so that the amount of other phases will be small.

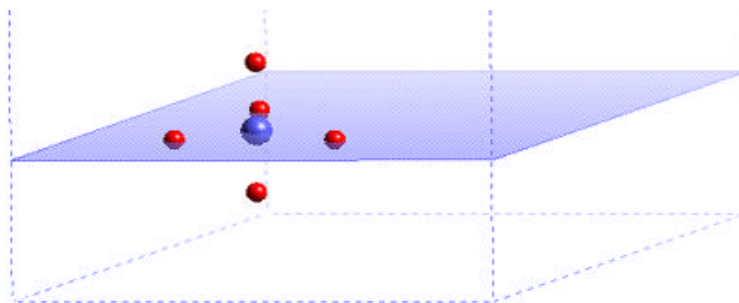
References

1. D. Ravichandran, S.T. Johnson, S. Erdei, R. Roy, and W.B. White, "Crystal Chemistry and Luminescence of the Eu^{2+} -Activated Alkaline Earth Aluminate phosphors," *Displays*, **19**[4] 197-203 (1999).
2. G. Yamaguchi and K. Suzuki, *Bull. Chem. Soc. Jap.*, **41** 93 (1968). As cited in M. Bettman and L.L. Turner, "On the Structure of $\text{Na}_2\text{O}\cdot 4\text{MgO}\cdot 15\text{Al}_2\text{O}_3$, a Variant of Beta-Alumina," *Inorg. Chem.*, **10**[7] 1442-6 (1971).
3. M. Bettman and C.R. Peters, "The Crystal Structure of $\text{Na}_2\text{O}\cdot \text{MgO}\cdot 5\text{Al}_2\text{O}_3$ with Reference to $\text{Na}_2\text{O}\cdot 5\text{Al}_2\text{O}_3$ and Other Isotypal Compounds," *J. Phys. Chem.*, **73**[6] 1774-80 (1969).
4. B.G. Dick and A.W. Overhauser, "Theory of the Dielectric Constants of Alkali Halide Crystals," *Phys. Rev.*, **112**[1] 90-103 (1958).
5. J.G. Park and A.N. Cormack, "Structural Chemistry of Alkaline Earth Hexa-Aluminates," *Mater. Res. Soc. Symp. Proc.*, **369** 457-62 (1995).
6. J.G. Park and A.N. Cormack, "Crystal/Defect Structures and Phase Stability in Ba Hexa-aluminates," *J. Solid State Chem.*, **121**[1] 278-90 (1996).
7. G.V. Lewis and C.R.A. Catlow, "Potential Models for Ionic Oxides," *J. Phys. C: Solid State Phys.*, **18**[6] 1149-61 (1985).
8. C.R.A. Catlow, A.N. Cormack, and F. Theobald, "Structure Prediction of Transition-Metal Oxides using Energy-Minimization Techniques," *Acta Crystallogr., Sect. B: Struct. Sci.*, **B40**[3] 195-200 (1984).
9. A.N. Cormack, G.V. Lewis, S.C. Parker, and C.R.A. Catlow, "On the Cation Distribution of Spinels," *J. Phys. Chem. Solids*, **49**[1] 53-7 (1988).
10. N.F. Mott and M.J. Littleton, "Conduction in Polar Crystals. I. Electrolytic Conduction in Solid Salts," *Trans. Faraday Soc.*, **34**[1] 485-99 (1938).
11. M. Bettman and L.L. Turner, "On the Structure of $\text{Na}_2\text{O}\cdot 4\text{MgO}\cdot 15\text{Al}_2\text{O}_3$, a Variant of Beta-Alumina," *Inorg. Chem.*, **10**[7] 1442-6 (1971).
12. B.M.J. Smets and J.G. Verlijsdonk, "The Luminescence Properties of Eu^{2+} and Mn^{2+} Doped Barium Hexa-aluminates," *Mater. Res. Bull.*, **21**[11] 1305-10 (1986).
13. L.G.V. Uitert, "An Empirical Relation Fitting the Position in Energy of the Lower d-Band Edge for Eu^{2+} or Ce^{3+} in Various Compounds," *J. Lumin.*, **29**[1] 1-9 (1984).

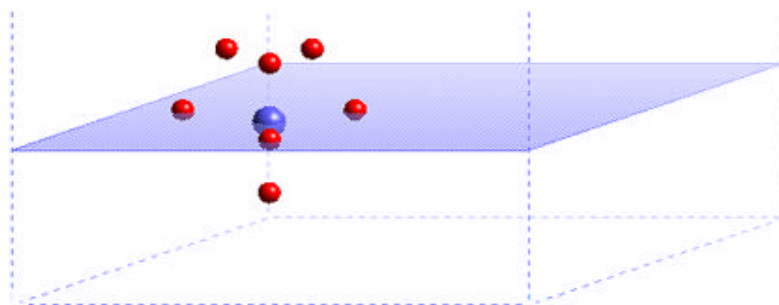
14. C.K. Jorgensen, "Partly Filled Shells Constituting Anti-Bonding Orbitals with Higher Ionization Energy Than Their Bonding Counterparts," pp. 49-82 in *Structure and Bonding*. Edited by J. D. Dunitz, P. Hemmerich, R. H. Holm, J. A. Ibers, C. K. Jorgensen, J. B. Neilands, D. Reinen, and R. J. P. Williams. Springer-Verlag, Berlin, Germany 1975.



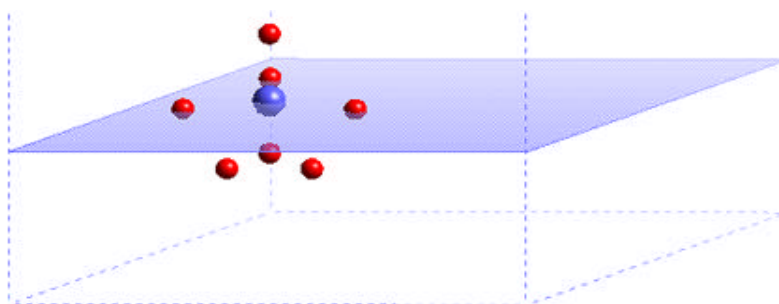
a) BR environment of BAM



b) anti-BR environment of BAM



c) BR environment of barium β'' -alumina



d) anti-BR environment of barium β'' -alumina

Figure 7.1. Comparison of BR and anti-BR positions.



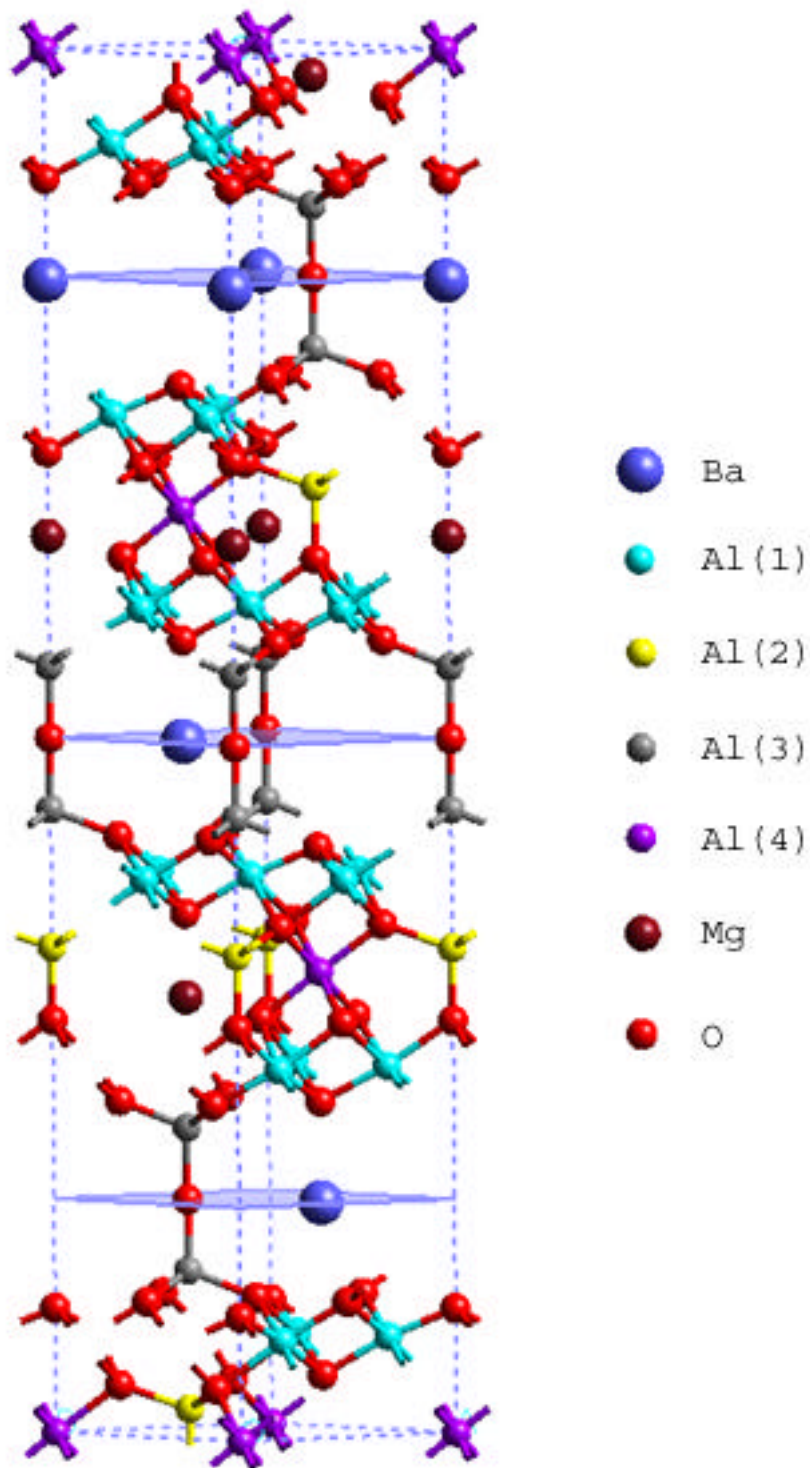


Figure 7.2. Unit cell of barium β'' -alumina.

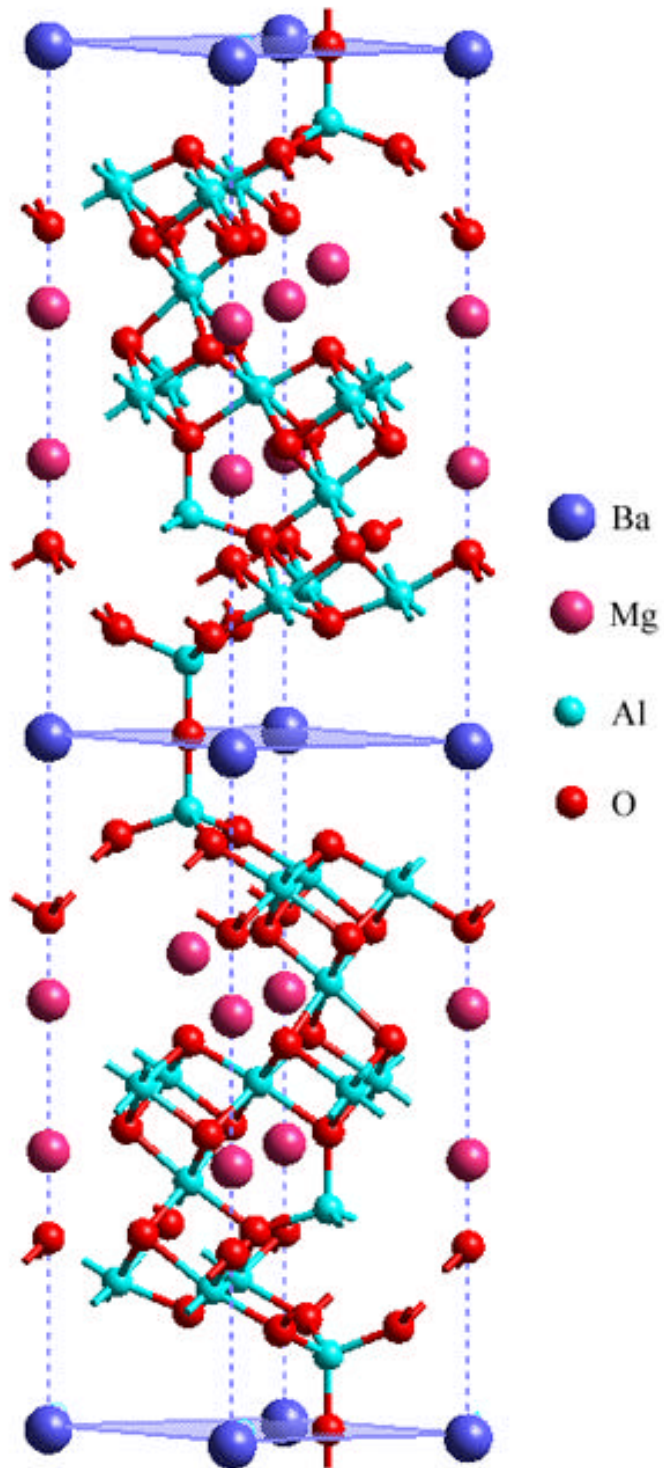


Figure 7.3. Primitive cell of barium β''' -alumina.

8. Summary and Future Work

8.1 Summary

Structural and defect properties of β -alumina-related barium phases have been investigated with the aid of computer simulation. The predicted optical behavior of the barium hexa-aluminates doped with Eu^{2+} ion has been studied and compared. Altogether five structures have been discussed: $\text{BaMgAl}_{10}\text{O}_{17}$ (BAM), $\text{Ba}_{0.75}\text{Al}_{11}\text{O}_{17.25}$ (barium-poor phase), $\text{Ba}_3\text{Mg}_3\text{Al}_{30}\text{O}_{51}$ (β'' phase), $\text{BaMg}_3\text{Al}_{14}\text{O}_{25}$ (β''' phase) and $\text{Ba}_3\text{Al}_{32}\text{O}_{51}$ (a hypothetical phase). Intrinsic and extrinsic defects have been calculated for each structure and compared, along with the Mg ion distributions in the spinel blocks and O ion distributions in the conduction plane. Ion-migration issues associated with Eu ion have also been discussed. The potential dependence of the simulation was also addressed.

Our work has suggested that BAM structures will have two different Mg distributions that will affect the defect properties. The two possible configurations can not be distinguished by the lattice energy. Both configurations will exist in the real material. Although two Mg distributions exist, the thermally predominant defect, a barium Frenkel defect, is the same for both configurations. The most significant change resulting from the Mg distribution is the oxygen interstitial position. The oxygen interstitial ion will reside in the mirror plane to form a two-bridge configuration at the mOB position, if the Mg distribution retains the mirror symmetry. However, if the Mg distribution destroys the mirror symmetry, the oxygen interstitial will stay inside the spinel block, in the half of the spinel block without Mg. It seems that the charge of Mg'_{Al} plays an important role in determining the position of the defect. Calculations of defect complexes and bond valence have verified the results that Eu^{3+} ion prefers Al(2) sites in the spinel block, instead of BR sites in the conduction plane, a result which is potential independent.

Ion migration studies suggest that Eu^{3+} ion can migrate into the spinel block at relatively low temperature with the help of Mg ion, but it will not migrate in the conduction plane, where barium and Eu^{2+} ions show active migration behavior. Oxygen

does not undergo long-range migration in the conduction plane, which implies that the formation of $\text{EuMgAl}_{11}\text{O}_{19}$ as suggested by Shozo et al. would not occur at the temperature when $\text{BaMg}(\text{Al}_9\text{Eu})\text{O}_{17}$ is more likely to be formed instead. Eu^{2+} ion seems to form clusters in the BAM structure, which will deteriorate the luminescent efficiency.

The defect properties of the barium-poor phase are different from BAM, because of the absence of Mg and the presence of oxygen interstitials in the conduction plane. The structural difference changes the location of defects. Eu^{3+} ion is found to occupy the Al(3) site, the other tetrahedral position, instead of the Al(2) site in order to compensate for the effective negative charges of oxygen interstitials in the mirror plane. Multiple configurations with different oxygen interstitial arrangements have been found to have very similar lattice energies. The d-band edge calculation for the europium ion has suggested that the observed broader and shifted emission band of Eu^{2+} ion in the barium-poor phase compared to BAM is the result of the multiple oxygen distributions that will change the ligand field of Eu^{2+} . The change of the ligand field is large enough to broaden and shift the emission band significantly to account for the two-band configuration that is seen in the measured emission spectrum. Eu^{3+} ions in the aluminum positions in the spinel block will also have the effect of shifting the emission band. The calculation also suggests that the two Mg distributions in BAM will change the emission spectrum to a continuously curved peak instead of a sharp peak.

A hypothetical structure $\text{Ba}_3\text{Al}_{32}\text{O}_{51}$ with aluminum vacancies inside the spinel blocks seems to have a lower lattice energy than the barium-poor and barium-rich phases, but its existence has not yet been demonstrated experimentally. Defect calculations on the $\sqrt{3} \times \sqrt{3}$ super-cell of this hypothetical phase show the same defect properties as the barium-poor phase.

Our study has suggested that the barium β'' and β''' phases have defect properties more like BAM than the barium-poor phase, because of similar chemical components and closely related structures. Several structures with different Mg distributions were also found to exist in these two phases. Among all the three phases (β , β'' and β'''), the β phase (BAM) is the most stable one which is the reason why BAM is widely used rather than the other barium hexa-aluminates. Because of the different site environments of BR sites in the β'' phase compared to BAM and because of the possibility of its intergrowth

with BAM, our study suggests that the formation of the β'' phase will shift the emission band significantly and degrade the designed emission properties of BAM:Eu²⁺ material. Europium ion in the β''' phase also shows an emission band shift with respect to BAM but to a small extent so there is no big influence of the formation of the β''' phase in the BAM material. The potential adjustment for different coordinations of Eu was not found to affect the simulation results.

8.2 Suggestions for Future Work

Since there is another phase of barium hexa-aluminate, 1.32BaO6Al₂O₃ (a barium rich phase that can intergrow with the barium-poor phase), the europium ion behavior should be studied further in this phase.

As we have found that Mg plays an important role in the Eu³⁺ migration into the spinel block, which will shift the emission band, other divalent cations should be considered to substitute for Mg to control this migration to hinder the luminescent degradation.

Because the Eu²⁺ cluster in BAM will decrease the luminescent intensity and Eu²⁺ ion migrates with an interstitialcy mechanism, substitution of barium with other ions like Ca may provide a way to separate Eu²⁺ ions so that the luminescent efficiency will be increased.

Many other phases such as CaAl₁₂O₁₉ and SrMgAl₁₀O₁₇ with similar structures to the barium-hexa-aluminates have also been used for Eu²⁺ hosts. And many other active ions of rare-earth elements can be doped in these phases. Our studies can be extended to the studies of active cations in different structures, which will help to design phosphor materials with specific luminescent properties.

Further calculation of the d-band edge of the Eu ion in the three positions, BR, Al(2) and Al(3) sites could be more accurately calculated by ab initio simulation, which would clarify the main reason for the luminescent degradation in BAM:Eu²⁺.